Université d'Ottawa · University of Ottawa

PERMISSION DE REPRODUIRE ET DE DISTRIBUER LA THÈSE

PERMISSION TO REPRODUCE AND DISTRIBUTE THE THESIS

NOM DE L'AUTEUR / NAME OF AUTHOR:	Jamal KURDI
ADRESSE POSTALE / MAILING ADDRESS:	~~P.O. Box 53217 Ottawa ON K1N 1C5~~ 20072 - 390 RIDEAU ST. OTTAWA, ON., K1N 5Y8
GRADE / DEGREE:	**ANNÉE D'OBTENTION / YEAR GRANTED**
Ph.D.(Chemical Engineering)	2003
TITRE DE LA THÈSE / TITLE OF THESIS:	
Molecular Engineering and Nanostructuring of Polymer Networks for High Performance Gas Separation Membranes	

L'auteur permet, par la présente, la consultation et le prêt de cette thèse en conformité avec les règlements établis par le bibliothécaire en chef de l'Université d'Ottawa. L'auteur autorise aussi l'Université d'Ottawa, ses successeurs et cessionnaires, à reproduire cet exemplaire par photograhie ou photocopie pour fins de prêt ou de vente au prix coûtant aux bibliothèques ou aux chercheurs qui en feront la demande.

Les droits de publication par tout autre moyen et pour vente au public demeureront la propriété de l'auteur de la thèse sous réserve des règlements de l'Université d'Ottawa en matière de publication de thèses.

The author hereby permits the consultation and the lending of this thesis pursuant to the regulations established by the Chief Librarian of the University of Ottawa. The author also authorizes the University of Ottawa, its successors and assignees, to make reproductions of this copy by photographic means or by photocopying and to lend or sell such reproductions at cost to libraries and to scholars requesting them.

The right to publish the thesis by other means and to sell it to the public is reserved to the author, subject to the regulations of the University of Ottawa governing the publication of theses.

N.B. LE MASCULIN COMPREND ÉGALEMENT LE FÉMININ

MAY, 4th, 2003 — DATE

(AUTEUR) SIGNATURE (AUTHOR)

Université d'Ottawa · University of Ottawa

Université d'Ottawa · University of Ottawa

FACULTÉ DES ÉTUDES SUPÉRIEURES ET POSTDOCTORALES

FACULTY OF GRADUATE AND POSTDOCTORAL STUDIES

KURDI, Jamal

AUTEUR DE LA THÈSE - AUTHOR OF THESIS

Ph.D. (Chemical Engineering)

GRADE - DEGREE

Chemical Engineering

FACULTÉ, ÉCOLE, DÉPARTEMENT - FACULTY, SCHOOL, DEPARTMENT

TITRE DE LA THÈSE - TITLE OF THE THESIS

Molecular Engineering and Nanostructuring of Polymer Networks for High Performance Gas Separation Membranes

André Tremblay

DIRECTEUR DE LA THÈSE - THESIS SUPERVISOR

EXAMINATEURS DE LA THÈSE - THESIS EXAMINERS

M. Dubé

X. Feng

B. Kruczek

T. Matsuura

J.-M. De Koninck, Ph.D.

LE DOYEN DE LA FACULTÉ DES ÉTUDES SUPÉRIEURES ET POSTDOCTORALES

SIGNATURE

DEAN OF THE FACULTY OF GRADUATE AND POSTDOCTORAL STUDIES

Molecular Engineering and Nanostructuring of Polymer Networks for High Performance Gas Separation Membranes

by

Jamal Kurdi

A thesis submitted to the Faculty of Graduate and Postdoctoral Studies
in partial fulfillment of the requirements for the degree of

DOCTOR OF PHILOSOPHY

in the Department of Chemical Engineering
UNIVERSITY OF OTTAWA

January 2003

STATEMENTS OF CONTRIBUTIONS OF COLLABORATORS

I hereby declare that I am the sole author of this thesis. Membrane preparation and characterization were performed by myself under the supervision and training received from Professor André Y. Tremblay. The X-ray diffractions measurements were contracted out to the Department of Earth Sciences at the University of Ottawa.

My supervisor Dr. Tremblay provided an excellent collaboration through the whole research work, day-to-day supervision, discussing and sharing ideas, continuous input and editorial comments for all of my written work. The quality of the research and publications were significantly improved through his collaboration.

Signature

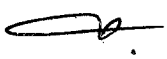

Date: January 6th, 2003

Jamal Kurdi

ABSTRACT

The architecturing and characterization of polymer-based materials at a molecular scale are of great importance in the development of novel rigid polymeric molecular sieves for high performance gas separation membranes. The new rapidly growing field of nanoscience technologies and material nanostructuring offers novel ways for creating nanoengineered material combinations. Intermolecular and supramolecular interactions among different molecules and clusters play an important role in the microscopic behavior of molecular architectures and molecular self-assembly. In this work, the coordination shell number of polyetherimide (PEI) membranes was determined from experimental X-ray diffraction data and found to be a key link between microscopic pair intermolecular interactions and macroscopic scale interactions. This link enabled us to determine the intermolecular force parameters required to understand material structuring at a molecular scale. These physical parameters are required in all models used in the determination of the micropore size distributions from gas adsorption isotherms.

Computational chemistry and physicochemical principles were useful to illustrate molecular architecturing and coordinating to form intermediate stable molecular complexes during membrane fabrication. These coordination complexes acted as pore forming templates that could be disrupted and removed after polymer coagulation to open the closed PEI network structure and increase the interconnectivity and accessibility among polymer micropores. Based on nanotechnology concepts, a uniform dispersion of nanoscopically-sized filler particles into a polymer network created novel materials with superior properties and characteristics attributed to the presence of ultra-large interfacial

area per unit volume. The adhesive (noncovalent interactions among different molecules) properties of nanoelement surfaces and polymer surfaces were the key for the creation of uniform polymeric molecular sieves. Narrowing the micropore size distribution is also possible when the adhesive energy between nanoparticles and polymer phase exceeds the cohesive energy of the pure polymer. Membranes were prepared using twelve metal-ligand complexes as filler additives that were uniformly dispersed into the PEI polymer solution before membrane casting. Membranes containing cobalt phthalocyanine (CoPc) showed the highest performance for oxygen separation from air. However, the performance was largely decreased upon annealing indicating a low nanostructure stability. Membranes containing magnesium phthalocyanine (MgPc) showed different characteristics and behaviors. These membranes had an excellent performance for oxygen separation from air that increased with increasing additive concentration. The membrane performance was maintained after the annealing process indicating high nanostructure stability. Their micropore size distribution was narrower than all membranes containing other additives as well as the base membrane without additive. The incorporation of MgPc into PEI polymer is a very successful method to produce stable polymeric molecular sieve membranes having high performance for oxygen separation from air.

RÉSUMÉ

L'architecture et la caractérisation de polymères à l'échelle moléculaire sont de grande importance dans le développement de tamis moléculaires polymériques rigides pour la fabrication de membranes de séparation de gaz a rendement élevé. La nouvelle discipline des technologies de nanosciences et de "nanostructuring" offrent de nouvelles routes pour créer des matériaux nanostructurés. Les interactions intermoléculaires et supramoléculaires parmi différentes molécules et agrégats jouent un rôle important dans le comportement microscopique des architectures moléculaires et l'auto-assemblage moléculaire. Dans ce travail, le nombre de coordination pour le polyetherimide (PEI) formant des membranes sélectives pour l'oxygène a été déterminé à partir des données expérimentales de diffraction de rayon X et c'est avéré être un lien important entre les interactions intermoléculaires microscopiques et les interactions macroscopiques. Ce lien nous a permis de déterminer les paramètres de force intermoléculaires exigés pour comprendre le matériel structurant sur une balance moléculaire. Ces paramètres physiques sont requis pour tous les modèles utilisés dans la détermination des distributions de micropores par l'adsorption de gaz.

La chimie informatique et les principes physico-chimiques sont utilisés pour illustrer l'architecture et la coordination moléculaire pour former des complexes intermédiaires moléculaires stables pendant la fabrication de la membrane. Ces complexes de coordination ont agit en tant que substance formant les pores qui peuvent être perturbés et enlevés après la coagulation du polymère pour ouvrir la structure fermée du réseau du PEI et pour augmenter l'inter-connectivité et l'accessibilité parmi les micropores du polymère. Basé sur des concepts de nanotechnologie, une dispersion uniforme des particules nanoscopiques dans le réseau du polymère a crée de nouveaux matériaux ayant des propriétés et caractéristiques attribuées à la présence d'une grande surface par volume unitaire. Les propriétés adhésives entre la surface des nanoelements et la surface du polymère est la clef pour la création de l'uniformité du tamis moléculaire. Le rétrécissement de la distribution des grandeurs de micropores est également possible entre le moment où l'énergie adhésive des nanoparticules et la phase du polymère

excèdent l'énergie cohésive du polymère propre. Plusieurs membranes ont été préparées en utilisant douze complexes métalliques uniformément dispersés dans la solution de polymère utilisée dans la préparation de la membrane. Les membranes contenant le phthalocyanine de cobalt (CoPc) ont montré le rendement le plus élevé pour la séparation de l'oxygène de l'air. Cependant, la performance de ces membranes diminue avec un processus de recuite indiquant une instabilité de la nanostructure tandis que les membranes contenant la phtalocyanine de magnésium (MgPc) montraient différentes caractéristiques et comportements. Ces membranes (PEI et MgPc) ont une excellente performance pour la séparation de l'oxygène de l'air qui a augmenté en augmentant la concentration de cet additif. Leur distribution de grandeur de micropores était plus étroite que toutes les autres membranes ainsi que la membrane de basse sans additif. En conclusion, l'incorporation de MgPc dans le polymère de PEI est une méthode très utile pour obtenir des membranes polymèriques a tamis moléculaires stables ayant un rendement élevé pour la séparation de l'oxygène à partir de l'air.

ACKNOWLEDGEMENTS

I would like to express my sincere appreciation and deep gratitude to Dr. André Y. Tremblay to whom this thesis and I, owe a lot. I thank him for many things he has done on my behalf, for devoting his valuable time to teach me both laboratory skills and theoretic approaches with generosity and patience; for helping me through his guidance, feedback, beneficial discussions and valuable comments. I have been impressed and motivated by his diligence in work, incredible enthusiasm and energy to renew and professionalism over solving difficult problems we have faced. I thank him a lot for his endless support and generous help that made this work possible.

I would like to thank Professor V. Petkov, Sofia University, Bulgaria, for making his RAD program for analysis of X-ray diffraction data available for free downloading through the internet.

Many thanks to all staff of the Department of Chemical Engineering who have always been very supportive during my entire graduate study. In particular, I would like to thank the technicians at our department, Louis Tremblay, Gérard Nina and Franco Ziroldo for their generous care and great assistance in all experimental facilities supplying and maintaining work. Their fast response and high skills were very helpful.

I must also thank all graduate students of our department with whom I have attended classes, worked for long hours and shared the common goal.

I would like to thank the Ontario Graduate Scholarship (OGS) and the University of Ottawa excellence scholarship programs for their generous financial support. Many thanks to Dr. André Y. Tremblay for providing me with a research assistantship during all of my graduate study through the Natural Science and Engineering Council of Canada (NSERC).

Finally and not least, I owe a tremendous debt to my parents for their constant love, emotional support and encouragement to be creative. With my new hope, I would like to dedicate this work to Amal, my new future.

TABLE OF CONTENTS

CHAPTER III

CHAPTER IV

CHAPTER V

CHAPTER VI

CHAPTER VII

CHAPTER VIII

CHAPTER IX

CHAPTER X

LIST OF TABLES

CHAPTER II

CHAPTER III

CHAPTER IV

CHAPTER V

CHAPTER VI

CHAPTER VIII

CHAPTER IX

LIST OF FIGURES

CHAPTER II

CHAPTER III

CHAPTER IV

CHAPTER V

CHAPTER VI

CHAPTER VII

CHAPTER VIII

CHAPTER IX

CHAPTER X

APPENDIX

CHAPTER I

INTRODUCTION

Membrane-based gas separation is a rapidly growing technology that has achieved $150 million/year business with an expected similar substantial growth in the near future (Baker, 2002). Gas separation membranes have many industrial applications such as H_2 recovery in refineries, CO_2 removal from natural gas, O_2 or N_2 production from air, dehydration of air or natural gas, recovery of hydrocarbon vapors or processing solvents from purge gases, and separation of different hydrocarbon vapors in petrochemical plants (Henis, 1994; Bhide and Stern, 1991; Baker et al. 1998; Baker et al., 2001a, b). To date, the separation of oxygen from air using membrane technologies is not competitive with other technologies as a higher membrane performance is required. Although a high performance liquid membrane with O_2/N_2 selectivity exceeding 20 can be achieved, the life of facilitated-transport membranes based on cobalt Schiff bases is less than one month (Johnson et al., 1987) and a demand for increasing membrane performance still exists (Baker, 2002). Research to improve gas separation performance of membranes is currently focused in two areas:

1. Optimizating membrane morphology such as the preparation of defect-free membranes having ultra-thin selective layers and sublayers with a negligible resistance to gas transport (Hachisuka et al. 1996, Pinnau, 1994, Koros and Fleming, 1993, Fritzsche et al. 1989, Pinnau and Koros, 1993).
2. Improving membrane materials by the synthesis of new materials such as polyimides (Mittal, 2001, Ohya et al. 1996), modifying material chemical structures (Won et al., 2000, Chowdhury et al., 2001, Tiemblo et al., 2002), incorporating additives into polymer network (Shonaike and Simon, 1999, Mahajan et al. 2002, Figoli et al. 2001), blending different polymers (Chung and Xu, 1998, Kapantaidakiset al. 1999, Kim et al. 1999, Shonaike and Simon, 1999) and architecturing the material molecular assembly such as structuring and molecular engineering of supramolecular polymers (Caruso and Antonietti, 2002, Ying, 2001, Ciferri, 2000).

The importance of the second area was emphasized in a recent review article (Baker, 2002), which concludes that the development of improved membrane materials is a continuing topic of research, and is particularly required for oxygen separation from air. This can be illustrated by a large number of different materials tested for oxygen permeability vs. O_2/N_2 selectivity and plotted by Robsen (1991) showing a strong trade off between permeability and selectivity. The movement beyond the upper bound Robsen (1991) is still a challenge that needs a breakthrough for competitive O_2/N_2 membrane separation. Singh and Koros (1996) emphasized that the challenge for advanced gas separation membranes can be overcome by enhancing the entropic selectivity through fabrication of a new generation of polymeric membrane materials having a molecular sieve structure. Therefore, the correlation structures/permeabilities/selectivity of polymeric membranes is a subject of many systematic studies (Pandey and Chauhan, 2001).

The general objective of this thesis is a contribution to the development of membrane technology in the field of gas separation, and particularly for oxygen separation from air. Our main goal within the membrane material development area was to tailor polymeric molecular sieves suitable for gas separation membranes. However, many obstacles had to be overcome before achieving this goal. The two most important challenges being;

1. Determination of intermolecular force interactions among similar and different molecules.
2. Characterization of polymeric membrane materials at the microscopic (< 2 nm) scale.

These two challenges are considered to be the two most important obstacles facing nanotechnology development according to the authors of the WTEC Panel Report on Nanostructure Science and Technology (Siegel, 1999).

The first challenge requires knowledge of molecular self-assemblies, supramolecular interactions, and the interactions between nanoscale building blocks and their surroundings. This is required for two reasons: first, the intermolecular force interactions represent essential physical parameters for the characterization of polymeric membrane materials at a molecular scale; and second, knowledge of the intermolecular

force interactions is required for predicting, molecular engineering and architecturing of the microstructure of membrane material assemblies.

The second challenge relates to the determination of the micropore size distribution of polymeric materials with pore sizes less than 2 nm (IUPAC, 1997). This is necessary to know the molecular sieve structure of polymeric materials to obtain narrow pore size distributions. This knowledge is also required and extremely important for material development in the area of catalysis and adsorption technologies (Ying, 2001).

The thesis deals with both challenges and additional significant fundamental contributions within the physical chemistry area have resulted. A membrane preparation method "coagulation post-leaching" was established in the first paper (chapter II). The objective was to gel a polyetherimide matrix containing dispersed stable templates followed by the breaking and removal of these templates in order to create micropores with a uniform size inside the polymer network structure. The influence of several variables in membrane preparation on the performance of the membranes for oxygen separation from air had to be addressed. The purpose of this paper was to explore membrane material architecturing and tailoring at a molecular scale. It is difficult to find works on the microstructure of membranes and their performance in the literature, due to the combined effects of membrane morphology optimization and material structuring (Pratsenko and Bil'dyukevich, 1994, Kesting et al., 1990, Kesting, 1989) and the challenge in the characterization of the microstructure of polymeric materials.

In the second paper (chapter III), we were seeking two targets: first, studying the supramolecular interactions during membrane preparation in order to illustrate the mechanism of architecturing the membrane material using the coagulation post-leaching preparation method; second, modeling the PEI structure at a molecular scale and determining the micropore size distribution of this polymeric membrane. Computational chemistry and physicochemical principles were useful means to achieve the two targets. The determination of pore size distributions for ultrafiltration membranes using nitrogen adsorption techniques was discussed in literature (Calvo et al., 1997). In this work, standard nitrogen adsorption method ASAP 2000M set by Micromeritics (GA, U.S.A.) was used to determine the nitrogen adsorption isotherms. The slit geometry Horvath-

Kawazoe model was used to calculate the micropore size distributions from nitrogen adsorption isotherms (Horvath and Kawazoe, 1983). The same interaction parameters for amorphous activated carbon were used for PEI membranes based on the abundance of carbon in the structure of PEI. This assumption is still an unsolved challenge in the literature (Dombrowski et al. 2000, Ravikovitch et al. 2000) and was partly solved in our later work. However, the results were useful for exploring the influence of architecturing of membrane materials on the shape of its micropore size distribution as well as the correlation between the total micropore volume of membranes and the corresponding air permeance and oxygen separation factor. The purpose of this exploration was to find out if a narrower micropore size distribution and permeation having greater sieving effects could be obtained.

Because the determination of the micropore size distribution of polymeric membrane materials was required in this work, it was necessary to verify simplifying assumptions used in gas adsorption techniques. The Horvath-Kawazoe model is a simple method because one equation is used to relate micropore size to relative pressure in the adsorption isotherms (Cheng and Yang, 1994). It is widely used to characterize microporous carbons and zoelites (Razmus and Hall, 1991, Baksh and Yang, 1992, Kruk et al. 1997). However, two essential problems exist in using this micropore characterization model: first, structural modeling at a molecular scale especially for amorphous networked solids (Gelb and Gubbins, 1999), and second, the determination of intermolecular force interaction parameters between the adsorbate and adsorbent (Baksh and Yang, 1992). It was reported that the agreement of the micropore size distribution of activated carbons calculated from nitrogen adsorption isotherms with one based on other experimental techniques is attributed to the selection of the suitable physical parameters (Korili and Gil, 2001). Others also reported that the accuracy of micorpore size distribution of organo-xerogels (microporous silica gel) obtained by HK model depends on the accuracy of the used interaction parameters (Newalkar and Komarneni, 2000). Neimark et al., 1998 reported that the most important factor that influenced the calculated micropore size by the non-local density functional theory (NLDFT) is the choice of the parameters of the adsorbate-adsorbate and adsorbate-adsorbent interactions. Ravikovitch et al. 2000 have also attributed the inconsistency in the micropore size distribution

calculated by NLDFT to the choice of these parameters. The uncertainty of these physical parameters and their considerable impact on the calculated pore size were discussed in the literature. It was considered that the variation in the values of these parameters is a major source of inaccuracy and discrepancy in the resulting micropore size distributions (Satio and Foley, 1991, Cheng and Yang, 1994). As this matter was not addressed in the literature for polymeric systems before, determination of the interaction parameters and the structural modeling of micropores for N_2-PEI system were the topic of the third paper, chapter IV. The same theoretical approach addressed in Horvath-Kawazoe (1983) paper to determine the intermolecular force parameters was used. The influence of these parameters on the determined micropore size distribution was explored.

Although we used, in the third paper (Chapter IV), the same physical parameters for nitrogen as in Horvath-Kawazoe paper, our literature survey indicated a discrepancy in the nitrogen physical parameters used by Horvath and kawazoe (1983) and the reported parameters found in other sources (Bretsznajder and Bandrowski, 1971, Soule et al. 2001, Poling et al. 2001, Ravikovitch et al. 2000 and 1997, Fernandes and Gavalas, 1999, Sonwane and Bhatia, 2000, Ohba et al. 2000, Razmus and Hall, 1991). Because of the importance of these physical parameters not only in the micropore characterization but also for predicting, molecular engineering and architecturing of the microstructure of membrane material assemblies (Balzani et al, 1998 and 2000; Lindoy and Atkinson, 2000), it was necessary to address the discrepancy in the reported parameters in the literature as well as exploring the valid methods for the determination of the intermolecular force parameters, which became the topic of the fourth paper, chapter V. The important point in this paper was to define the direct link between the molecular properties and macroscopic (bulk) properties of materials required for the determination of intermolecular force parameters.

In the literature, the intermolecular force parameters were assumed to be independent of pressure and temperature (Neimark et al. 1998, Hirschfelder et al. 1967, molecular theory). In another reference, they are temperature dependent and are usually determined based on statistical mechanics methods and molecular dynamic simulations (White et al. 2000). A simple method to determine these parameters at different

temperature was not given in the literature. This matter is required because adsorption isotherm has to be done at a certain temperature depending on the boiling point of the adsorbate gas. The parameters should be determined for the test temperature. The matter was explored for nitrogen and PEI in the fifth and sixth papers, chapters VI and VII respectively.

In the Horvath-Kawazoe model, the intermolecular interaction energy coefficient was calculated form the Kirkwood-Muller equation (Horvath and Kawazoe, 1983). However, it was reported that this equation yields a coefficient with a value larger than the experimental one. The discrepancy was attributed to the neglect of an electron correlation term (Salem, 1960). As this is an important matter in determination of interaction energy among a pair of molecules based on molecular properties, it was investigated in the fifth paper, chapter VI for nitrogen at different temperature and pressure.

The three fundamental papers (4, 5 and 6) are important works required to determine both the supramolecular interactions among molecules and the physical parameters used in characterization material structure at a molecular scale.

Through our published work, the third paper in chapter IV, the physical parameters in the Horvath-Kawazoe model for N_2-PEI system was established. Improving the accuracy of these parameters can be achieved using the approaches founded in the three fundamental papers (4, 5 and 6). However, because the difference in the interaction parameters leads to a small shift in the micropore size distribution with maintains the same shape as discussed in the third paper in chapter IV, it was not necessary at this time to improve the accuracy of these parameters. Another reason not to use the three fundamental papers, an improvement is still required for the characterization model. A new model for the determination of micropore size distribution from nitrogen adsorption isotherm was investigated by us based on the fundamental work, which was included in this thesis. The new work consists of three long papers in the final stage of preparation to be submitted in refereed journals and will not be included in this thesis because of space limitations.

Once accurate parameters for the characterization method were set, we could move towards the main goal of this thesis, narrowing the micropore size distribution of

PEI membrane materials. The Horvath-Kawazoe model was used for two reasons: first, it is an established known method, and second, it yields the correct shape of the micropore size distribution. Using the calculated physical parameters for N_2-PEI system found in the third paper, chapter IV, the Horvath Kawazoe model is reasonable because the intermolecular force distance parameter for PEI was determined by computational chemistry. This parameter has a significant influence on the mode of the micropore size distribution. The height of the peak in the distribution will have the same shift for all compared samples in case of deviation in the interaction energy parameter. Therefore, this provided a dependable characterization method for the last two papers in this thesis.

To improve the sieving structure of PEI, a literature survey was conducted. From the most found promising work, it was found that the incorporation of cobalt complexes such as Cosalen (Oxygen carrier) into polymeric membranes such as polycarbonate (Chen and Lai, 1996) or polyurethane (Chen et al. 2000) had the ability to improve membrane performance for O_2/N_2 separation. On the other hand, molecular building blocks consisting of cyclic, nanoscale cavity-containing coordination compounds can be used for architecturing porous nanostructured materials (Hupp and Nguyen, 2001). Macrocyclic liquid crystals such as porphyrins and phthalocyanines were also found to be suitable nano-meter scale molecular building blocks to tailor material properties (Kosal and Suslick, 2000, Suslick et al. 2000). Therefore, it was decided to investigate the incorporation of different metal complexes into polyetherimide membranes. The influence of metal complexes incorporated in polymeric membrane on the micropore size distribution was not investigated in literature and is the subject of the last two papers. The importance of this proposed work was to explore the ability of controlling the microporosity of polyetherimide membrane materials. The correlation between material structure of these membranes at a molecular scale and their performance for air separation is extremely important for the development of tailored polymeric membranes having molecular sieve structures.

Tailoring membrane materials and their characterization at a molecular scale are a necessity for the fabrication of polymeric molecular sieves with superior properties and characteristics required in many applications and particularly for air separation, the main topic of this thesis.

REFERENCES

Baker, R. W., "Future directions of membrane gas separation technology, Review", Ind. Eng. Chem. Res. 41(6), 1393-1411 (2002).

Baker, R. W., K. A. Lokhandwala, Z. He and I. Pinnau, "Processes Including PSA and Membrane Separation for Separating Hydrogen from hydrocarbons", U. S. Patent 6, 183, 628 (2001a).

Baker, W. R., A. Da Costa, I. Pinnau, R. D. Daniels and Z. He, "Membrane Augmented Polypropylene Manufacture", U.S. Patent 6,271,319 (2001b).

Baker, W. R., J. G. Wijmans and J. H. Kaschemekat, "Design of Membrane Vapor-Gas Separation Systems", J. Membrane Sci. 151 (1) 55-62 (1998).

Baksh, M. S. A/. and R. T. Yang, "Unique Adsorption properties and Potential Energy Profiles Of Microporous Pillared clays", AIChE J. 38 (9), 1357-1368 (1992).

Balzani, V., A. Credi, F. M. Raymo and J. F. Stoddart, "Artificial Molecular Machines", Angew. Chem. Int. Ed. 39, 3348-3391 (2000).

Balzani, V., M. Gómez-López and J. F. Stoddart, "Molecular machines", Acc. Chem. Res. 31, 405-414 (1998).

Bhide, B. O.and S. A. Stern, "A New Evaluation of Membranes Processes for the Oxygen Enrichment of Air", J. Membrane Sci. 62, 13-58 (1991).

Bretsznajder, S. and J. Bandrowski, "Prediction of Transport and Other Physical Properties of Fluids", Pergamon Press, Oxford, UK (1971).

Calvo, J I. P. Pradanos, A. Hernandez, W. R. Bowen, N. Hilal, R. W. Lovitt and P. M. Williams, "Bulk and surface characterization of composite UF membranes. Atomic force microscopy, gas adsorption-desorption and liquid displacement techniques", J. Membr. Sci. 128, 7-21 (1997).

Caruso, R. A., M. Antonietti, "Silica films with bimodal pore structure prepared by using membranes as templates and amphiphiles as porogens", Advanced Functional Materials. 12 (4), 307-312 (2002).

Chen, S. H., K. C. Yu, S. L. Houng, J. Y. Lai, "Gas transport properties of HTPB based polyurethane/cosalen membrane", J. Membrane Sci. 173(1), 99-106 (2000).

Chen, S. H. and J. Y. Lai, "Polycarbonate/(N,N'-dialicylidene ethylene diamine) Cobalt(II) complex Membrane for Gas Separation", J. Appl. Polym. Sci. 59, 1129-1135 (1996).

Cheng, L. S. and R. T. Yang, "Improved Horvath-Kawazoe Equations Including Spherical Pore Models for Calculating Micropore Size Distribution", Chem. Eng. Sci. 49 (16), 2599-2609 (1994).

Chowdhury, G., S. Deng, T. Matsuura, B. Laverty, "Development of thin-film composite hollow-fiber membranes from modified polyphenylene oxide for gas separation applications", J. Appl. Polym. Sci. 79 (2) 275-282 (2001).

Chung, T.S. and Z.L. Xu, "Asymmetric hollow fiber membranes prepared from miscible polybenzimidazole and polyetherimide blends", J. Membr. Sci. 147 (1), 35-47 (1998).

Ciferri, A., Ed., "Supramolecular Polymers", Marcel Dekker, Inc., New York (2000).

Dombrowski, R. J., D. R. Hyduke and C. M. Lastoskie, "Pore Size Analysis of Activated Carbons from Argon and Nitrogen Porosimetry Using Density Functional Theory", Langmuir 16, 5041-5050 (2000).

Fernandes, N. E. and G. R. Gavalas, "Molecular Dynamics Simulations of Diffusion in Mesoporous Glass", Ind. Eng. Chem. Res., 38 (3) 723-730 (1999).

Figoli, A., W. F. C. Sager, M. H. V. Mulder, "Facilitated oxygen transport in liquid membranes: Review and new concepts", J. Membrane Sci. 181 (1), 97-110 (2001).

Fritzsche, A. K., M. K. Murphy, C. A. Cruse, R. F. Malon and R. E. Kesting, "Characterization of Asymmetric Hollow Fiber membranes with Graded-Density Skins", Gas Sep. Purif. 3, 106-116 (1989).

Gelb, L. D. and K. E. Gubbins, "Pore size distributions in porous glasses: A computer simulation study", Langmuir 15 (2), 305-308 (1999).

Hachisuka, H., T. Ohara and K. Ikeda, "New Type Asymmetric Membranes having almost Defect free Hyper-Thin Skin Layer and Sponge-Like Porous Matrix", J. Membrane Sci. 116 (2), 265-272 (1996).

Henis, J. M. S., "Commercial and Practical Aspects of Gas Separation Membranes", in "Recent Development in Separation Science", D. R. Paul and Y. P. Yampol'skii, Eds., CRC Press, Boca Raton, FL (1994).

Hirschfelder, J.O., C. F. Curtiss, and R. B. Bird, "Molecular Theory of Gases and Liquids", John Wiley and Sons, Inc., New York, NY (1967).

Horvath, G. and K. Kawazoe, "Method for the calculation of effective pore size distribution in molecular sieve carbon", J. Chem. Eng. Jpn 16 (6), 470-475 (1983).

Hupp, J. T. and S. T. Nguyen, "Functional Nanostructured Molecular Materials", The Electrochemical Society Interface. Fall (2001).

IUPAC Manual of Symbols and Terminology, Appendix 2, Pt. 1, Colloid and surface Chemistry. Pure Appl. Chem. 31, 578 (1997).

Johnson, B. M., R. W. Baker, S. L. Matson, K. L. Smith, I. C. Roman, M. E. Tuttle and H. K. Lonsdale, "Liquid Membranes for the Production of Oxygen-Enriched Air. II. Facilitated-Transport membranes", J. Membrane Sci. 31 (1), 31-67 (1987).

Kapantaidakis, G. C., S. P. Kaldis, G. P.Sakellaropoulos, E. Chira, B. Loppinet and G. Floudas, "Interrelation between phase state and gas permeation in polysulfone/polyimide blend membranes", J. Polym. Sci. B37 (19), 2788-2798 (1999).

Kesting, R. E., "Solvent size effect: Solvents and solvent complexes viewed as transient templates which control free volume in the skins of integrally-skinned phase inversion membranes", J. Polym. Sci. C 27, 187-190 (1989).

Kesting, R E. A. K. Fritzsche, M. K. Murphy, C. A. Cruse, A. C. Handermann, R. F. Malon and M. D. Moore, "The second-generation polysulfone gas-separation membrane. I. The use of Lewis acid. Base complexes as transient templates to increase free volume", J. Appl. Polym. Sci. 40, 1557-1574 (1990).

Kim, M H. J. H. Kim, C. K. Kim, Y. S. Kang, H. C. Park and J. O. Won, "Control of phase separation behavior of PC/PMMA blends and their application to the gas separation membranes", J. Polym. Sci. B 37 (21), 2950-2959 (1999).

Kim, S. R., K. H. Lee and M. S. Jhon, "The Effect of Zn Cl_2 on the Formation of Polysulfone Membrane", J. Membrane Sci. 119 59-64 (1996).

Korili, S. A. and A. Gil, "On the application of various methods to evaluate the microporous properties of activated carbons", Adsorption 7 (3) 249-264 (2001).

Koros, W. J. and G. K. Fleming, "Membrane –Based Gas Separation", J. Membrane Sci. 83, 1-80 (1993).

Koros, W. J., M. R. Coleman, and D. R. B. Walker, "Controlled Permeability Polymer Membranes", Annu. Rev. Mater. Sci. 22, 47-89 (1992).

Kosal, M. E. and K. S. Suslick, "Microporous Porphyrin and Metalloporphyrin Materials", J. Solid State Chem. 152, 87-98 (2000).

Kruk, M., M. Jaroniec and J. Choma, "Critical Discussion of Simple Adsorption Methods Used to Evaluate the Micropore Size Distribution", Adsorption 3, 209-219 (1997).

Lindoy, L. F. and I. M. Atkinson, "Self-Assembly in Spramolecular Systems", The Royal Society of Chemistry, Cambridge, UK (2000).

Mahajan, P., R. Burns, M. Schaeffer, W. J. Koros, "Challenges in forming successful mixed matrix membranes with rigid polymeric materials", J. Appl. Polym. Sci. 86 (4), 881-890 (2002).

Mittal, K. L., Ed., "Polyimides and Other High temperature Polymers: Synthesis, Characterization and Applications", VSP, Utrecht, NL (2001).

Neimark, A. V., P. I. Ravikovitch, S. C. O'Domhnaill, M. Grun, F. Schuth and K. K. Unger, "Pore Size Analysis of MCM-41 Type Adsorbents by Means of Nitrogen and Argon Adsorption", Journal of Colloid and Interface science, 207, 159-169 (1998).

Newalkar, B. L. and S. Komarneni, "Synthesis and characterization of microporous silica prepared with sodium silicate and organosilane compounds", J. Sol-Gel Sci. Technol. 18 (3), 191-198 (2000).

Ohba, T., T. Suzuki and K. Kaneko, "Preformed Monolayer-induced Filling of Moleculaes in Micropores", Chemical Physics Letters, 326, 158-162 (2000).

Ohya, H., V. V. Kudryavtsev and S. I. Semenova, "Polyimide Membranes – Applications, Fabrications, and Properties", Kodansha LTD. and Gordon & Breach Science Publishers S. A., Tokyo, JP (1996).

Pandey, P. and R. S. Chauhan, "Membranes for gas separation", Progress in Polymer Sci. 26 (6), 853-893 (2001).

Pinnau, I, "Recent Advances in the Formation of Ultrathin Polymeric Membranes for Gas Separation", Polymers for Advanced Technologies 5, 733-744 (1994).

Pinnau, I. and W. J. Koros, "A Qualitative Skin Layer Formation Mechanism for Membranes Made by Dry/Wet Phase Inversion", J. Polym. Sci. B31, 419-427 (1993).

Poling, B. E., J. M. Prausnitz and J. P. O'Connell, "The Properties of Gases and Liquids, McGraw-Hill, New York, NY (2001).

Pratsenko and Bil'dyukevich, "Structure of casting solutions and its effect on the characteristics of polyamide membranes", Vysokomolekularnye Soedineniya. Seriya A. 36 (3), 457-460 (1994).

Ravikovitch, P. I., A. Vishnyakov, R. Russo and A. V. Neimark, "Unified approach to pore size characterization of microporous carbonaceous materials from N_2, Ar, and CO_2 adsorption isotherms", Langmuir 16 (5) 2311-2320 (2000).

Ravikovitch P. I., D. Wei, W. T. Chueh, G. L. Haller and A. V. Neimark, "Evaluation of Pore Structure Parameters of MCM-41 Catalyst Supports and Catalyst by Means of Nitrogen and Argon Adsorption", J. Phys. Chem. Part B, 101, 3671-3679 (1997).

Razmus, D. M. and C. K. Hall, "Prediction of Gas Adsorption in 5A Zeolites Using Monte Carlo Simulation", AIChE J. 37 (5) 769-779 (1991).

Robeson, L. M., "Correlation of Separation Factor versus Permeability for Polymeric membranes", J. Membrane Sci. 62, 165-185 (1991).

Saito, A. and H. C. Foley, "Curvature and parametric sensitivity in models for adsorption in micropores", AICHE J. 37 (3), 429-436 (1991).

Salem, L., "The Calculation of Dispersion Forces", Mol. Phys., 3, 441-452 (1960).

Shonaike G. O. and G. P. Simon, Eds., "Polymer Blends and Alloys", Marcel Dekker, Inc., New York, NY (1999).

Siegel, R. W., WTEC Panel Report on "Nanostructure Science and Technology, R&D Status and Trends in Nanoparticles, Nanostructured Materials, and Nanodevices", Loyola College Baltimore, MD 21210, USA (September, 1999).

Singh, A. and W. J. Koros, "Significance of entropic selectivity for advanced gas separation membranes", Ind. Eng. Chem. Res. 35 (4), 1231-1234 (1996).

Sonwane, C. G. and S. K. Bhatia, "Characterization of Pore Size Distributions of Mesoporous Materials from Adsorption Isotherms", J. Phys. Chem. B: 104 (39) 9099-9110 (2000).

Soule, A. D., C. A. Smith, X. Yang, C. T. Lira, "Adsorption Modeling with the ESD Equation of State", Langmuir, 17 (10) 2950-2957, 2001.

Suslick, K. S., N. A. Rakow, M. E. Kosal and J-H. Chou, "The Materials Chemistry of Porphyrins and Metalloporphyrins", J. Porphyrins Phthalocyanines 4, 407-413 (2000).

Tiemblo, P., J. Guzman, E. Riande, C. Mijangos, M. Herrero, J. Espeso and H. Reinecke, "Diffusion of small molecules through modified poly(vinyl chloride) membranes", J. Polym. Sci. B 40 (10) 964-971(2002).

White, A., F. J. Zerilli and H. D. Jones, "Ab Initio Calculation of Intermolecular Potential Parameters for gaseous Decomposition Products of Energetic Materials", DSTO Aeronautical and Maritime Research Laboratory, Australia (2000), pp. 1-43.

Won, J.M. H. Kim, Y. S. Kang, H. C. Park, U. Y. Kim, S. C. Choi and S. K. Koh, "Surface modification of polyimide and polysulfone membranes by ion beam for gas separation", J. Appl. Polym. Sci. 75 (12), 1554-1560 (2000).

Ying, J. Y., Ed., "Nanostructured Materials", Academic Press, San Diego, CA (2001).

CHAPTER II

The preparation of Defect-free Asymmetric Membranes for Gas Separations

J. Kurdi, and A. Y. Tremblay*

Department of Chemical Engineering, University of Ottawa, 161 Louis Pasteur, Ottawa, Ontario, K1N 6N5, Canada

*Corresponding author

André Y. Tremblay

Tel.: +1-613-562-5920; fax: +1-613-562-5172

E-mail address: tremblay@uottawa.ca

Article has been Published in: **Journal of Applied Polymer Science, Volume 73, Number 8, 1471-1482 (1999).**

CHAPTER II

Paper 1: The preparation of Defect-free Asymmetric Membranes for Gas Separations

J. Kurdi, and A. Y. Tremblay
Department of Chemical Engineering, University of Ottawa, 161 Louis Pasteur, Ottawa, Canada, K1N 6N5
Received 13 August 1998; accepted 18 December 1998

ABSTRACT

A technique was developed to prepare defect-free, asymmetric, polymer membranes for gas separation. The preparation method eliminates the need for coatings, which are usually required to render asymmetric, polymer based, membranes gas selective. In this method, a casting solution containing a polymer, solvent and salt additive is given a desired shape and immersed in a coagulation bath containing a non-solvent. The non-solvent is selected to have a low affinity for both the solvent and salt additive. After the complete coagulation of the membrane, the additive salt is leached out in a second bath. This leads to the formation of an asymmetric membrane having a well-interconnected porous network. The fine membrane structure is preserved by solvent exchange before it is finally dried.

Polyetherimide (PEI, Ultem® 1000) membranes were prepared from casting solutions containing 23, 25 and 26.5% (wt.) PEI, various amounts of lithium nitrate and N-Methyl-2-Pyrrolidinone (NMP). Membrane performance was determined for the separation of oxygen from air. The effects of polymer concentration, additive salt concentration and the drying process on oxygen permeance and the actual separation factor of the membrane are discussed. The addition of a small amount of solvent to the coagulation bath improved the leaching of the salt additive and produced membranes with a more open structure. A polymer concentration of 23% produced membranes with the highest performance. J Appl Polym Sci 73: 1471-1482, 1999

Key words: polyetherimide, air separation, asymmetric membrane, phase inversion, membrane preparation.

1 INTRODUCTION

The selection of a suitable polymeric membrane material and the method of preparation play an important role in increasing the performance of gas separation membranes. The structure of the membrane, which is determined by the material properties of the polymer and the mechanisms of formation, must be optimized to produce a membrane that has a high permeance and separation factor for a component in a mixture. Composite or asymmetric membrane structures are currently used for gas separations.[1] The desirable structural characteristics of an asymmetric membrane for gas separations are as follows:

1- Defect-free selective layer to avoid non–selective pore flow where gas transport occurs by viscous or Knudsen mechanisms.
2- The number of dead–ended pores should be minimized.
3- The number of selective pores, in which surface-diffusion of permeate gas is predominant[2], should be as large as possible.
4- The membrane should have a well-interconnected porous network structure to avoid high flow resistance.
5- The skin and overall cast film should be thin to obtain a high permeance.
6- The substantial resistance of the membrane sublayer to gas transport should be as low as possible.
7- Macrovoid-free structure to avoid the formation of a weak layer under the skin or avoid the presence of non-selective pores.
8- High mechanical strength to avoid compaction under high-pressure operation.

The selection of a suitable polymeric membrane material depends on the required separation task. Glassy polymers have a rigid structure and a high glass transition temperature. These properties make them suitable materials to form membranes with micropores having an excellent dimensional stability over a wide temperature range. Micropores are classified as pores or void volumes which are less than 2 nm, in width[3]. Glassy polymers are attractive materials to prepare membranes for the separation of permanent gas mixtures. This has been attributed to the flickering movement of the constituent polymer segments being moderated by the intrinsic rigidity of the polymer

backbone that produces subtle size selective transient gaps through which gas molecules can jump. High mobility selectivity of transient gas molecules can be obtained in glassy polymers.[4] Polyetherimide (PEI), one of these glassy polymers, is produced under the trade name Ultem® by General Electric, U.S.A. It is a high performance engineering amorphous thermoplastic resin.[5] Ultem® 1000 exhibits excellent mechanical, thermal and electrical properties. Its chemical resistance is good but may be attacked by halogenated hydrocarbons, dipolar aprotic solvents, cresol and concentrated acids and bases.[6,7] The chemical structure of polyetherimide is shown in Figure 2.1.[8] The aromatic imide units provide stiffness and heat resistance, while the swivel groups such as -O- and -$C(CH3)_2$- form flexible macromolecular chains which allow for good processability.[6] The intrinsic permeabilities of oxygen and nitrogen for a dense PEI film, at 35°C, were reported by Barbari et al.[9] as 0.4 and 0.05 Barrers respectively (1 Barrer = 10^{-10} [cm^3 (STP) cm / cm^2 s cm Hg]). Permeabilities and selectivities at 35°C, for many glassy polymer which can also be used for gas separation, have been reported elsewhere.[4] The intrinsic selectivity of oxygen over nitrogen[9] (at 35°C) for a dense PEI film is 7.6 which is higher than that for a dense polyethersulfone film (which is 5.7, reported by Wang et. al)[10] or for other glassy polymers reported by Koros et. al.[4] Although PEI polymer has a lower gas permeability, its higher intrinsic selectivities for He/N_2, CO_2/N_2 and O_2/N_2 makes this polymer an attractive membrane material.[11] However, membrane permeance can be increased by using a suitable preparation method that improves membrane morphology to obtain a high permeance without reducing membrane selectivity.

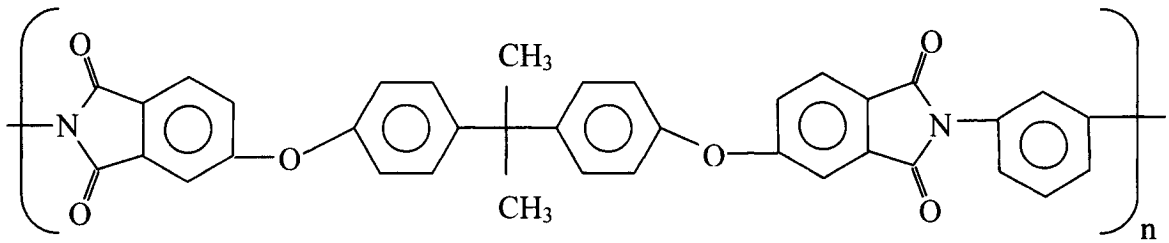

Figure 2.1 Structure of a PEI repeat unit.

Once the polymeric material is selected, the appropriate preparation method must be determined. Generally, the following techniques or combinations of them are used in the preparation of asymmetric polymeric membranes; Thermal Phase Inversion [12], Dry Phase

Inversion[13], Vapour Phase Inversion[14] and Wet Phase Inversion.[15] In all of these techniques, the resulting membrane structure will be affected by various formation mechanisms. These mechanisms involve one or several of the following basic processes; diffusion, evaporation, gellation, vitrification, crystallization, chemical reaction, phase conversion or separation, nucleation - growth, spinodal decomposition – coarsening, and coalescence.[16-20]

2 BACKGROUND

2.1 Preparation methods

The current industrial asymmetric membrane preparation techniques, for gas separations, are as follows; dry / wet phase inversion, phase inversion using Lewis acid:base complex solvents and dual-bath methods.

2.1.1 Dry / wet phase inversion

In this method, a partial evaporation step is used to form the skin layer on the surface of the membrane, followed by immersion in a non-solvent liquid medium to achieve an instantaneous phase inversion to form an interconnected open substructure.[21]

2.1.2 Phase inversion by using Lewis acid:base complex solvents[22]

Relatively high amounts of non-solvent can be added to the casting solution if the non-solvent forms a Lewis acid:base complex with the casting solvent. The skin formation through an evaporation step or diffusion driven process will be suppressed as a result of complex formation. Using an aqueous quench medium, a quick phase inversion occurs as a result of the rapid dissociation of the complex and the strong non-solvent environment of the resulting Lewis acid-water-solvent combination. Highly porous and integrally skinned asymmetric membranes can be obtained. However, if these membranes are to be used in gas separations, a silicon rubber layer must be applied over the membrane to seal defects present in the skin layer of the membrane.

2.1.3 Dual-bath method

The dual-bath method has been developed to take the advantages of both the delayed phase inversion and the instantaneous phase inversion.[23] The concept of this method is to first shortly immerse the cast membrane into a non-solvent bath to achieve a delayed phase inversion. Then, the cast film is immersed in a second non-solvent bath to achieve an instantaneous phase inversion in order to form an interconnected open substructure in the support layer.

2.2 Mechanisms of membrane formation

The formation of a skin and the type of phase inversion play an important role in obtaining a structure required for gas separation membranes.

2.2.1 Skin formation

An ultrathin skin layer is usually preferred to obtain a membrane with both a high permeate flux and separation factor. Two approaches can be used to form the skin layer:

a) A short evaporation is used to increase the polymer concentration in the top layer. This will play an important role in forming a dense skin layer. The evaporation process may be achieved by natural or forced convection.[24] However, highly volatile solvents such as chlorinated hydrocarbons are usually required.

b) The formation of the dense skin film can be induced by a diffusion driven process. This process occurs when the cast film is immersed in a non-solvent liquid medium that has a thermodynamically poor interaction with the casting solvent. In this case, the onset of demixing is delayed keeping the cast film as a viscous solution for a while during which the solvent diffuses easily from the outermost interface region of the cast film to the liquid quench medium. At the same time, the counter diffusion of the non-solvent will be delayed or reduced by the viscous nature of the casting solution. As a result of this multicomponent diffusion process, the rapid increase in the polymer concentration in the top layer of the cast film leads to the formation of a highly polarized gelled skin layer.[1,15,16]

2.2.2 Type of phase inversion

The wet phase inversion process, which causes the asymmetric structure, can be divided into two types;[25] delayed phase inversion (Membrane type I) and instantaneous phase inversion (Membrane type II)

a) Delayed Phase Inversion:

In the delayed phase inversion, the non-solvent liquid medium and the solvent in the casting solution have a poor mutual affinity. A dense skin layer is induced by the previously described diffusion driven process. In this situation, phase inversion proceeds slowly due to the dense top skin layer which suppresses the diffusion of the non-solvent into the cast film, and the weak non-solvent – solvent interaction which keeps the demixing process slow. Since this coagulation process is slow, the phase inversion will occur by nucleation and growth. The main disadvantages of type I membranes are a thick skin layer (> 1 μm) and a closed-cell structure that cause a very low permeate gas flux.[1]

b) Instantaneous phase inversion:

When the non-solvent in the liquid coagulation medium, has a strong thermodynamic interaction with the solvent in the casting solution, phase inversion is instantaneous. Because an instantaneous liquid-liquid demixing occurs, the rapid diffusion driven process forms a very thin skin layer. A rapid phase inversion will occur and the membrane structure formed by the spinodal decomposition and coarsening processes. Generally, membranes formed by this mechanism have a very thin microporous skin layer and a finger or sponge-like open interconnected substructure.[26]

2.3 The proposed method

As previously mentioned, the method used in membrane manufacture plays an important role in increasing the performance of an asymmetric membrane. The objective of this work was to prepare a membrane with a high separation factor and permeate gas flux from a single polymer without the need for a coating. It was proposed to achieve this by making a thin skinned type I membrane having a well-interconnected porous network structure. The following materials and steps were proposed to manufacture this membrane.

To prepare the casting solution, Polyetherimide (PEI, Ultem® 1000) was selected as a polymer due to its commercial availability and favourable characteristics. Anhydrous N-Methyl-2-Pyrrolidinone (NMP) was selected as a solvent because it is a powerful solvent for PEI compared to other solvents such as N,N-Dimethylacetamide or Dimethylformamide. When a more powerful solvent is used, a larger amount of the non-solvent is imbibed in the coagulated polymer.[20] Therefore an improvement in the porosity of the polymeric structure is to be expected.

A non-solvent medium having a thermodynamically moderate or poor interaction with the casting solvent was used in the coagulation bath. In such a case, there is a moderate delay time before the onset of demixing during which the diffusion driven process forms the dense skin layer. A shorter delay time, before demixing in type I membranes, has been linked to the formation of a thinner skin layer.[23] Isopropyl alcohol was used to satisfy the above requirements.

To overcome the problem of the closed-cell structure often seen in type I membranes, lithium nitrate was added to the casting solution as a complexing agent. Lithium nitrate has a thermodynamically poor interaction with the isopropanol coagulant. The coagulation process is expected to occur without dissociation or leaching out of the additive salt. After a complete coagulation, the additive salt will then be leached out by using a non-solvent having a good solubility for the salt. Methanol or water can be used to leach out the lithium nitrate. The final result of all these processes should be a skinned porous membrane having a well-interconnected open structure.

3 EXPERIMENTAL

3.1 Materials

Aromatic polyetherimide (Ultem® 1000) was supplied by the General Electric Co. in pellet form and used after drying in an oven at 150 °C for 8 hours. Lithium nitrate ($LiNO_3$) from Fisher Scientific Co., ON, Canada, was dried in the oven at 140 °C for 8 hours. Anhydrous 1-Methyl-2-Pyrrolidinone (99.5 %, reagent grade) was from Aldrich Chemical Co. Inc., (WI, U.S.A.). Methyl alcohol, (microscopic grade), hexanes (reagent grade), and isopropyl alcohol were supplied from BDH Inc., ON, Canada.

3.2 Membrane preparation

Two sets of experiments were used in order to verify the concepts of the new preparation method. In a first set of experiments issues surrounding the mechanisms involved in the preparation method were explored. In the second set of experiments, the effects of polymer and additive concentration were examined.

In the first set, casting solutions of composition shown in Table 2.1, were cast at room temperature (22°C) under a dry nitrogen atmosphere onto a clean glass plate using a knife gap of 250 μm. After 10 seconds, the film was immersed in a coagulation bath of isopropyl alcohol for one hour. The film was then transferred to a leaching bath of methyl alcohol or water for 12 hours. Finally, the film was solvent exchanged using hexane for 4 hours followed by drying for 24 hours at a temperature of 90 °C, and under 725 mm Hg vacuum pressure. Before the water-wet membranes were dried, they were solvent exchanged using an isopropanol bath for four hours followed by a hexane bath for four hours. All baths were used under laboratory conditions i.e. temperature 22 °C and atmospheric pressure.

Table 2.1 Membrane characteristics using various coagulation baths. Casting solutions were cast on a glass plate. After 10 seconds, the glass plate was dipped in a coagulation bath (held at 22 °C) for one hour. The membrane was then transferred to a leaching bath (held at 22 °C) for 12 hours. Unless otherwise stated, all membranes were tested at an operating pressure of 6.9 bar gauge, and the permeate discharged to atmosphere.

Case	Casting solution 23% PEI in NMP with % Li NO_3/PEI ratio (w/w)	Coagulation bath	Mutual affinity between solvent and non-solvent	Leaching bath	comments	Struct -ure	Memb -rane type
1	Without Li NO_3	Water[a] or Methanol[b]	Strong	-	High Flux No oxygen selectivity	Open	II
2	3.3% Li NO_3/ PEI (w/w)	Water[a] or Methanol[b]	Strong	-	High Flux No oxygen selectivity	Open	II
3	Without Li NO_3	Isopropanol[b]	Poor	Skip this step	No Flux[c]	Closed	I
4	Without Li NO_3	Isopropanol	Poor	Methanol[b]	No Flux[c]	Closed	I
5	Without Li NO_3	Isopropanol	Poor	Water[a]	No Flux[c]	Closed	I
6	3.3% Li NO_3/ PEI (w/w)	Isopropanol[b]	Poor	Skip this step	No Flux[c]	Open	I
7	3.3% Li NO_3/ PEI (w/w)	Isopropanol	Poor	Methanol[b]	Membrane selective for O_2, With a reasonable flux	Open	I
8	3.3% Li NO_3/ PEI (w/w)	Isopropanol	Poor	Water[a]	Membrane selective for O_2, With a reasonable flux	Open	I
9	Without Li NO_3	Isopropanol + 5 % NMP (v/v)	Poor	Methanol[b]	No Flux[c]	Closed	I
10	3.3% Li NO_3/ PEI (w/w)	Isopropanol + 5 % NMP (v/v)	Poor	Skip this step	Membrane selective for O_2, With a lower flux than in Case 7 and 8	Open	I
11	3.3% Li NO_3/ PEI (w/w)	Isopropanol + 5 % NMP (v/v)	Poor	Methanol[b]	Membrane selective for O_2, With best performance	Open	I

[a] Membranes were solvent exchanged with isopropanol for four hours then in hexane for four hours and dried at 90 ° C in a 725 mm Hg vacuum for 24 hours.

[b] Membranes were solvent exchanged using hexane for four hours, then dried at 90 ° C in a 725 mm Hg vacuum for 24 hours.

[c] There was no gas flux when feed pressure, was increased to 27.6 bar gauge, permeate discharge to atmosphere.

In the second set of experiments, the casting solution compositions listed in Table 2.2 were studied. The procedure described for case 11, Table 2.1 was used throughout the second set of experiments. After the membranes were solvent exchanged, they were tested for oxygen permeance and separation. They were then dried in a vacuum oven for 24 hours at a temperature of 90 °C, under a 725 mm Hg vacuum, and tested a second time for oxygen permeance and separation.

Table 2.2 The compositions of the casting solutions, which were used to produce membranes in the second part of this study.

PEI Concentration in NMP, % (w/w)	Li NO_3 / PEI, % (w/w)					
23	1.1	1.6	2.9	3.2	3.8	4.7
25	1.1	1.6	2.9	3.2	3.8	4.7
26.5	1.1	1.6	2.9	3.2	3.8	4.7

3.3 Membrane testing

The average oxygen permeance, (P_{O2}/ℓ) and oxygen separation factor, $\alpha_{O2/N2}$ were determined for two or more coupons from each cast membrane. All permeation experiments were carried out at a temperature of 22 °C. A cross-flow test cell having a permeate surface area of 20 cm^2 was used. Tests were performed using standard compressed air (Air Products Co., Canada) at a pressure of 12.8 bar gauge. The permeate was discharged to atmosphere. An air feed flow rate of 400 ml (STP)/min was used. The volumetric permeate gas flow rate was measured by a soap bubble flowmeter and the oxygen concentration in the permeate gas was determined using Gas Chromatography.

3.4 Oxygen permeance and separation factor $\alpha_{O2/N2}$ calculations[27]

The oxygen permeance in the nitrogen and oxygen mixture through the membrane, (P_{O2}/ℓ) can be defined in terms of the partial pressure difference of oxygen across a unit area of the membrane by using the following equation:

$$\left(P_{O2}/\ell\right) = \frac{Q_p y_{O2} T_s}{\Delta P A_m T_a} \qquad (1)$$

where Q_p is the volumetric flow rate of the permeate gas mixture at atmospheric pressure and temperature, T_a = 295 K, y_{O2} is the mole fraction of oxygen in the permeate gas, A_m is the surface area of the membrane, T_s = 273.16 K is the standard temperature, and ΔP is the difference in the oxygen partial pressure across the membrane which is given by the following equation:

$$\Delta P = P_f x_{O2} - P_P y_{O2} \tag{2}$$

where P_f and P_P are the absolute pressure in the upstream and downstream of the membrane respectively, x_{O2} is the fraction of oxygen in the feed gas (standard air).

A similar equation can be used to calculate the nitrogen permeance in the oxygen/nitrogen mixture:

$$\left(P_{N2}/\ell\right) = \frac{Q_P(1-y_{O2})T_s}{\left[P_f(1-x_{O2}) - P_P(1-y_{O2})\right]A_m T_a} \tag{3}$$

The permeance is typically expressed in units of GPU (Gas Permeation Unit), where:

$$1\ GPU = 1\times10^{-6}\frac{cm^3(STP)}{cm^2\ \sec\ cm\ Hg} \tag{4}$$

For standard air mixture permeating through the membrane, the actual separation factor of oxygen over nitrogen is given by the following equation:

$$\alpha(O_2/N_2) = \frac{[y_{O2}/(1-y_{O2})]}{[x_{O2}/(1-x_{O2})]} \tag{5}$$

4 RESULTS AND DISCUSSION

As previously mentioned, a first set of experiments was performed to explore the formation of the asymmetric membrane from the PEI, lithium nitrate and NMP casting solution system. Table 2.1 contains a list of various casting solution formulations, coagulation and leaching baths used to identify and discuss the concepts of the sequenced steps in the proposed preparation method.

Cases 1 and 2 in Table 2.1 illustrate the situation when the coagulation bath, water or methanol has a strong mutual affinity with the solvent, NMP. The coagulation process begins with an instantaneous liquid-liquid demixing (the membrane becomes opaque

soon after immersion and lifts off rapidly from the glass plate). A solid phase is formed by spinodal decomposition and coarsening to produce an open cell structure (membrane type II).[1] Microscopic examinations of cross-sections of the membranes produced in cases 1 and 2 show the presence of a fingerlike sublayer structure. Type II membrane is usually classified as a Microfiltration or Ultrafiltration membrane according to its end application.[16] Membranes of type II are usually not suitable for use directly as gas separation membranes unless a repair coating over the membrane is applied to seal the non-selective pores.[28] However, type II membranes can be used for gas separations if a selective (defect-free) dense skin layer is formed. As it is observed elsewhere,[26] the higher the polymer concentration in the casting solution, the denser the resulting membrane. A dense skin can be formed by an increase in the polymer concentration in the outermost top layer of the cast film. In the dual-bath method, the skin formation is achieved by a diffusion driven process and in the dry/wet phase inversion method by evaporation. The later method was further developed,[24] by using forced convection instead of normal evaporation to produce a defect-free ultrathin-skinned asymmetric membrane suitable for gas separation.

Cases 3 to 11 in Table 2.1 illustrate situations where the coagulation medium has low mutual affinity with the solvent NMP. In these cases Isopropanol was used as a coagulant. Upon immersing the cast film in the coagulation bath, it is observed that the membrane lifts off the glass plate after 2 to 3 minutes. This slower release from the glass plate indicates a delayed phase inversion. In this case, a diffusion driven process occurs before demixing to induce the formation of the skin layer. As the coagulation process continues, the solid phase is formed by the nucleation and growth to produce a closed cell structure (membrane type I).[1] Microscopic examinations of cross-sections of the membranes produced in cases 3 to 11 reveal the typical sponge like structure often found in type I membranes. As can be observed in case 3 to 6, a coagulation time of one hour in isopropanol was sufficient to form a tight structure through which there was no gas flux even when the feed air pressure was increased to 27.6 bar gauge.

To obtain a reasonable gas flux through type I membranes, a complexing agent which has a thermodynamically poor interaction with the non-solvent in the coagulation bath was added to the casting solution. The poor mutual affinity between isopropanol

and lithium nitrate can be observed in case 6. Because the leaching process was skipped in case 6, the membrane still had a closed cell structure. This indicated that leaching of the lithium nitrate did not occur in the coagulation bath.

When a leaching bath of methanol or water was used as in cases 7 and 8, membranes suitable for air separation were produced. Lithium nitrate is very soluble in either water or methanol. Both membranes had a reasonable permeate flux and oxygen separation factor. This suggests that using two separate steps, coagulation followed by leaching, yields a membrane having a well-interconnected porous structure.

As seen in case 9, the addition of NMP to the coagulation bath did not open the structure of the membranes produced from the casting solution which did not contain lithium nitrate. When 3.3% (wt. %) lithium nitrate was added to the casting solution and five percent of NMP (vol. %) were added to the isopropanol bath, the partial leaching of the lithium nitrate in the coagulation bath was observed as in case 10, Table 2.1. Comparing cases 6 and 10, the low permeate gas flux through the membrane in case 10 indicates that during coagulation in a bath containing 5% NMP in isopropanol, some lithium nitrate was leached out leaving a partially open structure. Therefore, the penetration of the non-solvent into the coagulating membrane film improved the final removal of lithium nitrate from the membrane in the leaching bath.

The presence of NMP in the coagulation bath reduces the difference in chemical potential across the nascent skin layer. This causes a slower outflow of solvent from the cast film into the coagulation medium. The diffusion driven transport is reduced as the content of the solvent increases in the coagulation bath. Then, the delay time before the onset of demixing will increase with a slower outflow of solvent giving a sufficient amount of time for the solvent to diffuse from the bulk of the casting solution to the depletion region under the skin layer. Therefore, the intermediate layer under the skin will have a moderate gradient in density offering a good uniform support for the thin skin layer.

The strong mutual affinity between the NMP in the non-solvent medium and the polymer will also affect the density of the resulting membrane. The presence of solvent in the imbibed quench medium has two effects, an increase in the amount of the coagulant required to achieve the polymer precipitation and an increase in the swelling

effect which forces the coagulant to imbibe inside the polymer film. Therefore, a total increase in the imbibed liquid into the nascent membrane will inherently lead to a decrease in density of the resulting skin layer and overall membrane.

Finally, as a result of this preliminary study, membranes produced using the technique described in case 11, Table 2.1, show substantial promise as air separation membranes. The technique offers the possibility of forming Type I, defect-free membranes that have good gas permeate flux. These membranes also have a strong mechanical structure because the formation of macrovoids was suppressed by the following: a delayed phase inversion, the addition of solvent to the coagulation bath[29] and the addition of lithium nitrate to the casting solution. Huang et al. [20] have observed that the amount of non-solvent required to precipitate the polymer is reduced when lithium nitrate is present in the casting solution.

Using the sequence of steps shown in case 11, Table 2.1, a second set of experiments was carried out based on the casting solutions described in Table 2.2. The effect of polymer concentration, additive salt concentration and the drying process on the performance of the membranes were studied before and after drying at 90 °C under 725 mm Hg vacuum pressure for 24 hours.

4.1 Effect of initial polymer concentration in the casting solution

In the second set of experiments, three polymer concentrations were used to determine the effect of polymer concentration in the casting solution on the performance of the membranes. The relationship between oxygen permeance and oxygen separation factor were plotted in Figure 2.2 for membranes produced from casting solutions shown in Table 2.2 As shown in Figure 2.2a) and b), the highest productivity, defined as the highest simultaneous oxygen permeance and oxygen separation factor, was obtained for membranes produced from casting solutions containing 23% by weight PEI.

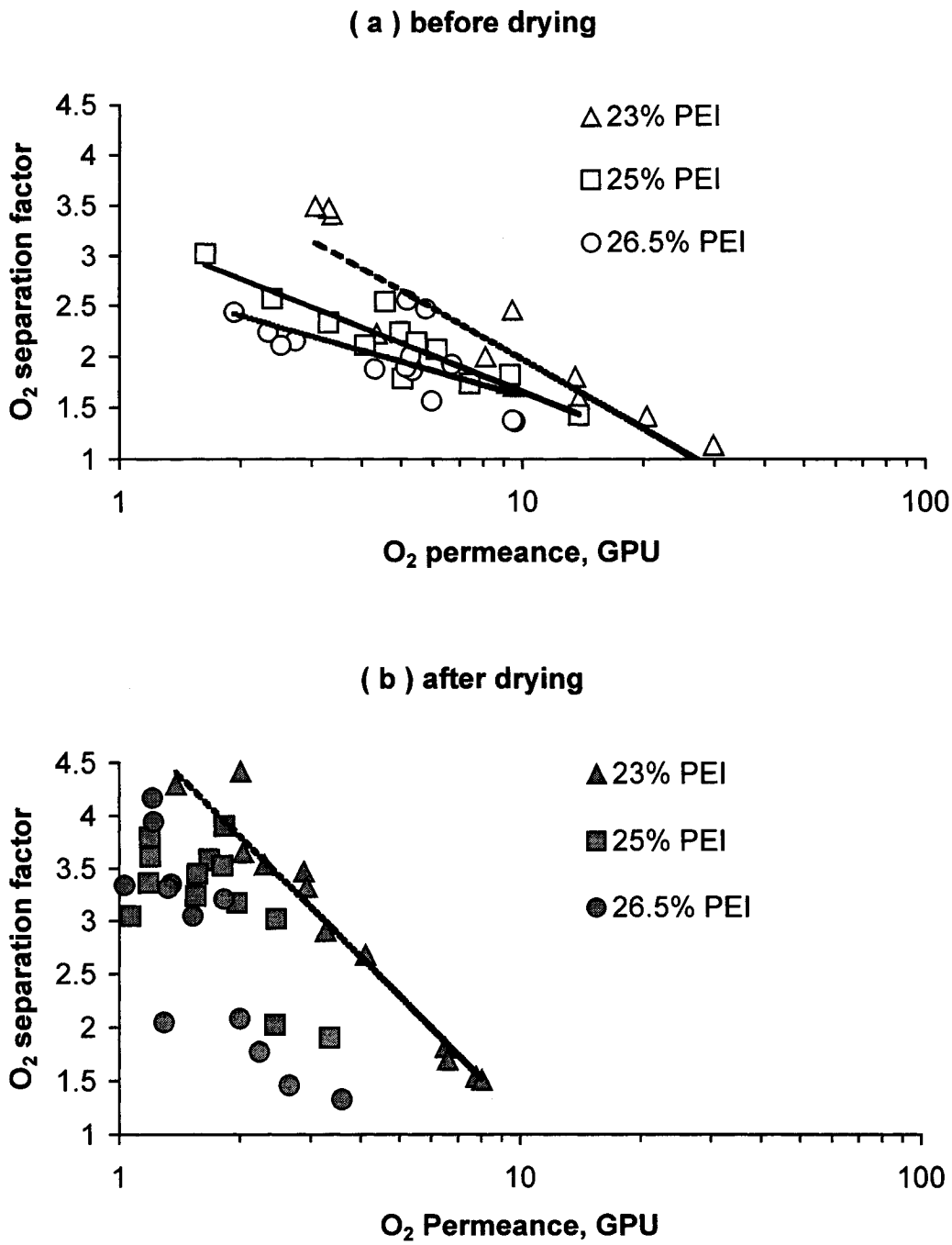

Figure 2.2 Plot of the oxygen separation factor vs. the oxygen permeance for the separation of air using membranes produced from casting solutions shown in Table 2.2, a) before drying and b) after drying at 90 ° C in a 725 mm Hg vacuum for 24 hours. Open symbols before drying, closed symbols after drying.

Changes in membrane morphology with decreasing polymer concentration in the casting solution can be explained by the following considerations:

1- In general, more dilute polymer solutions require greater amounts of non-solvent to precipitate the polymer.[20] Then a larger amount of imbibed non-solvent in the cast membrane leads to a more porous membrane structure.
2- In addition, the total thickness of the membrane decreases because the film shrinkage rate is higher due to increasing solvent outflow at lower polymer concentrations in the casting solution.[26]
3- It is also reported elsewhere[16] that the thickness of the dense top layer in type I membranes decreases with decreasing polymer concentration.

Therefore, a thinner skin layer of lower density, a thinner membrane film, and a high-porosity sublayer structure all decrease the membrane resistance to gas flow leading to high oxygen permeance while the less substantial substructure resistance maintains a high oxygen separation factor.[30]

4.2 Effect of lithium nitrate concentration in the casting solution

For all dried membranes produced from casting solutions described in Table 2.2, the oxygen permeance and the actual separation factor versus the ratio of $LiNO_3$ to PEI (% w/w) are shown in Figures 2.3 and 2.4 respectively. All trends in Figure 2.3 indicate that very little if any permeation occurs in the absence of lithium nitrate. This is in agreement with the preliminary work illustrated by cases 4, 5, and 9 listed in Table 2.1. From Figure 2.3, the oxygen permeance increases as the ratio of lithium nitrate in the casting solution increases. The rate of this increase is more pronounced at the lower polymer concentration of 23% PEI than at the 25% and 26.5% PEI concentrations.

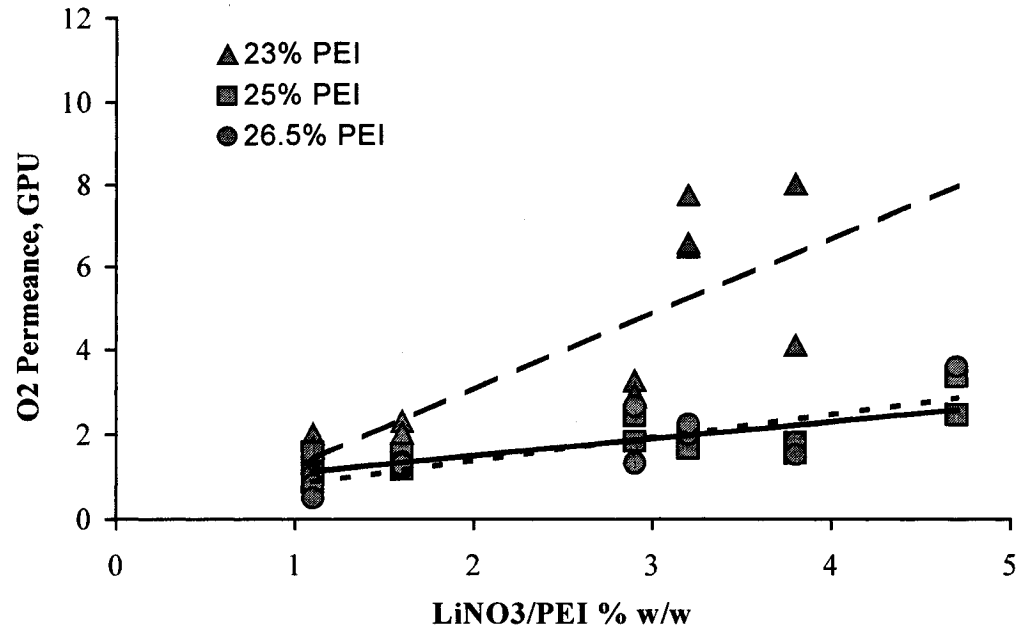

Figure 2.3 Plot of the oxygen permeance vs. the ($LiNO_3$/PEI) ratio in the casting solution for air separation for dried membranes produced from casting solutions shown in Table 2.2.

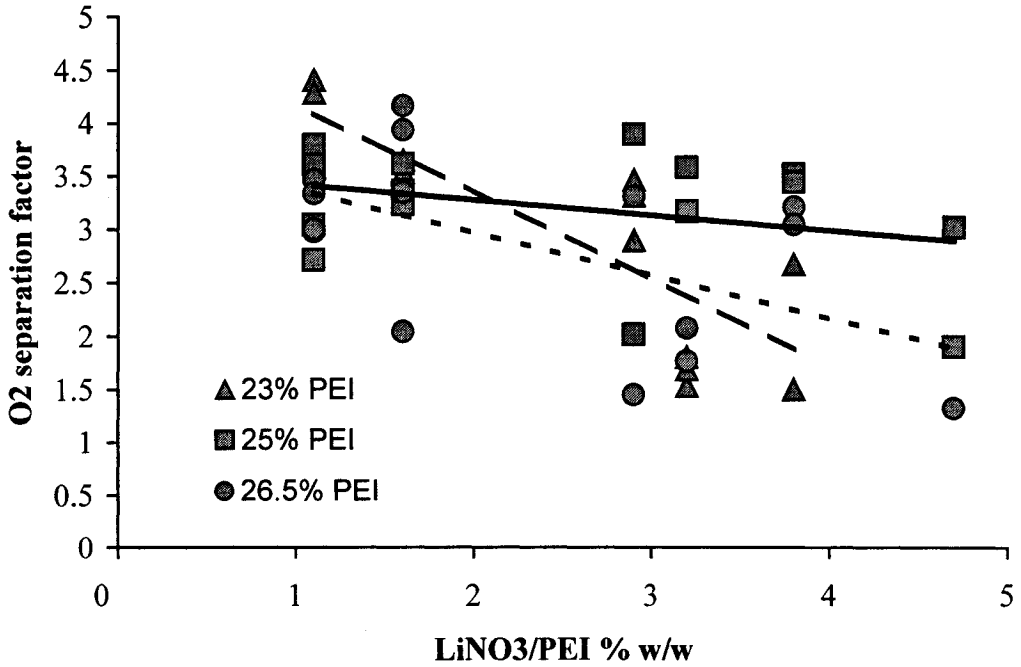

Figure 2.4 Plot of the oxygen separation factor vs. the ($LiNO_3$/PEI) ratio in the casting solution for air separation by using dried membranes produced from casting solutions shown in Table 2.2.

The following must be considered to explain the greater effect of the addition of lithium nitrate on the 23% PEI concentration:

- Decreasing PEI concentrations lead to an increase in membrane porosity and a thinner skin layer. Therefore, the leaching process is improved due to the easier penetration of the non-solvent into the nascent membrane and an easier outflow of lithium nitrate. Most of the total additive lithium nitrate will be leached leaving a well-interconnected porous structure. The magnitude of this effect will be accentuated at lower polymer concentrations as seen in Figure 2.3, the slope of the 23% PEI concentration is greater than that of the 25% and 26.5% PEI concentrations.
- For the same reason, the sublayer will be more open and have a higher porosity so that the substantial resistance of the substructure to gas transport will be very low or negligible. However in Figure 2.3, the slope of the oxygen permeance versus lithium nitrate ratio seems to be nearly identical at the higher concentrations of 25% and 26.5% PEI. This would indicate that there is a limit to the enhancement of leaching and that there is a possibility that some lithium nitrate remains entrapped in the 26.5% PEI membranes.

As shown in Figure 2.4, the oxygen separation factor decreases as the amount of lithium nitrate increases in the casting solution. This decline is more pronounced at the lower polymer concentration. Therefore, at the 23 % PEI concentration, only a small amount of lithium nitrate is required to produce a well interconnected porous network structure. Increasing $LiNO_3$ / PEI ratio to more than 2 % leads to a more open structure which causes a large increase in gas permeance accompanied by a large decrease in the oxygen separation factor. This decrease in the gas selectivity, due to increase in pore size, can be explained by an increase in viscous and Knudsen gas transport (non-selective mechanisms for separating O_2/N_2) with respect to the surface-diffusion which is a selective mechanism for separating oxygen from nitrogen.[2]

Above a $LiNO_3$ / PEI ratio of 2 %, the highest oxygen separation factor was obtained for a membrane produced from the 25% PEI casting solution. This indicates that $LiNO_3$ was still being leached out at the 25 % PEI level. Increasing the lithium

nitrate concentration above 2 % makes the support layer more open, while maintaining a reasonable skin density until the $LiNO_3$ / PEI ratio exceeds 4.7%.

As the polymer concentration increases to 26.5 %, a more dense and thicker skinned membrane is obtained. Leaching is more difficult leading to a decrease in the amount of lithium nitrate removed from the total amount of salt in the initial casting solution. A smaller number of pores and a less interconnected porous network structure will cause a significant resistance to gas transport especially through the sublayer.

4.3 Effect of drying

As mentioned previously membrane coupons were first tested after the solvent exchange step and then tested after drying. These results were initially plotted in Figure 2.2. As seen in Figure 2.2 a) and b), the drying process caused an increase in the oxygen separation factor and a decrease in the oxygen permeance. A decrease in the residual NMP content in the membrane polymer and a change in the physical and microstructure properties of the membrane material can explain the change in membrane performance.

The increase in the trace amount of residual NMP in the membrane polymer leads to an increase in swelling, a depression in the glass transition temperature (T_g) and a reduction in the polymer chain packing especially in the skin layer. Therefore, NMP acts as a plasticizer that makes polymer segments flexible and decreases the intermolecular and intramolecular interactions between the polymer chains. These changes decrease the resistance of the polymeric film to gas transport so that a higher gas permeance can be obtained.

The permeation rate of both oxygen and nitrogen increases with increase in the opening of the membrane network structure achieved by a greater amount of lithium nitrate in the casting solution. Because the oxygen separation factor is proportional to both the mobility and solubility selectivities, the change in the separation factor can be explained by the change in these two selectivities.

In the presence of residual NMP, opening membrane structure by increasing the amount of lithium nitrate in the casting solution leads to the following:

1. An increase in the diffusion coefficient due to a structure of lower density and higher network connectivity causes a decrease in the mobility selectivity.

2. An increase in the specific surface area which contains the residual NMP enhances the solubility selectivity of oxygen. Oxygen has a higher critical temperature than nitrogen. This makes oxygen more condensable and hence more soluble than nitrogen in most media.[4] In such a case, NMP acts as a liquid transport medium.
3. An increase in the free fractional volume of the polymeric membrane causes an increase in the glass transition temperature (t_g).[31] However, the presence of residual NMP causes a decrease in t_g. Both effects lead to a small overall change in t_g. Therefore, the rigidity of the membrane materials does not change significantly and hence the solubility selectivity remains high.

For these reasons, the decrease in the mobility selectivity will be partially compensated by an increase in the solubility selectivity so that a gradual decrease in the oxygen separation factor with increasing oxygen permeate flux would be obtained as it is shown in Figure 2.2a).

On the other hand, in the absence of residual NMP, increasing the opening of the membrane network structure leads to the following:

1. A decrease in the mobility selectivity due to an increase in the diffusion coefficient resulting from a structure of lower density and higher network connectivity.
2. An increase in the glass transition temperature which is attributed to an increase in the rigidity of the membrane materials. Then, the solubility selectivity tends to be lower and the mobility selectivity becomes dominant.

Therefore, a steep decrease in the separation factor with an increase in the oxygen permeate flux would be obtained as it is shown in Figure 2.2b).

The rigidity of the final membrane material plays an important role in determining the slope of the correlation between the separation factor and the oxygen permeance. As it is shown in Figure 2.2a) and 2b), the absolute value of the slope of the line increases with drying or with decreasing the polymer concentration in the casting solution. The increase in this slope can be attributed to an increase in the rigidity of the membrane

material. In conclusion, the rigidity of the polymer increases when NMP is removed or when the free fractional volume of the polymer increases.

The effect of the drying process on the relationship between the gas permeate flux and the oxygen concentration in the permeate which corresponds to the oxygen separation factor is shown in Figure 2.5 for membranes produced from casting solutions containing 23 % PEI. At a lower permeate flux (less than 7 GPU) where the membrane structure is less open, the mobility selectivity will dominate and be greatly affected by the increase in the packing density after the drying process due to the high initial packing density before drying. For instance, the highest oxygen concentration of 54.8 % was obtained for a flux 2.4 GPU. At higher permeate flux (more than 7 GPU), where the membrane has a more open structure, the solubility selectivity will be enhanced by the presence of residual NMP leading to a moderate decrease in the total oxygen selectivity. For instance, at a permeate flux of 21 GPU through the membrane without drying, an oxygen concentration 34 % was obtained in the permeate. However, the removal of the solvent and the non-solvent is necessary to obtain a stable membrane.

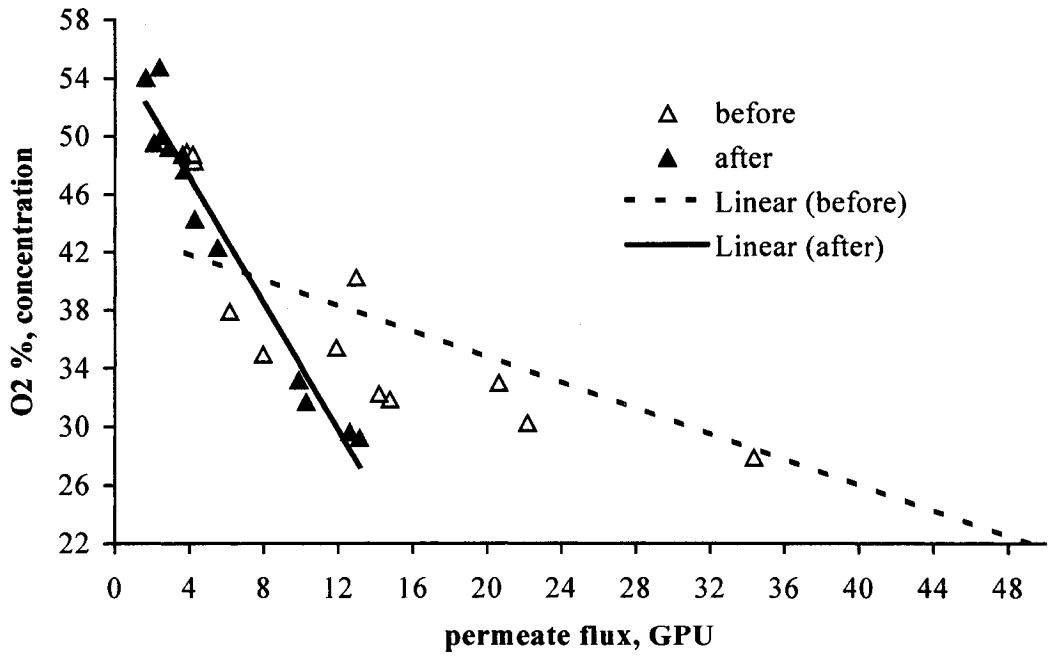

Figure 2.5 Plot of the permeance vs. the concentration of oxygen in the permeate for air separation by using dried membranes produced from casting solutions shown in Table 2.2.

A drying factor was defined as the absolute ratio of the increase in the oxygen separation factor divided by the decrease in the oxygen permeance for a given coupon. The drying factor vs. the ratio of $LiNO_3$ / PEI in the casting solution are plotted in Figure 2.6. Higher drying factors indicate greater improvement in membrane performance on drying. As can be observed in Figure 2.6, for all concentrations, the best improvement on drying was obtained at lower $LiNO_3$/PEI ratios. Reasonable fits were obtained for the 23 % (r^2=0.82) and 25 % (r^2=0.82) concentrations. The omission of one outlier at the 26.5 % PEI concentration produced a similar fit. There appears to be a maximum improvement at a median concentration of 25 % PEI. Explanations for this maximum are in good agreement with the results presented in Figure 2.4. As previously mentioned, $LiNO_3$ was still being leached out of the nascent membrane at the 25 % PEI level. Above this level, $LiNO_3$ was more difficult to leach out leading to a denser skin, a smaller number of pores and a less interconnected porous network structure.

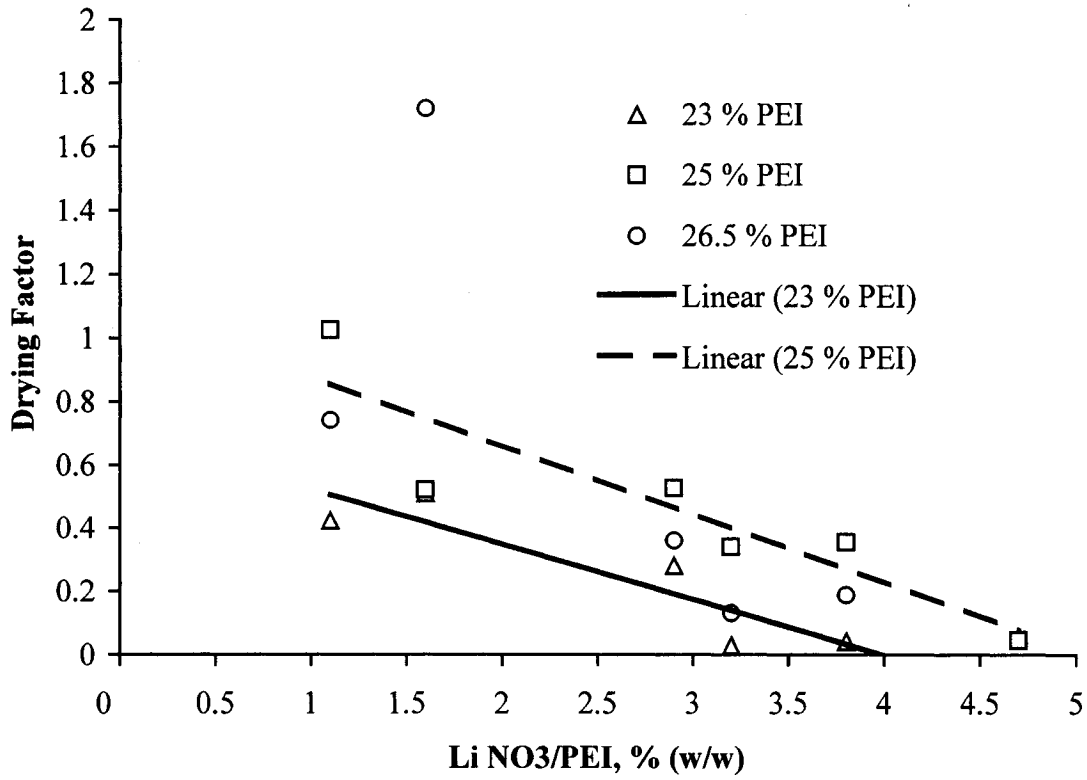

Figure 2.6 The $LiNO_3$/PEI ratio in the casting solution vs. the drying factor. The drying factor is the absolute increase in the oxygen separation factor divided by the decrease in the oxygen permeance as a result of drying membranes produced from casting solutions shown in Table 2.2.

5 CONCLUSIONS

1. A defect-free, asymmetric membrane having a skin with an intermediate layer and a well-interconnected porous structure can be produced for the separation of permanent gas mixtures, The proposed approach does not require an additional repair coating. Oxygen concentrations of more than 50 % in the permeate were obtained for air separation.
2. When isopropanol is used as a coagulating agent for a casting solution containing PEI/$LiNO_3$ /NMP, the coagulation process occurs without the leaching of lithium nitrate from the cast film.
3. The addition of NMP to the coagulation bath enhances the leaching of lithium nitrate in the second bath yielding a more open membrane.
4. Membranes produced from casting solutions containing 23 % PEI in NMP have higher performance (productivity) than the membranes produced from casting solutions in which the PEI concentration is greater than 23 %.
5. The lithium nitrate concentration in the casting solution can be adjusted to produce membranes that have the desired oxygen permeance or oxygen separation factor. It was also found that the addition of lithium nitrate to the casting solution had a greater effect at lower polymer concentrations.
6. The highest selectivity was obtained for a membrane produced from casting solutions containing 23% PEI when the $LiNO_3$ /PEI ratio was less than 2 % (w/w), or from casting solutions containing 25% PEI when the $LiNO_3$ /PEI ratio was above 2 % (w/w).
7. The presence of residual solvent (NMP) in the PEI membrane improves the solubility selectivity, which maintains the oxygen separation factor high at a higher gas permeance of more than 7 GPU. This is useful to obtain higher productivity. Unfortunately, the performance of the membrane is not stable and the solvent is usually removed slowly during the running time.

8. The rigidity of the membrane increases on drying at 90 °C under vacuum. This increase causes a different effect on the performance of the membrane at different porosities. For instance, testing membranes produced from casting solution containing 23 % PEI, the performance of the membrane was better before drying when the permeate flux was more than 7 GPU, while the performance of the membrane was better after drying when the permeate flux was less than 7 GPU.
9. Increasing $LiNO_3$ /PEI ratio in the casting solution causes a decrease in the drying factor.

NOMENCLATURE

A_m	the active permeation surface area of the membrane (cm^2)
ℓ	the effective thickness of the membrane (cm)
P_f	the absolute pressure at the upstream of the membrane (cm Hg)
P_p	the absolute pressure at the upstream of the membrane (cm Hg)
P_{N2}	the nitrogen permeability (cm^3 (STP) cm / cm^2 sec cm Hg)
P_{O2}	the oxygen permeability (cm^3 (STP) cm / cm^2 sec cm Hg)
(P_{N2}/ℓ)	the nitrogen permeance (cm^3 (STP) / cm^2 sec cm Hg)
(P_{O2}/ℓ)	the oxygen permeance (cm^3 (STP) / cm^2 sec cm Hg)
Q_p	the volumetric flow rate of the permeate gas mixture (cm^3 / sec)
T_a	the ambient temperature (° K)
T_s	the standard temperature (273.15 ° K)
x_{O2}	the mole fraction of the oxygen in the feed gas mixture (mole / mole)
y_{O2}	the mole fraction of the oxygen in the feed gas mixture (mole / mole)
$\alpha_{(O2/N2)}$	the actual separation factor for oxygen over nitrogen, dimensionless
ΔP	the oxygen partial pressure difference across the membrane (cm Hg)

REFERENCES

1. I. Pinnau, Recent Advances in the Formation of Ultrathin Polymeric Membranes for Gas Separation; Polymers for Advanced Technologies, Vol. 5, Nov 1994, pp. 733-744.
2. K. Kamada, J. Kamo, A. Motonaga, T. Iwasaki, and H. Hosokawa, Gas Permeation Properties of Conducting Polymer/Porous Media Composite Membranes I., Polymer Journal, Vol. 26, No. 2, 1994, pp 141-149.
3. IUPAC Manual of symbols and Terminology, Appendix 2, Part 1. Colloid and surface Chemistry. Pure Appl. Chem., 31, 1972, p 578.
4. W. J.Koros, M. R. Coleman, and D. R. B. Walker, Controlled Permeability Polymer Membranes, Annu. Rev. Mater. Sci., Vol 22, 1992, pp 47-89.
5. R. E. Findes, J. P. Bartolomucci, Polyetherimides offer strength and stiffness, Advanced Materials & Processes. Vol. 149, n 1, Jan 1996, p 47.
6. J. Bijwe, U. S. Tewari, P. Vasudevan, Friction and wear studies of bulk polyetherimide, Journal of Materials Science. Vol. 25, n 1B, Jan 1990, pp 548-556.
7. Sheng-Huei Hsiao, Chin-Ping Yang, Kuan-Yu Chu, Synthesis and properties of poly(ether imide)s having ortho-linked aromatic units in the main chain; Macromolecules. Vol. 30, n 2, Jan 27 1997, pp 165-170.
8. M. Alger, Polymer Science Dictionary, Chapman & Hall, London, 1997
9. T. A. Barbari, W. J. Koros and D. R. Paul, Polymeric Membranes Based on Bisphenol-A for Gas Separations, Journal of Membrane Science, 42, 1989, pp 69-86.
10. D. Wang, K. Li, and W. K. Teo, Gas Permselection Properties in Silicon-coated Asymmetric Polyehtersulfone Membranes, Journal of Applied Polymer Science, Vol. 66, 1997, pp 837-846.
11. D. Wang, K. Li, and W. K. Teo, Preparation and Characterization of Polyetherimide Asymmetric Hollow Fiber Membranes for Gas Separation, , Journal of Membrane Science, 138, 1998, pp 193-201.
12. G. B. Tanny, The surface tension of the polymer solutions and asymmetric membrane formation, J. Appl. Polym. Sci. 18, pp. 2149-2163.
13. R. E. Kesting, Concerning the microstructure of dry-RO membranes, J. Appl. Polym. Sci., 17 (6), (1973) 1771-1785.

14. L. Boens, F. W. Altena, C. A. Smolders, Asymmetric Membrane Structure As A Result Of Phase Separation Phenomena, Desalination, 32 (1980) 33-45.
15. W. J. Koros, and G. K. Fleming, Membrane –Based Gas Separation, Journal of membrane Science, 83 (1993) 1-80.
16. M. Mulder, Basic Principle of Membrane Technology, Kluwer Academic Publishers, Dordrecht, 1996.
17. C. S. Tsay, A. J. McHugh, Combined effects of evaporation and quench steps on asymmetric membrane formation by phase inversion, Journal of Polymer Science Part B-Polymer Physics. Vol. 29, n 10, Sep 1991, pp 1261-1270.
18. C. S. Tsay, A. J. McHugh, Mass transfer dynamics of the evaporation step in membrane formation by phase inversion, Journal of Membrane Science, Vol. 64, n 1-2, Nov 15 1991, pp 81-92.
19. S. Birgul Tantekin, William B. Krantz, Alan R. Greenberg, Dynamics of evaporation in polymer/solvent films - importance in asymmetric polymeric membrane formation, Polymer Preprints, Division of Polymer Chemistry, American Chemical Society. Publ by ACS, Books & Journals Division, Washington, DC, USA, Vol. 30, n 1, pp 36-37. Conference Information Papers Presented at the Dallas, Texas Meeting. Dallas, TX, USA. 19890409-19890414. Conference Code: 12346.
20. R. Y. M. Huang, X. Feng, Studies on solvent evaporation and polymer precipitation pertinent to the formation of asymmetric polyetherimide membranes, Journal of Applied Polymer Science, Vol. 57, n 5, Aug 1 1995, pp 613-621.
21. I. Pinnau, Jan. Wind, Klaus-Viktor Peinemann, Ultrathin multicomponent poly(ether sulfone) membranes for gas separation made by dry/wet phase inversion, Industrial & Engineering Chemistry Research, Vol. 29, n 10, Oct 1990, pp 2028-2032.
22. R. E. Kesting, A. K. Fritzsche, M. K. Murphy, A. C. Handermann, C. A. Cruse, and R. F.Malon, Process for Forming Asymmetric Gas Separation Membranes Having Graded Density Skins, US Patent, 4,871,494 (1989).
23. J. A. van't Hof, A. J. Reuvers, R. M. Boom, H. H. M. Rolevink and C. A. Smolders, Preparation of asymmetric gas separation membranes with high selectivity by a dual-bath coagulation method, Journal of Membrane Science. Vol. 70, n 1, May 20 1992, pp 17-30.

24. I. Pinnau, and W. J. Koros, Defect-free Ultrahigh Flux Asymmetric Membranes, US Patent, 4,902,422 (1990).
25. A. J. Reuvers, J. W. A. van den Berg, C. A. Smolders, Formation of Membranes by means of Immersion Precipitation, Journal of Membrane Science. Vol. 34, n 1, Nov 1 1987, pp 45-86.
26. C. S. Tsay, A. J. McHugh, Mass transfer modelling of asymmetric membrane formation by phase inversion, Journal of Polymer Science Part B-Polymer Physics. Vol. 28, n 8, Jul 1990, pp 1327-1365.
27. K. Ghosal, and B. D. Freeman, Gas Separation Using Polymer Membranes: An Overview, Polymers for Advanced Technologies, Vol. 5, n11, Nov. 1994, PP.673-697.
28. J. M. S. Henis, and M. K. Tripodi, Composite Hollow Fiber Membranes for Gas Separation: The Resistance Model Approach, Journal of Membrane Science, 8 (1981) 233
29. C. A. Smolders, A. J. Reuvers, R. M. Boom, L. M. Wienk, Microstructures in phase-inversion membranes. Part 1. Formation of macrovoids, Journal of Membrane Science. Vol. 73, n 2-3, Oct 9 1992, pp 259-275.
30. I. Pinnau, And W. J. Koros, Relationship between Substructure Resistance and Gas Separation Properties of Defect-Free Integrally Skinned Asymmetric Membranes, Ind. Eng. Chem. Res. Vol. 30, n 8, August 1991, pp1837-1840.
31. K. Fritzsche, C. A. Cruse, M. K. Murphy and R. E. Kesting, Polyethersulfone and Polyphenylsulfone Hollow Fiber Trilayer Membranes Spun fromLewis acid:base Complexes – Structure Determination by SEM, DSC, and Oxygen Plasma Ablation, Journal of Membrane Science, Vol. 54, n 1-2, Nov.15, 1990, pp 29-50.

CHAPTER III

The Influence of Casting Solution Structure on the Microporosity of Polyetherimide Gas Separation Membranes Prepared by the Coagulation Post-Leaching Method

J. Kurdi, and A. Y. Tremblay*

Department of Chemical Engineering, University of Ottawa, 161 Louis Pasteur, Ottawa, Ontario, K1N 6N5, Canada

*Corresponding author

André Y. Tremblay

Tel.: +1-613-562-5920; fax: +1-613-562-5172

E-mail address: tremblay@uottawa.ca

Article has been Published in: **Journal of Membrane Science, Volume 184, Number 2, 175-186 (2001).**

CHAPTER III

Paper 2: The Influence of Casting Solution Structure on the Microporosity of Polyetherimide Gas Separation Membranes Prepared by the Coagulation Post-Leaching Method

J. Kurdi, and A. Y. Tremblay
Department of Chemical Engineering, University of Ottawa, 161 Louis Pasteur, Ottawa, Canada, K1N 6N5
Received 19 January 2000; received in revised form 22 September 2000; accepted 12 October 2000

ABSTRACT

The microporosity and performance of polyetherimide (PEI) membranes produced by the coagulation post-leaching technique were investigated. Computational chemistry and chemical structure principles indicate that a lithium cation solvated in NMP (N-methyl-2-pyrrolidinone) forms a complex with two NMP molecules. This complex was determined to be stable in NMP and isopropanol but not in methanol or water. Increasing the additive ($LiNO_3$) concentration in the casting solution lead to a greater number of micropores in the 0.7 to 1.2 nm range, while the peak in the micropore distribution remained unchanged at 1.0 nm. Molecular mechanics calculations indicate that the PEI polymer chain can form coils having an inner section of 0.7 x 1.0 nm. Micropore measurements and computational chemistry results suggest that the inherent size of the PEI polymer coils remains unchanged on the addition of $LiNO_3$ but the number of polymer coils increases. A linear relation was found to exist between the permeance of the membranes to air and micropore volume. Larger micropores were present at higher $LiNO_3$ concentrations and caused a decline in the actual separation factor for these membranes. Journal of Membrane Science 184 (2001) 175-186.

Key words: Gas separations; Membrane preparation and structure; Polyetherimide; Microporosity; Asymmetric membrane; Coagulation post-leaching technique.

1 INTRODUCTION

As indicated by several workers, gas separation membranes that incorporate polymeric molecular sieves exhibit both high permeance and gas separation factor [1-3]. Stiffer polymers generally have higher mobility selectivity since their behavior is closer to that of molecular sieves [4]. Polymeric molecular sieves require the use of rigid materials and tailoring techniques to produce a very narrow and definite free volume distribution in the polymer matrix or specifically in the selective skin layer of asymmetric gas separation membranes.

The rigidity and the properties of a polymeric material are related to its chemical structure. A comparison of different families of polymeric materials and the effect of the polymer flexibility on membrane gas separations were illustrated by Koros et al. [5]. Robeson et al. [6] used a group contribution method to predict the gas permeability and permselectivity of aromatic polymers from their chemical structures.

When a rigid polymeric material is used, membrane morphology must be controlled to produce a membrane suitable for the separation of a specific gas mixture. The major aspects of the formation of asymmetric polymeric membranes by phase inversion for gas separations have been investigated [7-9]. Many efforts were exerted to produce membranes having a thinner defect-free skin layer containing voids or pores small enough to confine gas transport and achieve selective gas separation. The sub-layer should have open pores that are large enough to have negligible resistance to gas transport. Several phase inversion methods have been developed to form the selective skin layer of a membrane and to obtain an open sub-layer with negligible gas transport resistance. The formation of the skin layer can be achieved by: (1) volatile organic solvents such as halogenated hydrocarbons and an evaporation step prior to wet phase inversion [10]. (2) a delayed phase inversion step [11, 12] and (3) two solvents that have different affinities for the coagulant, a volatile solvent with low affinity for the coagulant and a non-volatile solvent with a strong affinity for the coagulant (evaporation induced delayed demixing) [9, 13].

In all cases, non-solvents or additive salts are added to the casting solution to obtain open structures with less resistance to gas transport. Polyetherimide flat-sheet

asymmetric membranes were prepared by phase inversion using a halogenated hydrocarbon as a volatile solvent, and various organic non-solvents as additives and coagulants [14]. Integral asymmetric polyetherimide hollow fiber membranes for gas separations were prepared form the NMP / ethanol system [15]. Kim et al. [16] studied the presence of $ZnCl_2$ in a polysulfone/NMP casting solution on membrane structure and the performance of ultrafiltration polysulfone membranes. The effect of low molecular weight additives on the structure of aromatic polyamide membranes was studied by Kraus et al. [17]. The role of additives, of both high- and low-molecular weight on the structure of the membranes was discussed by Wienk et al. [18]. Kim and Lee [19] studied the effect of polyethylene glycol (PEG) as a pore-forming agent in the casting solution on the formation of the structure and the permeation properties of ultrafiltration polysulfone membranes.

However, the effect of the additives on the pore size of the membranes was not studied in the work mentioned above. Early attempts at controlling the size and the effective number of pores on the surface of a polysulfone ultrafiltration membrane were performed by Tweddle et al. [20]. This was achieved by using inorganic acids in an aqueous gelation bath or by exposing the cast film to a mixture of air and HCl gas prior to the gelation process. The additive acid reacts with the basic solvent, which later dissociates in the aqueous gelation bath and leads to an increase in the average pore size and number of pores. Further development was achieved by Kesting [21-22] and led to the invention of a polysulfone gas separation membrane. Organic acids were used to form Lewis acid-base complexes in polymer/solvent casting solutions. These complexes are stable in the casting solution but can easily break-up into smaller parts in the gelation bath. Different complexes were used in the polysulfone/NMP casting solution and a linear relationship between complex molar volume and gas permeability was found [23-24]. Solvent complexes act as transient templates (spacers) to control the free volume in the membranes. However, both the dynamics of phase inversion, which leads to the formation of an asymmetric membrane structure, and the addition of the solvent complex to the polymeric casting solution play a role in changing the pore size distribution of the membranes.

Controlling morphology at the micropore level is essential to produce high performance gas separation membranes or molecular sieves from rigid polymeric materials. The objective of this work is to study changes in the microporosity of PEI membranes produced by the coagulation post-leaching preparation method [12]. The coagulation post-leaching preparation method uses a delayed wet phase inversion step where there is poor mutual affinity between solvent and non-solvent in the coagulation bath. Delayed wet phase inversion usually forms membranes having a closed structure. However, this unsuitable structure is avoided by incorporating an appropriate additive component into the casting solution and then post-leaching the additive component to open the membrane's structure.

Computational Chemistry and nitrogen adsorption were used to investigate the influence of lithium nitrate on the morphology of PEI membranes produced by the coagulation post-leaching method. Computational Chemistry was used to study the molecular structure of the additive component or its complex in the casting solution and in various solvents. Nitrogen adsorption was used to determine the pore size and pore size distribution of the final membranes.

2 COMPUTATIONAL CHEMISTRY

Computational chemistry is a useful tool to study the stereo-structure of molecules in vacuo or in a solution and the mutual interaction of a molecule with other molecules. Therefore, computational chemistry can be used to explain the mutual interactions of molecules in polymeric solutions used for membrane preparation or in the different media used during membrane formation. For a large system, molecular mechanics is a simple and efficient tool to estimate the structure of organic molecules and their coordination [25]. It can also be used to study the structure and steric interactions that occur in organometallics [26]. Molecular mechanics provide a convenient and rapid method to screen the possible connecting structures and predict metal complex stability that is based on the optimized structure that has the lowest deformation, steric strain or coordination energy [27]. The difference in the minimized total potential energy (differences in strain energies) between products and reactants can be considered to be a

qualitative estimation for the final stable structures of a chemical system [25]. Atomic charges in molecules can be determined by semi-empirical or *ab initio* quantum mechanics methods. The values of these charges are required to calculate the electrostatic energies (including hydrogen bonding) used in the molecular mechanics calculations [28].

3 COMPUTATIONAL DETAILS

All molecules studied in this work were built from their atoms according to their chemical formula obtained from the CRC Handbook of Chemistry and Physics [29]. The model builder in the HyperChem Pro 5.1 program (Hypercube Inc., Gainesville, FL, USA) was used to convert these formulas into three-dimensional structures. A preliminary Molecular Mechanics geometry optimization using a MM+ force field and atomic charges was carried out to obtain a starting structure for optimization. Then an *ab initio* geometry optimization with a large (6-31G**) basis set was performed on each molecule in order to obtain the ground state structures and to calculate the partial charge for each atom using a Mulliken population analysis. The structures of the molecules were then used in further studies.

Using the *ab initio* optimized structure of an NMP molecule, a solvent periodic box of size 2 x 2 x 2 nm was generated using Bender's FillCage macro program [30]. The number of molecules in the cage was calculated from the density of NMP at 25 °C. Solvent cages of size 2 x 2 x 2 nm were also generated for methanol and water. A geometry optimization for each solvent in the cage was achieved by using Molecular Mechanics using the MM+ force field and atomic charges. The densities and number of molecules in each cage are shown in Table 3.1 [31].

Table 3.1 Densities and the number of molecules in a 2 x 2 x 2 nm solvent cage [31].

Molecules	Molecular weight	Liquid densities at 25°C	Liquid molecular volume[a] [nm^3]	No. of molecules[b] in a 2 x 2 x 2 nm solvent cage
NMP	99.133	1.025	160.58×10^{-3}	50
Isopropanol	60.096	0.783	127.43×10^{-3}	63
Methanol	32.042	0.787	67.60×10^{-3}	118
Water	18.015	1.027	29.12×10^{-3}	275

[a] calculated from liquid densities at 25 °C

[b] calculated from liquid molecular volume.

Lithium nitrate was placed at the center of the NMP solvent cage to study the chemical interactions between lithium nitrate and the NMP solvent molecules. All coordination possibilities between lithium and NMP were considered: lithium without coordination and lithium coordinated to one, two, three, four, five or six NMP molecules. For each coordination number, the system of $LiNO_3$ in the NMP cage was optimized using Molecular Mechanics MM+ and partial atomic charges.

4 MEMBRANE CHARACTERIZATION

The membranes studied in this work were prepared by the coagulation post-leaching method [12, chapter II]. Polyetherimide membranes were produced using various amounts of lithium nitrate as an additive in a casting solution containing 23 % (wt) of PEI in NMP. The polymer solutions were cast on glass plates. The plates were immersed in isopropanol for 1 hour, then in methanol for 12 hours. They were solvent exchanged using hexane; air dried at room temperature then dried in a 725 mm Hg vacuum at 90 °C for 48 hours.

Coupons measuring 0.07 m in diameter were cut from the sheets and tested at room temperature with air at 13.79 absolute bar (200 psia). The permeate gas was discharged to the atmosphere and the actual separation factor determined using gas

chromatography. The permeance of the membranes was evaluated using a gas bubble flowmeter. Details on the evaluation of the actual separation factor and permeance were given by Kurdi and Tremblay [12, chapter II].

After being tested, the membrane coupons were cut into small strips and characterized in an automated porosity analyzer ASAP 2000M produced by Micromeritics (GA, U.S.A.). The micropore size and micropore size distribution of these membranes were obtained from nitrogen adsorption at a temperature of 77 K. A slit pore geometry was assumed and the Horvath-Kawazoe method used to interpret the data. The size of the micropores (voids measuring less than 2 nm in diameter) was determined from the relationship between the average potential energy of the adsorbate inside a pore and the free energy change upon adsorption [32].

5 RESULTS AND DISCUSSION

5.1 Structure of lithium nitrate in NMP

The lithium cation is a hard Lewis acid and coordinates with hard Lewis bases according to the principle of hard and soft acids and bases (HSAB). NMP, isopropanol, methanol and water are hard Lewis bases due to the presence of an oxygen donor atom in their structures [33]. Early literature results indicated that the most probable coordination number for lithium as a monovalent cation was two and to a less extent three [34]. Later, Izutsu et al. [35] reported that a lithium cation coordinates to four oxygen atoms in acetonitrile, DMF or DMSO. In water, Rudolph et al. [36] report that Li^+ coordinates to four molecules of water. As previously mentioned in this work, lithium nitrate was placed at the center of an NMP solvent cage to study the interactions between lithium nitrate and the NMP solvent molecules. NMP is a Lewis base interacting with the lithium cation, a Lewis acid. All coordination possibilities between lithium and NMP were considered: without complexation, lithium coordinated to one, two, three, four, five or six NMP molecules. For each coordination number, all molecules in the cage were optimized using molecular mechanics and the MM+ force field.

The total potential energy of the system was calculated and the results shown in Table 3.2. The lowest potential energy, -68.47 kcal, was obtained when a lithium cation

was coordinated to two NMP molecules. Coordination numbers, higher than two, yield positive potential energies due to a significant increase in the steric strain energy. These results are reasonable due to the fact that the change in the enthalpy of complexation can be attributed to two opposing factors; a negative component reflecting the enthalpy of formation of the lithium cation–oxygen donor bonds, and a positive component reflecting a loss of enthalpy as a result of unfavorable steric interactions [27]. Therefore, the most stable chemical structure for a lithium cation in NMP is a complex consisting of a lithium cation coordinated to two molecules of NMP solvent (Li^+-2NMP).

Table 3.2 The total potential energy of the solvent system and the dimension and volume of various Lithium - NMP complexes.

Number of NMP molecules coordinated to Li^+	Total potential energy of the system[a]	Liquid molar volume[b] of lithium complex	Effective diameter[c] of the complex when acts as a spacer [nm]
0	-47.76	6.6	0.29
1	-40.24	166.95	0.66
2	-68.47	327.35	1.0
3	+160.87	487.75	1.21
4	+963.25	648.15	1.41
5	+14.06	808.55	1.31
6	+33.48	968.95	1.33

[a] the energy in Kcal for the total solvent cage calculated using HyperChem Pro 5.1.

[b] volume in 10^{-3} nm^3 based on the liquid volume of lithium and NMP molecules [31].

[c] calculated using HyperChem Pro 5.1. measured by computational chemistry program.

5.2 The stability of the Li^+-2NMP complex in isopropanol, methanol and water

To explain membrane formation by the coagulation post-leaching method, the stability of the Li^+-2NMP complex was determined in pure isopropanol, methanol, and water using computational chemistry. A solvent cage (2 x 2 x 2 nm) containing isopropanol was generated and optimized using HyproChem Pro 5.1. The cage

accommodated a number of molecules corresponding to the density of the solvent at 25 ^{o}C as seen in Table 3.1. A number of isopropanol molecules having a liquid volume approximately equivalent to the sum of the liquid volume of Li^{+}, NO_3^{-} and two NMP molecules were deleted from the center of this isopropanol cage. Then, Li^{+}, NO_3^{-}, and two NMP molecules were placed in the center of the solvent cage. Interactions of lithium as a Lewis acid with each of the following Lewis-bases NO_3^{-}, NMP and isopropanol were studied by molecular mechanics optimization using the MM+ force field and previously determined atomic charges. The total potential energy of the system for each possible coordination case was calculated as shown in Table 3.3. Similar procedures were used for methanol and water. The results are shown in Tables 3.4 and 3.5 respectively.

Table 3.3 Stability of various complexes in isopropanol.

System Li^{+}, 2 NMP and NO_3^{-} in isopropanol cage	Total potential energy of entire system, Kcal
Without complexation	-3944.7
Li^{+} coordinates to one molecule of isopropanol	-3923.1
Li^{+} coordinates to two molecules of isopropanol	-3935.0
Li^{+} coordinates to two molecules of NMP	-3950.6

Table 3.4 Stability of various complexes in methanol.

System Li^{+}, 2 NMP and NO_3^{-} in methanol cage	Total potential energy of entire system, Kcal
Without complexation	-1983.3
Li^{+} coordinates to one molecule of methanol	-2073.3
Li^{+} coordinates to two molecules of methanol	-2320.2
Li^{+} coordinates to three molecules of methanol	-1694.9
Li^{+} coordinates to two molecules of NMP	-942.6

Table 3.5 Stability of various complexes in water.

System Li^+, 2 NMP and NO_3^- in water cage	Total potential energy of entire system, Kcal
Without complexation	-2958.7
Li^+ coordinates to one molecule of water	-2949.8
Li^+ coordinates to two molecules of water	-2994.2
Li^+ coordinates to three molecules of water	-2804.3
Li^+ coordinates to four molecules of water	-2077.3
Li^+ coordinates to two molecules of NMP	-2939.2

The stability of the Li^+-2NMP complex in isopropanol, methanol and water depends on the mutual and competitive interaction between any pair of these solvent molecules and may generally be attributed to the physico-chemical properties of the molecules. Computational chemistry results indicate that the lithium cation forms a complex with two NMP molecules had lowest potential energy in both NMP and isopropanol as shown in Tables 3.2 and 3.3. The lithium cation did not form a complex with isopropanol. Such a structure with isopropanol would lead to an increase in the potential energy of the system. The potential energies for a methanol solvent cage containing a lithium complex with different coordination bonds are listed in Table 3.4. These potential energies indicate that the Li^+-2NMP complex is not stable (higher system energy) in methanol. Lithium coordinated with two molecules of methanol is favored as indicated by a decrease in the potential energy of the system for this case, see Table 3.4. The potential energies were also calculated for water, see Table 3.5. The results indicate that the Li^+-2NMP complex is not stable in water, as the coordination of a lithium cation with two water molecules is favored.

The dielectric constants of the solvents used in this work are listed in Table 3.6. The higher the dielectric constant of the solvent, the weaker the electrostatic attraction between oppositely charged ions in solution which favors dissociation. Zhao and Freeman [37] have shown that ion association and the effect of the mutual ionic field are negligible in water and methanol while they are significant in isopropanol. This was attributed to the lower dielectric constant of isopropanol versus that of water and

methanol. This further suggests that the Li^+-2NMP complex is stable in isopropanol but not in methanol or water.

Table 3.6 Selected physico-chemical properties of the components studied in this work [31].

Molecule	V_{MV} m^3/Kmol	V_{ML} m^3/Kmol	ε
NMP	60.390×10^{-3}	96.699×10^{-3}	33.0
Isopropanol	42.160×10^{-3}	76.784×10^{-3}	18.3
Methanol	21.710×10^{-3}	40.702×10^{-3}	32.6
Water	12.370×10^{-3}	18.069×10^{-3}	78.5

5.3 Modeling the PEI polymer chain using computational chemistry and membrane microporosity in the absence of $LiNO_3$

A PEI repeat unit was built using the HyproChem program according to the structure found in the Polymer Science Dictionary [38]. This structure was optimized by switching alternatively between the molecular mechanics MM+ and CNDO semi-empirical quantum-mechanical calculation methods. Twelve repeat units were connected with each other to form a polymer chain. The chain was then optimized using the MM+ and CNDO methods. It was found, as shown in Figure 3.1, that the polymer chain forms a coil having an average inner rectangular cross-section measuring 0.7 nm x 1.0 nm.

These results were confirmed by experimental micropore measurements shown in Figure 3.2. The membrane produced from a 23 % (wt) PEI/NMP casting solution without $LiNO_3$ has a micropore size distribution with an onset at 0.7 nm, a maximum at 1.0 nm and a gradual decline after 1.2 nm. Micropores larger than 1.6 nm were not present in this membrane material. The onset of the pore distribution coincides exactly with the smallest dimension of the polymer coil. The maximum corresponds with the larger side of the rectangle and the point at which the curve declines corresponds to the diagonal of a rectangle measuring (0.7x1.0 nm) or 1.22 nm.

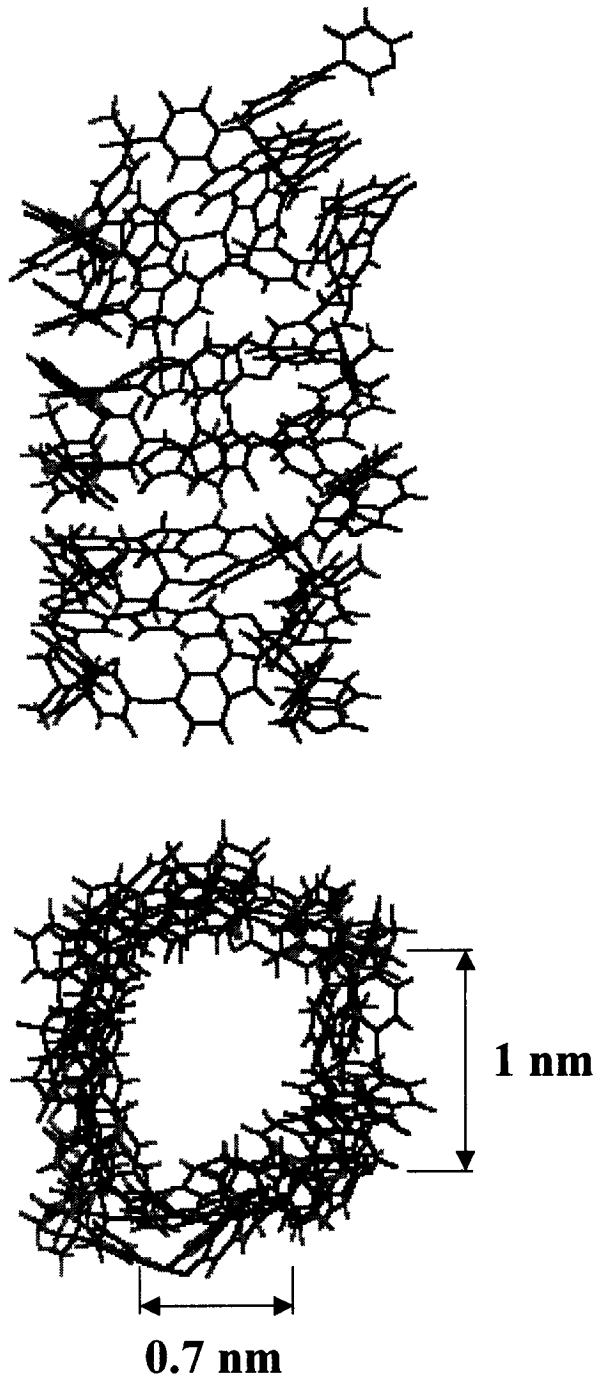

Figure 3.1 Twelve repeat units of PEI optimized by the MM+ molecular mechanics. The atomic charges were set by the CNDO semiempirical method. The bottom part of the figure is an axial view for the polymer coil seen in the top part.

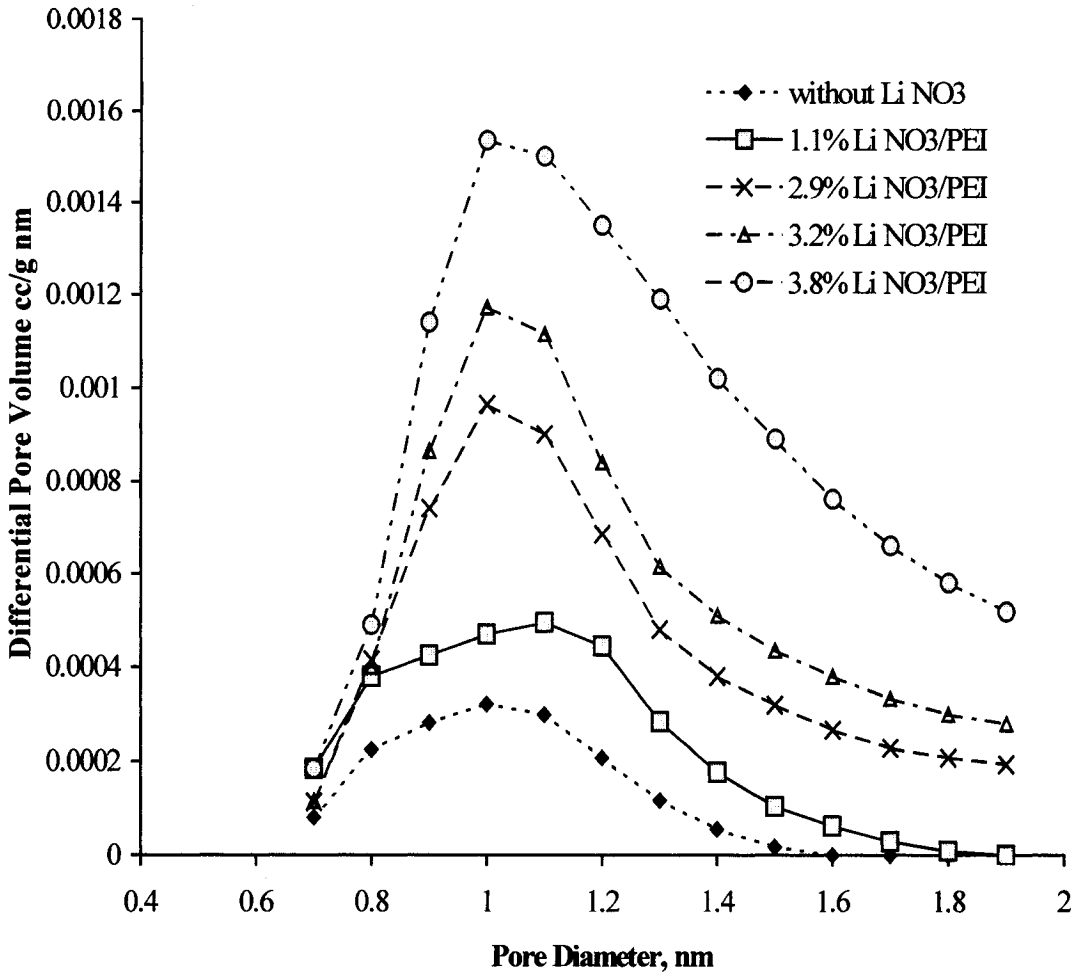

Figure 3.2 Micropore size distribution for PEI membranes produced by the coagulation post-leaching technique. Differential Pore Volume (cm^3/g nm) vs. micropore size in nm.

5.4 Modeling the PEI polymer chain using computational chemistry and membrane microporosity in the presence of $LiNO_3$

The differential pore size distributions of membranes produced from casting solutions having a different amount of lithium nitrate are also shown in Figure 3.2. As seen in Figure 3.2, increasing the amount of lithium nitrate in the casting solutions leads to an increase in the micropore volume of the membranes for all micropore sizes. The peak in the differential pore volume distribution is approximately 1 nm for all membranes. The shape of this distribution can be attributed to an intrinsic property of PEI that was

confirmed above using computational chemistry and the micropore size distribution for the polymer without the $LiNO_3$ additive.

From Figure 3.2, it is clear that all micropores have a diameter larger than 0.7 nm. This size is more than twice the size of lithium, 0.29 nm. Therefore, if lithium plays a role in the formation of micropores, it must be coupled with the solvent NMP to form these pores. Let us consider all the possible cases, lithium without complexation, lithium complexed with one, two, three, four and five NMP. The diameter of complexes that could act as spacers in pore formation were determined using HyperChem 5.1 and are reported in Table 3.2. When the lithium cation forms a complex with one NMP molecule, its dimension was calculated to be 0.66 nm which is also smaller than pores measured in the tested membranes. Therefore, the lithium cation should form a complex with two or more molecules of NMP.

The size of the pore formed by the polymer surrounding the lithium complex was also determined by computational chemistry. A chain of polyetherimide was built using twelve repeat units. Six (Li^+-2NMP) and six NO_3^- optimized by *ab initio* were placed inside the polymer coil. The total system was optimized using molecular mechanics. After each optimization, the atomic charges were reset on the polymer chain by the CNDO semiempirical method. The presence of Li^+-2NMP in the coil expanded the inner size of the coil to 0.7x1.2 nm as seen in Figure 3.3a). Lithium complexed with two NMP molecules has a dimension of 1nm. This is small enough to be accommodated inside the intrinsic pores of PEI and large enough to remain entrapped in the polymer phase during the gelation step of the coagulation post-leaching process.

The size of the pore within the polymer coil was determined after removing the six lithium complexes from the coil. The six Li^+-2NMP and six NO_3^- were deleted from the system shown in Figure 3.3a). Then a new optimization using molecular mechanics MM+ and CNDO was carried out. Figure 3.3b) shows the final optimized structure. The pore size of the coil changed from 0.7 x 1.2 nm to 0.7 x 1.0 nm. The bending and rotation of the PEI chain depends on the swivel groups (O, C $(CH_3)_2$) and the interval distance between them [1]. The presence of such a small number of swivel groups in PEI restricts the bending and rotation of the polymer chain. The result being that the polymer coil does not change significantly when the lithium complex is removed.

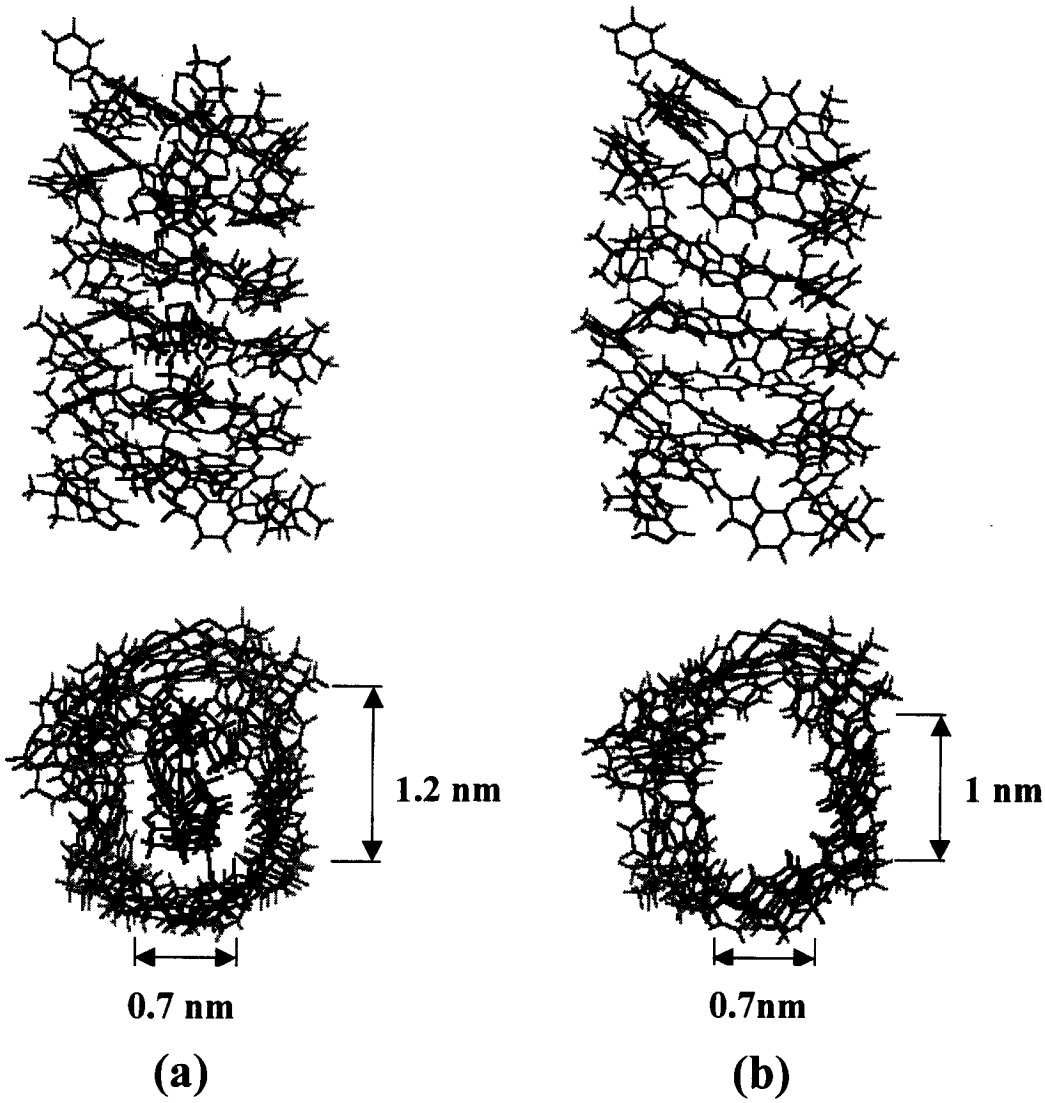

Figure 3.3 A chain of twelve repeat units of PEI optimized by MM^+ molecular mechanics. The atomic charges were set by the CNDO semiempirical method: (a) With 6(Li^+-2NMP, NO_3^-) optimized by MM^+, atomic charges were set by ab initio method (6-31 G**). (b) Molecule in Figure 3(a) optimized after removing the 6(Li^+-2NMP, NO_3^-). The bottom part of the figure is an axial view for the polymer coil seen in the top part of the figure.

5.5 The effect of micropore size distribution on membrane performance

The total micropore volume per unit weight of membrane was calculated by integrating the differential micropore volume curves, shown in Figure 3.2, through the range of 0.6 to 2.0 nm. The actual separation factor (α) and the air permeance have been plotted versus the total micropore volume and are shown in Figure 3.4 a) and b) respectively. As seen in Figure 3.2, at $LiNO_3$ concentrations of 2.9% and above, larger 2.0 nm pores appear in the distribution. The presence of these pores causes a decrease in the actual separation factor shown in Figure 3.4 a). Note that as the membranes produced without $LiNO_3$ had no permeate flow, it was impossible to determine the composition of the permeate and evaluate α for these membranes. The consequence of this is that the first point in Figure 3.4 a) corresponds to a $LiNO_3$ concentration of 1.1%.

As seen in Figure 3.4b), a linear correlation was established between gas permeance and micropore volume. The square of the regression factor for the linear correlation shown in 4b) is $r^2= 0.9381$. Micropore volumes were determined for membranes produced without the $LiNO_3$ additive although these membranes had no measurable permeate flow. The non-zero intercept of the permeance plot indicates that the polymer coils are an inherent feature of the PEI polymer and that a reasonable degree of connectivity between polymer coils is required for gas flow through the membrane. The addition of $LiNO_3$ to the casting solution promotes chain coiling and increases the number of micropores and the connectivity of these pores. However, as previously discussed, an excessive amount of additive causes the formation of larger micropores which decreases the actual separation factor. Controlling the formation of these larger micropores remains the key to improving the performance of these membranes.

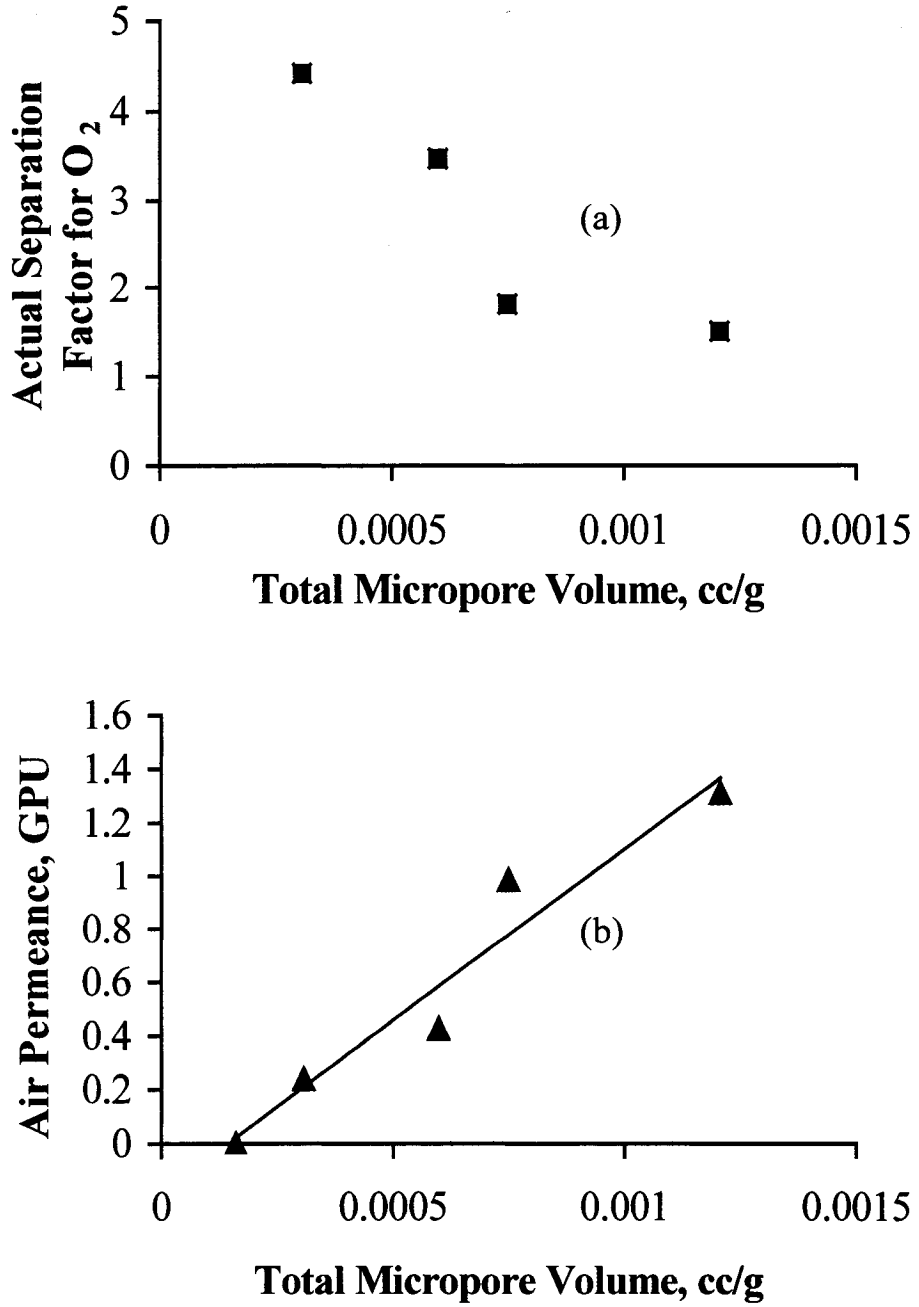

Figure 3.4 Membrane performance versus total micropore volume. (a) Actual separation factor for oxygen versus micropore volume. (b) Air permeance versus micropore volume (Regression factor squared for the linear regression in Figure 4 b) is r^2=0.9381).

5.6 Formation of micropores in the coagulation post-leaching technique

The formation of the micropores, measuring 0.7x1.0 nm, in membranes produced using the coagulation post-leaching method can be explained by the following steps as shown in Figure 3.5, as explained below:

- In the casting solution, Li^+ forms a complex with two NMP molecules.
- The complex promotes chain coiling within the solution.
- During the PEI coagulation step, the lithium complex is stable in isopropanol and remains entrapped inside the polymer gel.
- The mobility of the polymer chain is greatly reduced by further coagulation and it is impossible for the entrapped lithium complex to diffuse out of the polymeric gel.
- During the leaching process, the lithium complex is not stable in methanol and dissociates to its original building blocks. These blocks are smaller than the size of the intrinsic pores and can easily diffuse outside the polymeric gel.
- This leaves micropores measuring 0.7x1.0 nm in the membrane.

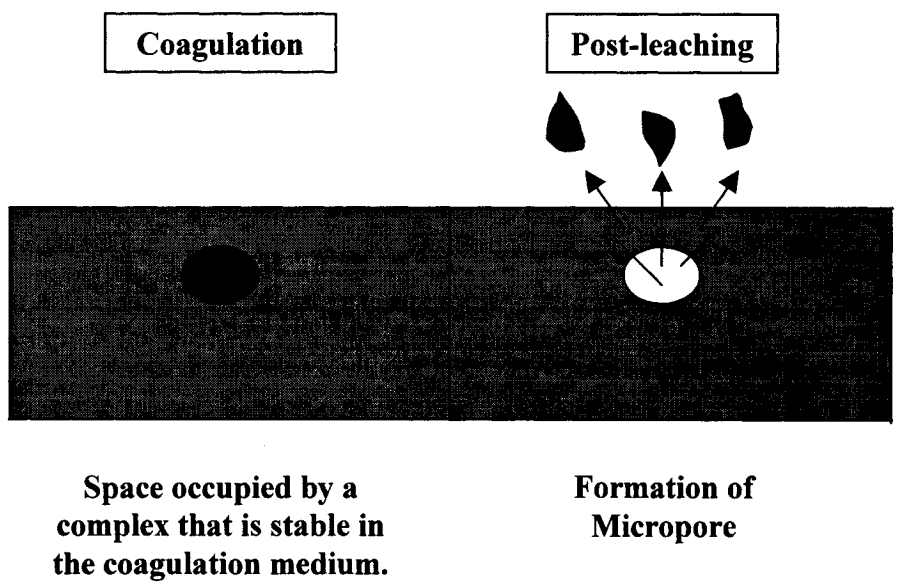

Figure 3.5 Formation of micropores in the coagulation post-leaching technique.

These results indicate that the steps involved in the coagulation post leaching process were successful in preserving the structure of the polymer present in the casting solution. This has considerable advantages in tailoring membranes for gas separations.

6 CONCLUSIONS

The preparation of PEI membranes for gas separation by the coagulation post-leaching method was studied using micropore measurements, chemical principles, and computational chemistry. PEI membranes show micropore size distributions with an onset at 0.7 nm and a maximum at 1.0 nm for all membranes. This pore size distribution is attributed to the inherent property of the PEI polymer chain to form coils having an inside pore measuring 0.7x1.0 nm.

Computational chemistry supported by chemical principles was used to study and explain the coagulation post-leaching preparation method. In this method, the lithium cation forms a complex with two NMP molecules. During membrane formation, the complex, which is stable in the NMP solution and isopropanol, is entrapped in voids present in the polymeric gel structure. It is not leached out of the membrane at the polymer coagulation stage. The complex is not stable in methanol and leaches out leaving an open microporous structure. At $LiNO_3$ concentrations of 2.9% and above, larger 2.0 nm pores appear in the micropore distribution. The presence of these larger micropores reduces the actual separation factor of oxygen from air. A linear correlation was established between membrane permeance and the total micropore volume of the membrane.

The results of this work indicate that the inherent properties of the polymer, the casting solution structure, and the preparation method play an important role in determining the final microporous nature of the membrane. Computational chemistry offers considerable promise in explaining membrane microstructure and in the design and development of new membrane preparation methods that involve tailoring casting solutions to affect membrane microporosity.

LIST OF SYMBOLS

X_A Mole fraction of oxygen

X_B Mole fraction of nitrogen

V_{MV} Molar Van der Waals Volume, [m^3/kmol]

V_{ML} Liquid Molar Volume, [m^3/kmol]

Greek Symbols

α Actual separation factor of oxygen over nitrogen

$= [X_A/X_B]_{Permeate} / [X_A/X_B]_{Retentate}$

ε Dielectric constant

Abbreviations

CNDO Complete Neglect of Differential Overlap, self-consistent field method for semi-empirical quantum-mechanical calculations.

GPU Gas permeation unit; 1 GPU= $1x10^{-6}$ cm^3(STP)/cm^2/s/cmHg.

MM+ Force field used in molecular mechanics calculations.

NMP N-Methyl-2-pyrrolidone

PEI Polyetherimide

REFERENCES

[1] H. Ohya, V. V. Kudryavtsev and S. I. Semenova, Polyimide Membranes – Applications, Fabrications, and Properties, Kodansha LTD. and Gordon & Breach Science Publishers S. A., Tokyo, 1996.

[2] A. Singh and W. J. Koros, Significance of Entropic Selectivity for Advanced Gas Separation Membranes, Ind. Eng. Chem. Res. 35 (1996) 1231-1234.

[3] A. Singh and W. J. Koros, Pyrolytic carbon Membranes for Air Separations, Membrane Journal 7 (1997) 15-21.

[4] Y.-T. Chern and B.-S. Wu, preparation of Composite Membranes with Polyimides and Poly(amide-imide)s Skin via Interfacial Condensation for Air Separation, J. Appl. Polym. Sci. 63 (1997) 693-701.

[5] W. J.Koros, M. R. Coleman and D. R. B. Walker, Controlled Permeability Polymer Membranes, Annu. Rev. Mater. Sci., 22 (1992) 47-89.

[6] L. M. Robeson, C. D. Smith and M. Langsam, A Group Contribution Approach to Predict Permeability and Permselectivity of Aromatic Polymers, J. Membr. Sci. 132 (1997) 33-54.

[7] W. J. Koros and G. K. Fleming, Membrane –Based Gas Separation, J. membr. Sci. 83 (1993) 1-80.

[8] R. E. Kesting and A. K. Fritzsche, Polymeric gas Separation Membranes, John Wiley and Sons, Inc., New York, 1993.

[9] M. Mulder, Basic Principle of Membrane Technology, Kluwer Academic Publishers, Dordrecht, 1996.

[10] I. Pinnau and W. J. Koros, Defect-free Ultrahigh Flux Asymmetric Membranes, US Patent 4,902,422, 1990.

[11] J. A. van't Hof, A. J. Reuvers, R. M. Boom, H. H. M. Rolevink and C. A. Smolders, Preparation of asymmetric gas separation membranes with high selectivity by a dual-bath coagulation method, J. Membr. Sci. 70 (1992) 17-30.

[12] J. Kurdi and A. Y. Tremblay, Preparation of Defect-Free Asymmetric Membranes for Gas Separations, J. Appl. Polym. Sci. 73 (1999) 1471-1482, (chapter II in this thesis).

[13] J.-J. Shieh and T.-S. Chung, Phase –Inversion Poly(ether imide) Membranes Prepared from Water-Miscible/ Immiscible Mixture Solvents, Ind. Eng. Chem. Res. 38 (1999) 2650-2658.

[14] K.-V. Peinemann, Method for producing an integral, asymmetric membrane and the resultant membrane, US patent 4,673,418, 1987.

[15] D. Wang, K. Li and W. K. Teo, Preparation and Characterization of Polyetherimide Asymmetric Hollow Fiber Membranes for Gas Separation, J. Membr. Sci. 138 (1998) 193-201.

[16] S. R. Kim, K. H. Lee and M. S. Jhon, The Effect of Zn Cl_2 on the Formation of Polysulfone Membrane, J. Membr. Sci. 119 (1996) 59-64.

[17] M. A. Kraus, M. Nemas and M. A. Frommer, the Effect of Low Molecular Weight Additives on the Properties of Aromatic Polyamide Membranes, J. Appl. Polym. Sci. 23 (1979) 445-452.

[18] I. M. Wienk, R. M. Boom, M. A. M. Beerlage, A. M. W. Bulte, C. A. Smolders and H. Strathmann, Recent Advances in the Formationof Phase Inversion Membranes Made from Amorphous or Semi-Crystalline Polymers, J. Membr. Sci. 113 (1996) 361-371.

[19] J.-H. Kim and K.-H. Lee, Effect of PEG on Membrane Formation by Phase Inversion, J.Membr. Sci. 138 (1998) 153-163.

[20] T. A. Tweddle, O. Kutowy, W. I. Thayer and S. Sourirajan, Polysulfone Ultrafiltration Membranes, Ind. Eng. Chem. Prod. Res. Dev. 22 (1983) 320-326.

[21] R. E. Kesting, The Solvent Size Effect: Solvents and Solvent Complexes Viewed as Transient Templates which Control Free Volume in the Skins of Integrally-Skinned Phase Inversion Membranes, J. Polym. Sci., Part C 27 (1989) 187-190.

[22] R. E. Kesting, A. K. Fritzsche, M. K. Murphy, A. C. Handermann, C. A. Cruse, and R. F.Malon, Process for Forming Asymmetric Gas Separation Membranes Having Graded Density Skins, US Patent 4,871,494, 1989.

[23] R. E. Kesting, A. K. Fritzsche, M. K. Murphy, C. A. Cruse, A. C. Handermann, R. F. Malon and M. D. Moore, The Second-Generation Polysulfone Gas-Separation Membrane. I. The Use of Lewis Acid:Base Complexes as Transient Templates to Increase Free Volume, J. Appl. Polym. Sci. 40 (1990) 1557-1574.

[24] R. E. Kesting, A. K. Fritzsche, C. A. Cruse and M. D. Moore, The Second-Generation Polysulfone Gas-Separation Membrane. II. The Relationship between Sol Properties, Gel Macrovoids, and Fiber Selectivity, J. Appl. Polym. Sci. 40 (1990) 1575-1582.

[25] P. Comba and T. W. Hambley, Molecular Modeling of Inorganic Compounds, VCH, Weinheim, 1995.

[26] B. P. Hay and O. Clement, Metal Complexes, in P. V. R. Schleyer (Ed.), Encyclopedia of Computational Chemistry, Volume 3, John Wiley and Sons, New York, 1998, pp. 1580-1587.

[27] B. P. Hay, D. Zhang and J. R. Rustad, Structure Criteria for Rational Design of Selective Ligands. 2. Effect of Alkyl Substitution on Metal Ion Complex Stability with Ligands Bearing Ethylene-Bridged Ether Donors, Inorgan. Chem. 35 (1996) 2650-2658.

[28] A. K. Rappe and W. A. Goddard III, Charge Equilibration for Molecular Dynamic Simulations, J. Phys. Chem. 95 (1991) 3358-3363.

[29] D. R. Lide, CRC Handbook of Chemistry and Physics, CRC Press, New York, 1998.

[30] T. Bender, HyproChem Excel Macro, Carleton University, Ottawa, 1999, (available from www.hyper.com).

[31] C. L. Yaws, Chemical Properties Handbook, McGraw-Hill, New York, 1999.

[32] G. Horvath and K. Kawazoe, Method for the Calculation of the Effective Pore Size Distribution in Molecular Sieve Carbon, Journal of Chemical Engineering of Japan, 16 (1983) 470-475.

[33] R. G. Pearson, Chemical hardness, Wiley-VCH, Weinheim, Germany, 1997.

[34] A. A. Grinberg, An Introduction to the Chemistry of Complex Compounds, J. R. Busch and R. F. Trimble, Jr. (Eds.), Progamon Press, London, 1962.

[35] K. Izutsu, T. Nakamura, K. Miyoshi and K. Kurita, Potentiometric study of Complexation of Lithium Ions in Some Solvents Related to Lithium Batteries, Electrochimica Acta 41 (1996) 2523-2527.

[36] W. Rudolph, M. H. Brooker and C. C. Pye, Hydration of Lithium Ion in Aqueous Solution, J. Phys. Chem. 99 (1995) 3793-3797.

[37] Y. Zhao and G. R. Freeman, Solvent Structure Effects on Electrical Conductivities of Small-Ion Salts Compared to Large-Ion Salts in C_1-C_4 Alcohols and Water, Can. J. Chem. 75 (1997) 559-566.

[38] M. Alger, Polymer Science Dictionary, Chapman and Hall, London, 1997.

CHAPTER IV

The Determination of Interaction Parameters in the Characterization of Polyetherimide Gas Separation Membranes using the Horvath-Kawazoe Model

J. Kurdi, and A. Y. Tremblay*

Department of Chemical Engineering, University of Ottawa, 161 Louis Pasteur, Ottawa, Ontario, K1N 6N5, Canada

*Corresponding author:
André Y. Tremblay
Tel.: +1-613-562-5920; fax: +1-613-562-5172
E-mail address: tremblay@uottawa.ca

Article has been Published in: **Desalination 148, 341-346 (2002).**

CHAPTER IV

Paper 3: The determination of interaction parameters in the characterization of polyetherimide gas separation membranes using the Horvath-Kawazoe model

J. Kurdi, and A. Y. Tremblay
Department of Chemical Engineering, University of Ottawa, 161 Louis Pasteur, Ottawa, Canada, K1N 6N5
Received 8 February 2002; accepted 8 April 2002

ABSTRACT

The Horvath-Kawazoe (HK) model is widely used to characterize microporous carbons and zeolites. The use of the HK model in this application has been extensively studied and interaction parameters exist to relate gas adsorption isotherms to the microporosity of these materials. However, interaction parameters for the HK model do not exist for polymeric materials, which limits its use in characterizing such systems. In this work, the HK parameters for the nitrogen-polyetherimide system were determined from molecular properties and computational chemistry. The interaction energy coefficients required to calculate interaction parameters in the HK model were determined from the polarizability and diamagnetic susceptibility of PEI using the Kirkwood-Muller equations. The parameters were used in the HK method to model a nitrogen adsorption isotherm at 77.2 K and determine the micropore size distribution of a PEI gas separation membrane. The relation between the differential heat of adsorption and pore size distribution, which is the basis of the HK model, was studied for nitrogen adsorption on PEI using different interaction parameters and estimates of the diameter of the PEI chain. The influences of these parameters on the calculated pore size distribution were discussed. The validity of the pore size distribution was examined by comparing the dominant pore size with the d-spacing obtained from X-ray diffraction on PEI. Good agreement was obtained between these values on using a suitable structural model that represents the wall thickness of the adsorbent and includes the polar property of PEI in determining HK parameters. Desalination 148 (2002) 341-346.

Keywords: Gas separation; Characterization; Polyetherimide; Nitrogen adsorption; Horvath-Kawazoe; Interaction parameters.

NOMENCLATURE

A_{N2}	pair interaction energy coefficient of nitrogen [J cm^6/molecule]
$A_{N2\text{-}PEI}$	pair interaction energy coefficient of N_2-PEI [J cm^6/molecule]
c	velocity of light in vacuum [299792458 m/s]
d	sum of the adsorbate and adsorbent diameters [nm]
d_A	diameter of the adsorbate [nm]
d_s	diameter of the adsorbent [nm]
IP	Interaction energy parameter given by equation (2), [J cm^4]
m	electron mass [9.109389754 10^{-31} Kg]
N_{AV}	Avogadro's number [molecule/mole]
N_{N2}	number of molecules per unit area of liquid nitrogen surface [molecules/cm^2]
N_{PEI}	number of molecules per unit area of solid PEI surface [molecules/cm^2]
l	distance between molecular center of the two opposite pore walls [nm]
n_r	refractive index [dimensionless]
P	absolute pressure [Pa]
P_o	saturated pressure [Pa]
q_{diff}	differential heat of adsorption [J/mole]
R_g	gas constant [J/mole K]
T	absolute temperature [K]

Greek Symbols

α_{N2}	polarizability of nitrogen [cm^3/molecule]
α_{PEI}	polarizability of PEI [cm^3/molecule]
ΔH_{vap}	normal molar heat of vaporization of nitrogen [Joule/mole]
μ	dipole moment [Debye]
ρ	density [molecules/cm^3]
σ	distance between center of the adsorbate and the center of the wall of the solid at zero interaction energy [nm]
χ_{N2}	diamagnetic susceptibility of nitrogen [cm^3/molecule]
χ_{PEI}	diamagnetic susceptibility of PEI [cm^3/molecule]

1 INTRODUCTION

With the increased use of nanostructured materials, there is a need for simple and comprehensive approaches by which the microporosity of various types of materials can be determined. The HK model [1] is widely used in evaluating the microporosity of various molecular sieves. The characterization of microporosity is required in many applications such as catalysis, adsorption and molecular sieving processes.

Asymmetric glassy polymeric gas separation membranes rely on a dense skin layer to confine gas transport and achieve a selective separation [2, 3, chapter II and III]. As this skin layer contains pores or voids of molecular dimension (< 2 nm), it is necessary to find and use reliable techniques that are suitable to determine the size and shape of these pores. Semi-empirical models derived by Dubinin et al. [4-6], Jaroniec et al. [7-8] and Horvath-Kawazoe [1] are widely used to calculate the micropore size distribution from adsorption isotherms. These models are based on the relation between micropore size and the adsorption potential energy of a gas molecule in a micropore of a given geometry. This relation is based on the mechanism of adsorption in micropores that is considered to be pore filling rather than surface coverage or capillary condensation. The potential energy in a micropore is enhanced due to the overlap of the potential fields of the opposite walls inside the micropore [9-10]. The parameters used in the above models are available for various porous carbons and zeolites but have not been determined for polymers or other nanostructured materials. Obtaining such important parameters for various N_2-polymer interactions will enhance the use of nitrogen adsorption for the characterization of polymeric materials, especially the characterization of gas separation membranes.

In this paper, the interaction parameter and polymer chain thickness required in the HK model were determined in order to calculate the micropore size distribution of a polyetherimide membrane from a nitrogen adsorption isotherm. The calculation procedures are discussed and the influence of the interaction energies and diameter of a PEI chain on the resulting pore size distribution illustrated. Computational chemistry [11] was used to determine the chain thickness of PEI. The validity of the determined parameters was confirmed by comparing the dominant pore size obtained from the HK model to X-ray diffraction experiments performed on the polymeric membrane [12].

2 EXPERIMENTAL

Polyetherimide (PEI) membranes were prepared by the coagulation post leaching method from a solution containing 23% PEI in N-Methyl pyrrolidinone and 4.7% ($LiNO_3$/PEI) by weight [2-3, chapters II and III]. The membrane coupons were cut into small strips and characterized by nitrogen adsorption in an automated micropore analyzer ASAP 2000M [13]. The amount of N_2 adsorbed on the membrane was determined over a pressure ranging from 0.001 mm Hg to 760 mm Hg at a liquid nitrogen temperature of 77.2 K. The HyperChem computational chemistry program [11] was used to model and optimize the structure of polyetherimide as explained elsewhere [3, chapter III].

3 THEORY

The HK model and its variations offer a method to relate gas adsorption isotherm measurements with the pore size of an adsorbent. For slit shaped pores, Horvath and Kawazoe derived the following equation [1];

$$R_g T \ln(p/p_o) = N_{AV} \frac{IP}{\sigma^4 (l-d)} \times \left[\frac{\sigma^4}{3(l-d/2)^3} - \frac{\sigma^{10}}{9(l-d/2)^9} - \frac{\sigma^4}{3(d/2)^3} + \frac{\sigma^{10}}{9(d/2)^9} \right] \quad (1)$$

where R_g is the gas constant, T is the absolute temperature, p is the applied pressure, p_o is the saturation pressure, N_{AV} is Avogadro's number, l is the distance between the molecular center of the two opposite pore walls, d is the sum of the adsorbate diameter and the adsorbent diameter, σ is the distance between the center of the adsorbate and the center of the wall of the solid at zero interaction energy and IP is the interaction parameter. The value of IP was determined from the following equation [13];

$$IP = N_{N2} A_{N2} + N_{PEI} A_{N2\text{-}PEI} \quad (2)$$

where N_{N2} and N_{PEI} are the number of molecules per unit area of surface for nitrogen and PEI respectively. The value of N_{N2} was determined from the bulk density of nitrogen at its normal boiling point. The value of N_{PEI} was determined from the bulk density of PEI. A_{N2} and $A_{N2\text{-}PEI}$ are the interaction energy coefficients for nitrogen and nitrogen-PEI respectively. The value of A_{N2} was calculated from Kirkwood-Muller equation for similar

molecules. The interaction energy coefficient for N_2-*PEI* was calculated from the Kirkwood-Muller equation for dissimilar molecules [1];

$$A_{N2-PEI} = \frac{6mc^2 \alpha_{N2}\alpha_{PEI}}{\frac{\alpha_{N2}}{\chi_{N2}} + \frac{\alpha_{PEI}}{\chi_{PEI}}} \tag{3}$$

where m and c are the mass of an electron and velocity of light in vacuum respectively, α_{N2} and α_{PEI} are the polarizability of nitrogen and PEI respectively; χ_{N2} and χ_{PEI} are the diamagnetic susceptibility of nitrogen and PEI respectively.

The diamagnetic susceptibility of PEI was calculated from the chemical structure of PEI using the group contribution method [14]. The polyetherimide repeat unit has a dipole moment. This implies that the total polarizability of PEI will be the sum of its static and dynamic polarizabilities. The static polarizability component α_{PEI} (static) was calculated from the refractive index, n_r using Lorenz-Lorentz equation [15]. The dynamic (polar) interaction energy component was determined by equating the polar interaction energies as defined in [16] to that found in Kirkwood-Muller and solving for α_{PEI} (polar). The dipole moment of PEI was calculated using the PM3 semiempirical method in the HyperChem program [11].

The HK model considers that the differential heat of adsorption, q_{diff} in a micropore is related to the gas pressure upon adsorption and can be calculated from the following equation;

$$q_{diff} = R_g T \ln\left(\frac{p}{p_o}\right) + \Delta H_{vap} \tag{4}$$

where ΔH_{vap} is the normal heat of vaporization of nitrogen [17], p is the applied pressure and p_o is the saturation pressure.

4 RESULTS AND DISCUSSION

The influence of the interaction parameter (IP) and the thickness of the PEI chain on the differential adsorption energy were evaluated. Table 4.1 summarizes all the required quantities to determine parameters in the HK model. Two interaction parameters were determined for nitrogen-PEI; one based on the static polarizability of PEI (i.e. ignoring its orientation dipole) and the other based on the sum of the static and dynamic polarizabilities.

Table 4.1 Summary of the information used evaluating of the HK parameters. All quantities were temperature corrected to 77.2 K.

Parameters	N_2 [Reference]	PEI [Reference]	Units
Diameter of adsorbate, d_A	0.3 [1]		nm
Thickness of adsorbent, d_s		0.49 [*]	nm
Density, ρ	1.74E+22 [1]	1.29E+21 [18]**	molecule/cm^3
Surface density No., N	6.70E+14 [1]	1.185E+14 [*]**	molecule/cm^2
Refractive index, n_r	1.19876 [19]	1.658 [18]	
Dipole moment, μ	0	5.704 [*]	Debye
Diamagnetic susceptibility, χ	1.99E-29 [19]	5.64E-28 [*]**	cm^3/molecule
Static polarizability, α	1.74E-24 [19]	6.6643E-23 [*]**	cm^3/molecule
Polar polarizability, α at 77.2 K	0	5.302E-23 [*]**	cm^3/molecule
Total polarizability, α	1.74E-24	1.197E-22 **	cm^3/molecule
Interaction energy coefficient, A_{N2}	4.25E-66	8.29E-63	J cm^6
$A_{N2\text{-}PEI}$	3.41383E-64		J cm^6
$d = d_A + d_s$	0.79		nm
$\sigma = 0.858\ (d/2)$ [1]	0.339		nm
Interaction Parameter, IP based on static polarizability of PEI	3.56E-50		J cm^4
Interaction Parameter, IP based on the static and polar polarizabilities of PEI	4.32E-50		J cm^4

* This work using the mentioned equations.
** For PEI, a repeat unit was used to represent a molecule of adsorbent.

The interaction parameter depends on the molecular properties of PEI as discussed above. Two models were studied to determine the entity of the adsorbent surface: (1) the surface consists of atoms that are in direct contact with the nitrogen molecules (2) the surface of the adsorbent is considered to be all the atoms in the

molecule comprising the surface. For the first case, the PEI surface would be considered as carbon atoms as they are the main constituent of PEI. In this case the wall thickness is equal to the effective diameter of a carbon atom, 0.34 nm, as taken by Horvath-Kawazoe [1]. While in the second approach, the effective diameter of the PEI chain would be taken as the wall thickness. In this case the chain width was determined from HyperChem. Figure 4.1 shows a segment of several optimized polyetherimide chains with two lines passing through the center of two neighboring chains. The distance between neighboring chains was measured by the program at different positions in the optimized structure. The thickness of five chains was also measured at several points and averaged giving a chain diameter of 0.49 nm.

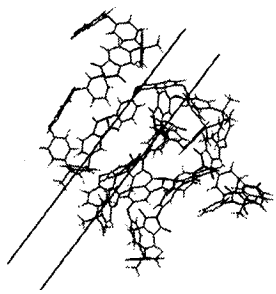

Figure 4.1 Optimized polyetherimide coil and two lines showing the effective distance between two neighboring chains.

The differential heat of adsorption was plotted vs. slit pore width in Figure 4.2 as seen in this figure, the estimate of the chain diameter has a considerable effect on the differential adsorption energy and hence the pore size distribution. It can also be seen from this figure that at a given slit width the estimate of chain thickness plays a greater role in determining the differential adsorption energy than polar/non-polar considerations.

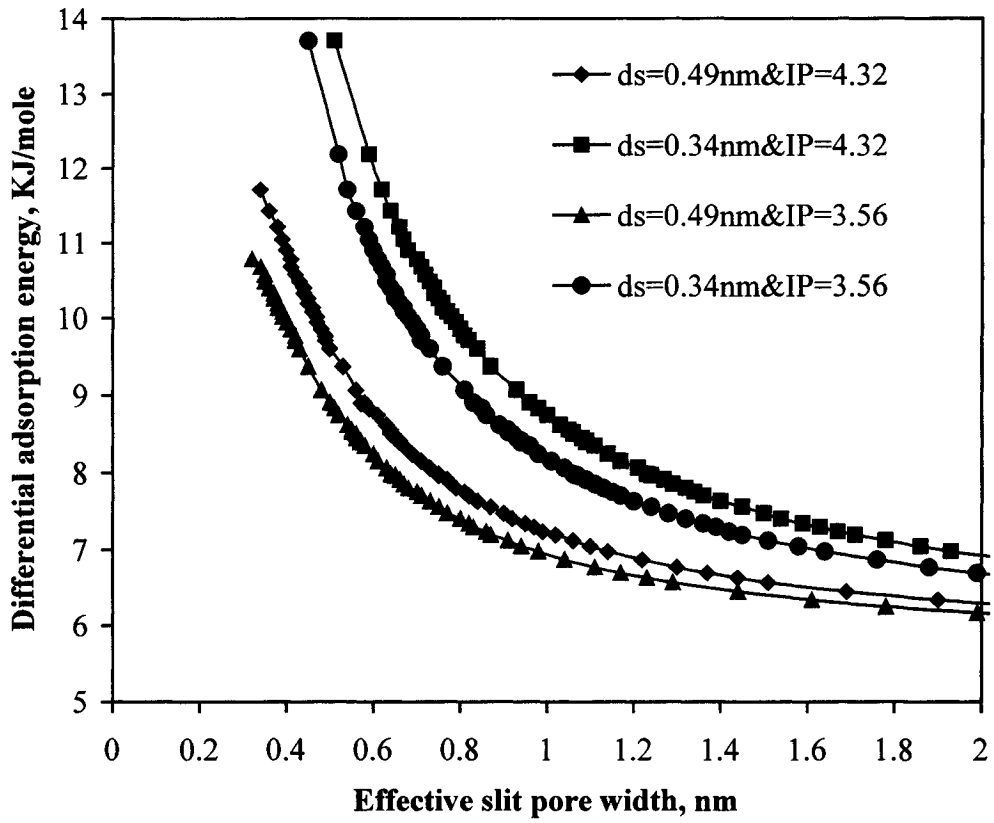

Figure 4.2 The influence of the adsorbent wall thickness (d_s) and interaction parameter (IP) on the differential adsorption energy (IP units 1E-50 J cm^4).

As previously described, polyetherimide (PEI) membranes prepared by the coagulation post leaching method were tested in an ASAP 2000M microporosimeter. The differential pore volume was plotted versus the slit pore width as shown in Figure 4.3. The dominant pore size corresponding to the maximum differential pore volume for the case of d_s = 0.34 nm is 0.7 nm while for d_s = 0.49 nm, it is 0.48 nm. The second structural model is closest to the reported value of the d-spacing = 0.524 nm for polyetherimide (Ultem 1000) as determined from X-ray diffraction measurements [12]. The results indicate that using a chain width determined from computational chemistry to estimate d_s offers a better prediction of pore size than the approach based on the effective diameter of carbon, the main element in the PEI chain.

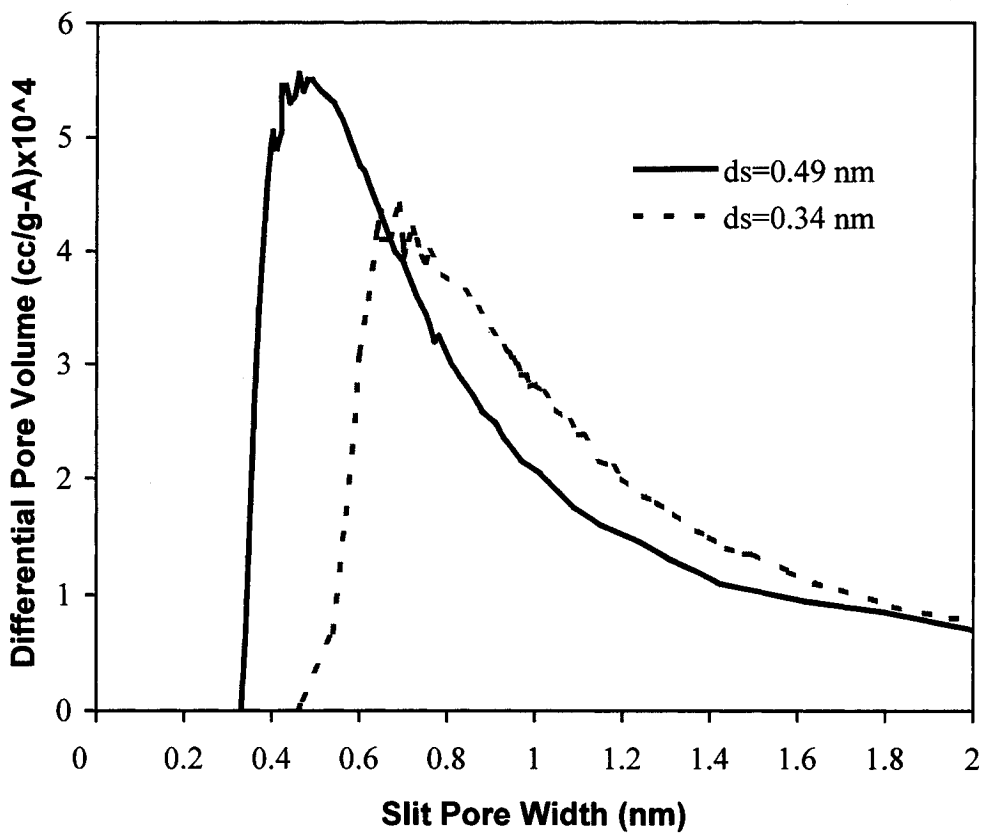

Figure 4.3 The differential pore volume versus pore size for two values of d_s for a value of IP = 4.32×10^{-50} J cm^4 in both cases.

5 CONCLUSIONS

The parameters required in the HK model were determined for the adsorption of nitrogen on PEI. These parameters predict pore sizes that are in agreement with X-ray diffraction measurements on PEI. The polar nature of polyetherimide should be included in determining IP as this affects the resulting pore size distribution. The atomic/molecular representation of the surface is critical in estimating the value of the structural parameter d_s for inclusion in the HK model. The HyperChem program was helpful in determining this value. Larger pore sizes are predicted by the HK model when the parameters for carbon are used. The results indicate the importance of parameter determination in interpreting gas adsorption isotherms to obtain valid micropore size distributions.

REFERENCES

1. Horvath, G. and K. Kawazoe, Method for the calculation of effective pore size distribution in molecular sieve carbon, Journal of chemical engineering of Japan, 16 (6), (1983) 470-475.
2. J. Kurdi and A. Y. Tremblay, Preparation of defect-free asymmetric membrane for gas separations", Journal of Applied Polymer Science, 73 (8) (1999) 1471-1482, chapter II.
3. J. Kurdi and A. Y. Tremblay, The influence of casting solution structure on the microporosity of polyetherimide gas separation membranes prepared by the coagulation post-leaching method, Journal of Membrane Science, 184 (2), (2001) 175-186, chapter III.
4. M. M. Dubinin and Stoeckli, Homogeneous and heterogeneous micropore structures in carbonaceous adsorbents, Journal of colloid and interface science, 75 (1), (1980) 34-42.
5. H.F. Stoeckli, F. Kraehenbuehl, L. Ballerini and S. De Bernardini, Recent developments in the Dubinin equation, Carbon, 27 (1), (1989) 125-128.
6. D. D. Do, Adsorption Analysis: Equilibria and Kinetics, Imperial College Press, London. 1998, pp. 171-190.
7. J. Choma and M. Jaroniec, Influence of the pore geometry on the micropore size distribution function of active carbon, Adsorption Science and Technology, 15 (8), (1997) 571-581.
8. M. Jaroniec, K. P. Gadkaree and J. Choma, Colloids surfaces A: Physicochem. Eng. Aspects 118 (1996) 203-210.
9. S. J. Gregg and K. S. W. sing, Adsorption, surface area and porosity, Academic Press, New York. 1982, pp. 195-247.
10. H. K. Shethna and S. K. Bhatia, interpretation of adsorption isotherms at above-critical temperatures using a modified micropore filling model, Langmuir, 10 (1994) 870-876.
11. HyperChem Pro 5.1 program (Hypercube Inc., Gainesville, FL, USA).
12. R. H. Vora, S. H. Goh and T.-S. Chung, Synthesis and properties of fluoro-polyetherimides, Polymer Engineering and Science, 40 (6) (2000) 1318-1329.
13. ASAP 2000M made by Micromeritics (GA, USA).
14. R.S. Drago, Physical Methods for chemist, Saunders College Publishing, Orlando, FL. 1992.
15. C. J. F. Bottcher, Theory of Electric polarizability, Volume 1: Dielectric in static fields, Elsevier Scientific Publishing Company, Amsterdam. 1973 p173.
16. K. S. Pitzer, Inter- and intramolecular forces and molecular polarizability, in Advances in chemical physics, I. Prigogine (Ed.), Volume II, Interscience Publishers, Inc. New York. 1959, pp. 59-83.
17. B. E. Poling, J. M. Prausnitz and J. P. O'Connell, The properties of gases and liquids, McGraw-Hill, New York. 2001.
18. Ultem PEI polyetherimide datasheet, Boedeker Plastics, Inc., 904 West 6th Street, Shiner, Texas 77984, USA.
19. D. R. Lide (ed), CRC Handbook of Chemistry and Physics, CRC Press, Boca Raton, 2000-2001.

CHAPTER V

Experimental Determination of the Local Microscopic Structure and Intermolecular Force parameters of Amorphous Liquids and Solids

J. Kurdi, and A. Y. Tremblay*

Department of Chemical Engineering, University of Ottawa, 161 Louis Pasteur, Ottawa, Ontario, K1N 6N5, Canada

*Corresponding author

André Y. Tremblay

Tel.: +1-613-562-5920; fax: +1-613-562-5172

E-mail address: tremblay@uottawa.ca

CHAPTER V

Paper 4: Experimental determination of the local microscopic structure and intermolecular force parameters of amorphous liquids and solids

J. Kurdi, and A. Y. Tremblay
Department of Chemical Engineering, University of Ottawa, 161 Louis Pasteur, Ottawa, Canada, K1N 6N5

ABSTRACT

The local microscopic structure and intermolecular force parameters of amorphous liquid nitrogen and polyetherimide (PEI, Ultem® 1000) were investigated. An approach was established for the determination of these parameters based on X-ray diffraction measurements and cohesive energy. The proposed approach is different from other methods in removing ideal assumptions and the need to fit the parameters through a mathematical potential function that is responsible for the discrepancy in the parameters in the literature. Structural parameters obtained from X-ray diffraction measurements and interpreted using the RAD program for amorphous materials were found to be in excellent agreement with those calculated from computational chemistry. The structural parameters determined for nitrogen were also in good agreement with those found in the literature based on experimental measurements. Two PEI films were prepared using different solutions to examine the determination of the intermolecular force parameters. The results indicated that the mesoporous and macroporous morphology of the tested PEI films has no influence on the determined parameters as long as the purity of the dense structure was maintained. This is in consistent with the fact that the intermolecular force parameters are intrinsic molecular properties of a pure polymer representing the chemical structure that leads to an intrinsic local microscopic structure.

Keywords: Intermolecular force parameters, Polyetherimide, Membrane microstructure, X-ray diffraction, Nitrogen adsorption.

1 INTRODUCTION

Local microscopic structures and intermolecular forces are responsible for most physical and thermodynamic properties of materials. Knowledge of intermolecular forces and the local molecular structure of a material are important in solving a wide class of problems [1] in physics, chemistry, biology, supramolecular chemistry [2], molecular machines [3], and the simulation of molecular systems such as molecular dynamics and Monte Carlo simulations [1].

An essential starting point in the study of intermolecular forces is the microscopic structure of materials. The organization or arrangement of the structure of an ensemble of similar or different molecules and the interaction energies among neighboring molecules are attributed to intermolecular forces. The balance between the intermolecular attractive and repulsive forces determines the distances between a reference molecule and each of the nearest surrounding molecules under many body effects. This leads to a definite local intrinsic density, which can be represented by the first spherical coordination unit in amorphous liquids and solids [4] or by a unit cell in a crystal and an ordered substance [5]. The first coordination unit represents a group of molecules that are weakly bonded to each other in a small cluster or crystal.

For a given material, the properties and phase states of a molecular cluster are different from that of the isolated molecule due to the intermolecular interactions among molecules in the same cluster and are different from that of the bulk material due to the interactions among clusters [6-7]. Because the cluster (coordination unit or unit cell) is the microstate or the local microstructure by which the bulk phase is assembled, it is necessary to study these clusters to bridge the gap between thermodynamic formalisms and molecular properties. Several books have been devoted to the review of intermolecular forces [1,8-12] and other books devoted to the review the structures and dynamics of clusters using different intermolecular spectroscopies [6, 13-14].

Intermolecular forces are usually expressed by their corresponding potential energies, equal to the integration of these forces with respect to the pair intermolecular distance between two molecules [9]. The potential energy as a function of the pair intermolecular distance can be represented mathematically by a potential model which contains two parameters: (1) the intermolecular force energy parameter, $\varepsilon(r_{equi})$ (which

corresponds to the minimum interaction energy of a pair of molecules) and (2) the intermolecular force distance parameter, σ_o (which corresponds to the zero potential energy of a pair of molecules).

The determination of these two intermolecular force parameters, in the literature, is based on three approaches: 1) in the first approach, computational chemistry is used such as *ab initio* [15], semiempirical [16], or empirical [17-18] methods and 2) in the second approach, macroscopic experimental measurements such as critical properties [19], viscosity [20-21], spectroscopic measurements [9, 22-23], beam scattering [21] and bulk properties having functional dependence on the intermolecular forces are used [21]. In these two approaches, a pair potential model (such as Lennard-Jones 6-12 potential or exp-6 potential) is required to link the energy of the molecular system to its structure as a function of separation distance. In the first approach, the intermolecular force parameters are adjustable constants that can be determined by fitting the pair potential model to the computed *ab initio*, semiempirical or empirical potential energy while in the second approach, an appropriate relation is required between one of the material properties (such as second virial coefficient, viscosity, compressibility factor, ...etc) and the potential model. The intermolecular force parameters in the model have to be adjusted to fit an experimental property of interest. 3) In the third approach, the intermolecular force parameters are variables in the Lennard-Jones potential model within a set of equations in the non-local density functional theory (NLDFT) established for calculating the minimum grand thermodynamic potential as a function of fluid density. Then these parameters are adjusted in order to reproduce the bulk properties at the normal boiling point of the gas (i.e. P = 1 atm) [24-26].

The three approaches use different assumptions in deriving intermolecular force parameters. In the first approach, the intermolecular parameters determined by computational chemistry are assumed to be the pair intermolecular interaction energy in vacuum independent of pressure, but as a function of temperature. Statistical mechanics methods such as molecular dynamic, Monte Carlo or Multipole Expansion methods [15] are then used to account for the increase in temperature from zero Kelvin to a specified temperature and to calculate the average or optimum potential of many random or selected orientations and configurations. In the second approach, the intermolecular

force parameters or force constants are adjustable constants independent of pressure and temperature. To validate this assumption, many efforts were done to establish a universal relation between the force constants and a material property. These end results are only applicable to specific properties and classes of materials [21]. In the third approach, the Lennard-Jones intermolecular force parameters used in the non-local density functional theory are determined at the normal boiling point of the gas (i.e. P = 1 atm) and then assumed to be independent of both pressure and temperature [24].

The use of these different assumptions leads to the reporting of several values of the interaction parameters for the same component. This makes the selection of the correct intermolecular force parameters rather difficult. The significance of the discrepancy in the reported force parameters should be illustrated. Due to the mutual influence of force energy and distance on each other, the combination of both experimental microstructure and energy measurements would provide independent information on these interaction parameters and offer a more direct calculation of the two force parameters. It is proposed to achieve this by determining the intermolecular force distance from X-ray diffraction experiments and the intermolecular force energy from the coordination number obtained by X-ray diffraction and the cohesive energy. Since the intermolecular force parameters for many materials such as polyetherimide are not available in the literature, a suitable and valid method for the determination of these parameters for large non-spherical molecules must be investigated.

Intermolecular forces can be measured directly using Surface Force Apparatus (*SFA*) and Atomic Force Microscopy (*AFM*) [8]. However, molecularly smooth surfaces are difficult to obtain and coarse surfaces lead to unreliable and less accurate estimates of force parameters.

Our present ability to isolate one or two molecules is rather limited. Interaction parameters are most often determined from bulk material properties. One advantage of this is that the molecular properties will include many body effects. The results will also represent a real statistical average intermolecular distance and energy under the instrumental test conditions. This consideration is more realistic than the results obtained for two ideal, isolated molecules and can be applied to both crystalline and amorphous materials.

In amorphous liquids or solids, the atoms surrounding a given reference atom are never exactly the same as the ones around another reference atom as in ordered crystals. X-Ray scattering will be influenced by the random structure and will provide an average statistical picture representing the material structure at the experimental conditions (temperature and pressure during X-ray measurements). In this paper, methods to obtain the structural parameters of amorphous liquids or solids will be described. Using these structural parameters, the determination of intermolecular force parameters was applied to two case studies: amorphous liquid nitrogen and amorphous polyetherimide.

2 THEORETICAL BACKGROUND

Intermolecular forces are meant to represent all the possible interactions among molecules. Atoms are linked through ionic or covalent bonds to form molecules. These molecules are held together in a larger structure by intermolecular cohesive or adhesive forces through non-covalent interactions or coordination bonds. The intermolecular coordination bonds cover all kinds of interactions that do not lead to the formation of a chemical bond. Intermolecular forces are attributed to electromagnetic forces, which are essentially electrostatic in origin [8-9]. These forces determine the properties of gases, liquids and solids, their static (equilibrium) and dynamic (e.g. Viscous and time-dependent) behaviors in pure bulk, mixtures, or in the interfaces (surfaces) and are responsible for the formation of material structures.

At a single condition (T, P), the organization of the equilibrium structures of an ensemble of molecules is a result of the balance of the attractive and repulsive forces between each pair of molecules having the lowest chemical potential (molar Gibbs free energy). At a phase transition condition such as boiling or melting point, an interaction potential energy among molecules is responsible for the change in the phase or state of the material (gas, liquid, many solid phases). This interaction potential energy depends on the interaction energy coefficient and the equilibrium distance among molecules under certain conditions (temperature and pressure).

2.1 Local microscopic structure of an ensemble of molecules

The local microscopic structure of an ensemble of molecules is required to link the cohesive energy and hence the thermodynamic properties to the pair intermolecular forces. The coordination number, distance and bond angle for amorphous liquids or solids can be determined from the radial local density function. This function can be obtained by the following methods:

2.1.1 Computer simulation

In this method, computer simulations are used to provide the detailed structure of a molecular ensemble. Molecular simulations require a potential model to determine the intermolecular interactions among molecules and to optimize the structure by minimizing the total potential energy of the ensemble. Using the Debye formula and the configuration structure optimized by a semi-empirical quantum mechanics method, the reduced structure factor was calculated and compared with one obtained from X-ray experiments [27-28].

The reverse Monte Carlo technique can also be used. A random configuration of atoms or molecules is generated by computer and then the radial distribution function is calculated and compared with the one obtained from X-ray experiments. A molecule is moved and the new position is accepted if a better fit is obtained otherwise the move is rejected [29-32]. However, many optimized configurations are often obtained and the global minimum is not known.

2.1.2 Reference interaction site model (RISM)

RISM is used to link the structure to the thermodynamic properties and pair correlation function especially for non-spherical molecules and polymers [33-36]. The RISM model was combined with the reverse Monte Carlo method to increase the reliability of the simulation results. However, Radnai et al. (1994) suggested a careful examination with respect to the reliability of the simulated results [37].

2.1.3 Molecular mechanic optimization

Goudeau et al. 2000 [38] used molecular mechanics (COMPASS forcefield) and dynamic simulations in which the intermolecular forces are represented by empirical parameters in the Lennard-Jones 9-6 potential and the electrostatic interaction functional forms to calculate the surface tension and cohesive energy of some amorphous polymers. However, the fitting of the intermolecular force parameters depend on the mathematical equations used, the initial random structures and the six-order combination rule for dissimilar components, which requires further improvements as reported elsewhere [17-18, 38].

2.1.4 Intermolecular spectroscopic methods

Intermolecular spectroscopy techniques are useful methods by which the molecular constants such as polarizability, electric multipole moments and Lennard-Jones parameters can be determined. For instance, the collision-induced far infrared absorption coefficient of compressed gases is related to an intermolecular potential model. The intermolecular force parameters are calculated as adjustable variables in order to fit experimentally determined absorption coefficients [13].

Clusters or aggregates in the condensed matter of a gas mixture were confirmed and studied by spectroscopic techniques along with molecular dynamic simulations [6]. Knowing the number of molecules in each cluster provides us with the number of molecules surrounding a reference molecule that is a coordination number required to link the microscopic parameters to the macroscopic properties of materials.

2.1.5 X-ray diffraction method

The local microscopic atomic structure of amorphous materials can be determined from the X-ray diffraction measurements through the pair correlation function [4, 39]. In amorphous solids, the surrounding atoms around an arbitrary atom are never exactly the same as the ones around another arbitrary atom. Therefore, we have to deal with an average statistical variables rather than exactly defined variables. Let us take an arbitrary atom in the isotropic polymer bulk (dense phase), the number of the surrounding atoms,

$N(r)$ that lie at a distance between r and $r + dr$ away from a central reference atom is equal to:

$$N(r) = \left(4/3\right)\pi\left[\left(r + dr\right)^3 - r^3\right]\rho(r) = 16\pi r^2 \rho(r)dr \qquad (1)$$

where $\rho(r)$ is the local atomic density (atoms per unit volume).

As r increases, the local atomic density reaches its maximum at a distance σ_{min}, which is equivalent to the center-center average distance of the first coordination shell from a central reference atom. With a further increase in r, the local atomic density will go through many alternate maxima and minima with a decreasing magnitude and at a large r, the local atomic density will reach the value of the atomic bulk density. The pair correlation function or pair distribution function $g(r)$ is equal to:

$$g(r) = \rho(r)/\rho(\infty) \qquad (2)$$

This function provides us with the most frequent pairwise distance among centers of higher dense spaces where a large number of electrons exist. Within the range of possible non-covalent interactions, the most frequent pairwise distance that is larger than usual intramolecular distances (covalent bonds) should represent an intermolecular distance. This fact can be exploited to determine the effective statistical average intermolecular force distance, σ_{min}, which is equal to r corresponding to maximum $g(r)$ in the first peak [4]. The number of neighboring molecules for closest approach and random packing from a central reference molecules is equal to the coordination number, which is equivalent to surface area of the first peak as reported elsewhere [4, 37].

The diffraction technique can be selected to obtain the structural information at a required scale. A short wavelength and a wide angle are suitable to determine the structure at atomic scale distances. For instance, calculating molecular electric moments (dipole, quadrupole, or other multipole) from X-ray diffraction data requires radiations of wavelength shorter than 0.1 nm (i.e. Mo or Ag X-ray tubes) in order to adequately resolve sharp features of atomic density i.e. intramolecular distance [40] while a longer wavelengths and a smaller angle are suitable for features 1 nm or larger [41]. Because the intermolecular distance is usually larger than 0.2 nm, wavelength of 0.154 nm and wide-angle X-ray diffraction measurements are suitable to study this structural range.

2.2 Microscopic and macroscopic intermolecular interactions

The total equilibrium or minimum energy of an ensemble of molecules is attributed to the molecular heat of formation resulting from the intramolecular interactions within a molecule and the cohesive or adhesive energy resulting from the intermolecular interactions among molecules. At an equilibrium (steady state at constant pressure and temperature) and a constant total system energy, a molecules' ensemble will have definite inherent properties (physical and thermodynamic properties) within a stable phase. In one phase (gas, liquid or solid), material properties are determined by equations of state and heat capacity (C_p or C_v) while at phase transitions, structural changes take place as a result of reorganizing, forming or breaking the non-covalent bonds within a coordination shell or cluster. Because the ensemble is still under the same temperature and pressure conditions, the chemical potential for the different phases will not change but the change in the phase will lead to a jump in the thermodynamic properties due to forming or breaking the coordination (non-covalent) bonds or reorganizing the structure of the coordination unit.

The properties and the strength of the cohesive energy of condensed phases are attributed to the coordination interaction energies (energies of the non-covalent bonds) between a reference molecule and other neighboring molecules within the coordination unit. In Van der Waals liquids or solids, under close packing, a small molecule can contact 12 other molecules. Therefore, the total bulk energy will be equal to 12 newly formed pair-interaction energies minus 6 broken pair-interaction energies [8, 10]. For classical intermolecular vibrations, the total interaction energy of each reference molecule with its surrounding molecules within a cluster is the sum of the pairwise interaction energies and is given by the following equation [8, 10]:

$$\Delta U(r_{equi}) = \frac{1}{2} N_{AV} n_c \varepsilon(r_{equi}) \qquad (3)$$

where N_{AV} is Avogadro's number, n_c is the effective coordination shell number which is equal to the number of neighboring molecules that have coordination interactions (non-covalent bonds) among them within a cluster. The variable $\Delta U\ (r_{equi})$ is equal to the intermolecular coordination interaction energy per mole, which represents the molar

cohesive energy that holds molecules together in a liquid or solid phase. $\varepsilon(r_{equi})$ is the pairwise equilibrium intermolecular force energy parameter (well depth) that is a function of intermolecular force distance and can be given by the following equation [9]:

$$\varepsilon(r_{equi}) = \frac{A_{\text{int}}}{r_{equi}^{6}} \tag{4}$$

Where A_{int} is a phenomenological pairwise interaction energy coefficient between two molecules or atoms and r_{equi} is the thermodynamic equilibrium distance between these two molecules.

Equation (3) represents a direct relationship between the macroscopic property (cohesive energy) and the microscopic property (pairwise intermolecular force energy parameter). The molar cohesive energy of a pure liquid or solid can be 4 to 6 times the pairwise interaction energy [8]. For liquids, the enthalpy or latent heat of vaporization is related to the internal energy of vaporization (cohesive energy) by the following equation [8,42]:

$$\Delta H^{vap} = \Delta U(r_{equi}) + P(V_g - V_L) = \Delta U(r_{equi}) + Z_g R_g T_B \tag{5}$$

where P is the absolute pressure, Z_g is the gas compressibility factor, R_g is the universal gas constant, T_B is boiling point, V_g and V_L are molar volumes of gas and liquid respectively. For solids, the heat of vaporization and the boiling temperature should be replaced, in equation (5), by the heat of sublimation and the sublimation temperature respectively [8].

For small molecules, the transition from the gas phase to a condensed liquid or solid phase is attributed to the formation of non-covalent bonds among molecules. However, as the molecular weight increases, the intramolecular bonds, which are shorter and stronger than the non-covalent bonds, become increasingly significant in keeping atoms together in the condensed phase (liquid or solid). Excluding the influence of strong non-covalent bonds such as hydrogen bonds, the higher the molecular weight, the higher the boiling point, which may exceed the decomposition temperature of the molecule. Therefore, most high molecular weight solids cannot be evaporated or sublimated without destroying their molecular structure. Their experimental vapor-liquid phase transition curve, which represents the formation of the non-covalent bonds, cannot be obtained. In this case, solubility parameters are used to obtain interaction energies,

because they are derived from the energy required to convert a liquid to a gas [42]. Hansen solubility parameters (*HSP*) [42] are based on the total energy of vaporization of a liquid and consist of several individual parts that are directly related to intermolecular interactions. According to the type of interactions, the parameter can also be divided into three parts: non-polar, polar and hydrogen bonding components. The cohesive energy at a given set of conditions (usually 1 atm and room temperature) can be given by the following equation:

$$\Delta U(r_{equi}) = V(\delta_d^2 + \delta_p^2 + \delta_H^2) \tag{6}$$

Where δ_d, δ_p, and δ_H are the dispersion, polar and hydrogen bonding components of the Hansen solubility parameters. Therefore, the cohesive energy (required in equation (3) to determine the intermolecular force energy parameter) can be determined experimentally from the heat of vaporization and work of expansion, or the Hansen solubility parameters and molar volume.

3 EXPERIMENTAL

3.1 Computational chemistry

3.1.1 Structure of an isolated pair of nitrogen molecules

Two nitrogen molecules were assembled in the computational chemistry HyperChem Pro 5.1 program [43]. The structure of the two nitrogen molecules was optimized using a molecular quantum *ab initio* method and a large basis set (6-31G**). A molecular dynamic simulation was used along with the *ab initio* method to increase the system temperature to a specified value [44]. The average distance between the two molecules was calculated from the pairwise distances between atoms using the following equation:

$$\frac{n_r}{r_{equi}^6} = \sum_{ij}^{n_r} \frac{1}{r_{ij}^6} \tag{7}$$

where r_{ij} is all the possible pairwise distances between each atom in one molecule and all other atoms in other molecules and n_r is the number of r_{ij} used in equation (7). The

reason for using this average in equation (7) is that the physical (non-covalent) interaction energy between a pair of molecules falls off with the sixth power of the separation distance based on quantum mechanics [9]. The optimization was also repeated using the *AM1* semiempirical method instead of the *ab initio* method. Other computation methods could also be used but two are sufficient for the purpose of this study.

3.1.2 Optimization of a cluster of nitrogen molecules

A cluster of 14 molecules of nitrogen was built in the HyperChem Pro 5.1 program [43] and optimized by the semiempirical *AM1* method at 0 K in vacuum. A molecular dynamics simulation was used to optimize the structure at a temperature of 65 K. At both temperatures and after several long simulation runs, we found that only 12 molecules remained in a close cluster while two molecules were found to have moved a far distance away from the cluster. The pair average intermolecular distance was calculated using equation (7) for all possible pairs in the 12-molecule cluster.

3.1.3 Optimizing equilibrium distance between PEI chains

The equilibrium distance between two closely packed polyetherimide chains was calculated from computational chemistry program and was discussed in our previous work, chapters III and IV [45-46].

3.2 X-ray diffraction experiments

Two samples of polyetherimide were prepared for testing by wide-angle X-ray diffraction:

1. Membrane cast using NMP: Polyetherimide (Ultem 1000, GE [47]) membrane was prepared by the coagulation post leaching method described in Kurdi and Tremblay, chapters II and III [46, 48], from a casting solution containing 23% by weight polymer concentration and 4.7% (w/w) Li NO_3/PEI. The membrane was dried and annealed in a vacuum oven at temperature 90 °C and 725 mm Hg vacuum pressure for 48 hours. The resulting membrane was opaque and had

asymmetric structure as evident by scanning electron microscopy. It had a dense skin layer with an average thickness 10 μm (chapter X in this thesis).

2. Clear film cast using $CH_2 Cl_2$: A symmetric film was cast from a solution of 23% polyetherimide (Ultem® 1000) in dichloromethane (Analar, BDH) at room temperature (23°C) and a nitrogen atmosphere on a clean glass plate using a knife gap of 250 μm and the membrane dried in air at lab conditions for one day and finally dried and anealed in a vacuum oven at temperature 90 °C and 725 mm Hg vacuum pressure for 48 hours. The resulting film was transparent and had a symmetric structure as observed by scanning electron microscopy.

The membrane and the film were cut into 32 mm diameter coupons. The X-ray diffraction measurements of both samples were carried out in reflection geometry at room temperature (23°C) using a Philips diffractometer (PW3710) and Cu k_α radiation source operated at 45 kv and 40 mA. The wavelength of radiation is (λ_1 = 0.154056 nm and λ_2 = 0.154439 nm, λ_2/λ_1 = 0.5). The data were collected by step scanning $\Delta(2\theta) = 0.02^\circ$ from $(2\theta) = 3^\circ$ to 35° range. Background scattering data was obtained at the same experimental conditions without the sample in place.

4 CALCULATIONS

4.1 Pair radial correlation function

The pair radial correlation function of liquid nitrogen at 65 K and polyetherimide samples at room temperature 298.15 K were calculated using the RAD program [39]. For liquid nitrogen at 65 K, the interference function or reduced intensity function "distinct structure function" $H_d(k)$ vs scattering angle k, [1/A] was taken from Narten et al. 1980 [49] and used in the RAD program to obtain the molecular pair correlation function. Then, the local molecular density of liquid nitrogen at 65 K was plotted versus radial distance as shown in Figure 5.1. For polyetherimide at 298.15 K, the effective thickness of the PEI samples was calculated from the bulk density of polyetherimide [50]. The linear absorption coefficient of polyetherimide was calculated from the sum of the mass attenuation (absorption) coefficients of atoms in PEI obtained from the International Tables for Crystallography, Table 4.2.4.3 [51], The atomic number and the dispersion

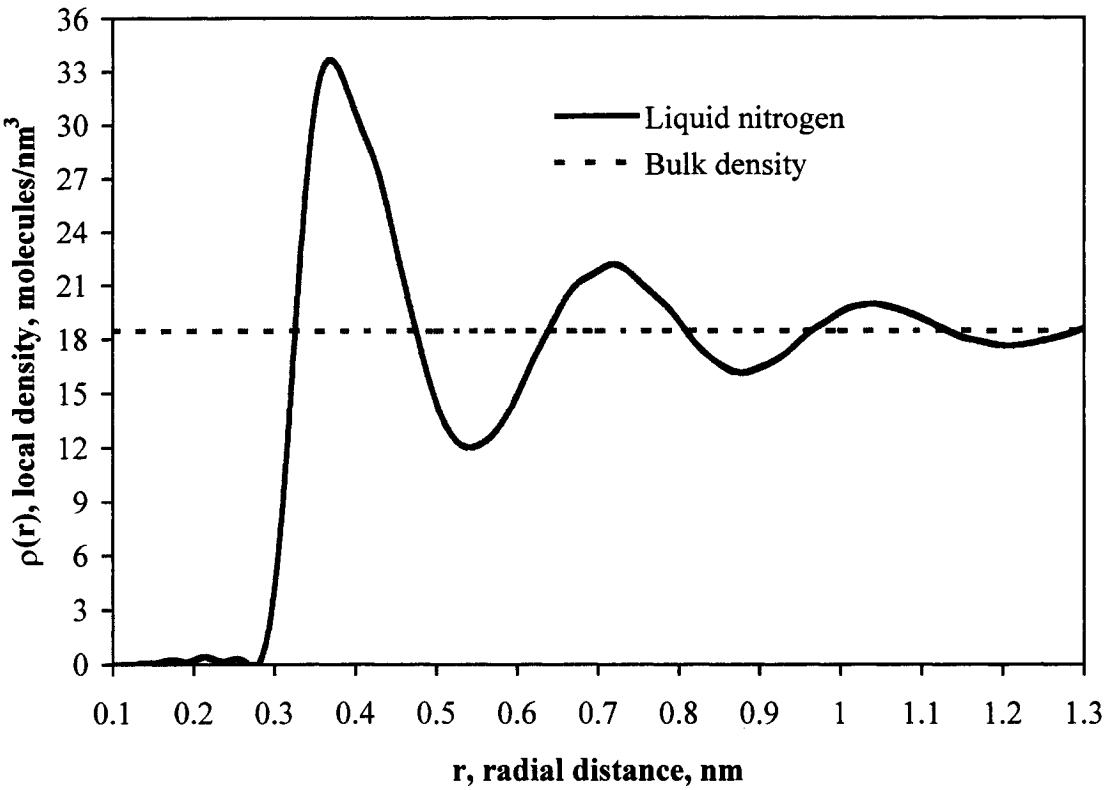

Figure 5.1 Pair molecular density distribution function for liquid nitrogen.

correction for atoms were obtained from the International Tables for Crystallography [51]. The number and atomic concentration of each atom type in PEI was calculated from the structure of one repeat unit of PEI obtained from the Polymer Science Dictionary [52]. The parameters used for the PEI samples in the RAD program are shown in Table 5.1.

Table 5.1 Parameters for PEI samples, used in the RAD program.

Parameters	PEI (Ultem 1000)	Units/Notes
Bulk density of PEI	1.27	g/cm^3
Linear absorption Factor	7.13	cm^{-1}
Bulk atomic density	89.05	$atoms/nm^3$
Damping factor	0.005	dimensionless
Effective thickness	0.00341	cm, PEI clear film
Effective thickness	0.00415	cm, PEI membrane
One repeat unit of PEI = $C_{37}N_2O_6H_{24}$ = (444.4 + 28 + 96 + 24.2 = 592.6 g / mole)		

In the RAD program, the data are corrected for background, polarization and absorption. The missing data for low angle scattering was extrapolated to zero. The corrected data was smoothed and normalized to electronic units. Then the atomic pair correlation functions were obtained through Fourier transformations. A recommended damping factor of 0.005 was used to suppress spurious ripples arising from series termination [39, 53]. The influence of the recommended damping in our results was tested and it is less than 0.002 nm. Detailed information about the different steps in obtaining the pair correlation function or pair distribution function, *g(r)* as a function of the radial distance from X-ray scattering data can be found elsewhere [39, 41, 51, 53-55]. The local atomic densities of the clear PEI film and PEI membrane cast using NMP as a function of the radial distance were plotted in Figures 5.2 and 5.3 respectively.

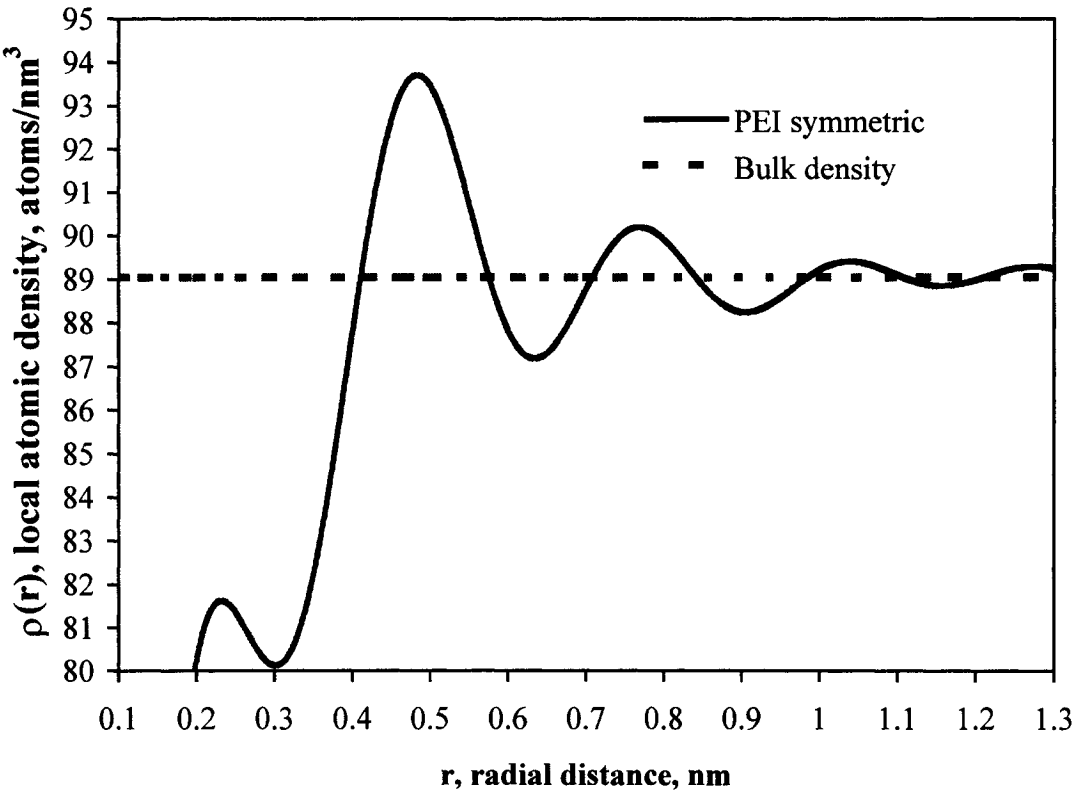

Figure 5.2 Pair atomic density distribution function for PEI clear film.

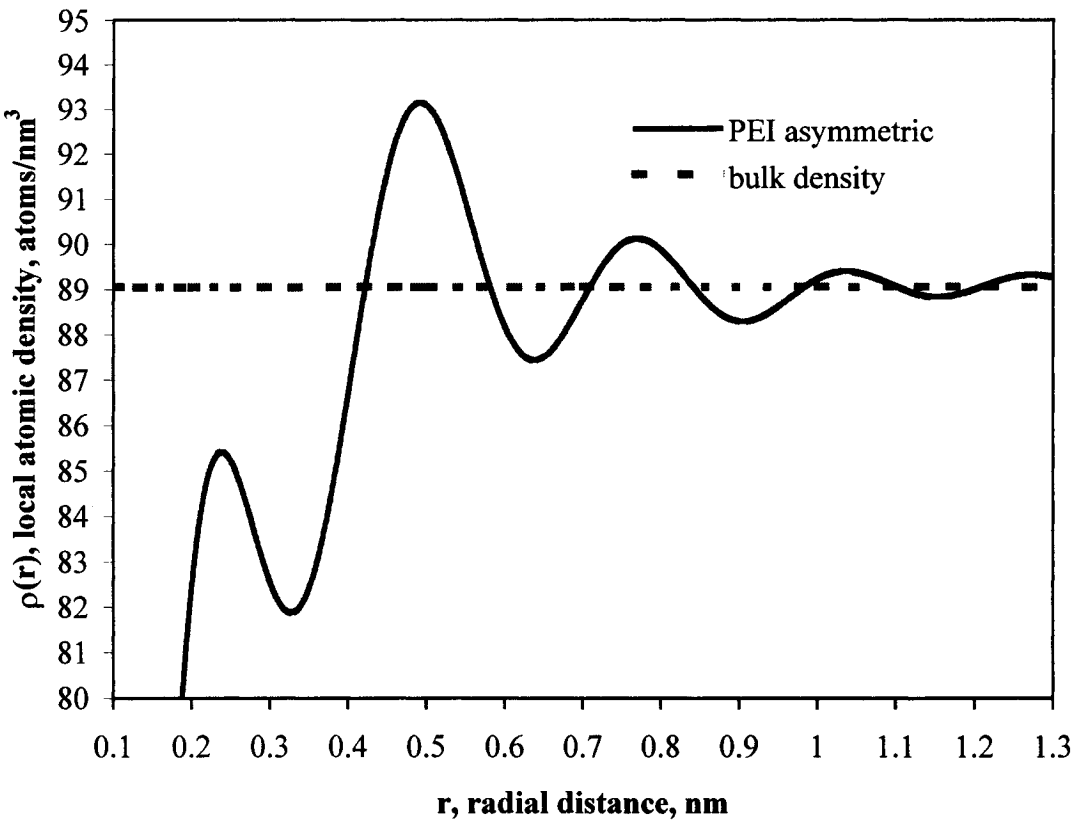

Figure 5.3 Pair atomic density distribution function for PEI membrane.

4.2 Structural parameters of liquid nitrogen and PEI samples

The coordination distances of the liquid nitrogen at 65 K and the two PEI films at 298.15 K were obtained from the atomic density functions in Figures 5.1, 5.2, and 5.3 respectively. They were determined by simply considering the intermolecular force distance equal to the radial distance corresponding to the maximum local atomic density for each peak starting from the strongest peak (number 1), then the next peak (number 2) and so on. In Figures 5.2 and 5.3 for PEI samples, the weak peak before the peak of maximal intensity was excluded as it is related to the weak or non-conventional hydrogen bond [C – H ... A] among PEI chains, where A is a proton acceptor in the PEI [56-57]. The radial distance corresponding to the maximum density of this weak peak is equal to 0.24 nm. This is in the usual range for weak hydrogen bonds [C – H ... A] in organic components [57].

The number of non-covalently bonded atoms or molecules in each coordination unit can be calculated from the area under the corresponding peak [4]. This area is determined by the integration of the pair atomic density function (in Figures 5.1, 5.2 and 5.3) from the radial distance at the minimum density at the beginning of the peak to the radial distance at the minimum density at the end of the peak [37]. The thickness of each consecutive coordination unit is obtained from the distance between successive minima in the atomic density distribution curves, Figures 5.1, 5.2, and 5.3. As the coordination unit distance r_u is the radial distance from the middle of the spherical shell to the center of the sphere, then the outer radius of the shell is equal to the sum of the coordination unit distance and half the thickness of the coordination unit $(\delta_u/2)$. Therefore, the volume of each coordination unit excluding the first one, V_u is given as follows:

$$V_u = \frac{4}{3}\pi\left[\left(r_u + \frac{\delta_u}{2}\right)^3 - \left(r_u - \frac{\delta_u}{2}\right)^3\right] \tag{8}$$

The volume of the first coordination unit can be calculated as a complete sphere. Finally, the coordination number of each peak is calculated from the product of the corresponding volume of the coordination unit and the average atomic density.

It is worth noting that the first coordination unit should have the highest average molecular density number and this density number should decrease with increasing radial distance until it becomes equal to the bulk density number (number of molecules per unit volume). This decrease in the density number for higher coordination shells is attributed to the larger volume involved in the calculation of the density number. However, it is possible to include the second, third and higher coordination numbers into the first coordination number to have one effective coordination number, n_c. The total interaction energy of a reference molecule with the surrounding molecules in all coordination units is equal to the sum of the pairwise interaction potential energy (given by equation 4) for all coordination units and by using equation (3), we obtain the following equation:

$$\Delta U(r_{equi}) = \frac{1}{2} N_{Av} n_c \frac{A_{A-A}}{r_{equi}^6} = \frac{1}{2} N_{Av} n_{c1} \frac{A_{A-A}}{r_{equi}^6} + \frac{1}{2} N_{Av} n_{c2} \frac{A_{A-A}}{r_2^6} + \frac{1}{2} N_{Av} n_{c3} \frac{A_{A-A}}{r_3^6} + \ldots\ldots \tag{9}$$

Rearrange equation (9), the effective coordination number n_c, which is corresponding to total interaction energy with all shells but with a pair coordination distance equal to the first coordination distance, can be calculated from the following equation:

$$n_c = n_{c1} + n_{c2}\left(\frac{r_{equi}}{r_2}\right)^6 + n_{c3}\left(\frac{r_{equi}}{r_3}\right)^6 + n_{c4}\left(\frac{r_{equi}}{r_4}\right)^6 + \ldots\ldots \quad (10)$$

The effective coordination number of PEI samples and liquid nitrogen was calculated using three coordination shells in equation (10). Using fourth and higher coordination shells in equation (10) had no significant effect on the total coordination number. The effective coordination number of PEI was divided by the number of atoms in one repeat unit (69 atoms) in order to obtain a result based on the number of repeat units rather than the number of atoms. The effective coordination number for N_2 and both PEI samples were reported in Table 5.2.

Table 5.2 Properties of liquid nitrogen (at 65 K and saturated pressure) and PEI samples (at 298.15 K and 1 atm) and their structural and intermolecular force parameters.

Properties	Liquid N_2	PEI clear film	PEI membrane	units
Bulk density	0.8596	1.27	1.27	g/cm^3
Molar volume, V_M	32.589	466.598	466.598	cm^3/mole
Non-polar *HSP* [a]		19.6	19.6	[Joule/cm^3]$^{0.5}$
Polar *HSP* [a]		16.6 [d]	16.6 [d]	[Joule/cm^3]$^{0.5}$
Non-polar cohesive energy, ΔU_d	5449.3 ± 109	179248.5 ± 1295	179248.5 ± 1295	J/ mole
Polar cohesive energy, ΔU_p		64745.2	64745.2	J/ mole
Total cohesive energy	5449.3 ± 109	243993.7 ± 4880	243993.7 ± 4880	J/ mole
Effective coordination number (*XRD*) [b]	24 ± 0.5	116 ± 0.5	117 ± 0.5	atom / coordination unit
Effective coordination number (*XRD*) [b]	12	1.68	1.69	molecule / coordination unit
Intermolecular force distance parameter (*XRD*) [b]	0.369 ± 0.002	0.483 ± 0.002	0.492 ± 0.002	nm
Intermolecular force energy parameter [c], ε	1.5E-21	4.82E-19	4.79E-19	Joule/pair of molecules
Intermolecular force energy parameter [c], ε/κ_B	109 ± 4	34911	34613	K/pair of molecules
Intermolecular force energy parameter [c], ε/κ_B		506 ± 20	502 ± 20	K/average pair of atoms

[a] Hansen Solubility Parameter, [b] X – Ray Diffraction, [c] Using cohesive energy and [d] including hydrogen bonding.
Note: for PEI, repeat unit is expressed by a molecule or mole.

The coordination angle can be calculated from the first and second coordination shell distance using the following equation [4]:

$$\theta_u = 2\sin^{-1}\left(\frac{r_2}{r_1}\right) \tag{11}$$

4.3 Effective intermolecular force parameters

The effective intermolecular force energy parameters of liquid nitrogen at 65 K and the two PEI samples at 298.15 K were calculated using equation (3). The effective coordination number, n_c was calculated from X-ray diffraction measurements using equation (10), the cohesive energy of liquid nitrogen at 65 K was calculated from the difference in the molar internal energy between liquid and gas phase at a vapor pressure corresponding to the same temperature (i.e. 65 K and 0.174 bar) obtained from the *NIST* webbook [58]. The cohesive energies of one repeat unit of PEI for non-polar and polar part at 298.15 K were determined from the Hansen solubility parameters of PEI (Ultem 1000), found elsewhere [42].

The effective pair intermolecular force energy was divided by Boltzmann's constant, converting it to Kelvin as usually reported in the literature [21].

5 RESULTS AND DISCUSSION

5.1 Radial atomic density distribution function

The local microscopic structure of amorphous liquid nitrogen (at 65 K and 0.174 bar) and two PEI samples having different porosities (as amorphous solids at 298.15 K and 1.013 bar) were represented by the radial pair atomic density distribution function determined from Wide angle X-ray Diffraction within a range of less than 1.2 nm around a reference site. This local micro-structural data was represented as shown in Figures 5.1, 5.2 and 5.3. Table 5.3 lists the values of r_1, r_2, r_3 and the differences between the center of these shells for liquid nitrogen and both PEI samples. As noticed from Table 5.3 the distance between the successive shells is much lower for both PEI samples than it is for nitrogen that can be attributed to the larger average intermolecular distance of PEI relative to nitrogen. This can also be observed by the lower coordination angle for PEI

(θ_u =103-105°, obtained from equation (11) compared to that of liquid nitrogen (θ_u = 155°).

Table 5.3 Radius of coordination shells and coordination angles for Nitrogen and PEI samples.

Material	r_1 (nm)	r_2 (nm)	r_3 (nm)	$r_2 - r_1$ (nm)	$r_3 - r_2$ (nm)	θ_u *(degree)*
Nitrogen	0.369	0.72	1.04	0.351	0.32	155
PEI clear film	0.483	0.769	1.039	0.286	0.27	103
PEI membrane	0.492	0.77	1.037	0.278	0.267	105

As shown in Table 5.3, slight differences were found between the two PEI samples. The distance between the two successive shells is slightly lower in the membrane cast using NMP than that for the clear film cast using CH_2Cl_2. The first coordination distance or angle is slightly greater in the membrane cast using NMP solvent. These results are attributed to the presence of slight residue of NMP slovent that is more difficult to be removed compared to dichlormethane used in preparing the clear PEI film. The residual NMP solvent acts as a plasticizer in polyimides [59]. However, drying and annealing of the polymeric membrane did remove a significant amount of the residual solvent and leads to approach the local equilibrium intermolecular distance of the pure polymeric material. This can be observed in Figures 5.2 and 5.3 by the slight differences between the two PEI samples.

5.2 Intermolecular force distance parameter

Intermolecular force distance parameters of liquid nitrogen and two PEI samples were determined from X-ray diffraction measurements using the RAD program as well as from computational chemistry. The excellent agreement with all results by both techniques and for both liquid nitrogen and PEI, shown in Table 5.4, indicates the validity and the applicability of the proposed approach in the determination of the intermolecular force distance parameter. The experimental error in this parameter using X-ray diffraction was found elsowhere [60] to be ± 0.002 nm. However, the error in the intermolecular force distance parameter of two isolated nitrogen molecules is greater than

0.002 nm while it is within the experimental error when a cluster of nitrogen is used. This is because nitrogen molecules can form clusters in a liquid phase. For PEI samples, the difference between the intermolecular force distance parameter is slightly greater than the experimental error due to the presence of a trace amount of NMP slovent in the PEI membrane prepared using NMP.

Table 5.4 The effective pair intermolecular force distance parameter of Liquid N_2 and polyetherimide, as determined in this work using X-ray diffraction and computational chemistry.

Material, Conditions and Method (all results from this work)	σ, nm
Liquid N_2 (at 65 K and 0.17404 bar), *XRD* [b]	0.3690
Two isolated N_2 (at 0 K), *ab initio* Large basis 6-31 G**	0.3693
Two isolated N_2 (at 65 K), *ab initio* Large basis 6-31 G** and *MD* [e]	0.3208
Isolated cluster of 12 N_2 (at 0 K), *AM1* semiempirical	0.3710 [f]
Isolated cluster of 12 N_2 (at 65 K), *AM1* semiempirical	0.3688
Polyetherimide, symmetric membrane (at 298.15 K and 1.01325 bar), *XRD* [b]	0.483
Polyetherimide, asymmetric membrane (at 298.15 K and 1.01325 bar), *XRD* [b]	0.492
Polyetherimide (at 0 K), *MM+* and *CNDO* semiempirical	0.49

[b] X - Ray Diffraction measurements
[e] Molecular Dynamics simulation
[f] an average distance between pair of molecules in the cluster using equation (7).

As there are many experimental studies for liquid nitrogen, the results of this work were compared to those found in the literature. The equilibrium intermolecular force distance parameter, σ_{equi} represents the thermodynamic equilibrium average distance of a pure material between a pair of molecules at the experimental conditions and when the system is at its minimum potential energy. The intermolecular force distance parameter, σ_o is usually defined as that corresponding to a system having a zero potential energy. We used the following relation to convert between these two parameters [8, 61]:

$$\sigma_{equi} = \sqrt[6]{2}\,\sigma_o \qquad (10)$$

The equilibrium pair intermolecular force distance parameter determined in this work was compared with the one determined in the literature based on direct experimental

measurements as shown in Table 5.5. An excellent agreement exists between these values. It is also clear that a small change in the intermolecular force distance due to the change in the temperature and pressure can be detected by X-ray diffraction measurements. At 65 K and corresponding saturated pressure, the error in this parameter does not exceed the experimental error (0.002 nm).

Table 5.5 Comparing the effective equilibrium pair intermolecular force distance parameter of Liquid N_2 determined in this work with literature values that are based on experimental work at specified conditions.

Method, Conditions and reference	σ, nm
XRD (at 65 K, saturated pressure), this work	0.3690
RISM[g] (at 65 K, saturated pressure)	0.3700[h] [36]
XRD[b] (solid tetragonal γ N_2, at temperature 20.5 K and 4015 atm)	0.3514[f] [62]
XRD[b] (solid cubic α N_2, at temperature 25 K and 1 atm)	0.3590[f] [63]
XRD[b] (at 64 K, saturated pressure)	0.3690 [60]
XRD[b] (at 77 K, saturated pressure)	0.3730 [60]
Infrared spectrum measurement (at 77 K, saturated pressure)	0.3700 [22]

[b] X - Ray Diffraction measurements
[f] an average distance between pair of molecules in the cluster using equation (7).
[g] Reference Interaction Site Model
[h] from σ_o using equation (10)

5.3 Intermolecular force energy parameter

The link between microscopic and macroscopic properties is the key to calculate the intermolecular force energy parameters through using equation (3). This link was established and confirmed to give a valid result as discussed elsewhere [10]. The method for the determination of the coordination number from X-ray diffraction measurement was discussed as mentioned above and its value for nitrogen was determined as 12, see Table 5.2. Computational chemistry (semiempirical *AM1*) was also used to calculate the number of nitrogen molecules in a stable cluster, which can represent this structural parameter. An excellent agreement was found between the two different methods indicating the validity of the method to determine the parameter from X-ray diffraction experiments. We also found that this result is in good agreement with the coordination number reported for nitrogen [10, 37]. The same method for the determination of the

coordination number for other materials was also reported in the literature confirming the applicability of the approach [64-65]. The experimental error in the determined coordination number using X-ray diffraction was reported to be ± 0.5 atom/coordination unit [60].

In addition to the coordination number, the cohesive energy is required to determine the intermolecular force energy parameter. The error in the cohesive energy can be mainly attributed to the experimental error in the enthalpy of vaporization. This can be due to the insignificant error in the work of expansion in equation (5) compared to the error in the heat of vaporization that is reported to be ± 2% [66]. Therefore, the error in the cohesive energy in this work was considered to be ± 2%. The maximum error in the determination of the intermolecular force energy parameter using equation (3) based on the error in the cohesive energy obtained from the heat of vaporization measurements and the error in the coordination number obtained from the X-ray diffraction measurements was esitmated to be 4 %. The last error was calculated form the final results obtained from using the extreme errors for all variables in equation (3).

5.4 Accuracy of the intermolecular force parameters

The intermolecular force parameters determined in this paper for liquid nitrogen were compared with others, which were obtained from potential models as adjustable parameters and reported in the literature, as shown in Table 5.6. In this work, the accuracy of these parameters was estimated through the errors in the coordination shell number and the intermolecular force distance obtained from the X-ray diffraction measurements as well as the error in the cohesive energy obtained from the experimental heat of vaporization as discussed above. Because the intermolecular force parameters have a direct link to two properties: the cohesive energy and the pairwise intermolecular interaction energy coefficient, it is important to examine the accuracy of these parameters through the errors in these two properties. The cohesive energy and the pairwise intermolecular interaction energy coefficient of liquid nitrogen were determined using equation 3 and 4 respectively. The intermolecular force parameters determined in this work were considered as references to calculate the errors in both properties. The results

were included in Table 5.6. It is clear that the estimated properties using reported parameters for liquid nitrogen obtained from potential models as adjustable parameters have significant errors in the predicted cohesive energy between 5 and 74 % that are much greater than the error 2 % estimated in this work. The error in the pairwise intermolecular interaction energy coefficient is between 44 and 81 % when the intermolecular force parameters are calculated as adjustable parameters. This error is much greater than the one estimated in this work (6 %). This can be attributed to the fitting process and the non linear nature of the different potential models.

Table 5.6 Compare the determined intermolecular force parameters of liquid nitrogen at equilibrium and minimum potential energy with ones obtained as adjustable parameters in literature. Resulting errors in the cohesive energy and the pairwise intermolecular interaction energy coefficient were included.

Temp. K	ε/k_B K	σ_{min} nm	ΔU J/mol.	% ΔU Error	A_{int} J nm^6	% A_{int} Error	Remarks and references
65	**109.2**	**0.369**	**5449.3**	**2**	**3.81E-24**	**6**	from experiments, this work
77.35	**99.6**	**0.373**	**4967.7**	**2**	**3.70E-24**	**6**	from experiments, this work
	95.05	0.415	4741.8	14	6.71E-24	78	from compressibility data [61]
77	94.45	0.401	4711.8	15	5.45E-24	44	fitting parameters in L-J potential and N-L-Density Functional Theory[26,67]
77.35	91.5	0.413	4564.7	18	6.29E-24	67	Reference [68]
77	104.2	0.408	5198.2	5	6.61E-24	76	Reference [69]
	35.3	0.372	1761.0	74	1.29E-24	68	from Cheung-Powles by computer simulation [70]
77	101.5	0.406	5063.5	8	6.26E-24	66	L-J and Monte Carlo simulation [71]
77	78.52	0.300	3917.1	31	0.79E-24	81	Reference [72]

[h] from σ_o using equation (10).

5.5 Intermolecular force parameters as intrinsic molecular properties

In this work, two polyetherimide samples were prepared using different techniques: a clear PEI film cast from dichloromethane solution and PEI membrane obtained by coagulation post leaching method using NMP casting solution. The two samples have a different mesoscopic and macroscopic morphology.

The influence of the porosity in the determination of intermolecular force parameters was investigated by characterizing the two films using nitrogen adsorption technique. Both samples were examined for their differences. The clear PEI film was symmetric, colorless and transparent while the membrane cast from NMP solution and prepared by phase inversion process was asymmetric and opaque with a light yellow color. Microscopic examinations of cross-sections verified the symmetric and asymmetric structures of the two films.

Permeation test according to our previous work, chapter II and III in this thesis [46, 48], showed that the clear symmetric PEI film has a very low permeation (for air separation into oxygen and nitrogen, the air permeance is 0.03 *GPU* and the separation factor is 4.68) compared to a higher permeation in the asymmetric PEI membrane (the permeance is 6 *GPU* and the separation factor is 1.15).

The pore size distribution of each film was calculated from nitrogen adsorption isotherms at 77.2 K using the Horvath-Kawazoe slit model as explained elsewhere, chapter IV in this thesis [45, 72], and the results are shown in Figure 5.4. The maximum differential adsorption volume takes place approximately at the same slit width but its intensity is substantial for the asymmetric PEI membrane compared to barely detectable for the clear symmetric PEI film. This can be attributed to the lower accessibility of nitrogen gas at very low pressure to the micropores within the dense polymer structure of PEI clear film. Nitrogen adsorption technique requires accessible high surface area to be useful in the determination of the micropore size distribution.

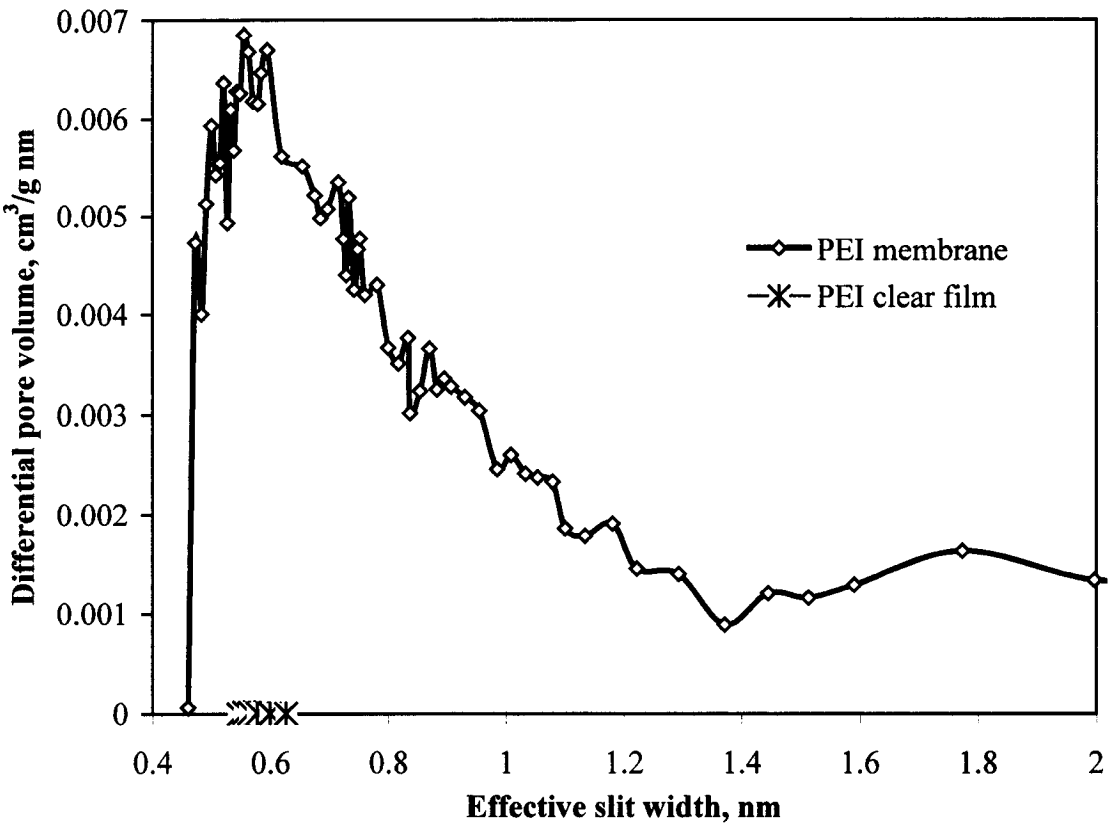

Figure 5.4 Micropore size distribution of PEI samples.

The difference between the intermolecular force distance parameters of two PEI samples, shown in Table 5.2, is 0.01 nm that is exceeding the experimental error (0.002 nm). This can be attributed to a very small amount of residual NMP in the membrane cast from NMP solution. As found elsewhere [73], a small amount of impurity may have large effects on material characterization. Although there is a large difference in the mesoscopic and macroscopic morphology between the two PEI films, the difference in the intermolecular force distance is still very small (0.01 nm) indicating the presence of a dense structure of approximately pure PEI polymer in both samples. The drying and annealing of the two films lead to improve the purity of the dense structure in both PEI samples. The small difference in the intermolecular force distance parameter can be considered as an experimental error due to the presence of a very small amount of impurities. It is clear that the intermolecular force parameters are intrinsic molecular properties of a material (PEI in this study) and are not influenced by the mesoscopic and macroscopic morphology of the porous materials as long as the purity is maintained. It

was shown by others [74] that the d-spacing of aromatic polyesters obtained by wide angle X-ray diffraction and the intrinsic gas permeability are well correlated. The intrinsic gas permeability is influenced by the chemical structure of the polymer as indicated by Robeson's group contribution approach [75]. This also confirmed that the intrinsic properties are related to the local microscopic structure of materials, which can be examined by X-ray diffraction techniques within the suitable distance scale. However, the X-ray diffraction technique was rather insensitive in identifying small changes in the porosity of the PEI samples. This can be attributed to the amorphous nature of the membrane and the wavelength of the X-ray used in this work. X-ray diffraction technique can meausre the most frequent pairwise distance between molecular segments. The presence of different micropore sizes that are close to each other leads to overlap the X-ray diffraction peaks and forms one diffuse peak. This makes the diffraction technique less sensitive to small changes in the microporosity of the amorphous materials. However, the most frequent pairwise distance of density-density correlation can be obtained from X-ray diffraction data within the selected range of possible intermolecular interactions. This pairwise distance correlation represents a statistical average distance available for non-covalent interactions among molecules. The sum of pairwise noncovalent atom-atom energy interactions can be applied for non-spherical molecules and polymers as found elsewhere [33-36].

6 CONCLUSIONS

An approach for the determination of the local microscopic structure and intermolecular force parameters of amorphous liquids and solids was established. The key link between the microscopic and macroscopic properties of materials was found through the non-covalent intermolecular interactions within a coordination shell unit (cluster). The thermodynamic equilbrium structure at a molecular scale of a pure material can be determined from the X-ray diffraction measurements as the most frequent pairwise density-density correlation distance. This represents a statistical average of the inverse of the sixth power of pairwise distances (based on quantum mechanics) among molecules within a cluster in a condensed matter as seen in equation (7). The effective coordination

shell number can be obtained from the pair density-density correlation function using X-ray diffraction data. This coordination number is required to determine the pairwise intermolecular energy parameter (microscopic properties) using equation (3). The error in the coordination shell number obtained from the X-ray diffraction data was estimated to be 4 %.

Structural parameters obtained from X-ray diffraction measurements interpreted using RAD program for amorphous materials were found to be in excellent agreement with those calculated from the optimization of a nitrogen cluster in computational chemistry. These results were also in agreement with those found in the literature when the structural parameters for nitrogen were determined based on experimental measurements.

To examine the applicability of the proposed method on amorphous solids such as PEI, two polyetherimide films were prepared using different techniques; a symmetric film cast from a di-chloromethane/PEI solution while the other cast from a N-Methyl-2-Pyrrolidinone/lithium nitrate/PEI solution and prepared by coagulation post leaching method found elsewhere (chapters II and III in this thesis). Although the two films have different mesoscopic and macroscopic structure, a slight difference was observed in the radial density correlation functions that can be attributed to the presence of a trace of residual NMP in the membrane cast using this solvent. Drying and annealing of PEI samples were useful to reduce the difference in the microstructure of the dense material. The difference in the intermolecular force distance parameter due to presence of NMP impurity was found to be 0.01 nm between the two PEI samples. Due to this small difference, the results confirmed that the values obtained for the intermolecular force distance parameter were not influenced by the mesoporous and macroporous morphology of the PEI films. It is an intrinsic molecular property of the pure polymer material.

The discrepancy in the reported intermolecular force parameters was explained through the large errors in the calculation of cohesive energies and intermolecular energy coefficients. These errors are attributed to ideal assumptions, mathematical trends for the intermolecular interaction potential and considering these parameters as adjustable variables. Reducing these errors through the use of this proposed approach is an important step to understand material structure at a molecular scale. The parameters are

required to quantify the intermolecular and supramolecular interactions in condensed matter.

NOMENCLATURE

$A_{A\text{-}A}$	pair equilibrium intermolecular energy coefficient [J nm^6/molecule]
Ab initio	a quantum mechanics method by which each orbital is determined from the sum of a basis set (primitive geometric functions) [43].
AM1	Austin model 1, a semiempirical, Self-Consistent Field method for computational chemistry calculation [43].
AFM	Atomic Force Microscopy [8]
C_p	heat capacity at constant pressure [J/mol K]
C_v	heat capacity at constant volume [J/mol K]
CNDO	a semiempirical quantum mechanics calculation with Complete Neglect of the Differential Overlap [43]
COMPASS	an empirical molecular mechanics (force field) method [17-18]
g(r)	pair distribution function
GPU	Gas Permeation unit, [1 x 10^{-6} cm^3 (STP) / (cm^2 sec cm Hg)], [48]
HSP	Hansen Solubility Parameter
M_W	molecular weight of one repeat unit of the polymer [Kg/mole]
MD	Molecular Dynamic method to simulate the motion of atoms or molecules in a molecular system [43]
MM+	An empirical Molecular Mechanics (force field) method [43]
n_r	number of r_{ij} used in equation (4), [dimensionless]
N_{AV}	Avogadro's number [molecule/mole]
n_c	effective coordination number [dimensionless]
NIST	National Institute of Standards and Technology
P	absolute Pressure [Pa]
PEI	Polyetherimide polymer (Ultem 1000), [47]
RISM	Reference Interaction Site Model, [33]
R_g	gas constant [Joule/mole K]

r_{ij}	all the possible distances between an atom in one molecule and all other atoms in other molecules [nm]
r_{equi}	effective average pair intermolecular force distance at equilibrium [nm]
r_u	radius of coordination shell taken at the middle of the shell [nm]
$r_1, r_2, r_3,$	equal to r_u corresponding to coordination shell 1, 2, 3, respectively [nm]
SFA	Surface Force Apparatus [8]
T	absolute temperature [K]
T_B	boiling point at a given pressure [K]
V	solid molar volume [m^3/mole]
V_g	gas molar volume [m^3/mole]
V_L	liquid molar volume [m^3/mole]
V_u	volume of coordination unit or shell [nm^3/shell]
XRD	X-Ray Diffraction
Z_g	Gas compressibility factor [dimensionless]

Greek Symbols

ΔH^{vap}	molar heat of vaporization at a given condition [Joule/mole]
δ_u	thickness of the coordination shell [nm]
$\Delta U(r_{equi})$	molar cohesive energy at equilibrium [Joule/mole]
$\varepsilon(r_{equi})$	pair equilibrium intermolecular force energy parameter [Joule/molecule]
θ_u	coordination shell angle [degree]
$\rho(r)$	Local atomic or molecular density
$\rho(\infty)$	bulk density
σ_{equi}	pair equilibrium intermolecular force distance parameter at minimum potential energy [nm]
σ_o	pair intermolecular force distance at zero intermolecular potential energy [nm]

REFERENCES

[1] Kaplan, I. G. and Translation editors: S. Fraga and M. Klobukowski, " theory of molecular interactions", Elsevier, Amsterdam, NL (1986).

[2] Lindoy, L. F. and I. M. Atkinson, "Self-Assembly in Spramolecular Systems", The Royal Society of Chemistry, Cambridge, UK (2000).

[3] Balzani, V., A. Credi, F. M. Raymo and J. F. Stoddart, "Artificial Molecular Machines", Angew. Chem. Int. Ed. 39, 3348-3391 (2000).

[4] Elliott, S. R. "Physics of Amorphous Materials", second edition, Longman Scientific and Technical; and John Wiley and Sons, Inc., New York, NY (1990).

[5] Kitaigorodsky, A. I., "Mixed Crystals", Springer-Verlag, Berlin Heidelberg, DE (1984).

[6] Scoles, G., Ed., "The Chemical Physics of Atomic and Molecular Clusters", Proceeding of the International School of Physics, Elsevier Science Publishers, North-Holland, NL (1990).

[7] Berry R. S. and B. M. Smirnov, "Two-state approximation for aggregate states of clusters", Journal of Chemical Physics, 114 (15), 6816-6823 (2001).

[8] Israelachvili, J., "Intermolecular and Surface Forces", Second Edition, Academic Press Inc., San Diego, CA (1991).

[9] Maitland, G. C., M. Rigby, E. B. Smith and W. A. Wakeham, "Intermolecular Forces: their origin and determination", Clarendon Press, Oxford, UK (1981).

[10] Stone, A. J., "The theory of Intermolecular Forces", Clarendon Press, Oxford, UK (1996).

[11] Gans, W. and J. C. A. Boeyens, "Intermolecular Interactions", Plenum Press, New York, NY (1998).

[12] Margenau, H. and N. R. Kestner, "Theory of intermolecular Forces", Pergamon press Ltd., Oxford, UK (1969).

[13] Kranendonk, J. V., Ed., "Intermolecular Spectroscopy and Dynamical Properties of Dense Systems", Proceeding of the International School of Physics, North-Holland Publishing Company, Amsterdam, NL (1980).

[14] Haberland, H., Ed., "Clusters of Atoms and Molecules, Theory, Experiment, and Clusters of atoms", Springer-Verlag, Berlin, DE (1995).

[15] White, A., F. J. Zerilli and H. D. Jones, "Ab Initio Calculation of Intermolecular Potential Parameters for gaseous Decomposition Products of Energetic Materials", DSTO Aeronautical and Maritime Research Laboratory, Australia (2000), pp. 1-43.

[16] Stewart, J. J. P., "MOPAC: A Semiempirical Molecular Orbital Program", Journal of Computer-Aided Molecular Design, (Special Issue), 4 (1) 1-105 (1990).

[17] Yang, J., Y. Ren, A. Tian, and H. Sun, "COMPASS Force Field for 14 Inorganic molecules, He, Ne, Ar, Kr, Xe, H_2, O_2, N_2, NO, CO, CO_2, NO_2, CS_2, and SO_2, in Liquid Phases", Journal of Physical Chemistry, B., 104 (20), 4951-4957 (2000).

[18] Bunte S. W. and H. Sun, "Molecular modeling of energetic materials: The parameterization and validation of nitrate esters in the COMPASS force field", Journal of Physical Chemistry B. 104 (11), 2477-2489 (2000).

[19] Stiel, L. I. and G. Thodos, "Lennard-Jones Force Constants Predicted from Critical Properties", J. Chem. Eng. Data, 7 (2), 234-236 (1962a).

[20] Bromley, L. A. and C. R. Wilke, "Viscosity Behavior of gases", Industrial and Engineering Chemistry, 43 (7), 1641–1648 (1951).

[21] Hirschfelder, J.O., C. F. Curtiss, and R. B. Bird, "Molecular Theory of Gases and Liquids", John Wiley and Sons, Inc., New York, NY (1967).

[22] Long, C. A., G. Henderson and G. E. Ewing, "The infrared Soectrum of the $(N_2)_2$ Van der waals Molecule", Chemical Physics 2 485-489 (1973).

[23] Cohen, R. C. and R. J. Saykally, "Vibration-Rotation-Tunneling Spectroscopy of the Van der Waals Bond: A new look at intermolecular forces", J. Phys. Chem., 96, 1024–1040 (1992).

[24] Ravikovitch, P. I., S. C. O'Domhnaill, A. V. Neimark, F. Schuth and K. K. Unger, "Capillary Hysteresis in Nanopores: Theoretical and Experimental Studies of Nitrogen Adsorption on MCM-41", Langmuir, 11 4765-4772 (1995).

[25] Lastoskie, C. M., N. Quirke and K. E. Gubbins, "Structure of Porous Adsorbents: Analysis Using Density Functional Theory and Molecular Simulation", in "Equilibria and Dynamics of Gas adsorption on Heterogeneous Solid Surfaces", W. Rudzinski, W. A. Steele and G. Zgrablich, Eds., Studies in Surface Science and Catalysis, Volume 101, Elsevier Science, Amsterdam, NL (1997), pp. 745–775.

[26] Neimark, A. V., P. I. Ravikovitch, S. C. O'Domhnaill, M. Grun, F. Schuth and K. K. Unger, "Pore Size Analysis of MCM-41 Type Adsorbents by Means of Nitrogen and Argon Adsorption", Journal of Colloid and Interface science, 207, 159-169 (1998).

[27] Jacobson, S. H., "Molecular modeling Studies of Polymeric Gas Separation and Barrier Materials: Structure and Transport Mechanisms", Polymers for Advanced Technologies, 5 (11) 724-732 (1994).

[28] Shimazu, A., T. Miyazaki and K. Ikeda, "Interpretation of d-spacing Determined by Wide Angle X-ray Scattering in 6FDA-based Polyimide by Molecular Modeling", Journal of Membrane Science, 166 (1) 113-118 (2000).

[29] Petkov, V., G. Holzhueter, U. Troege, Th. Gerber and B. Himmel, "Atomic-scale structure of amorphous TiO2 by electron, X-ray diffraction and reverse Monte Carlo simulations", Journal of Non-Crystalline Solids, 231 (1-2) 17-30 (1998).

[30] Arai, T. and R. L. McGreevy, "RMC Modelling of the Structure of Expanded Liquid Mercury Along the Co-existence Curve", Journal of Physics: Condensed Matter, 10, 9221-9230 (1998).

[31] Kang, S., C. Park, M. Saito and Y. Waseda, "Reverse Monte Carlo Simulation for Determining the Partial Structural Functions of Ge O_2 Glass from the Anomalous X-ray Scattering and Neutron Diffraction Data", Materials Transactions, JIM, 40 (6), 552-555 (1999).

[32] Howe, M. A., "Orientational Correlations in the Liquid Halogens", Molecular Physics, 69 (1) 161-174 (1990).

[33] Chandler, D. and H. C. Andersen, "Optimized Cluster Expansions for Classical Fluids, II. Theory of Molecular Liquids", The Journal of Chemical Physics, 57 (5) 1730–1937 (1972).

[34] Janssen, R. H. C., S. Wang, E. Nies and P. Cifra, "Lattice Polymers with Nearest-neighbor Interactions: A Comparison of Polymer RISM Theory Employing Atomic Closures and Monte Carlo Simulations", Macromolecules, 32 (2) 471-479 (1999).

[35] Kojima, K. and K. Arakawa, "Computation of the Correlation Functions for Fluids Composed of Diatomic Molecules by means of the Method of Integral Equations", Bulletin of the Chemical Society of Japan, 51 (7), 1977 –1981 (1978).

[36] Kojima, K. and K. Arakawa, "Correlation Functions Calculated by Using Reference Interaction Site Model Equations for Diatomic Molecular Fluids", Bulletin of the Chemical Society of Japan, 53 (7), 1995 –1800 (1980).

[37] Radnai, T., I. Bako, P. Jedlovszky and G. Palinkas, "A Reverse Monte Carlo and RISM Integral Equation Study of Liquid Nitrogen", Molecular Physics, 83 (3) 459 – 470 (1994).

[38] Goudeau, S., J. Galy, J. F. Gerard, R. Fulchiron and J. L. Barrat, "Modelling Surface Properties of Linear Amorphous Polymers", Materials Research Society Symposium – Proceedings, 629 (2000) pp. FF9.2.1-FF9.2.6.

[39] Petkov, V., "RAD, A Program for Analysis of X-ray Diffraction Data from Amorphous Materials for Personal Computers", J. Appl. Cryst. 22, 387-389 (1989). (last upgraded: Sept., 2001).

[40] Spackman, M. A., "Molecular Electric Moments from X-ray Diffraction Data", Chemical Reviews, 92, 1769-1797 (1992).

[41] Roe, R-J., "Methods of X-Ray and Neutron Scattering in Polymer Science", Oxford University Press, Inc., New York, NY (2000).

[42] Hansen, C. M., "Hansen Solubility, Parameters: A User's Handbook", CRC Press, Boca Raton, FL (2000).

[43] HyperChem Pro 5.1 program, Hypercube Inc., Gainesville, FL, USA.

[44] Miller, J, support staff, Hypercube Inc., Gainesville, FL (2002).

[45] Kurdi, J. and A. Y. Tremblay, "The Determination of Interaction Parameters in the Characterization of Polyetherimide Gas Separation Membranes Using Horvath-Kawazoe Model", Desalination, 148, 341-346 (2002), (chapter IV in this thesis).

[46] Kurdi, J. and A. Y. Tremblay, "The influence of casting solution structure on the microporosity of polyetherimide gas separation membranes prepared by the coagulation post-leaching method", J. Membrane Sci. 184 (2), 175-186 (2001), (chapter III in this thesis).

[47] Ultem 1000, GE Plastics, One Plastics Avenue, Pittsfield, MA 01201, U. S. A.

[48] Kurdi, J. and A. Y. Tremblay, "Preparation of Defect-Free Asymmetric Membrane for Gas Separations", Journal of Applied Polymer Science, 73 (8) 1471-1482 (1999), (chapter II in this thesis).

[49] Narten, A. H. and E. Johnson, "Atom Pair Potentials of Liquid Nitrogen from Diffraction Data", Journal of Chemical Physics, 73 (3), 1248 –1255 (1980).

[50] Ultem PEI polyetherimide datasheet; Boedeker Plastics, Inc., 904 West 6th Street, Shiner, Texas 77984, USA.

[51] Wilson, A. J. C. (Ed.), "International Tables for Crystallography", Volume C, Mathematical, Physical and Chemical Tables, Kluwer Academic Publishers, Dordrecht, NL (1992).

[52] Alger, M., "polymer Science dictionary", second edition, Chapman and Hall, New York, NY (1997).

[53] Klug, H. and L. E. Alexander, "X-Ray Diffraction Procedures: For Polycrystalline and Amorphous Materials", A Wiley-Interscience Publication: John Wiley and Sons, New York, NY (1974).

[54] Waseda, Y., "The Structure of Non-Crystalline Materials: liquid and Amorphous Solids", McGraw-Hill International Book Company, New York, NY (1980).

[55] Waring, J. R., R. Lovell, R. Mitchell and A. H. Windle, "Radial Distribution Functions of Non-Crystalline Polymers and Their Applications to the Structural Analysis of PMMA", Journal of materials Science, 17, 1171–1186 (1982).

[56] Nasr, S. "H-bonding in Amorphous Acetamide CH_3CONH_2 as Studied by X-ray Scattering", Journal of Chemical Physics. 115 (14) 6569-6577 (2001).

[57] Desiraju, G. R. and T. Steiner, "The Weak Hydrogen Bond: In Structural Chemistry and Biology, Oxford University Press, New York, NY (1999).

[58] NIST Chemistry Webbook, "Thermophysical Properties of Fluid Systems", NIST Standard Reference Database Number 69 - July 2001 Release.

[59] Nishino, T., M. Kotera, N. Inayoshi, N. Miki and K. Nakamae, "Residual Stress and Microstructures of aromatic Polyimide with different Imidization Processes", Polymer, 41, 6913-6918 (2000).

[60] Furumoto, H. W. and C. H. Shaw, "X-ray Diffraction in Liquids–Nitrogen, Oxygen, and their Mixtures", The Physics of Fluids, 7 (7), 1026–1029 (1964).

[61] Bretsznajder, S. and J. Bandrowski, "Prediction of Transport and Other Physical Properties of Fluids", Pergamon Press, Oxford, UK (1971).

[62] Schuch, A. F. and R. L. Mills, "Crystal Structures of the three Modifications of Nitrogen 14 and Nitrogen 15 at High Pressure", The Journal of Chemical Physics, 52 (12) 6000-6008 (1970).

[63] Jordan, T. H., H. W. Smith, W. E. Streib and W. N. Lipscomb, "Single-Crystal X-Ray Diffraction Studies of α-N_2 and β-N_2", The Journal of Chemical Physics, 41 (3) 756-759 (1964).

[64] Nield, V. M. and P. T. Verronen, "The Structure of Expanded Mercury", Journal of Physics: Condensed Matter, 10, 8147–8153 (1998).

[65] Radnai, T. and H. Ohtaki, "X-ray Diffraction Studies on the Structure of Water at High Temperatures and Pressures", Molecular Physics, 87 (1), 103–121 (1996).

[66] Jacobsen, R. T., R. B. Stewart and M. Jahangiri, "Thermodynamic Properties of Nitrogen from Freezing Line to 2000 K at Pressures to 1000 Mpa", J. Phys. Chem. Ref. Data, 15 (2), 735-909 (1986).

[67] Ravikovitch P. I., D. Wei, W. T. Chueh, G. L. Haller and A. V. Neimark, Evaluation of Pore Structure Parameters of MCM-41 Catalyst Supports and Catalyst by Means of Nitrogen and Argon Adsorption", Journal of Physical Chemistry B. 101(19), 3671-3679 (1997).

[68] Sonwane, C. G. and S. K. Bhatia, "Characterization of Pore Size Distributions of Mesoporous Materials from Adsorption Isotherms", J. Phys. Chem. B: 104 (39) 9099-9110 (2000).

[69] Ohba, T., T. Suzuki and K. Kaneko, "Preformed Monolayer-induced Filling of Moleculaes in Micropores", Chemical Physics Letters, 326, 158-162 (2000).

[70] Razmus, D. M. and Hall, C. K., "Prediction of Gas Adsorption in 5A Zeolites Using Monte Carlo Simulation", AIChE Journal, 37 (5) 769-779 (1991).

[71] Ravikovitch, P. I., A. Vishnyakov, R. Russo and A. V. Neimark, "Unified approach to pore size characterization of microporous carbonaceous materials from N_2, Ar, and CO_2 adsorption isotherms", Langmuir 16 (5) 2311-2320 (2000).

[72] Horvath, G. and K. Kawazoe, "Method for the calculation of effective pore size distribution in molecular sieve carbon", Journal of chemical engineering of Japan,16 (6), 470-475 (1983).

[73] Ha, D. H., S. Byon, Y.-I. Kim, "Correction of impurity effects on the characterization of YBCO superconductor", Physica C, 333 (1-2) 72-78 (2000).

[74] Charati, S. G.; Houde, A. Y.; Kulkarni, S. S.; Kulkarni, M. G., Transport of Gases in Aromatic Polyesters: Correlation with WAXD Studies" J. Polym. Sci., B: Polym. Phys., 29 (8), 921-931 (1991).

[75] Robeson, L. M.; Smith, C.D.; Langsam, M. "A group contribution approach to predict permeability and permselectivity of aromatic polymers" J. Membrane Sci., 132 (1), 33-54 (1997).

CHAPTER VI

Determination of Intermolecular Force Parameters and the Interaction Energy Coefficient for Non-polar Liquids as a Function of Temperature

J. Kurdi, and A. Y. Tremblay*

Department of Chemical Engineering, University of Ottawa, 161 Louis Pasteur, Ottawa, Ontario, K1N 6N5, Canada

*Corresponding author
André Y. Tremblay
Tel.: +1-613-562-5920; fax: +1-613-562-5172
E-mail address: tremblay@uottawa.ca

CHAPTER VI

Paper 5: Determination of intermolecular force parameters and the interaction energy coefficient for non-polar liquids as a function of temperature

J. Kurdi, and A. Y. Tremblay
Department of Chemical Engineering, University of Ottawa, 161 Louis Pasteur, Ottawa, Canada, K1N 6N5

ABSTRACT

The equilibrium pair intermolecular force parameters, the interaction energy coefficient and the coordination number of liquid nitrogen were investigated along the nitrogen liquid-gas phase transition curve. The methods of calculating these parameters as a function of temperature from the properties' data were illustrated. A set of equations was derived to calculate these parameters at different temperatures from critical properties. The parameters for liquid nitrogen, calculated from these derived equations, are in good agreement with experimental observations. Using the results of the above methods, it was possible to investigate the discrepancy between theory and experiment in the determination of the intermolecular interaction energy coefficient. The excess repulsive electron-correlation energy responsible for this discrepancy was determined for liquid nitrogen at different equilibrium intermolecular force distances corresponding to different boiling points. It was found that the minimum excess repulsive electron-correlation energy coefficient occurs at an intermolecular distance of 0.393 nm and boiling point 112 K. At this distance, electron-correlation obeys the quantum mechanics virial theorem. Indeed, the results explain the influence of temperatures on the length, energy and stability of the coordination non-covalent bonds among liquid nitrogen molecules.

Keywords: Critical properties; Vapour-liquid equilibria; Intermolecular force parameters; nitrogen; interaction energy coefficients; microscopic scales

1 INTRODUCTION

Intermolecular force parameters are intrinsic properties of an ensemble of similar or different molecules. They represent the interaction among molecules that leads to an inherent structure having its own static and dynamic properties. In a single phase, bulk material structures and properties are influenced by the applied conditions (temperature and pressure) according to the equation of state and the heat capacity obeying the static and steady state of the equilibrium thermodynamic laws.

In the gas phase, the intermolecular forces are responsible for the condition-dependent deviation of the ideal gas law (Maitland, 1981). In the condensed phases (liquids or solids), the formation of weak non-covalent bonds among similar or different molecules are reasons for material condensation and bulk phase transition (Beck et al. 1990). The denser structures and the higher interaction energies of liquids or solids than those of gases can be more easily observed by diffraction measurements (Ben-Naim, 1992 and Waseda, 1980) and calorimeter experiments (Lerchner et al. 1999).

At the same temperature and pressure on the phase transition curve, molecules in the gas phase have a larger vibration-rotation (VR) frequency contribution (leading to larger density relaxation) than that in the liquid phase (Gayathri and Bagchi, 1999). The VR frequency contribution in the gas phase carries enough energy to work against external pressure and keeps molecules apart with the longer range of repulsive forces dominating among molecules. However, the resonance-energy transfer contribution in the gas phase is smaller than in the liquid phase (Gayathri and Bagchi, 1999). This is reflected in the observed thermal conductivity and speed of sound (NIST, 2002) where the gas phase has lower values than the ones for the liquid phase. On the other hand, in the liquid phase, the VR frequency contribution has not enough energy to overcome the external pressure and molecules become close enough to share their electrons in weak non-covalent bonds. Mutual electromagnetic interactions among molecules leads to an increase in the resonance-energy transfer contribution, which explains the larger thermal conductivity and higher speed of sound in condensed phases.

Major changes in the molecular properties occur at the liquid-gas phase transition curve. The heat of vaporization required to determine the intermolecular force

parameters can be only determined along this curve from calorimetric experiments (Giauque and Clayton, 1933). Therefore, we have limited this study to the intermolecular forces of nitrogen along the gas-phase transition curve.

Hirschfelder et al.1954, considered these physical parameters as adjustable force constants independent of temperature and pressure. Recently, White et al., 2002, considered them dependent on temperature only. This work considers the influence of both temperature and pressure on the intermolecular force parameters based on experimental measurements. At one condition, the determination of the local microscopic structure and the intermolecular force parameters from experimental X-ray diffraction and cohesive energy was illustrated in our previous work (Kurdi and Tremblay, chapter V).

In this paper, the influence of temperature and pressure on various intermolecular parameters that include: the coordination number, intermolecular force parameters, interaction and excess repulsive correlation energy coefficients were discussed. These parameters were determined for liquid nitrogen along the saturated liquid-gas transition curve as a function of boiling point. Equations were derived to calculate these parameters at the saturated curve from critical properties.

The influence of temperature on the interaction and excess repulsive correlation energy coefficients was also investigated. The critical distance at which the mutual resonance-energy transfer contribution among molecules starts to be insignificant was also determined.

2 APPROACHES

2.1 Calculation of the intermolecular force parameters at different conditions

The equilibrium pair intermolecular force parameters of a liquid or solid can be determined accurately at certain temperatures and pressures from X-ray diffraction and cohesive energy measurements. The intermolecular force distance parameter and the coordination shell number can be obtained from the pair radial distribution function as explained elsewhere (Kurdi and Tremblay, chapter V). The equilibrium pair

intermolecular force energy parameter at a given temperature and pressure (T,P) can be obtained from the following equation (Stone, 1996):

$$\Delta U(T,P) = \frac{1}{2} N_{AV}\, n_c(T,P)\varepsilon(T,P) \tag{1}$$

where $\Delta U(T,P)$ is the molar cohesive energy, N_{AV} is the Avogadro's number, $n_{c(T,P)}$ is the coordination shell number and $\varepsilon(T,P)$ is the pair equilibrium force energy parameter.

The influence of temperature and pressure on structural parameters can be related directly to the change in the bulk density of the liquid. The intermolecular force distance parameter has a linear relationship with the third power of liquid molecular volume, $[V_L(T,P)/N_{AV}]^{(1/3)}$, when a homogeneous contraction or expansion is assumed (Radnai and Ohtaki, 1996). Therefore, the equilibrium pair intermolecular force distance at different conditions, (T,P), can be given as follows:

$$\sigma_{equi}(T,P) = m_s\left(\frac{V_L(T,P)}{N_{AV}}\right)^{1/3)} + C_s \tag{2}$$

where m_s is the slope of the linear relationship and C_s is a constant that can be calculated from the fitting of at least two experimental points in the above equation.

Because the calculation of the coordination number obtained from the pair radial distribution density functions was determined from X-ray diffraction based on the area of the peak between its two minima, a linear relationship between the coordination number and the density that pass through the origin (0,0) will be achieved as found elsewhere (Nield and Verronen, 1998; Radnai and Ohtaki, 1996). The coordination number at different conditions is then inversely proportional to the molar volume given as follows:

$$n_c(T,P) = n_c(T_R,P_R)\left[\frac{V_L(T_R,P_R)}{V_L(T,P)}\right] \tag{3}$$

where the subscript R refer to a reference temperature or pressure. It is often to take the boiling point at 1 atm but it could be any other conditions.

The saturated liquid molar volume used in equations (2) and (3) can be calculated along the liquid-gas phase transition curve as a function of temperature and critical properties of a component by using Rackett equation (Poling et al. 2001) as follows:

$$\left[\frac{V_L(T,P)}{V_L(T_R,P_R)}\right] = Z_c^{\Phi} \tag{4}$$

where Z_c is the critical compressibility factor and Φ is given by the following equation:

$$\Phi = \left[1-(T/T_c)\right]^{(2/7)} - \left[1-(T_R/T_c)\right]^{(2/7)} \tag{5}$$

where T_c and T_R are the critical and the reference temperatures respectively.

The influence of temperature on the cohesive energy can be obtained from the temperature dependence of heat of vaporization through Watson's equation (Reinhard and Drefahl, 1999) as follows:

$$\frac{\Delta H_v(T,P)}{\Delta H_v(T_b)} = \left(\frac{1-(T/T_c)}{1-(T_b/T_c)}\right)^n \tag{6}$$

where $\Delta H_v(T,P)$ is the normal heat of vaporization, T_b is the normal boiling point, and n is a constant given by the following equations:

$$n = 0.30 \qquad if\,(T_b/T_c) < 0.57 \tag{7}$$

$$n = 0.74(T_b/T_c) - 0.116 \qquad if\, 0.57 \le (T_b/T_c) \le 0.71 \tag{8}$$

$$n = 0.41 \qquad if\,(T_b/T_c) > 0.71 \tag{9}$$

It is worth noting that Watson's equation cannot be used with compounds, which exhibit a strong association in the vapor phase (Reinhard and Drefahl, 1999).

The cohesive energy can be calculated from the heat of vaporization using the following equation (Smith, 1990):

$$\Delta H_v(T,P) = \Delta U(T,P) + P(V_g(T,P) - V_L(T,P)) \tag{10}$$

where $V_g(T,P_s)$ and $V_L(T, P_s)$ are the molar volume of the gas and the liquid respectively. Equation (10) is applied at saturated conditions.

The equilibrium pair intermolecular force distance at saturated pressure can be calculated from the critical properties as a function of temperature by combining equations (2), (4) and (5) as follows:

$$[\sigma_{equi}(T,p) - C_s] = [\sigma_{equi}(T_R,P_R) - C_s]\frac{(Z_c^{(1/3)})(1-T/T_c)^{(2/7)}}{(Z_c^{(1/3)})(1-T_R/T_c)^{(2/7)}} \tag{11}$$

The coordination number at different temperatures and saturated pressures can also be calculated from combining equations (3), (4) and (5) to obtain the following equations:

$$n_c(T,P) = n_c(T_R,P_R)\frac{Z_c^{(1-T_R/T_c)^{(2/7)}}}{Z_c^{(1-T/T_c)^{(2/7)}}} \tag{12}$$

The cohesive energy at different temperatures and saturated pressures can be obtained by combining equations (6) and (10) as follows:

$$\frac{\Delta U(T,P_s)+P_s(V_g(T,P_s)-V_L(T,P_s))}{\Delta U(T_b)+P_s(T_b)(V_g(T_b)-V_L(T_b))} = \left(\frac{1-(T/T_c)}{1-(T_b/T_c)}\right)^n \tag{13}$$

where $P_s(T_b)$ is equal to 101325 [Pa]. Equation (13) can be used to calculate the cohesive energy at different temperatures and with equations (1) and (12), it is possible to calculate the intermolecular force energy parameter at different temperatures from critical properties and the compressibility of the liquid and gas phases.

2.2 Direct method of calculating the interaction energy coefficient

Intermolecular interaction energy coefficient is an essential parameter in the determination of interaction energies among molecules. It is of great importance to investigate the influence of temperature on this parameter and its components. The total interaction energy coefficient can be easily calculated from the pair intermolecular force parameters using the known Fritz London equation (Hirschfelder, 1967):

$$-\varepsilon(T,P) = \frac{-A_{\text{int}}(T,P)}{\sigma_{equi}^6(T,P)} \tag{14}$$

where $A_{int}(T,P)$ is the total interaction energy coefficient that includes both the attractive and the repulsive interactions at a thermodynamic equilibrium distance $\sigma_{equi}(T,P)$.

The pair intermolecular interaction energy coefficient is related to the electronic and magnetic properties of molecules and their electrostatic and electrodynamics' interactions. Many methods such as London, Slater-Kirkwood and Kirkwood-Muller formulae were developed to calculate the attractive dispersion energy (Pitzer, 1959). According to the Kirkwood-Muller approach, the attractive dispersion energy is proportional to the polarizability and diamagnetic susceptibility (Muller, 1936). However, a correction term, which accounts for the repulsive forces of electrons, was

earlier discussed by Vinite, 1932. Muller considers this term to vanish if molecules have a single-electron spherical symmetry (Muller, 1936). In 1960, Salem discussed the problems in the calculation of the dispersion energies. He considered that the discrepancy between theory and experiments is attributed to the neglect of this electron-correlation term (Salem 1960).

Therefore, according to Salem, the pair attractive dispersion energy between two molecules, $\varepsilon_{attr}(T,P)$ is given by the Kirkwood-Muller-Salem formula that includes the electron correlation term as follows:

$$-\varepsilon_{attr}(T,P)=\frac{-3m_eC^2\chi\alpha}{\sigma^6_{equi}(T,P)}+\frac{e^2\alpha}{2\sigma^6_{equi}(T,P)}\sum_{i\neq j}\langle r_i\cdot r_j\rangle \qquad (15)$$

where e and m_e are the charge and mass of electron respectively, C is the velocity of light in vacuum, χ is the diamagnetic susceptibility, α is the polarizability, $\sigma_{equi}(T,P)$ is the equilibrium separation distance between the two molecules, and $\sum_{i\neq j}\langle r_i\cdot r_j\rangle$ is the explicit electron correlation term. All the above properties are determined for a single molecule. The attractive energy is considered as a negative number while the repulsive energy is a positive number. It is worth noting that equation (15) can only be applied on non-polar molecules where the dipole moment is equal to zero. For polar molecules other polar terms should be added.

As the Lennard-Jones (6-12) potential model is found to have the general features of real intermolecular potential energy (as discussed by Maitland et al. 1981 and Israelachvili, 1992) and also with respect to the quantum-mechanical virial theorem (March and Mucci, 1993; Hirschfelder et al. 1967), an equilibrium occurs when the attractive potential energy is equal to twice of the negative value of the repulsive kinetic energy. Therefore the total interaction energy between two molecules can be obtained by taking out a half of equation (15), i.e. dividing equation (15) by 2 as follows:

$$-\varepsilon(T,P)=\frac{-3m_eC^2\chi\alpha}{2\sigma^6_{equi}(T,P)}+\frac{e^2\alpha}{4\sigma^6_{equi}(T,P)}\sum_{i\neq j}\langle r_i\cdot r_j\rangle \qquad (16)$$

In fact, the maximum magnitude of the pair interaction energy is equal to the upper negative limit of equation (16) when the second term on the right hand side of the equation becomes zero. This second term represents an excess repulsive electron

correlation energy due to a deviation in the intermolecular interaction energy from following the quantum-mechanical virial theorem and the Lennard-Jones (6-12) potential model. The deviation is caused by an electron correlation as discussed elsewhere (Vinti, 1932 and Salem, 1960). Therefore, the excess of the repulsive electron correlation energy coefficient can be defined in equation (16) as follows:

$$A_{corr}(T,P) = \frac{e^2\alpha}{4}\sum_{i\neq j}\langle r_i \cdot r_j \rangle \tag{17}$$

Combining equation (14) and (16) with setting the excess of the repulsive correlation energy coefficient to zero, the maximum interaction energy coefficient, $A_{int,max}(T,P)$ can be given by the original Kirkwood-Muller equation as follows:

$$-A_{\text{int,max}}(T,P) = -\varepsilon_{\max}(T,P)\sigma^6_{equi}(T,P) = \frac{-3m_eC^2\chi\alpha}{2} \tag{18}$$

The subscript (max) was added to distinguish the maximum values of these parameters from their actual values. The actual interaction energy coefficient can be obtained by combining equations (14), (16), (17) and (18) as follows:

$$-A_{\text{int}}(T,P) = -A_{\text{int,max}}(T,P) + A_{corr}(T,P) \tag{19}$$

The excess of the repulsive electron correlation energy coefficient $A_{corr}(T,P)$, can be obtained through combining equations (1), (14), (18) and (19) as follows:

$$A_{corr}(T,P) = \frac{3}{2}m_eC^2\chi\alpha - \frac{2\Delta U(T,P)\sigma^6_{equi}(T,P)}{N_{AV}n_c(T,P)} \tag{20}$$

Equation (18), (19) and (20) are useful equations for direct calculation of the intermolecular force parameters from experimental bulk measurements of a condensed matter.

3 RESULTS AND DISCUSSION

The methods discussed to determine the various intermolecular parameters: coordination number, intermolecular force parameters and interaction energy coefficients were applied to liquid nitrogen along the gas-liquid phase transition curve from the triple point 63.151 K to the critical point 126.192 K as defined by Nowak et al. (1997). The results were

also used to calculate the interaction energy coefficient and the excess repulsive electron correlation energy coefficient. The procedures of calculations, results and discussion are explained in the following sections.

3.1 Coordination number of liquid nitrogen at different conditions

The effective coordination shell number of liquid nitrogen at different temperatures and corresponding saturated pressures was calculated from the experimental liquid molar volume found elsewhere (Nowak et al. 1997) and a reference coordination number at 65 K obtained from X-ray diffraction measurement (Kurdi and Tremblay, chapter V) using equation (3). The coordination number at different temperatures was also calculated from the critical properties of nitrogen obtained from Nowak et al. (1997) by using equation (12) derived by us. The results shown in Figure 6.1 indicate an excellent agreement between the above two methods. Providing the molecules' ensemble with energy is required to increase temperature. This leads to a decrease in the coordination number due to an increase in the vibration-rotation frequency (Beck et al. 1990) causing an increase in the intermolecular force distances, breaking some of the non-covalent bonds within the cluster that leads to a decrease in the number of molecules in each coordination shell. The steep decrease in the coordination number near the critical point indicates that each molecule starts to have enough energy to surpass the attractive forces towards other molecules and some of non-covalent bonds were broken leading to a smaller cluster. Forming a cluster through non-covalent bonds becomes impossible when the energy of a molecules' ensemble exceed the energy corresponding to the critical point. The percolation of the coordination bond occurs at a critical coordination number, which corresponds to the minimum coordination number as it approaches zero (Nield et al. 1991; Arai and McGreevy, 1998). The critical coordination number for nitrogen was found to be equal to 4.436 as seen in Figure 6.1. The coordination number was not taken as integer number because it represents the statistical average of many clusters having different coordination numbers.

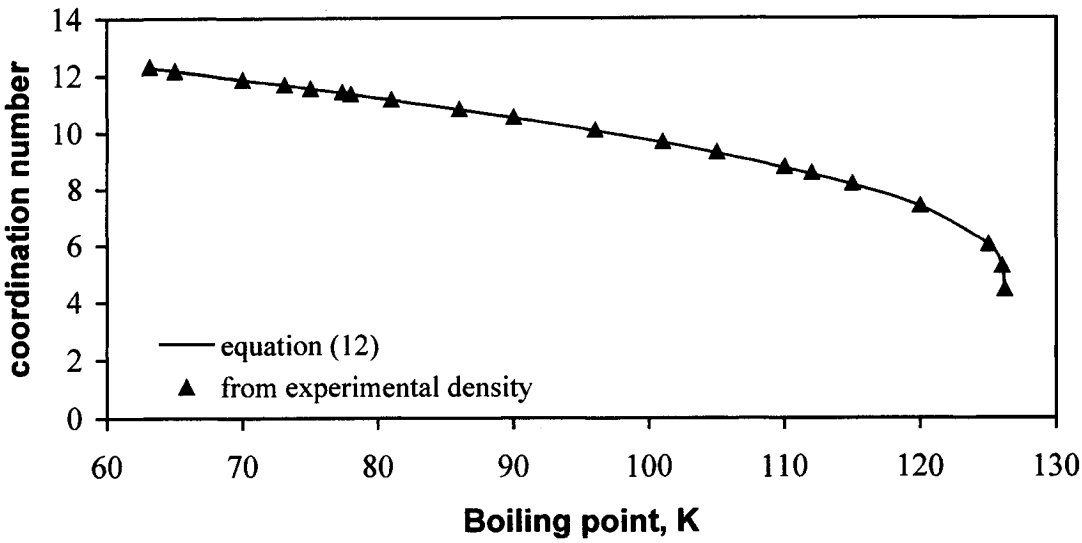

Figure 6.1 Coordination number at different temperatures for liquid nitrogen at saturated pressure.

These results agree with the observation of decreasing the heat of vaporization with increasing temperature along the liquid-gas phase transition curve (Reinhard and Drefahl, 1999). This can be attributed to a decrease in the number of non-covalent bonds per one molecule. The zero heat of vaporization at the critical point does not means that the non-covalent bond has zero interaction energy but indicates the absence of non-covalent bonds.

3.2 Equilibrium pair intermolecular force energy parameter for liquid nitrogen

The equilibrium pair intermolecular force energy for liquid nitrogen at different temperatures and saturated pressures was calculated using equation (1) from the molar cohesive energy and the coordination number obtained from equation (3). The molar cohesive energy was determined by using equation (10). The saturated pressure, molar vapor volume and molar liquid volume of nitrogen were taken from experimental data found elsewhere (Nowak et al. 1997). The heat of vaporization of saturated nitrogen was obtained from Jacobsen et al. (1986) and Din (1961). On the other hand, the intermolecular force energy parameter was also calculated from the molar cohesive

energy obtained from the critical properties and the difference between the gas and liquid molar volume using equation (13). As the results show in Figure 6.2, the agreement is not exact at all temperature ranges but a slight deviation was found near the critical point. The lower precision of equation (13) is attributed to the accuracy of Watson equation that is used to account for the change of the heat of vaporization with temperature. However, an excellent agreement is found when the temperature is far from the critical point (in case of nitrogen T < 110 K). The decrease in the equilibrium pair intermolecular force energy parameter with increasing nitrogen boiling point is attributed to the increase in the molecular chemical potential and vibration-rotation frequency (Beck et al. 1990) that causes an increase in the intermolecular distance and hence a decrease in the molecular cohesive energy. The change becomes very large as temperature approaches the critical point.

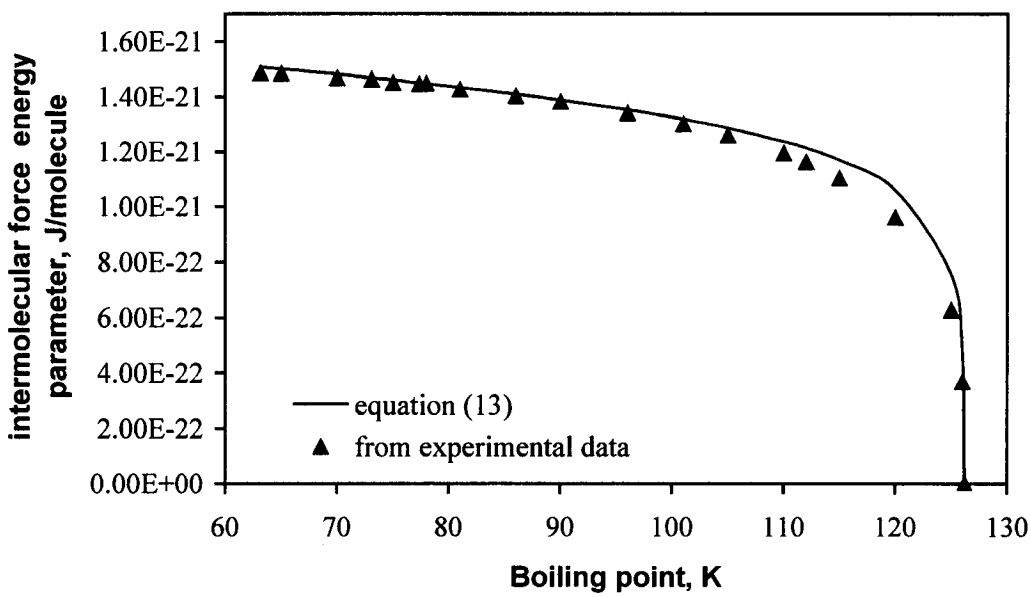

Figure 6.2 Intermolecular force energy parameter at different temperatures for liquid nitrogen at saturated pressure.

3.3 Intermolecular force distance parameter for liquid nitrogen

The equilibrium pair intermolecular force distance parameter of liquid nitrogen at different temperatures and saturated pressures was calculated from the experimental molar volume using equation (2). Two reference X-ray diffraction measurements at 65 K

and 77 K found elsewhere (Kurdi and Tremblay, Chapter V; Furumoto and Shaw, 1964) were used to calculate the slope and the constant in equation (2). The parameter was also calculated from the critical and normal properties using equation (11). The results were plotted in Figure 6.3 and show a slight increase in the intermolecular distance with increasing nitrogen boiling point. It is worth noting that a very small change in the intermolecular distance has a significant change in the interaction energy because energy is proportional to the reverse of distance to the power of six.

A very steep increase in the intermolecular distance can be observed near the critical point indicating that the molecules start to have enough chemical potential energy and vibration-rotation frequency to break down their intermolecular non-covalent bonds. Both calculation methods are in excellent agreement.

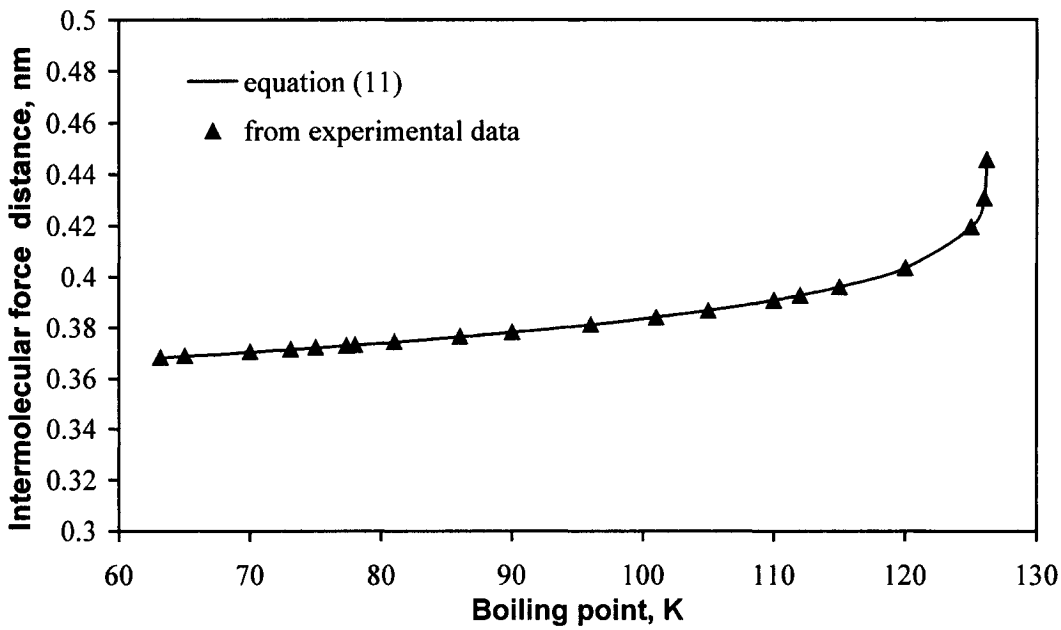

Figure 6.3 Intermolecular force distance at different temperatures for liquid nitrogen at saturated pressure.

3.4 Intermolecular interaction energy coefficient for liquid nitrogen

The intermolecular force interaction energy coefficient and the excess in the repulsive electron correlation energy coefficient of liquid nitrogen at different temperatures were calculated by using equations (14) and (20) respectively and plotted in Figure 6.4. The

non-polar polarizability of liquid nitrogen was calculated from the dielectric constant obtained from CRC Handbook of Chemistry and Physics (Lide, 2002-2003) using the Clausius-Mossotti equation (Bottcher, 1973). The diamagnetic susceptibility is independent of temperature and was also obtained from the CRC Handbook of Chemistry and Physics (Lide, 2002-2003). As shown in Figure 6.4, the intermolecular interaction energy coefficient increases slightly with increasing temperature because liquid nitrogen is a non-polar component and its polarizability is slightly increased by increasing temperature (Bottcher, 1973). The excess repulsive electron correlation energy decreases slightly, as seen in Figure 6.4, leading to a very small contribution in increasing the total actual energy coefficient. The drop in the energy coefficient near the critical point should not be considered because the non-covalent bonds start breaking down at this point.

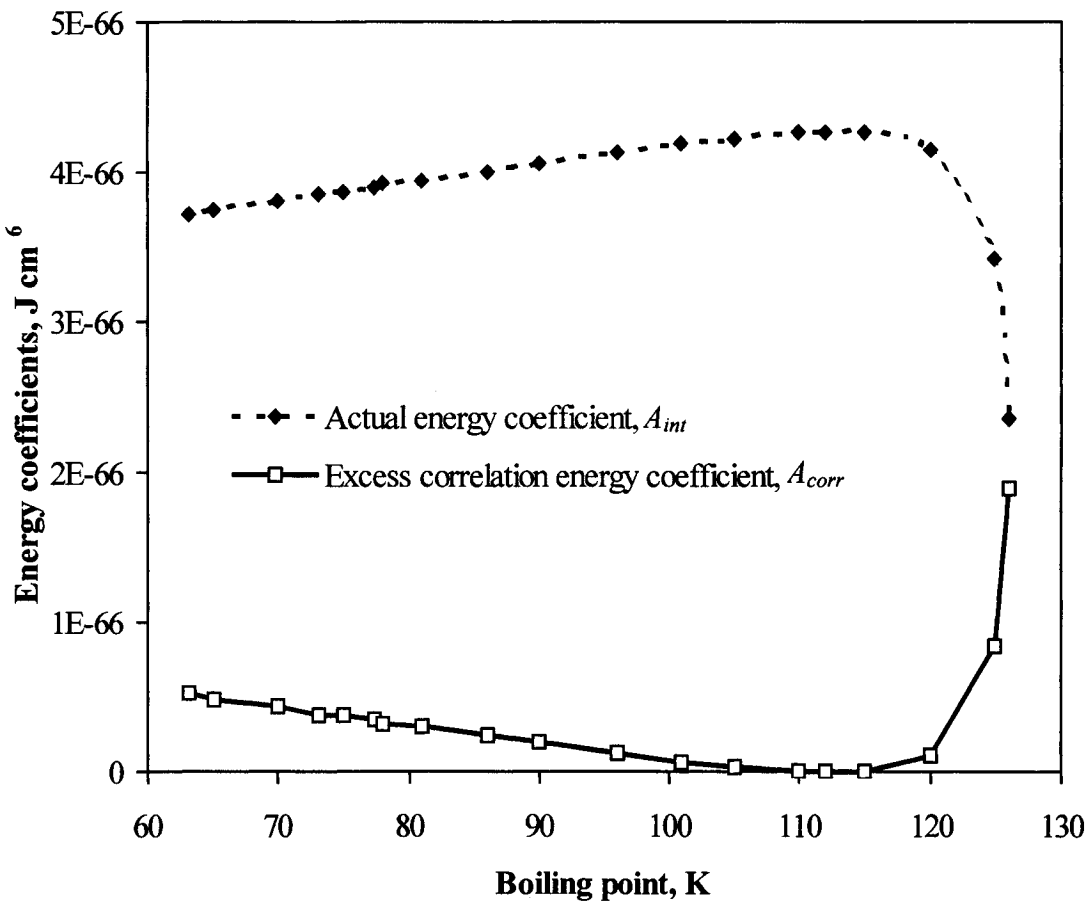

Figure 6.4 Energy and excess correlation energy coefficients at different temperatures for liquid nitrogen at saturated pressure.

3.5 Excess repulsive electron-correlation energy coefficient

Contrary to the interaction energy coefficient and as shown in Figure 6.4, the excess repulsive correlation energy coefficient decreases with increasing nitrogen boiling point due to an increase in the intermolecular distance. Then it increases at temperatures close to the critical point due to an increase in the vibration-rotation frequency of molecules that causes an increase in the non-covalent bond length. Increasing the intermolecular distance leads to an improper electron-correlation within the non-covalent bonds causing an increase in the repulsive energy that contributes to breaking the non-covalent (physical) bonds.

As it was discussed by Salem (1960) and Pitzer (1959), the discrepancy between experiments and theory for the calculation of the intermolecular interaction energy coefficients is due to the neglect of the explicit electron correlation term shown in equation (16). To clarify this discrepancy, we have calculated the intermolecular interaction energy coefficients of some noble gases and nitrogen using Kirkwood-Muller formula neglecting the correlation term. The diamagnetic susceptibility and the polarizability of the liquid phase of these gases at 1 atm were obtained from the CRC Handbook of Chemistry and Physics (83^{rd} ed., 2002-2003). The intermolecular force energy and distance parameters were obtained form the reported values for each gas based on the most extensive literature work (Dham et al. 1989, 1990, Kurdi and Tremblay, chapter V). The intermolecular interaction energy coefficient was then calculated using equation (14). The difference between the two calculated interaction energy coefficients is the excess in the repulsive electron-correlation energy coefficient. The percentage of this excess correlation coefficient as a part of the interaction energy coefficient obtained from the Kirkwood-Muller formula was determined. As shown in Table 6.1, the excess repulsive electron-correlation coefficients for N_2, Ar, Kr and Xe are significant and it increases by increasing the total interaction energy coefficients. This term represents 8.08 % of the total interaction energy coefficient of liquid nitrogen at normal conditions (1 atm and corresponding boiling point). For larger interaction energy, this percentage becomes higher for some selected noble gases shown in Table 6.1, for instance, it is equal to 28% for Xe. These values represent considerable part of the total interaction energy that should not be neglected.

Table 6.1 Properties and parameters for liquified N2, Ar, Kr and Xe at their boiling point and 1 atm. The percentage deviation due to the excess electron-correlation energy coefficient was included.

Properties and parameters	N_2	Ar	Kr	Xe	units
α	1.74E-24	1.64E-24	2.48E-24	4.04E-24	cm^3/molecule
χ	1.99E-29	3.21E-29	4.82E-29	7.56E-29	cm^3/molecule
$A_{int,max}$ eq (18)	4.25E-66	6.47E-66	1.47E-65	3.75E-65	J cm^6
ε	1.43E-21	1.98E-21	2.78E-21	3.90E-21	J
σ_{equi}	3.73E-8	3.76E-8	4.01E-8	4.37E-8	cm
A_{int}, eq (14)	3.85E-66	5.60E-66	1.16E-65	2.70E-65	J cm^6
A_{corr}, eq (20)	3.96E-67	8.68E-67	3.12E-66	1.05E-65	J cm^6
$\left(\frac{A_{corr}}{A_{int,max}}\right)*100$	9.3	13.4	21.2	28	%

Note: Interaction parameters were defined for a pair of molecules.

3.6 Intermolecular and excess electron-correlation energy coefficients

The total interaction and excess repulsive electron correlation energy coefficients of liquid nitrogen were plotted in Figure 6.5 as a function of the intermolecular force distance. The total pair intermolecular energy coefficient increases slightly with an increase in the intermolecular distance (or in the boiling point of nitrogen as in Figure 6.4) due to a very small increase in the liquid polarizability. This indicates that the change in the intermolecular force distance has insignificant influence on the total interaction energy coefficient. However, there is a critical intermolecular distance where non-covalent bonds start to break down. We have found that the interaction energy coefficient of liquid nitrogen reaches its maximum value at a distance of 0.393 nm as shown in Figure 6.5 before it starts to drop significantly at a distance of 0.404 nm because of two reasons: first, the improper distance for an optimum electron-correlation leads to an increase in the anti-binding electrons contribution that is responsible for

repulsive forces and second, molecules start to lose their mutual significant resonance-energy transfer contribution due to an increase in the intermolecular force distance. The critical maximum intermolecular distance that determined before the total noncovalent bonds are broken was found to be 0.431 nm.

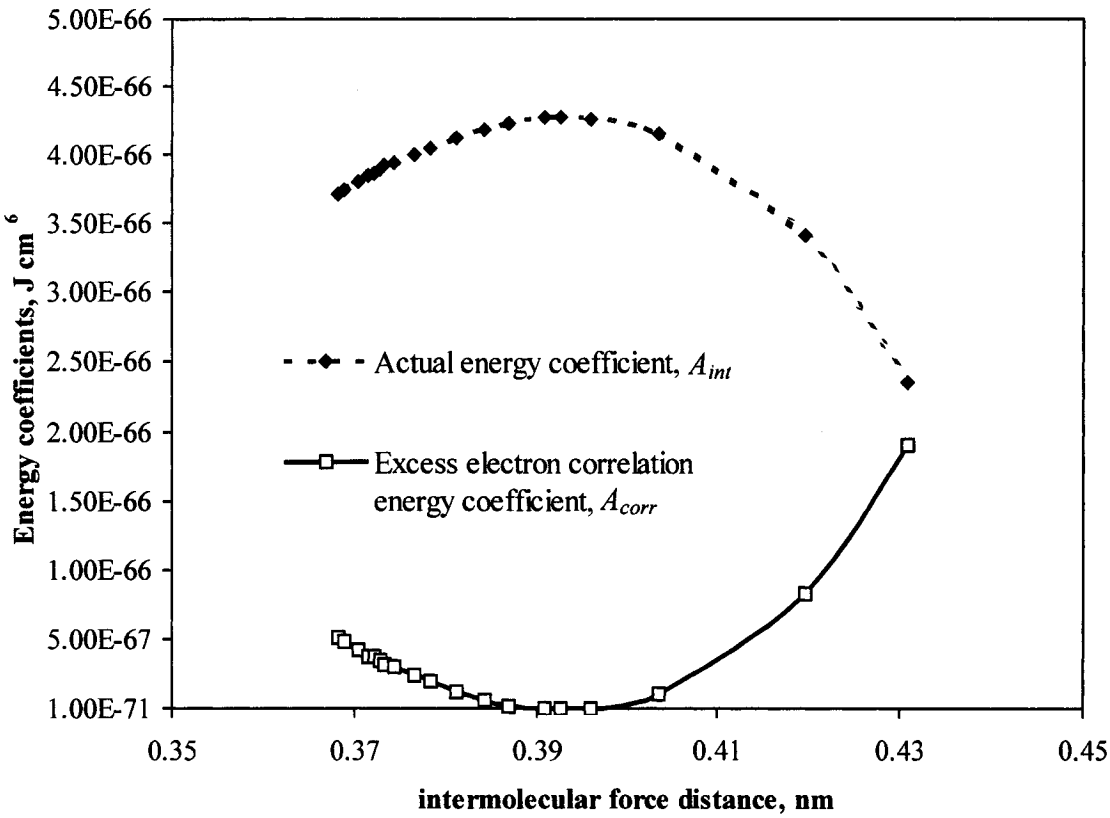

Figure 6.5 Actual energy coefficient and excess correlation energy coefficient vs. intermolecular force distance at different temperatures for liquid nitrogen at saturated pressure.

On the other hand, the excess in the repulsive electron-correlation energy coefficient is very sensitive to intermolecular distance. It has an appreciable value at low temperatures then it decreases with increasing temperature due to an increase in the intermolecular force distance as shown in Figure 6.5. The excess correlation energy coefficient reaches its minimum at intermolecular distance equal to 0.393 nm. This can be considered the optimum distance for the non-covalent bond between nitrogen molecules. At this distance, the attractive energy is equal to twice the repulsive energy

between two nitrogen molecules that is consistent with the quantum-mechanical virial theorem. A further increase in the boiling point of nitrogen leads to an increase in the vibration-rotation (VR) frequency contribution causing an increase in the intermolecular distance at which the electron-correlation becomes again in repulsive positions. A decrease in the ability of electrons to correlate properly is the reason for an increase in the repulsive energy between two molecules during the increase in the intermolecular distance.

4 CONCLUSIONS

The intermolecular force parameters of liquid nitrogen along the gas-liquid phase transition curve from the triple point to the critical point were determined from bulk properties. These physical parameters are influenced by the applied temperature and pressure conditions. A more significant change occurs as the conditions approach the critical point.

The effective coordination shell number was determined as it is necessary to link a bulk material properties and behaviors to microscopic ones. The decrease in this number is due to an increase in the kinetic energy leading to the break-up of some non-covalent bonds that are responsible for material condensation. The increase in the vibration-rotation frequency is attributed to the increase in the molar Gibbs free energy resulting from increasing the pressure and temperature of the system. The coordination number becomes zero when all the non-covalent bonds are broken and the resulted gas phase loses its ability to be condensed. The smallest critical coordination number for liquid nitrogen was found to be 4.436 near the critical point.

The intermolecular force distance parameter increases slightly with increasing nitrogen boiling point due to a decrease in the liquid molar density. However, it has a significant influence on the excess repulsive electron-correlation energy coefficient. The smallest deviation in this coefficient from what is predicted by the quantum mechanical virial theorem was found at intermolecular distance 0.393 nm. At this distance, an optimum electron correlation was achieved. We have also found that a critical

intermolecular distance of 0.431 nm for liquid nitrogen represents the longest stable non-covalent bond that may exist.

At temperatures well below the critical point of liquid nitrogen, we found that the interaction energy coefficient increases with increasing temperature due to an increase in the molecular polarizability of nitrogen. The repulsive correlation energy coefficient decreases with increasing temperature due to the increase in the intermolecular force distance that is controlled by the mutual vibration-rotation (VR) frequency contribution among molecules (Gayathri and Bagchi, 1999).

A set of equations were derived to determine the coordination shell number and the intermolecular force parameters form critical properties at nitrogen boiling points corresponding to different pressures. These equations were found to have a good agreement with the parameters calculated from properties' data obtained from the literature.

The discrepancy between theory and experiment in the determination of intermolecular interaction energy coefficient was attributed to the excess repulsive electron-correlation energy coefficient. An equation to calculate this correlation was established based on the Kirkwood-Muller formula, cohesive energy data and parameters obtained from X-ray diffraction measurements.

In conclusion, the determination of the various intermolecular force parameters and the coordination shell number at different temperatures is an essential step for understanding how a material can structuring itself under different conditions and starts to form a small cluster of molecules that is a first block for material self-assembly.

NOMENCLATURE

$A_{int}(T,P)$	pair equilibrium intermolecular force energy coefficient [J nm^6/molecule]
$A_{corr}(T,P)$	pair equilibrium excess repulsive electron-correlation energy coefficient [J nm^6/molecule]
C	velocity of light in vacuum [299792458 m/s]
C_s	constant in equation (2), [nm]
e	electron elementary charge [1.60217733 10^{-19} C]
m_e	electron mass [9.109389754 10^{-31} Kg]

m_s	slope in equation (2), [dimensionless]
n	constant is given by equations (7, 8 and 9), [dimensionless]
N_{AV}	Avogadro's number [molecule/mole]
$n_c(T,P)$	effective coordination shell number [dimensionless]
NIST	National Institute of Standards and Technology
P	absolute pressure [Pa]
P_s	saturated pressure [Pa]
P_R	reference pressure [Pa]
R_g	gas constant [Joule/mole K]
T	absolute temperature [K]
T_b	boiling point at a given pressure [K]
T_c	critical temperature [K]
T_R	reference temperature [K]
$V_L(T,P_s)$	liquid molar volume at saturated condition [nm^3/mole]
$V_g(T,P_s)$	gas molar volume at saturated condition [nm^3/mole]
Z_c	critical compressibility factor [dimensionless]
W_{attr}	attractive dispersion energy [J]
$W_{repulsive}$	repulsive dispersion energy [J]
W_{corr}	excess repulsive electron-correlation energy [J]

Greek Symbols

$\alpha(T, P)$	non-polar polarizability [nm^3/molecule]
$\Delta H_v(T,P)$	molar heat of vaporization at a given condition [Joule/mole]
$\Delta H_v(T_b)$	normal molar heat of vaporization [Joule/mole]
$\Delta U(T,P)$	molar cohesive energy at equilibrium [Joule/mole]
$\Delta U(T_b)$	normal molar cohesive energy at equilibrium [Joule/mole]
$\Delta Z(T,P)$	difference between gas and liquid compressibility factors [dimensionless]
$\varepsilon(T,P)$	pair equilibrium intermolecular force energy parameter [Joule/molecule]
Φ	Defined by equation (5), [dimensionless]

$\sigma_{equi}(T,P)$ pair equilibrium intermolecular force distance parameter at minimum potential energy [nm]

$\sum_{i \neq j} \langle r_i \cdot r_j \rangle$ explicit electron-correlation term [J nm^3/C^2]

χ diamagnetic susceptibility [nm^3/molecule]

REFERENCES

Arai, T. and R. L. McGreevy, "RMC Modelling of the Structure of Expanded Liquid Mercury Along the Co-existence Curve", Journal of Physics: Condensed Matter, 10, 9221-9230 (1998).

Beck, R. D., M. F. Hineman and J. W. Nibler, "Stimulated Raman Probing of Supercooling and Phase Transitions in Large N_2 Clusters Formed in Free Jet Expansions", Journal of Chemical Physics, 92 (12), 7068–7078 (1990).

Ben-Naim, A., "Statistical thermodynamics for Chemists and Biochemists", Plenum Press, New York, NY (1992).

Bottcher, C. J. F., "Theory of Electric Polarization", Elsevier Scientific Publishing Company, Amsterdam, NL (1973).

Dham, A. K., A. R. Allnatt, W. J. Meath and R. A. Aziz, "The Kr-Kr Potential Energy Curve and Related Physical Properties; The XC and HFD-B Potential Models", Mol. Phys. 67 (6), 1291-1307 (1989).

Dham, A. K., W. J. Meath, A. R. Allnatt, R. A. Aziz and M. J. Slaman, "XC and HFD-B Potential Energy Curves for Xe-Xe and Related Physical Properties", Chem. Phys. 142, 173-189 (1990).

Din, F., "Thermodynamic functions of gases", volume 3, Butterworths and Co., London, UK (1961), pp 72- 161.

Furumoto, H. W. and C. H. Shaw, "X-ray Diffraction in Liquids–Nitrogen, Oxygen, and their Mixtures", The Physics of Fluids, 7 (7), 1026–1029 (1964).

Gayathri N. and B. Bagchi, "Computer simulation study of the density and temperature dependence of fundamental and overtone vibrational dephasing in nitrogen: Interplay between different mechanisms of dephasing", Journal of Physical Chemistry. 103 (48), 9579-9590 (1999a).

Gayathri N. and B. Bagchi, "Subquadratic quantum number dependence and other anomalies of vibrational dephasing in liquid nitrogen: Molecular dynamics simulation study from the triple point to the critical point and beyond", Physical Review Letters. 82 (24), 4851-4854 (1999b).

Giauque, W. F. and J. O. Clayton, "The heat capacity and entropy of nitrogen. Heat of vaporization. Vapor pressures of solids and liquids. The reaction 0.5 N_2 + 0.5 O_2 = NO from spectroscopic data", J. Am. Chem. Soc., 55, 4875-4889 (1933).

Hirschfelder, J.O., C. F. Curtiss, and R. B. Bird, "Molecular Theory of Gases and Liquids", John Wiley and Sons, Inc., New York, NY (1967a).
Hirschfelder, J.O., "Intermolecular Forces", John Wiley and Sons, Inc., New York, NY (1967b).

Israelachvili, J., "Intermolecular and Surface Forces", Second Edition, Academic Press Inc., San Diego, CA (1991).

Jacobsen, R. T., R. B. Stewart and M. Jahangiri, "Thermodynamic properties of nitrogen from freezing line to 2000 K at pressures to 1000 Mpa", J. Phys. Chem. Ref. Data, 15 (2) 735-909 (1986).

Kurdi, J. and A. Y. Tremblay, "Experimental determination of the local microscopic structure and intermolecular force parameters of amorphous liquids and solids", Journal of Physical Chemistry, Part B., Submitted (chapter V in this thesis).

Lerchner, J., A. Wolf and G. "Wolf, Recent Developments in Integrated Circuit Calorimetry", J. Therm. Anal. Cal., 57, 241-251 (1999).

Lide, D. R., Ed., "CRC Handbook of Chemistry and Physics", 83rd ed., CRC Press, Boca Raton, 2002-2003.

Maitland, G. C., M. Rigby, E. B. Smith and W. A. Wakeham, "Intermolecular Forces: their origin and determination", Clarendon Press, Oxford, UK (1981).

March, N. H. and J. F. Mucci, "Chemical physics of free molecules", Plenum Press, New York, NY (1993).

Muller, A., "The Van der Waals Potential and the Lattice Energy of a n-CH_2 Chain Molecule in a Paraffin Crystal", Proceedings of the Royal Society of London, Series A: Mathematical and Physical Sciences, 154 (A 883) 624 – 639 (1936).

Nield, V. M. and P. T. Verronen, "The Structure of Expanded Mercury", Journal of Physics: Condensed Matter, 10, 8147–8153 (1998).

Nield, V. M., M. A. Howe and R. L. Mcgreevy, "The Metal-Non-Metal Transition in Expanded Caesium", Journal of Physics: Condensed Matter, 3, 7519-7525 (1991).

NIST Chemistry Webbook, "Thermophysical Properties of Fluid Systems", NIST Standard Reference Database Number 69 - July 2001 Release.

Nowak, P., R. Kleinrahm and W. Wagner, "Measurement and correlation of the (P, ρ, T) relation of nitrogen II. Saturated-liquid and saturated-vapour densities and vapour pressures along the entire coexistence curve", J. chem. Thermodynamics, 29, 1157-1174 (1997).

Pitzer, K. S., "Inter- and Intramolecular Forces and Molecular Polarizability", in "Advances in Chemical Physics", I. Prigogine Ed., Volume II, Interscience Publishers, Inc. New York, NY (1959), pp. 59-83.

Poling, B. E., J. M. Prausnitz and J. P. O'Connell, "The Properties of Gases and Liquids, McGraw-Hill, New York, NY (2001).

Radnai, T. and H. Ohtaki, "X-ray Diffraction Studies on the Structure of Water at High Temperatures and Pressures", Molecular Physics, 87 (1) 103–121 (1996).

Reinhard, M. and A. Drefahl, "Handbook for Estimating Physicochemical Properties of Organic Compounds", John Wiley and sons, Inc., New York, NY (1999).

Salem, L., "The Calculation of Dispersion Forces", Mol. Phys., 3, 441-452 (1960).

Smith E. B., "Basic Chemical Thermodynamics", Clarendon Press, Oxford, New York, NY (1990).

Stone, A. J., "The theory of Intermolecular Forces", Clarendon Press, Oxford, UK (1996).

Vinti, J. P., "A Relation between the Electric and Diamagnetic Suceptibilities of Monatomic Gases", Physical Review, 41, 813-817 (1932).

Waseda, Y., "The Structure of Non-Crystalline Materials: liquid and Amorphous Solids", McGraw-Hill International Book Company, New York, NY (1980).

White, A., F. J. Zerilli and H. D. Jones, "*Ab Initio* Calculation of Intermolecular Potential Parameters for gaseous Decomposition Products of Energetic Materials", DSTO Aeronautical and Maritime Research Laboratory, Australia (2000), pp. 1-43.

CHAPTER VII

The Influence of Temperature on Intermolecular Force Parameters for Polyetherimide

J. Kurdi, and A. Y. Tremblay*

Department of Chemical Engineering, University of Ottawa, 161 Louis Pasteur, Ottawa, Ontario, K1N 6N5, Canada

*Corresponding author
André Y. Tremblay
Tel.: +1-613-562-5920; fax: +1-613-562-5172
E-mail address: tremblay@uottawa.ca

CHAPTER VII

Paper 6: The influence of temperature on intermolecular force parameters for Polyetherimide

J. Kurdi, and A. Y. Tremblay
Department of Chemical Engineering, University of Ottawa, 161 Louis Pasteur, Ottawa, Canada, K1N 6N5

ABSTRACT

An approach was established to calculate the influence of temperature on the structural and energy parameters of amorphous polymers in their glassy state based on equations of state. The coordination number, cohesive energy and Hansen solubility parameters of polyetherimide (PEI, Ultem® 1000) were determined at different temperatures. The predicted cohesive energy was in good agreement with that calculated using Chickos' empirical equation (1993) and the results of molecular dynamics simulations performed on Ultem 1000 (Goudeau et al., 2000). The coordination number and the cohesive energy were used to determine the intermolecular force energy parameter. The intermolecular force distance parameter of PEI at different temperatures was calculated based on its experimental linear thermal expansion. The contribution of non-polar and polar components to the cohesive energy was discussed. Using the polar component, the intermolecular dipole moment of PEI at different temperatures was determined and found to be in good agreement with the one determined using computational chemistry. The results of this work are useful in explaining many physical phenomena in polymer systems at different temperatures such as the increase in the adsorption of water by PEI with increasing temperature.

Keywords: Cohesion, amorphous polyetherimide, Intermolecular force parameters, Hansen solubility parameters.

1 INTRODUCTION

The equilibrium intermolecular force parameters of condensed matter are intrinsic energetic and structural properties responsible for various static and dynamic characteristic interactions of similar or different molecules. These parameters are of great importance as fundamental principles in the study of phenomena such as self-assembly in supramolecular systems (Lindoy and Atkinson, 2000), molecular machines (Balzani et al, 1998), adsorption, adhesion, molecular simulations and their related application such as fluid (gas or liquid) separations, the characterization of porous solids, and the predication of the properties of surface, interface and bulk solids (Israelachvili, 1992; Hirschfelder et al. 1967; Maitland et al. 1981; Vlachos and Katsoulakis, 2000).

The new rapidly growing field of nanoscience technology especially in molecular machines must understand and control materials at the atomic and molecular scale. Richard P. Feynman (1959) had no doubt that the scientists would one day have the ability to control the arrangement of things on a molecular scale. This challenge leads to the proposal of a fundamentally new *"bottom-up"* approach which means starting from atoms and molecules in order to predict, at the macroscopic scale, all structural, physical and chemical properties of matter as well as the dynamic behavior of materials (Balzani et al, 1998). Intermolecular force interactions, such as non-covalent bonds among molecules are essential to interconnect the microscopic or atomic and macroscopic scales in materials (Balzani et al, 1998 and 2000; Lindoy and Atkinson, 2000). Therefore, it is important to have the ability to accurately determine the real intermolecular force interactions among molecules under different conditional settings.

Many different values for the intermolecular force parameters for the same component are reported in literature (Kurdi and Tremblay, chapterV in this thesis). This is largely due to the fact that the intermolecular force interactions were based on different potential models and theories that relate one or more macroscopic properties of materials to an average molecular potential. The reporting of several inconsistent intermolecular force parameters for the same component was demonstrated in the literature. For example, Ravikovitch et al. (2000) attributed the possible inconsistencies in the calculation of the pore size distributions using density functional theory (DFT) to the

choice of these parameters. Kurdi and Tremblay (chapter IV in this thesis) showed the significant influences of these parameters on the calculated pore size distribution using Horvath-Kawazoe method. It is also found that the intermolecular force parameters calculated from one bulk property would not be accurate to predict other properties (Hirschfelder et al. 1967). Assumptions related to the constant nature of the interaction parameters with respect to temperature and pressure can lead to unrealistic solutions or analyses for related physical phenomena (chapter V in this thesis). Therefore, the determination of realistic intermolecular interactions is an essential step to have accurate parameters by which the *bottom-up* approach can be used to predict the properties of new materials.

The approach to determine intermolecular force parameters based on experimental measurements was established by Kurdi and Tremblay (chapter V in this thesis) for both liquid and solid condensed matter. The influence of temperature and pressure on these parameters along the vapor-liquid phase transition curve was also investigated and applied for nitrogen gas (chapter VI in this thesis). In this paper, an approach was established to determine the influence of temperature on the intermolecular force parameters of amorphous polymers such as polyetherimide. We also have established a method to determine the equilibrium intermolecular dipole moment corresponding to the polar cohesive intermolecular interactions in bulk amorphous solids.

As the Hansen solubility parameters and the various intermolecular parameters are calculated at given conditions (temperature and pressure), which may not necessarily lie at the gas-liquid phase transition curve, it is important to determine these parameters at different conditions. The objective of this work is to investigate the influence of temperature on various intermolecular force parameters of amorphous solids. There is an increasing need for this research as polymers are being used at ever increasing temperatures in structural and membrane separation applications. Polyetherimide (Ultem 1000) was used as a case study in this work.

2 THEORY AND CALCULATIONS

2.1 Calculation of the molar volume of a polymer repeat unit

The molar volume of a repeat unit of a solid polymer at different conditions can be obtained from the Double-domain Modified Tait equation (Beiter and Ishii, 1996; Chang et al., 1996; Zoller, 1989; Cho and Sanchez, 1999) giving as follows:

$$V_M(T,P) = v_o(T)\left[1 - C\ln\left(1 + \frac{P}{B(T)}\right)\right] + v_t(T,P) \qquad (1)$$

where:

$$\left.\begin{aligned} v_o(T) &= b_{1m} + b_{2m}\overline{T} \\ B(T) &= b_{3m}\exp\left(-b_{4m}\overline{T}\right) \\ v_t(T,P) &= 0 \end{aligned}\right\} for T > T_t$$

$$\left.\begin{aligned} v_o(T) &= b_{1s} + b_{2s}\overline{T} \\ B(T) &= b_{3s}\exp\left(-b_{4s}\overline{T}\right) \\ v_t(T,P) &= b_7\exp\left(b_8\overline{T} - b_9 P\right) \end{aligned}\right\} for T < T_t$$

T and P are the absolute temperature and pressure respectively.

Transition temperature, $T_t = b_5 + b_6 P$

$\overline{T} = T - b_5$

and $C = 0.0894$ is a universal constant.

2.2 Calculation of the coordination number of a solid polymer

The coordination number of a polymer repeat unit at different conditions, $n_c(T, P)$, can be calculated from the molar volume of one repeat unit, $V_M(T, P)$, and one coordination number at reference conditions obtained experimentally from the X-ray diffraction measurement as explained elsewhere (Kurdi and Tremblay, chapter V) using the following equation:

$$n_c(T,P) = n_c(T_R,P_R)\left[\frac{V_M(T_R,P_R)}{V_M(T,P)}\right] \qquad (2)$$

The subscript R means reference temperature or pressure condition.

2.3 Calculation of the Hansen solubility parameters of PEI

Two suitable methods can be applied to calculate the solubility parameters of glassy solids at different temperatures: (1) using equation of state and (2) using empirical equation recommended by Chickos et al. (1993).

(1) Using equation of state

The total solubility parameter of a glassy polymer below its glass transition temperature, T_g, can be calculated from its cohesive and volumetric properties (cohesive energy density), which can be obtained from the experimental equation of state (PVT relationship). The direct determination of the internal pressure, $\pi(T)$, offers a possible method to calculate the cohesive energy at different temperatures using the following equation (Allen et al. 1961):

$$\pi(T) = \left(\frac{\partial U}{\partial V}\right)_T = T\frac{\alpha_V}{\beta_T} \tag{3}$$

In equation 3, the volumetric expansion coefficient, α_V of a polymer in the glassy state can be calculated from modified Tait's equation of state using the following equation (Seitz, 1993):

$$\alpha_V = \frac{1}{V_M}\frac{dV_M}{dT} \tag{4}$$

The isothermal (bulk compliance) compressibility, β_T, is the reciprocal of the bulk modulus ($\beta_T = 1/B(T)$) which can be calculated from the molar elastic wave Rao-function (additive group contribution molar function) using the following equation (Van Krevelen, 1997):

$$B(T) = \frac{1}{\beta_T} = \frac{M_W}{V_M}\left(\frac{U_R}{V_M}\right)^6 \tag{5}$$

The molar elastic Rao-function, U_R is independent of temperature or polymeric phase state and can be calculated from the additive group contributions found in Table (14.2) cited in Van Krevelen (1997), (for PEI, U_R= 26880 [$(cm^3/mol)*(cm/s)^{(1/3)}$]). M_w is the molecular weight of PEI.

The total cohesive energy of a solid at different temperatures was calculated from the internal pressure obtained by equation (3) through the numerical differential of the cohesive energy with respect to molar volume at constant temperature. The total solubility parameter can then be calculated from the cohesive energy using the following equation:

$$\delta_t = \sqrt{\frac{\Delta U(T)}{V_M}} \tag{6}$$

The dispersion solubility parameter at different temperatures was calculated numerically from the volumetric expansion coefficient using the following equation (Hansen and Beerbower, 1971):

$$\frac{d\delta_d}{dT} = -1.25\alpha_V \delta_d \tag{7}$$

The total polar solubility parameters was then calculated from the following equation:

$$\delta_{P+H} = \sqrt{\delta_t^2 - \delta_d^2} \tag{8}$$

The total polar, dispersion and total solubility parameters of Ultem 1000 were calculated from the above equations in addition to using solubility parameters at 298.15 K obtained from (Hansen 2000) as a reference point.

(2) Using the empirical equation recommended by Chickos et al. (1993)

The temperature dependence of the heat of sublimation for a wide range of solid materials was studied by Chickos et al. 1993. Using their recommended empirical equation and calculating the cohesive energy by subtracting ($2R_gT$) from the heat of sublimation, the following equation was obtained:

$$\Delta U(T) = \Delta U(298.15) + \left[2R_g(298.15 - T)\right] - 32(T - 298.15) \tag{9}$$

where the constant 32 is in units of [J/K]. The solubility parameters can be calculated from the cohesive energy or vice verse by using equation (6).

2.4 Calculate the pair intermolecular force parameters

The influence of temperature on the intermolecular force distance parameter can be obtained from the change in the experimental linear expansion coefficient, $\alpha_L(T)$, and considering the same change in $\sigma_{equi}(T)$ as the linear expansion. Therefore, the following equation can be used:

$$\frac{d\sigma_{equi}(T)}{dT} = \sigma_{equi}(T)\alpha_L(T) \tag{10}$$

The pair intermolecular force energy parameter can be calculated at each temperature from the total cohesive energy, $\Delta U(T)$, the coordination number, $n_c\ (T,P)$, and the intermolecular force distance parameter, σ_{equi}, using the following equation (Stone, 1996):

$$\Delta U(T) = \frac{1}{2} N_{AV}\, n_c(T,P)\varepsilon(T) \tag{11}$$

where N_{AV} is the Avogadro's number.

2.5 Calculate the intermolecular dipole moment of PEI

The intermolecular dipole moment of solids can be calculated from the polar part of the cohesive energy including hydrogen bonding, $\Delta U(polar)$. The total polar component of the pair intermolecular cohesive energy can be given by the following equation (Maitland, 1981):

$$\varepsilon(polar) = \frac{\mu^4}{3(4\pi\,\varepsilon_o)^2 k_B T\,\sigma_{equi}^6} + \frac{\mu^2\alpha(nonpolar)}{(4\pi\,\varepsilon_o)\sigma_{equi}^6} \tag{12}$$

where μ is the intermolecular dipole moment, κ_B is the Boltzmann constant, ε_o is the electric permittivity in vacuum and T is the absolute temperature. In the electrostatic system, the factor $(4\pi\varepsilon_o)$ is equal to 1, but in the S.I. unit, it is equal to 1.1126E-10 [coulomb^2/J m] and the intermolecular dipole moment, μ has a unit of [Coulomb m] (Stone, 1996).

The contribution of the non-polar polarizability of a molecule can be calculated from the dielectric constant measured at moderate-frequency alternating field, $\varepsilon(\omega)$ using the Clausius-Mossotti equation (Bottcher, 1973):

$$\alpha(nonpolar) = \frac{3}{4\pi N_V}\left[\frac{\varepsilon(\omega)-1}{\varepsilon(\omega)+2}\right] \quad (13)$$

The moderate-frequency alternating field should be determined from the change in the dielectric constant with the electrical field frequency. The dielectric constant at a certain moderate-frequency is only related to the non-polar polarizability (i.e. electronic and atomic contributions) if the change in the frequency is fast enough so that there is no time for the permanent dipole to orient itself with that electrical field. With a further increase in frequency, a steep decrease in the dielectric constant is observed because of a decrease in the atomic contribution to polarizability. At a frequency higher than 10^{14} Hz (Simpson and Clair, 2002), the atomic polarizability will not be influenced by changes in the frequency of the electric field leading to have a pure electronic polarizability (Bottcher, 1973). The dielectric constant in equation (13) should be measured at a frequency where there are complete atomic and electronic contributions for polarizability but no dipole contribution.

3 EXPERIMENTAL

A symmetric membrane was cast from a solution consisting of 23% by weight polyetherimide (Ultem 1000 from GE) and 77% by weight dichloromethane on a clean glass plate inside a glove bag using a casting blade gap of 250 μm. A low flow of dried nitrogen gas stream at room temperature (23°C) was used through the glove bag during the casting process and then for one day to dry the membrane. Finally, the membrane was dried in an oven at temperature 90°C and 725 mm Hg vacuum pressure for 24 hours. The X-ray diffraction measurements and the calculation of the structural parameters were used as explained elsewhere (Kurdi and Tremblay, chapter V in this thesis).

4 COMPUTATIONAL CHEMISTRY

A repeat unit of polyetherimide (Ultem 1000) was assembled using the HyperChem Pro 5.1 program according to the structure found in the polymer science dictionary (Alger, 1997). The geometrical structure was optimized by molecular mechanics MM+ and the

atomic charge then by the semiempirical method PM3. The optimization was repeated alternatively between the two methods. Initially, a small part of the structure was separated and optimized in order to have a stable convergence for the whole structure. Finally, the geometrical structural of the PEI repeat unit was optimized by PM3 to a RMS gradient less than 1E-6. The geometrical optimization in the HyperChem program is for the structure at temperature 0 K and absolute vacuum pressure.

To obtain a structure at different temperatures, a molecular dynamic simulation at a specified temperature was used on top of the semiempirical PM3 method. The dipole moment of the isolated PEI repeat unit was calculated using a single point, PM3.

5 RESULTS AND DISCUSSION

5.1 Coordination number of PEI at different temperatures

The relation between pressure, bulk molar volume and temperature (PVT) of polyetherimide (Ultem 1000) can be obtained from Tait's modified equation of state, equation (1). The adjustable experimental parameters of this equation for Ultem 1000 were obtained from General Electric Plastics (design solution center, 2002). By definition, the parameters b_{1s} and b_{1m}, used in equation (1), must be equal in an amorphous polymer at zero pressure to obtain a continuous $v_o(T)$ term (Chang et al. 1996). The experimental molar volume of Ultem® 1000 at 298.15 K and 1 atm was obtained from Boedeker Plastics, Inc. and from Simon el al. (1997) for other temperatures and 1 atm. The molar volume of PEI versus temperature was plotted in Figure 7.1. The results show an excellent agreement between the experimental data and Tait's modified equation of state.

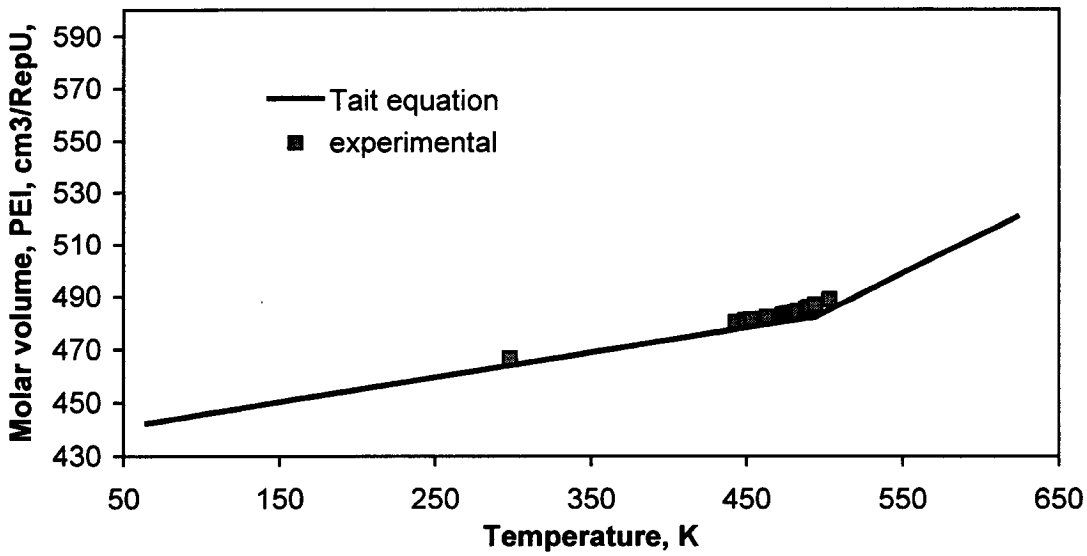

Figure 7.1 Volume of one repeat unit of PEI at 1 atm and different temperatures.

The coordination number of polyetherimide (Ultem 1000) at different temperatures was calculated from the coordination number at 298.15 K obtained from our previous work and using equation (2). The results were plotted in Figure 7.2, which shows two different slopes below and above the glass transition temperature. The change in the coordination number in the range close to the glass transition temperature is not sharp and a more precise experimental measurement of the molar volume such as that measured by Simon et al. (1997) must be used.

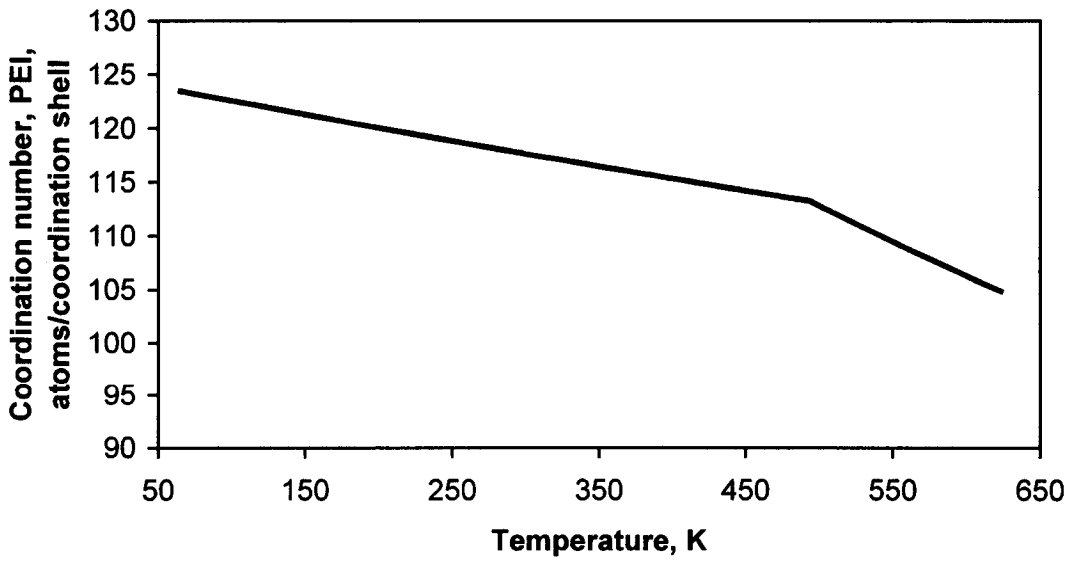

Figure 7.2 Coordiantion number of PEI at 1 atm and different temperatures.

5.2 Cohesive energy and Hansen solubility parameters of PEI

The Hansen solubility parameters of polyetherimide (Ultem 1000) in the temperature range of 65 to 450 K were determined. The weak polar and hydrogen bonding solubility components were considered as one total polar component since there is no need to separate them in this work. All variables were calculated for polyetherimide (Ultem 1000) within the above temperature range and a reference solubility at 298.15 K obtained from Hansen (2000) was used as a starting point for the numerical solution of the differential equations used above. The volumetric expansion coefficient was calculated from equation (4) based on Tait's equation of state (1). The isothermal compressibility, β_T of PEI was calculated from the molar volume and the molar elastic Rao-function, U_R which is independent of temperature or polymeric phase state and it was calculated from the additive group contributions of the chemical structure of the PEI repeat unit found in Table (14.2) cited in Van Krevelen (1997), and its value was determined to be U_R= 26880 $[(cm^3/mol)*(cm/s)^{(1/3)}]$. The internal pressure was then calculated using equation (3).
The total cohesive energy of PEI at different temperatures was calculated from the internal pressure obtained by equation (3) through the numerical differential of the cohesive energy with respect to molar volume at constant temperature. The total solubility parameter was then calculated from the cohesive energy and molar volume using equation (6).

The dispersion solubility parameter at different temperatures was calculated numerically from the volumetric expansion coefficient using equation (7) and the total polar solubility parameters including hydrogen bonding were then calculated using equation (8). The total solubility parameter of PEI was calculated using equation (9) and (6). Calculations were limited to temperature range lower than the glass transition temperature by at least 20 K. The results are shown in Figure 7.3, which indicate a slight decrease in the total solubility of PEI with increasing temperature. This trend is usually seen in non-polar materials. The non-polar component of the Hansen solubility parameter decreases with increasing temperature, consistent with a decrease in the heat of sublimation with increasing temperature (Reinhard and Drefahl, 1999). This slight decrease is due to the low volumetric expansion coefficient for PEI. The polar

component (including hydrogen bonding) of the Hansen solubility parameter increases with increasing temperature due to the increase in the molecular polarizability.

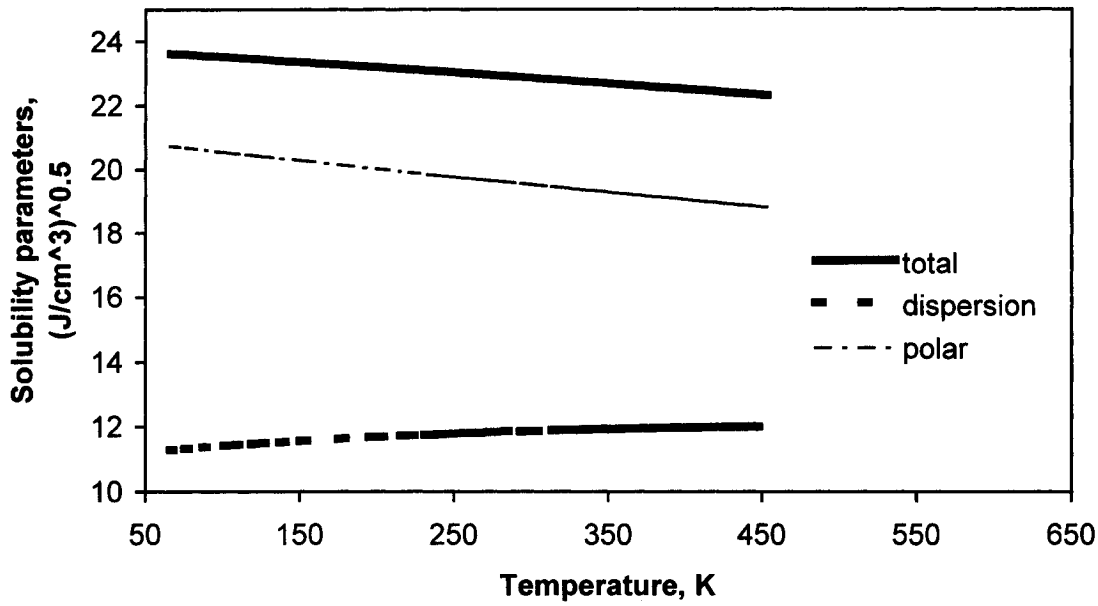

Figure 7.3 Solubility parameters of solid PEI at 1 atm and different temperatures.

To validate our results, the total cohesive energy of PEI corresponding to the calculated solubility parameters using equations (3) were compared with two other sources, using the empirical equation (9) of Chickos et al. (1993) and the results obtained by Goudeau et al. (2000) from the molecular dynamics simulation and the equation of state as shown in Figure 7.4. Below the glass transition temperature (T_g), our results agree well with Chickos' empirical equation for solids. However, below (T_g), the cohesive energy calculated by Goudeau el al. (2000) is slightly lower than our results and than the experimental cohesive energy. The slight discrepancy in Goudeau's was mentioned in their paper. The results of Goudeau et al. (2000) show the change in the cohesive energy at temperatures close to the glass transition temperature. Above T_g, our results agree well with Goudeau's results. The excellent agreement in the cohesive energy at different temperatures calculated in this work as shown in Figure 7.4 and those two literature sources indicates the validity of our results.

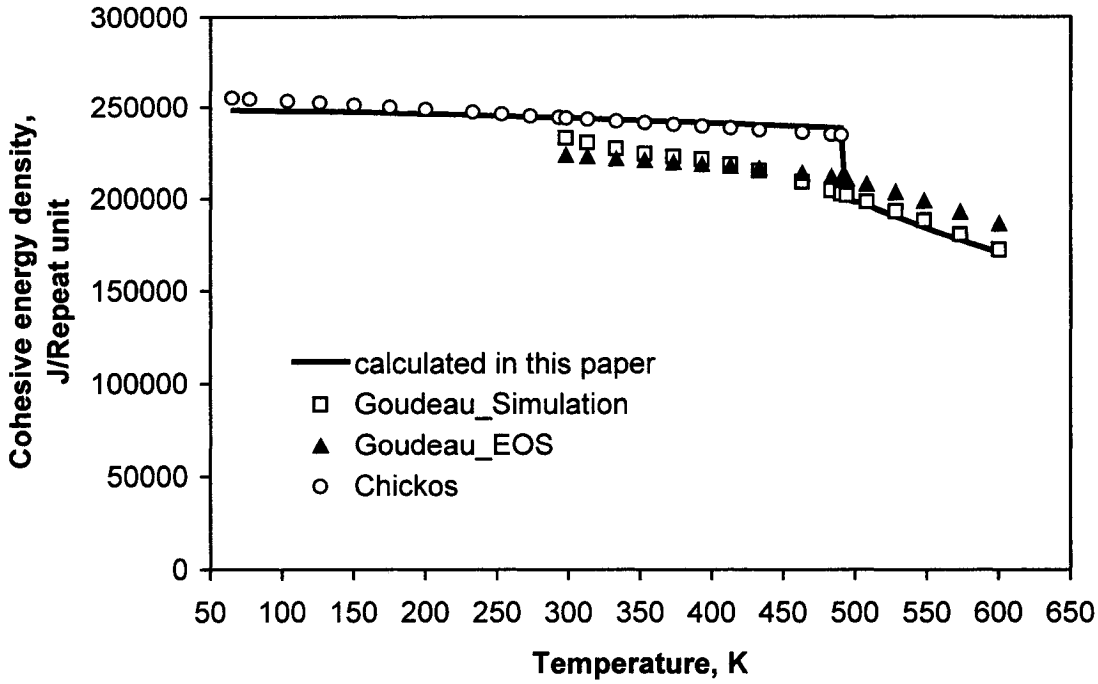

Figure 7.4 Cohesive energy density of solid PEI at 1 atm and different temperatures.

5.3 Intermolecular dipole moment of PEI

The intermolecular dipole moment of the polyetherimide was calculated at different temperatures from the cohesive energy using an equation derived from the combination of equations (12) and (11) as follows:

$$\left(\frac{\mu^2}{4\pi\varepsilon_o}\right)=\frac{3k_BT}{2}\left(-\alpha(nonpolar)+\sqrt{\alpha(nonpolar)^2+\frac{8\Delta U(polar)r_e^6}{3k_BTN_{AV}n_c(T,P)}}\right) \qquad (14)$$

The non-polar polarizability of PEI was calculated at different temperatures from the experimental dielectric constant at a frequency of 1 KHz obtained from GE-plastics (2002) and equation (13). The dipole moment was calculated from equation (14) and by computational chemistry using the PM3 semiempirical method. The results are shown in Figure 7.5. Excellent agreement was found above 50 K between the calculated intermolecular dipole moment using equation (14) and computational chemistry results. This verifies the validity of the calculated polar cohesive energy at different temperatures.

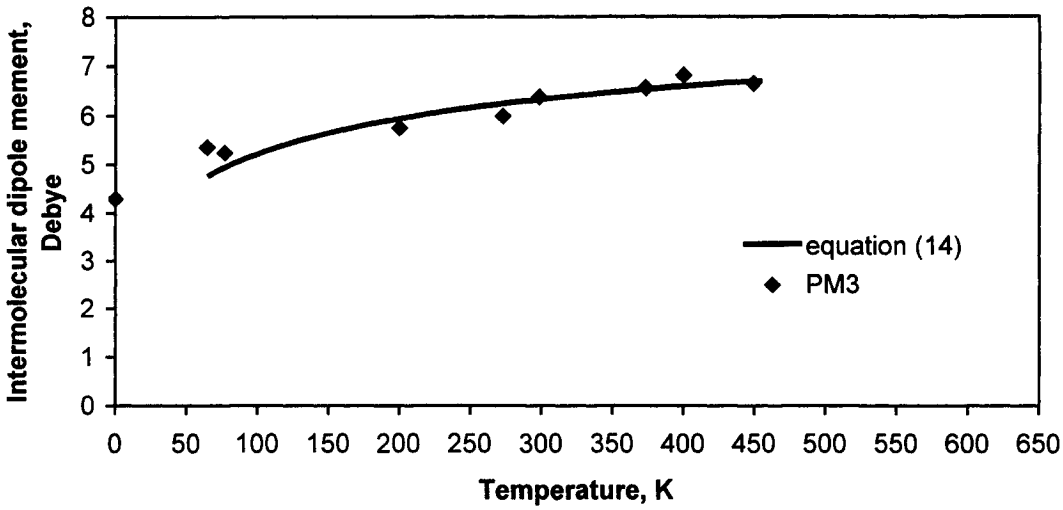

Figure 7.5 Intermolecular dipole moment of PEI at 1 atm and different temperatures.

5.4 Intermolecular force parameters of PEI

The intermolecular force distance parameter for PEI was calculated at different temperatures using equation (10) from the linear thermal expansion coefficient obtained from GE-Plastics (2002) and the intermolecular force distance at 298.15 K obtained from our previous work (Kurdi and Tremblay, chapter V). The results are shown in Figure 7.6. The slight increase in the intermolecular distance with increasing temperature is attributed to the thermal expansion of the polymer.

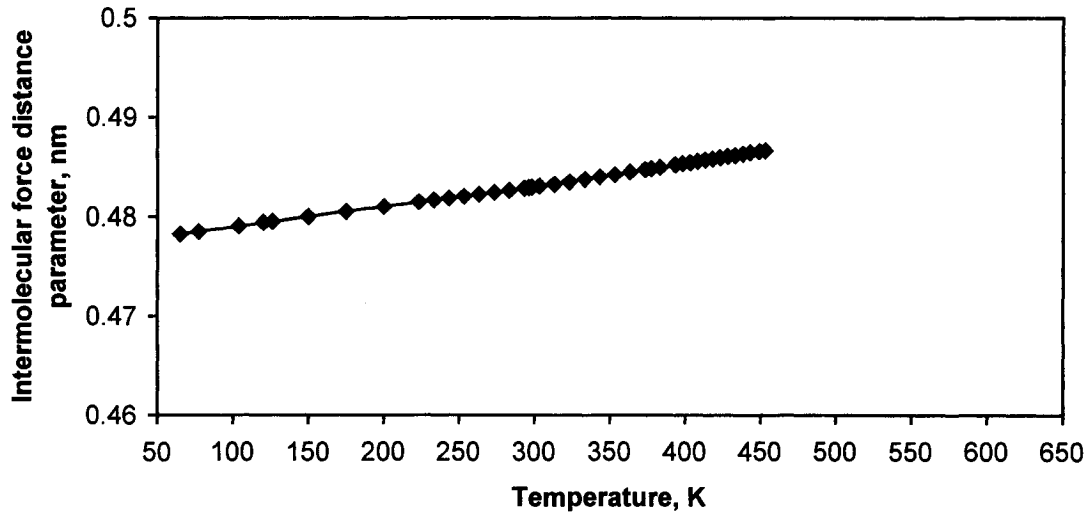

Figure 7.6 Intermolecular force distance parameter of PEI at 1 atm and different temperatures.

The intermolecular force energy parameter at different temperatures was calculated from the non-polar, polar and total cohesive energy, and the coordination number using equation (11). The results are shown in Figure 7.7. The total intermolecular force energy increased with increasing temperature, due to an increase in the polarizability of PEI and the intermolecular dipole moment. The decrease in the nonpolar component is in agreement with the slight decrease of the non-polar solubility parameter as previously shown in Figure 7.3 while the polar component had a more significant influence on the total intermolecular force energy parameter. These results were also confirmed by the experimental observation of Merdas et al. (2000). They found that the adsorption of water in PEI on a mass basis increased with increasing temperature.

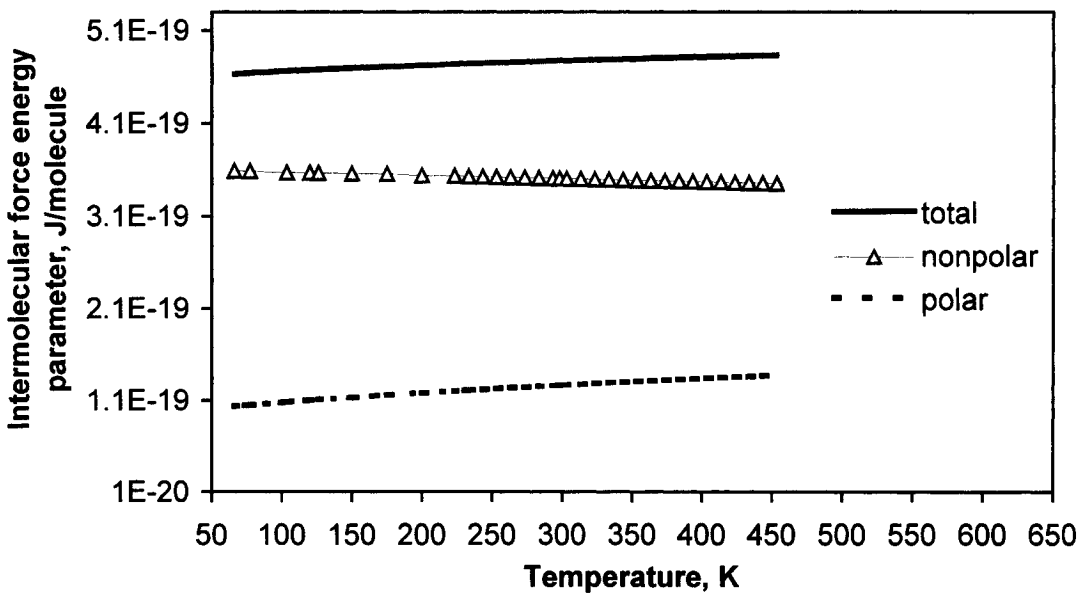

Figure 7.7 Intermolecular force energy parameter of PEI at 1 atm and different temperatures.

6 CONCLUSIONS

An approach to determine the structural and energy parameters of polyetherimide (Ultem 1000) at different temperatures was established based on Tait's equation of state. The method is useful to calculate the cohesive energy and the Hansen solubility parameters of amorphous polymers at different temperatures. Good agreement was found for the

cohesive energy determined in this work and the one obtained from Chickos' empirical equation (1993) for solids and the molecular dynamics simulations by Goudeau et al. (2000). The non-polar and polar components of these parameters were also determined. The increase in the polarity of PEI provides us with a reasonable explanation for the increase in the water adsorption into PEI polymer with increasing temperature (Merdas et al. 1999). The coordination number of PEI was a useful parameter to link between microscopic and macroscopic scale parameters. The parameters determined above were used to calculate the intermolecular force parameters of PEI at different temperatures. An equation was derived to determine the intermolecular dipole moment of solids from the coordination number, intermolecular force parameters, polar cohesive energy and non-polar polarizability. The dipole moment of the PEI repeat unit was also determined from computational chemistry (PM3, semiempirical method) and showed a good agreement with the one obtained from equation (14). All parameters in this work displayed a temperature dependence and therefore these changes should not be ignored in calculations of polymer physical properties.

NOMENCLATURE

b_{1m}	intercept of melt-state *V-T* line at zero pressure [m^3/Kg]
b_{2m}	slope of melt-state *V-T* line at zero pressure [m^3/Kg K]
b_{3m}	material constant to calculate *B(T)* of melt-state [Pa]
b_{4m}	material constant to calculate *B(T)* of melt-state [1/ K]
b_{1s}	intercept of solid-state *V-T* line at zero pressure [m^3/Kg]
b_{2s}	slope of solid-state *V-T* line at zero pressure [m^3/Kg K]
b_{3s}	material constant to calculate *B(T)* of solid-state [Pa]
b_{4s}	material constant to calculate *B(T)* of solid-state [1/K]
b_5	glass transition temperature at zero pressure, $b5 = Tt(P=0)$ [K]
b_6	material constant that represents the rate of change of glass transition temperature with pressure, $b_6 = dT_g(P)/dP$ [K/Pa]
b_7	material constant to calculate volume shrinkage due to crystallization [m^3/Kg]

b_8	material constant to calculate volume shrinkage due to crystallization [1/K]
b_9	material constant to calculate volume shrinkage due to crystallization [1/Pa]
$B(T)$	temperature dependent factor or Tait parameter [pa].
C	dimensionless universal constant or Cutler's constant (C=0.0894).
$MM+$	empirical Molecular Mechanics (force field) method
M_W	molecular weight of one repeat unit of the polymer [Kg/mole]
N_{AV}	Avogadro's number [molecule/mole]
$n_c(T,P)$	effective coordination shell number [dimensionless]
N_V	density number per unit volume [molecule/nm^3]
P	absolute pressure [Pa]
P_R	reference pressure [Pa]
R_g	gas constant [Joule/mole K]
T	absolute temperature [K]
$\overline{T}$	difference between the applied temperature and the glass transition temperature at zero pressure [K]
T_R	reference temperature [K]
T_t	transition temperature [K]
U_R	molar elastic Rao-function [(m^3/mole)*(m/s)$^{(1/3)}$]
V_M	molar volume of a repeat unit of polymer [m^3/mole]

Greek Symbols

$\alpha_L(T)$	linear expansion coefficient [1/K]
$\alpha(non\text{-}polar)$	non-polar polarizability [nm^3/molecule]
α_V	volumetric expansion coefficient [1/K]
β_T	isothermal bulk compressibility (compliance) [1/Pa]
δ_d	dispersion component of the Hansen solubility parameters [(Joule/m^3)$^{0.5}$]
δ_{p+H}	total polar component (including hydrogen bonding) of the Hansen solubility parameters [(Joule/m^3)$^{0.5}$]

δ_t	total Hansen solubility parameter [(Joule/m^3)$^{0.5}$]
∂U	change in the internal energy at constant temperature [Joule/mole]
$\Delta U(polar)$	total polar molar cohesive energy at equilibrium [Joule/mole]
$\Delta U(T)$	molar cohesive energy at equilibrium [Joule/mole]
∂V	change in the volume at constant temperature [m^3/mole]
ε_o	electric permittivity of vacuum [=1.1126E-10 Coulomb^2/J m]
$\varepsilon(polar)$	total polar components of the pair equilibrium intermolecular force energy parameter [Joule/molecule]
$\varepsilon(T)$	pair equilibrium intermolecular force energy parameter [Joule/molecule]
$\varepsilon(\omega)$	dielectric constant at alternating electric frequency, ω, [dimensionless]
κ_B	Boltzmann constant (R_g/N_{AV}) [= 1.380658E-23 J/K]
μ	intermolecular dipole moment of one repeat unit of the polymer [Coulomb m]
$v_o(T)$	molar volume of a repeat unit of polymer at zero pressure and as a function of temperature [m^3/mole].
$v_t(T, P)$	volume shrinkage term to account for crystallization [m^3/mole].
$\pi(T)$	internal pressure of polymer as a function of pressure [pa]
$\sigma_{equi}(T)$	pair equilibrium intermolecular force distance parameter at minimum potential energy [nm]

REFERENCES

Alger, M., "polymer Science dictionary", second edition, Chapman and Hall, New York, NY (1997).

Allen, G., D. Sims and G. J. Wilson, "Intermolecular Forces and Chain Flexibilities in Polymers. III – Internal Pressures of Polymers below their Glass Transition Temperatures", Polymer, 2, 375–799 (1961).

Balzani, V., A. Credi, F. M. Raymo and J. F. Stoddart, "Artificial Molecular Machines", Angew. Chem. Int. Ed. 39, 3348-3391 (2000).

Beiter, K. and K. Ishii, "Incorporating Dimensional Requirements into Material Selection and Design of Injection Molded Parts", Engineering Plastics (Rapra), 9, 435-456 (1996).

Boedeker Plastics, Inc., "Ultem PEI polyetherimide datasheet", 904 West 6th Street, Shiner, Texas 77984, USA.

Bottcher, C. J. F., "Theory of Electric Polarization", Elsevier Scientific Publishing Company, Amsterdam, NL (1973).

Chang, R. Y., C. H. Chen and S. K. Su, "Modifying the Tait Equation with Cooling-Rate Effects to Predict the Pressure-Volume-Temperature Behaviors of Amorphous Polymers: Modeling and Experiments", Polymer Engineering and Science, 36 (13), 1789-1795 (1996).

Chickos, J. S., S. Hosseini, D. G. Hesse, J. F. Liebman, " Heat capacity Corrections to a Standard State - A Comparison of New and Some Literature Methods for Organic Liquids and solids", Structural Chemistry. 4 (4) 271-278 (1993).

Cho, J. and I. C. Sanchez, "PVT Relationships and Equations of State of Polymers", in "Polymer Handbook", A. Abe and D. R. Bloch, Eds., John Wiley and Sons, Inc., New York, NY (1989), pp. VI/591-VI/601.

GE Plastics, One Plastics Avenue, Pittsfield, MA 01201, U. S. A.

Goudeau, S., J. Galy, J. F. Gerard, R. Fulchiron and J. L. Barrat, "Modelling Surface Properties of Linear Amorphous Polymers", Materials Research Society Symposium – Proceedings, 629 (2000) pp. FF9.2.1-FF9.2.6.

Hansen, C. M., "Hansen Solubility, Parameters: A User's Handbook", CRC Press, Boca Raton, FL (2000).

Hansen, C. M. and A. Beerbower, "Solubility Parameters", In "Kirk-Othmer Encyclopedia of Chemical technology", Supplement volume, second edition, A. Standen, Ed., Interscience, New York, NY (1971), pp. 889-910.

Hirschfelder, J.O., "Intermolecular Forces", John Wiley and Sons, Inc., New York, NY (1967).

HyperChem Pro 5.1 program, Hypercube Inc., Gainesville, FL, USA.

Israelachvili, J., "Intermolecular and Surface Forces", Second Edition, Academic Press Inc., San Diego, CA (1991).

Kurdi, J. and A. Y. Tremblay, "The Determination of Interaction Parameters in the Characterization of Polyetherimide Gas Separation Membranes Using Horvath-Kawazoe Model", Desalination, 148, 341-346 (2002), chapter IV.

Kurdi, J. and A. Y. Tremblay, "Experimental determination of the local microscopic structure and intermolecular force parameters of amorphous liquids and solids", Journal of Physical Chemistry, Part B., Submitted, chapter V.

Lindoy, L. F. and I. M. Atkinson, "Self-Assembly in Supramolecular Systems", The Royal Society of Chemistry, Cambridge, UK (2000).

Maitland, G. C., M. Rigby, E. B. Smith and W. A. Wakeham, "Intermolecular Forces: their origin and determination", Clarendon Press, Oxford, UK (1981).

Merdas I., F. Thominette and J. Verdu, "Humid aging of polyetherimide. II. Consequences of water absorption on thermomechanical properties", Journal of Applied Polymer Science, 77 (7) 1445-1451 (2000).

Ravikovitch, P. I., A. Vishnyakov, R. Russo and A. V. Neimark, "Unified approach to pore size characterization of microporous carbonaceous materials from N_2, Ar, and CO_2 adsorption isotherms", Langmuir 16 (5) 2311-2320 (2000).

Reinhard, M. and A. Drefahl, "Handbook for Estimating Physicochemical Properties of Organic Compounds", John Wiley and sons, Inc., New York, NY (1999).

Seitz J. T., The estimation of mechanical Properties of Polymers from Molecular structure", J. Appl. Polym. Sci. 49 (8) 1331-1351 (1993).

Simpson, J. O. and A. K. St. Clair, "Fundamental Insight on Developing Low Dielectric Constant Polyimides", NASA Langley Research Center, Hampton, VA 23681-0001, (2002).

Simon S.L., D. J. Plazek, J. W. Sobieski and E. T. Mcgregor, "Physical Aging of A Polyetherimide – Volume recovery and its Comparison to Creep and enthalpy Measurements, Journal of Polymer Science, Part B-Polymer Physics 35 (6) 929-936 (1997).

Stone, A. J., "The theory of Intermolecular Forces", Clarendon Press, Oxford, UK (1996).

Van Krevelen, D. W., "Properties of Polymers", Elsevier, Amstrdam, NL (1997).

Vlachos, D. G. and M. A. Katsoulakis, "Derivation and Validation of Mesoscopic Theories for Diffusion of Interacting Molecules", Physical Review Letters, 85 (18), 3898–3901 (2000).

Zoller, P., "PVT Relationships and Equations of State of Polymers", in "Polymer Handbook", J. Brandrup and E. H. Immergut, Eds., John Wiley and Sons, Inc., New York, NY (1999), pp. VI/475-VI/483.

CHAPTER VIII

The Influence of Cobalt Complexes on the Microporosity and Performance of Polyetherimide Gas Separation Membranes

J. Kurdi, and A. Y. Tremblay*

Department of Chemical Engineering, University of Ottawa, 161 Louis Pasteur, Ottawa, Ontario, K1N 6N5, Canada

*Corresponding author

André Y. Tremblay

Tel.: +1-613-562-5920; fax: +1-613-562-5172

E-mail address: tremblay@uottawa.ca

CHAPTER VIII

Paper 7: The Influence of Cobalt Complexes on the Microporosity and Performance of Polyetherimide Gas Separation Membranes

J. Kurdi, and A. Y. Tremblay
Department of Chemical Engineering, University of Ottawa, 161 Louis Pasteur, Ottawa, Canada, K1N 6N5

ABSTRACT

The microporosity and gas separation performance of polyetherimide membranes containing Cobalt complexes was investigated. A total of nine Cobalt complexes were selected mostly based on their affinity for oxygen. Membranes were cast from polyetherimide (PEI)/N-methylpyrrolidinone (NMP) solutions containing 1, 3, 7, 10, and 15% of Cobalt additive. The results indicate that increasing the concentration of the Cobalt additive leads to an increase in the total micropore volume of membrane. Cobalt(II) phthalocyanine produces a membrane having a micropore size distribution whose mode and average is greater by 0.09 – 0.12 nm than all other membranes produced in this work. This membrane had the best performance above a permeance of 0.36 GPU. Below the permeance of 0.36 GPU, the addition of Cobalt(II) 2,3-naphthalocyanine to PEI gave the best performance. All additives increased the intrinsic microporosity of the PEI network. Most additives formed nanostructured materials with a unique microporosity defined by pores at the nanoparticle-PEI polymer interface. The results also show a clear correlation between the performance of a gas separation membrane and its microporous structure.

Keywords: Cobalt complexes, microporosity, polyetherimide, gas separation membranes, nanoparticles, molecular engineering.

1 INTRODUCTION

The engineering of novel structures at the molecular and supramolecular levels is an interdisciplinary field that links nanomaterial synthesis, structure and properties relationships (Ying, 2001, Ciferri, 2000). Tailoring of high surface area materials with regular pore structures at an atomic to nanometer scale is important in the development of new materials having superior characteristics and properties for adsorption, separation and catalysis applications (Ying, 2001, Pinnavaia and Thorpe, 1995, Tanev et al., 1994, Davis, 1993).

Architecturing porous nanostructured materials can be achieved by using molecular building blocks consisting of cyclic, nanoscale cavity-containing coordination compounds (Hupp and Nguyen, 2001). Macrocyclic liquid crystals such as porphyrins and phthalocyanines were found to be suitable nano-meter scale molecular building blocks to tailor material properties (Kosal and Suslick, 2000, Suslick et al. 2000).

Metallic chelates that are usually used as oxygen carriers were reviewed for applications such as gas separation and catalytic activation of dioxygen in various oxidation reactions (Li and Govind, 1994, Martell and Sawyer, 1988, Niederhoffer et al. 1984, Simándi, 1992). However, it was found that these oxygen carriers in solution suffer from dimerization and irreversible oxidation (Taylor et al. 1989, 1992, Imamura and Lunsford, 1985). Collman et al. (1975, 1978) used a picket fence molecular structure to prevent the dimerization of iron porphyrin and to provide a nonacidic environment. It was also found that binding or incorporating of the metal complexes to microporous solids or molecular sieves leads to an increase in their stability and activity (Taylor et al. 1989, 1992, Drago et al. 1980, Wang et al. 2000, Lei et al. 2000).

The effect of oxygen carriers on gas permeability and selectivity is based on the method of incorporating or binding the metal complex-membrane material and their possible interactions. For instance, chelate membranes containing Schiff base oxygen carriers were prepared from poly(vinyl alcohol)/poly(N-salicylidene allyl amine) blends. The permeability and selectivity of oxygen over nitrogen were increased on increasing the Cobalt(II) content (Choi et al. 1995). The same results were also found for adding Cosalen to Cobalt(II)-neutralized sulfonated EPDM (Ethylene-Propene-Diene

terpolymer) ionomer membranes (Zhang and Lin, 1999, 1995). Chen and Lai (1996) found that the increase in the content of oxygen carrier (Cosalen) additive in polycarbonate membrane leads to a decrease in the permeability of oxygen and nitrogen gases but an increase in the selectivity of oxygen over nitrogen. They have attributed this influence to an increase in the packing density within the membrane, increase in the Cosalen content in the membrane as indicated by X-ray diffraction, and the domination of gas diffusion over gas solubility. The same conclusion was also obtained for adding Cosalen to polyurethane membranes (Chen et al. 2000).

It is worth noting that these results were also influenced by permeation test conditions such as temperature, upstream pressure or pressure difference across the tested membrane. In systems such as Cobalt porphyrin bonded to Vycor glass (Nishide et al. 1995, 1994) or Cosalen blended to Cobalt (II)-neutralized sulfonated EPDM (Ethylene-Propene-Diene terpolymer) ionomer membranes (Zhang and Lin, 1999, 1995), the permeability and selectivity of oxygen decreased with increasing upstream pressure or pressure differences, while nitrogen permeability remained constant. Increasing temperature lead to a decrease in the selectivity and an increase in the oxygen permeability of the membrane. The influence of adding oxygen carriers on oxygen/nitrogen membrane separation was attributed to a structural diffusion factor by using X-ray diffraction measurements (Chen and Lai, 1996) or using diffusion model (Nishide et al. 1995).

The change in the micropore size and micropore size distribution due to the use of different types of additives was not previously investigated. The microporous structure-gas separation performance relationship is very important in the 0.3 to 2 nm range. Three groups of Cobalt complexes: First group, Cobalt(II) ligated to Schiff-bases and benzoylacetonate, second group, neutral and cationic Cobaltocenes and the third group, unsubstituted and substituted Cobalt(II) phthalocyanines were added into polyetherimide/N-methylpyrrolidone solutions and cast into asymmetric flat membranes. The microporous structure of these membranes was determined using nitrogen adsorption and Horvath-Kawazoe slit model. The performance of these membranes for oxygen/nitrogen separation was also tested and the structure-performance relationship discussed.

2 EXPERIMENTAL

2.1 Materials

Polyetherimide (PEI, Ultem® 1000) was supplied from the General Electric Plastics in pellet form and was dried in a vacuum oven (725 mm Hg vacuum) at 140°C for 24 hours. Anhydrous 1-methyl-2-pyrrolidinone (Aldrich, 99.5 %, reagent grade, water < 0.005%) was supplied from Sigma-Aldrich Canada Ltd, ON., Canada. Methyl alcohol (BDH, microscopic grade), hexanes (BDH, reagent grade), and isopropyl alcohol (OmniSolv®, EM Science, water 0.05% max) were supplied by VWR CANLAB, QC, Canada. The nine different Cobalt complexes used in this work are shown in Table 8.1. They were supplied from Sigma-Aldrich Canada Ltd, ON., Canada and from Strem Chemicals, INC., MA, USA. These Cobalt complexes and N-methylpyrrolidinone were used as supplied but under dry nitrogen atmosphere. All other solvents were used without any further purification. Ultra high purity gases, nitrogen and helium (PRAX AIR, Ottawa, ON., CA) were used. Medical air (PRAXAIR, Ottawa, ON., CA) was used to test the membrane for oxygen separation. All gases were used as supplied without any further purification.

2.2 Membrane preparation

Casting solutions made from polyetherimide (PEI), 1-Methyl-2-pyrrolidinone anhydrous (NMP) and one of the additives shown in Table 8.1 were prepared under nitrogen atmosphere in a glove bag placed inside a fume hood. The ratio of PEI/NMP by weight was always (23/77) while many ratios of additive/PEI by weight were specified to be 1, 3, 7, 10 and 15%. One membrane sample was prepared without additives.

For each sample, the additive was first combined with NMP in a Nalgene polypropylene jar with a screw cap under nitrogen atmosphere and rolled at room temperature for many days until a clear solution was obtained. The polymer was added to the NMP solution under nitrogen atmosphere, sealed and rolled again for many days until a homogenous clear solution was obtained. The resulting solution was cast at room temperature onto a clean glass plate using a knife having a gap of 250 microcmeter and then quickly immersed in a coagulation bath of isopropyl alcohol for 5 minutes. The

Table 8.1 Cobalt complexes used in this study.

Group	Abbreviations	Cobalt complex name	Chemical structure
1	Co(salen)	Catalog No. # 274712 N,N'-Bis(salicylidene)ethylenediamine Cobalt(II) salt hydrate	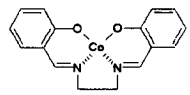
	CoSMDPT Co(salmdpt) Co(NMesalpr)	Catalog No. # 360155 Bis(salicylideniminato-3-propyl)methylaminoCobalt(II)	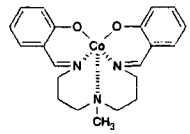
	Co-Jacobsen Ligand	Catalog No. # 27-0525 (1R,2R)-(-)-1,2-Cyclohexanediamino-N,N'-bis(3,5-di-t-butylsalicylidene)Cobalt (II)	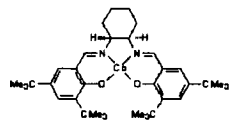
	Co-benzyol acetonate	Catalog No. # 316881 Cobalt(II) benzoylacetonate	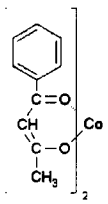
2	Cobaltocene $CoCp_2$	Catalog No. # 33,916-4 Bis(cyclopentadienyl)Cobalt	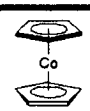
	$CoCp_2PF_6$ Cobaltocenium-PF_6	Catalog No. # 27,981-1 Bis(cyclopentadienyl)Cobalt(III) hexafluorophosphate	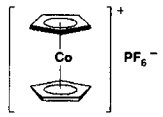
3	CoPc	Catalog No. # 30,769-6 Cobalt(II) phthalocyanine	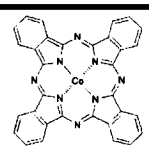
	$CoF_{16}Pc$	Catalog No. # 44,664-5 Cobalt(II) 1,2,3,4,8,9,10,11,15,16,17,18,22,23,24,25-hexadecafluoro-29H,31H-phthalocyanine	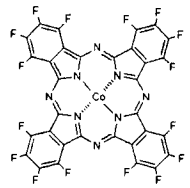
	Co(2,3-NPc) CoNPc	Catalog No. # 38,192-6 Cobalt(II) 2,3-naphthalocyanine	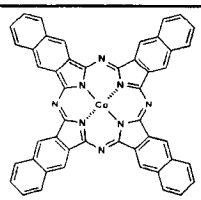

All additives in Table 8.1 were supplied from Aldrich, Sigma-Aldrich Canada LTD, ON., Canada except Co-Jacobsen Ligand was supplied from Strem Chemicals, Inc., MA, USA.

coagulated film was immersed in methanol for 16 hours and moved to a bath of hexanes for two days. The membrane was taken out to normal atmosphere for three days, before three circular coupons of 65 mm diameter were cut for each membrane and used in the permeation test. The remaining sections were cut into small strips and used in the nitrogen adsorption measurements. This ensured that microporous measurements were performed on material that originated from the same cast sheet.

2.3 Determination of the micropore size distribution

Approximately 1 gram of strips were precisely weighed, filled in the sample tube and degased at a pressure of 0.002 ± 0.0005 mm Hg and temperature 40 °C for 12 hours. The isotherm was measured by an automated volumetric porosity analyzer ASAP 2000M produced by Micromeritics (GA, USA). Ultra high purity gases, nitrogen and helium (PRAXAIR, Ottawa, ON., CA) were used in the porosimeter. Liquid nitrogen was used in the sample bath to keep temperature at 77 K. The micropore size distribution was determined from the isotherm measurements using the Horvath-Kawazoe slit model. The parameters required in this model were determined as explained elsewhere (Kurdi and Tremblay, chapter IV in this thesis).

2.4 Permeation test

A cross-flow test cell having a permeate surface area of 20 cm^2 was used. Medical grade air (PRAXAIR) at a pressure of 12.8 barg (200 psig) was fed to the cell. The flow of the retentate was set at 400 ml (STP)/min and the permeate discharged to atmosphere. The volumetric permeate gas flow rate was measured by a bubble flowmeter and the oxygen concentration in the permeate gas was determined using Gas Chromatography. Due to the difference in the thermal conductivity between oxygen and nitrogen, oxygen concentration in the permeate was corrected using the following equation (Academy of China, 1972):

$$y_{corr} = \frac{\left(\frac{y}{40}\right)*100}{\left(\frac{y}{40}\right)+\left(\frac{100-y}{42}\right)} \qquad (1)$$

where y is the oxygen concentration (%) in the permeate calculated by gas chromatography and y_{corr} is the corrected one. Oxygen permeance and nitrogen permeance were determined as explained elsewhere (Kurdi and Tremblay, chapter II). The total gas permeance is the sum of permeances of oxygen and nitrogen. The selectivity was considered to be the ratio of oxygen permeance to nitrogen permeance.

3 RESULTS AND DISCUSSION

3.1 Influence of additives on the microporosity of PEI membranes

Preliminary experiments in our laboratory were used to establish a membrane preparation technique for the PEI/NMP/Cobalt complex system. The limitations in using a single preparation method for all additives is that it is suitable for some but not for all. Therefore, some additives had to be excluded from our study in case of unsuitability of the preparation method.

All additives shown in Table 8.1 were soluble in NMP except the Co-Jacobsen Ligand. This additive was partially soluble in NMP leaving solid particles in the resulting membrane. This caused considerable variability in the separation and permeance results from membranes containing the additive. These membranes had pinholes as evidenced by the non-selective nature of the membranes. It was also found that the additive Cobaltocene was partially leached out in the methanol bath as observed by the yellowish colour of the bath. The leaching process left a very open membrane that was not selective for oxygen/nitrogen separations. These problems were not encountered with other additives listed in Table 8.1.

The micropore size distributions were calculated from nitrogen adsorption isotherms using the Horvath-Kawazoe (HK) slit model. This distribution is limited to pores less than 2 nm where the HK characterization method is valid and the micropore size range is suitable for gas separation. The results are shown in Figures 8.1, 8.2 and 8.3 for all membranes. Each membrane contains 3% (w/w) of additive with respect to the weight of PEI. Membranes were made from each additive listed in Table 8.1. Comparing these micropore size distributions with the sample without additives, it is clear that all additives lead to an increase in the micropore volume of membranes.

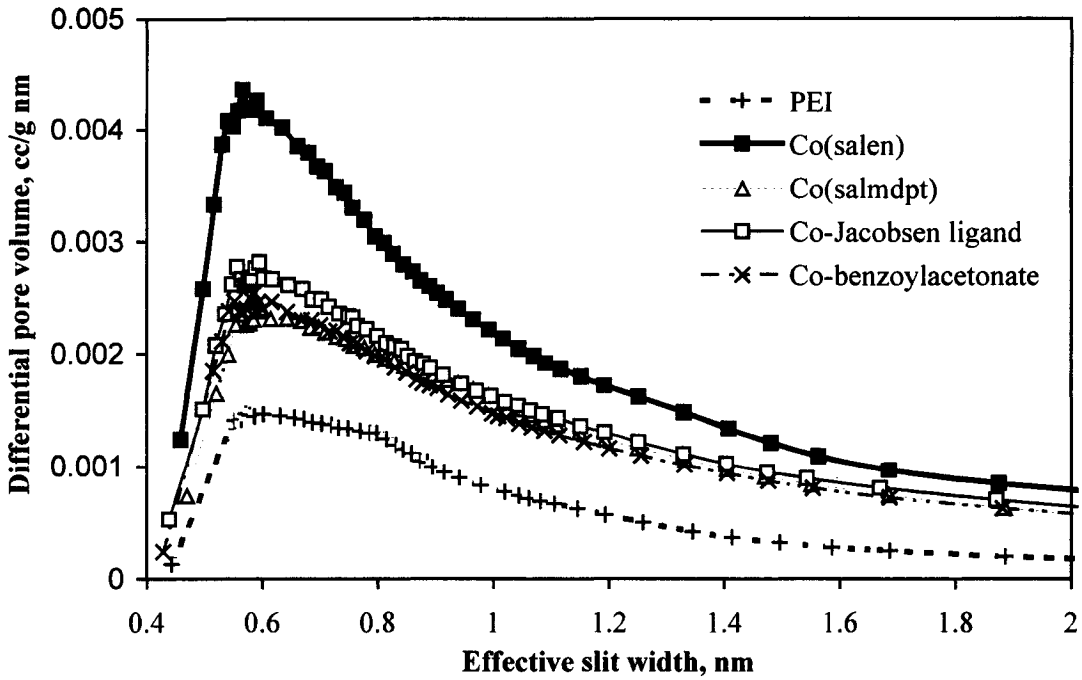

Figure 8.1 Micropore size distribution for PEI membranes containing group (1) additives shown in Table 8.1 and basecase without additive. Differential pore volume (cm^3/g nm) vs. effective slit width in nm.

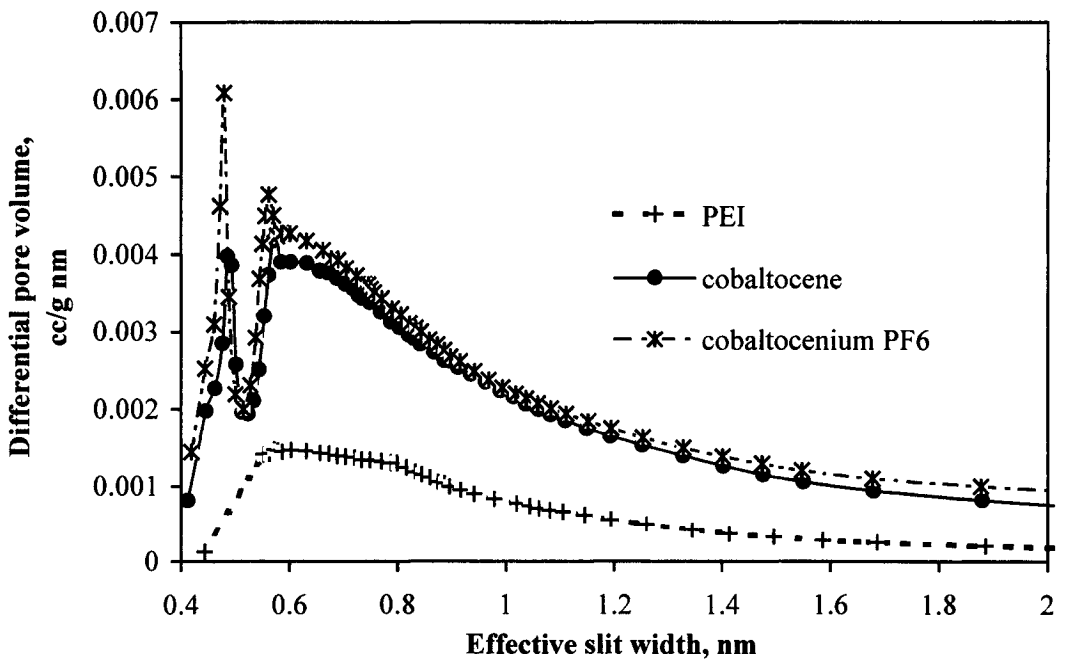

Figure 8.2 Micropore size distribution for PEI membranes containing group (2) additives shown in Table 8.1 and basecase without additive. Differential pore volume (cm^3/g nm) vs. effective slit width in nm.

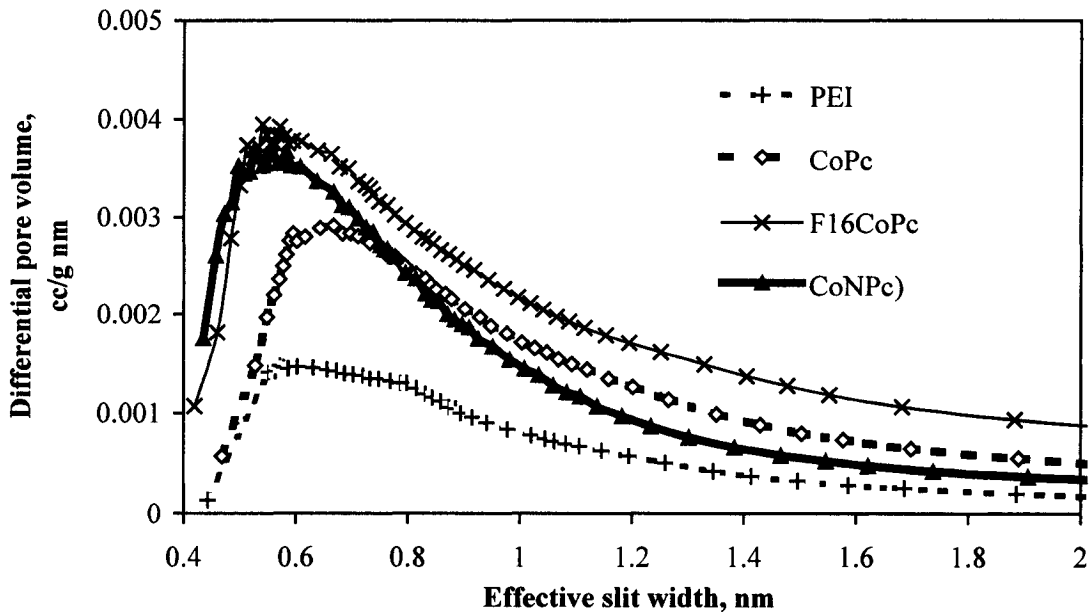

Figure 8.3 Micropore size distribution for PEI membranes containing group (3) additives shown in Table 8.1, and basecase without additive. Differential pore volume (cm^3/g nm) vs. effective slit width in nm.

Micropore size distributions of membranes containing Cobalt(II) chelates from group 1 (Table 8.1): Co(salen), Co(salmdpt), Co(Jacobsen ligand) and Co(benzoyl acetonate) are shown in Figure 8.1. The most frequent slit width (mode) for the Co(salen)/PEI membrane is approx. 0.57 nm which corresponds to a differential micropore volume of 0.0043 cc/g nm. This membrane has a higher differential micropore volume compared to 0.0024-0.0028 cc/g nm for other membranes containing the last three additives. The larger micropore volume in the Co(salen)/PEI membrane compared to membranes from the other additives can be explained based on the structure and properties of these Co(II) chelates. Co(salen) is reported to have a planar structure while Co(salmdpt) has a trigonal bipyramidal structure (Jone et al., 1979). Co-Jacobsen ligand has a similar chemical structure to Co(salen) but with extended hydrocarbon substituents that make the molecule more bulky. The Co(salen) forms structures quite readily due to its planar geometry whereas Co(salmdpt), Co-Jacobsen, and Co(benzoylacetonate) are more bulky and do not readily stack into nanosized aggregates. Micropores will also be created in the interstitial spaces between the polymer and nanoparticles. In domains within the PEI matrix where the Co(salen) is disordered, it will exist as fine randomly arranged flat platelets with an open structure having a high

connectivity. The presence of these platelets within the PEI polymers molecules will create a more open and accessible polymer network as evidenced by the substantial increase in the microporosity of the membrane for Co(salen) in Figure 8.1, while maintaining the shape of the micropore size distribution. The resulting micropore size distributions have the characteristic signature of the PEI without additives with a mode at approx 0.57 nm and a gradual decline to 2 nm. The planar Co(salen) gave the highest accessibility as evidenced by the greater micropore volume obtained for this additive over other group 1 compounds in Figure 8.1.

Micropore size distributions of membranes containing neutral and cationic Cobaltocene group 2 additives (Table 8.1) are shown in Figure 8.2. These additives were also used as supporting electrolytes in conductive polymer films (Galal et al. 1997). Both additives produced similar micropore size distributions having double peaks but with a little larger differential pore volume for the Cobaltocenium-PF_6 additive. The first peak was attributed to the microporosity of Cobaltocene-methanol clathrate. The resolution of this peak attests to the sensitivity of the micropore characterization technique. This peak disappeared on heating the membranes in a vacuum oven at 90 °C for 24 hours. The peak was not present when methanol was not used in preparing the membrane.

Porphyrins can form clathrate lattices by hosting different guest solvents (Byrn et al. 1993, 1991). For example, methanol as a guest molecule forms a "herring-bone" array of porphyrin molecules forming chain structures. Beauvais et al. (2000) reported that Cobalt complexes form octahedral species with small protic solvents such as methanol that participate in bridging between metal centers. The resulting network structure consists of an array of one-dimensional channels with a minimum internal diameter of 0.48 nm (Beauvais et al. (2000)) which is in agreement with the size of the first peak in Figure 8.2. The second peak has the same micropore size as polyetherimide membrane without additives leading to the conclusion that the dispersion of the nanophases of both Cobaltocene and Cobaltocenium-PF6 causes an increase in the connectivity and accessibility of microporous polyetherimide membranes.

Micropore size distributions of membranes containing unsubstituted and peripherally substituted phthalocyanines are shown in Figure 8.3. Phtalocyanines (known systematically as tetra-aza-tetra-benzoporphyrines) are planar 18-π-electron heterocyclic

aromatic coordination compounds having a variety of architectural forms and high stability (Kobayashi et al., 2002). Metal phthalocyanines show remarkable aggregation at low concentrations (Lever et al. 1986) and low solubility in common organic solvents (Drechsler and Hanack, Ch 8 in Atwood et al. 1996). Peripherally substituting phthalocyanines with elements or organic group improve the phthalocyanines' solubility and coupling to different polymers (Wohrle et al. 1993). This was clearly observed through the difficulty and longer time to dissolve CoPc in NMP solvent compared to the other substituted phthalocyanines listed in group 3 Table 8.1. CoPc had a lower affinity to PEI and yielded a larger interstitial spacing between the phases of the phthalocyanine and polymer. This agrees with the shift in the mode of the micropore distribution for PEI and PEI with group 1 additives vs. that of PEI with CoPc where the mode changes from 0.57 to 0.66 as seen in Figures 8.1 and 8.3.

Both CoNPc and $CoF_{16}Pc$ have a higher affinity to the PEI polymer leading to a shift in the mode from 0.57 to 0.54 nm. The larger differential micropore volume for membranes containing CoNPc or $CoF_{16}Pc$ compared to CoPc is attributed to the better solubility of these two additives in the PEI-NMP solution that leads to smaller nanoparticles dispersed in the PEI polymer network and a higher nanoparticle-polymer interfacial area. For a micropore of size larger than 0.8 nm; membranes produced with $CoF_{16}Pc$ additive have the largest differential volume among the three additives, this can be attributed to the highest ability to keep organic solvents such as methanol in its disordered structure. The aggregation of $CoF_{16}Pc$ into a disordered structure was observed by Hipps et al. (2002). This explanation is also supported in the literature. The donor-acceptor intermolecular hardness decreases in the following order $CoF_{16}Pc$ > CoPc > CoNPc (Cardenas-Jiron et al., 2001) that indicates $CoF_{16}Pc$ has a better affinity to a hard base donor HBD solvent such as methanol. The removal of solvent causes a more open structure in the resulting membranes.

The CoNPc aggregate is the better organized in this group due to the aromatic substituents that increase the π–π stacking interactions leading to microporous nanoscale structures (Inabe, 2000). In addition to this, PEI has an irregularly shaped, nonlinear, kinked polymer chain with rigid segments and several swivel points (Ohya et al. 1996). This is illustrated in the characteristic micropore size distribution found in the membrane

produced from PEI and those made from several additives as seen in Figures 8.1, 8.2 and 8.3. The more extended double phenyl arms of the CoNPc will have greater steric interactions to penetrate the intrinsic microporous network caused by the irregularly shaped polymer. The planar cross-shaped CoNPc will also lead to the creation of micropores at the interface of the CoNPc-PEI polymer. These considerations will lead to a change in the shape of the micropore distribution where the mode and the micropore volume above 0.8 nm both decrease. This is a departure from the PEI characteristic micropore size distribution found in Figures 8.1, 8.2 and 8.3 indicating a substantial and beneficial change in the microporous structure of the membrane.

The influence of additive concentration on the micropore size distributions of the membranes was also examined. Using the CoPc additive at concentrations 3, 7 and 10% (w/w), the differential micropore volume versus effective slit width was plotted in Figure 8.4. It is clear that increasing the concentrations of this additive leads to a general increase in the microporosity of the PEI matrix as seen in Figure 8.4. As previously explained, this is due to an increase in the number of dispersed additive nanophases. The spacing in the interfaces provides increased connectivity and accessibility within PEI network structure. The same observation was found for other additives but was not included in this work.

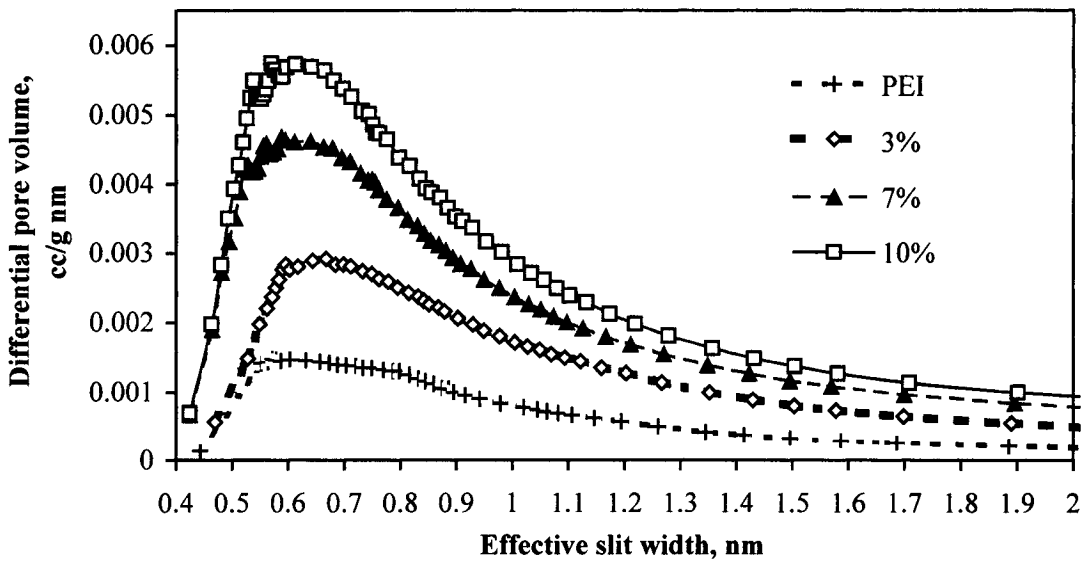

Figure 8.4 Micropore size distribution for PEI membranes containing CoPc additive at concentrations 3, 7 and 10 % (w/w), and basecase without additives. Differential pore volume (cm^3/g nm) vs. effective slit width in nm.

3.2 Influence of additives on the O_2/N_2 separation of PEI membranes

The air permeance of membranes containing all additives in Table 8.1 except Cobaltocene were plotted as a function of additive concentration in Figure 8.5 for groups (1 and 2) and in Figure 8.6 for group (3). Increasing the concentration of any additive leads to a general increase in the membrane permeance. This is consistent with the increase in the total micropore volume of the membranes as shown in Figure 8.4. Membranes containing Co-benzoylacetonate have higher permeance and a larger slope with greater concentrations than membranes containing other additives in group (1 and 2). This can be explained by the higher affinity of this additive to isopropanol used as the primary gelation bath in making the membrane, which increases the dynamics of the phase inversion process causing a thinner selective skin layer at the surface of the membrane compared to other additives in groups 1 and 2. On the other hand, the slope of the permeance vs. concentration plot for membranes containing Cobaltocenium-PF6 is lower since it has less affinity to isopropanol and yields a thicker skin than other membranes in groups (1 and 2).

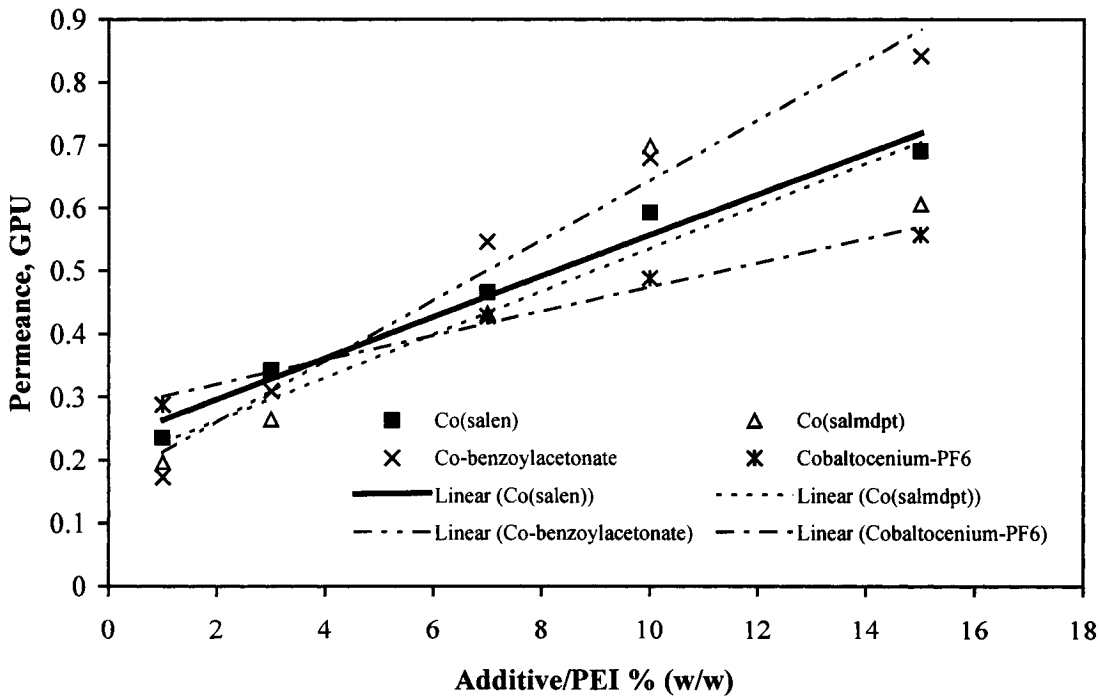

Figure 8.5 Plot of the total permeance, GPU vs. the percentage of the (additive/PEI) ratio in the casting solution for air separation by membranes containing group (1 and 2) additives shown in Table 8.1. Membranes containing Cobaltocene and Co-Jacobsen Ligand were not included because of its very high permeance.

The permeance of membranes cast from group (3) additives at different concentrations were plotted in Figure 8.6. Increasing the concentration of a single additive leads to an increase in membrane permeance that was attributed to the increase in the total micropore volume of the membranes produced as discussed above. Looking at the slopes for all three additives in group 3, a larger slope was obtained for membranes containing CoPc. This was attributed to the dynamics of the phase inversion process. CoPc has a higher affinity to isopropanol than others in this group which leads to the formation of thinner skins at the surface of the membrane. The lower permeances of membranes containing CoNPc is attributed to the smaller micropore sizes for these membranes as indicated by the lower differential micropore volume for slit width larger than 0.8 nm as seen in Figure 8.3.

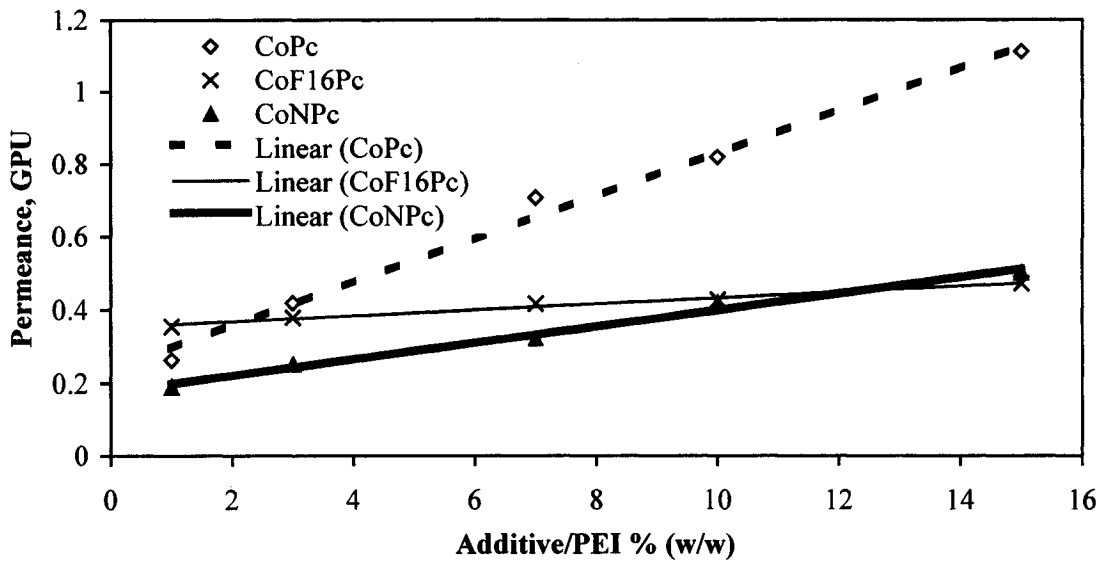

Figure 8.6 Plot of the total permeance, GPU vs. the percentage of the (additive/PEI) ratio in the casting solution for air separation by membranes containing group (3) additives shown in Table 8.1.

The selectivities of membranes of groups (1 and 2) at different additive concentrations were plotted in Figure 8.7. The selectivity trade off with membrane permeance is clear when Figure 8.7 is compared with Figure 8.5. Increasing permeance leads to a decrease in the selectivity for all membranes containing additives in groups (1 and 2). The selectivity of membranes in group (3) at different additive concentrations were plotted in Figure 8.8. Comparing with Figure 8.6, the same trade off between selectivity and permeance was observed.

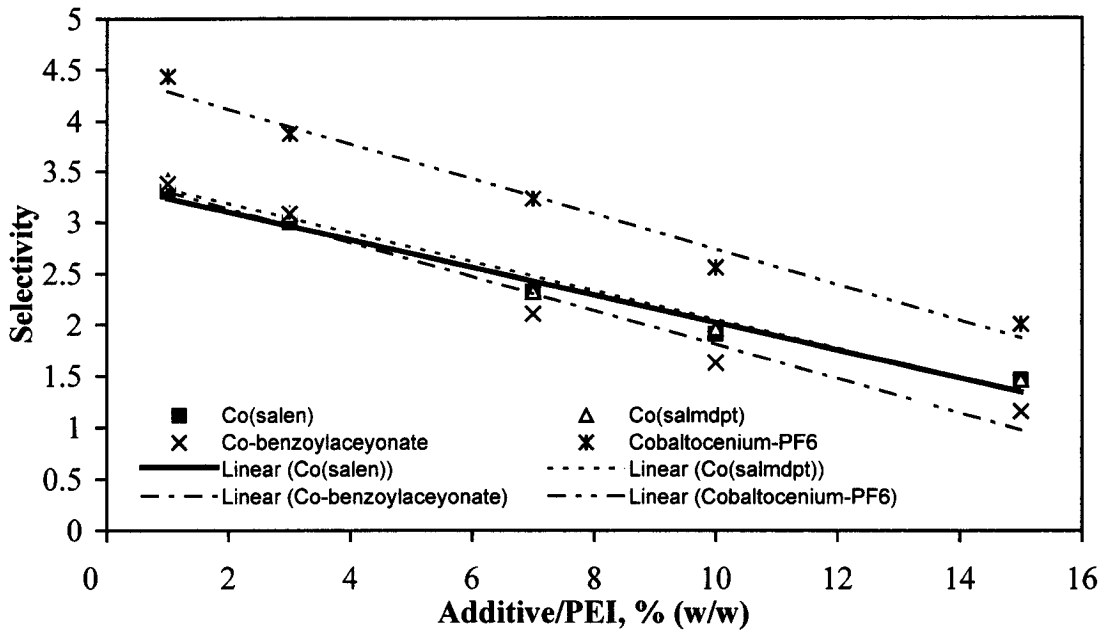

Figure 8.7 Plot of O_2/N_2 selectivity vs. the percentage of the (additive/PEI) ratio in the casting solution for air separation by membranes containing group (1 and 2) additives shown in Table 8.1. Membranes containing cobaltocene and Co-Jacobsen Ligand were not included as they had no air separation.

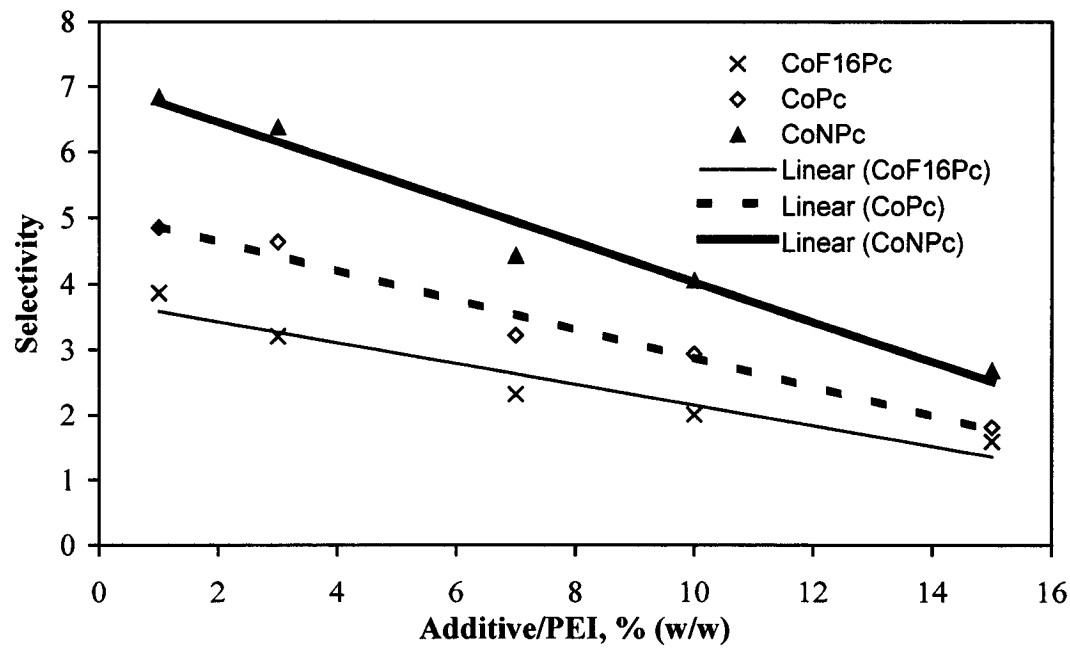

Figure 8.8 Plot of O_2/N_2 selectivity vs. the percentage of the (additive/PEI) ratio in the casting solution for air separation by membranes containing group (3) additives shown in Table 8.1.

In order to discuss membrane performance for air separation, the trade off between selectivity and permeance was plotted in Figure 8.9 for groups (1 and 2). All additives of group (1 and 2) produced membranes with similar performance. However, membranes containing Cobaltocenium-PF6 showed a higher performance at low permeance (less than 0.55 GPU) corresponding to lower additive concentrations. This can be attributed to the beneficial change in the micropore size distribution as seen in Figure 8.2. The decrease in the membrane performance with increasing the concentration of Cobaltocenium-PF6 can be attributed to an increase in the differential micropore volume of larger slit sizes resulting from methanol removal discussed earlier in this work.

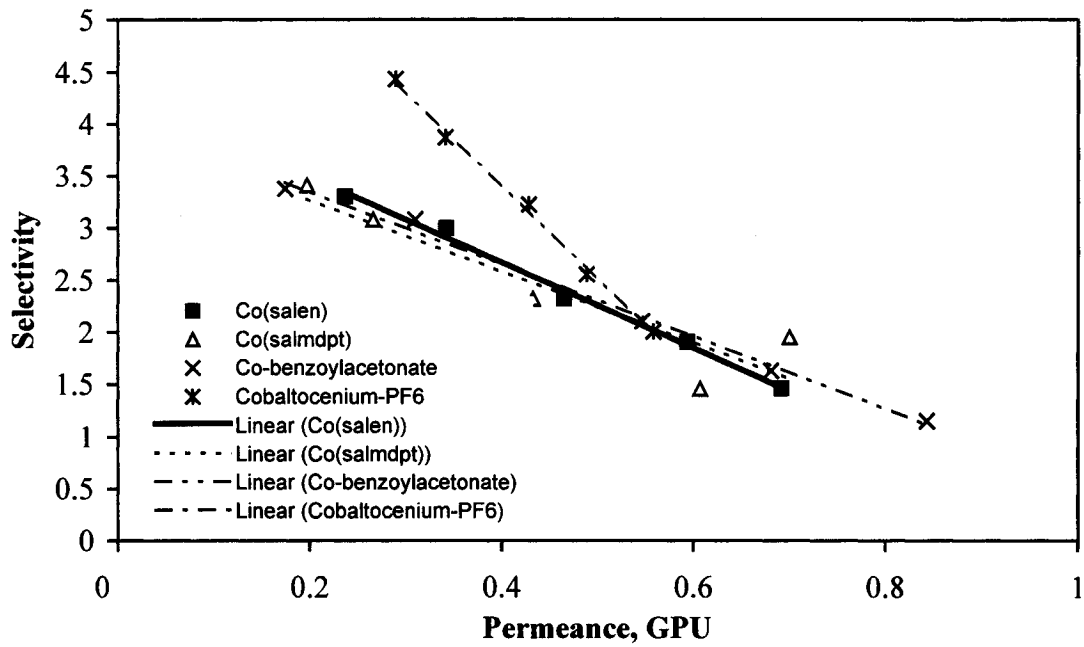

Figure 8.9 Performance plot of O_2/N_2 selectivity vs. the total permeance, GPU for air separation by membranes containing group (1 and 2) additives shown in Table 8.1.

The performance of membranes containing additives from groups (2 and 3) has been plotted in Figure 8.10. Membranes containing CoNPc show the best performance for air separation when the permeance is less than 0.36 GPU matching the expectations of the more narrow micropore size distribution in Figure 8.3. Membranes containing the additive CoPc had the best performance at a permeance greater than 0.36 GPU where the flat planar of CoPc produces a microporous network having a mode with 0.1 nm larger than the CoNPc as seen in Figure 8.3. The shape of the micropore size distribution is also different where the CoPc produces greater microporosity above 0.8 nm than CoNPc.

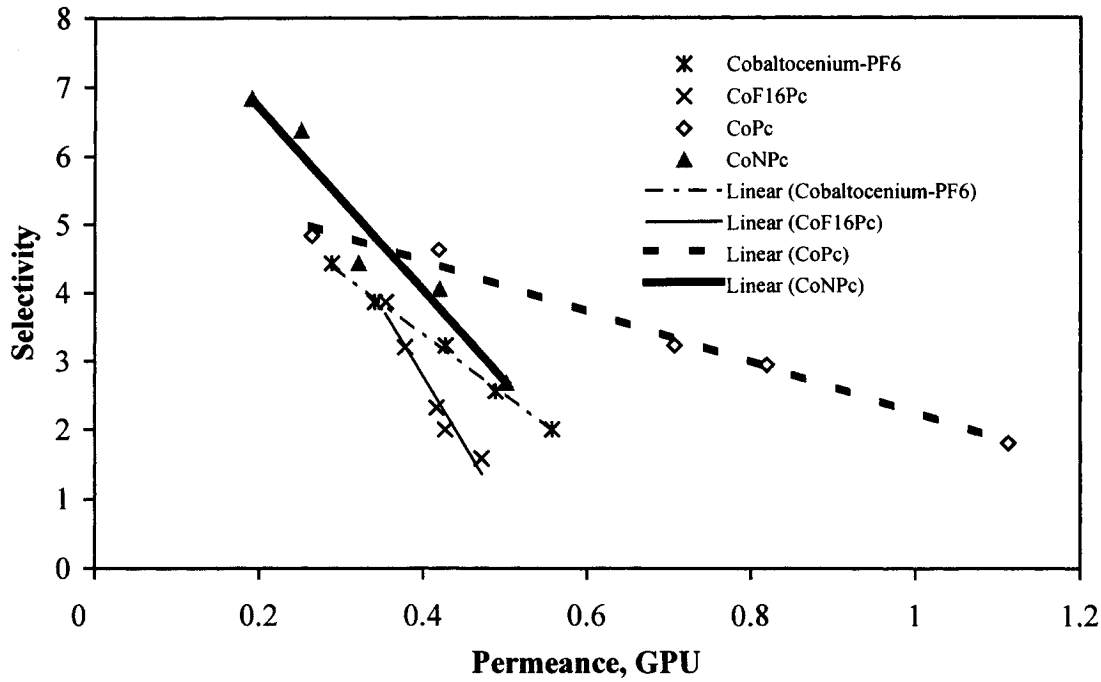

Figure 8.10 Performance plot of O_2/N_2 selectivity vs. the total permeance, GPU for air separation by membranes containing group (3) additives shown in Table 8.1. Membrane containing Cobaltocenium-PF_6 was included for the purpose of comparison.

4 CONCLUSIONS

Incorporating Cobalt chelates into polyetherimide membranes is a useful method to increase the microporosity and gas separation performance of the polymeric membranes. Increasing the concentration of one additive into polyetherimide membranes leads to an increase in the microporosity, an increase in the gas permeance and a decrease in the gas selectivity. In most cases, increases in microporosity were attributed to an increase in the connectivity and accessibility of the polymer network. The shift in the mode of the pore volume distribution was observed and attributed to spacing within the nanoparticles and at the interface between the nanoparticles-PEI polymer.

CoPc additive lead to a membrane with a mode of 0.66 nm, and the best air separation performance when the permeance is greater than 0.36 GPU. For gas permeance below 0.36 GPU, membrane produced using CoNPc had a better air separation performance. The two Cobalt chelates that displayed the best performance for gas separation contained phenyls surrounding the metal chelate ring. This increased

performance was attributed to both steric interactions with the polymer chain and a more structured nanophase due to the π-interactions of the phenyl groups.

The results indicate that phtalocyanine nanoparticles can be used to enhance the performance of polyetherimide gas separation membranes.

REFERENCES

Academy of China, Physics Institute of Dalian, "Gas Chromatography", Science Press Inc. of China, China (1972).

Beauvais, L. G., M. P. Shores and J. R. Long, "Cyano-Bridged Re_6Q_8 (Q= S, Se) Cluster-Cobalt(II) Framework Materials: Versatile Solid Chemical Sensors", J. Am. Chem. Soc. 122, 2763-2772 (2000).

Byrn, M. P., C. J. Curtis, Y. Hsiou, S. I. Khan, P. A. Sawin, S. K. Tendick, A. Terzis and C. E. Strouse, "Porphyrin Sponges: Conservation of Host Structure in over 200 Porphyrin-Based Lattice Clathrates", J. Am. Chem. Soc. 115, 9480-9497 (1993).

Byrn, M. P., C. J. Curtis, I. Goldberg, Y. Hsiou, S. I. Khan, P. A. Sawin, S. K. Tendick and C. E. Strouse, "Porphyrin Sponges: Structural Systematics of the Host Lattice", J. Am. Chem. Soc. 113, 6549-6557 (1991).

Chen, S. H. and J. Y. Lai, "Polycarbonate/(N,N'-dialicylidene ethylene diamine) Cobalt(II) complex Membrane for Gas Separation", J. Appl. Polym. Sci. 59, 1129-1135 (1996).

Chen, L., H. Xu and C-Z Yang, "The Study of Metal-Schiff Base Coordinated Polyurethane", Polym. Adv. Technol. 8, 335-338 (1996).

Chen, S. H., K. C. Yu, S. L. Houng, J. Y. Lai, "Gas transport properties of HTPB based polyurethane/Cosalen membrane", J. Membrane Sci. 173(1), 99-106 (2000).

Choi, M. J., C. K. Park and Y. M. Lee, "Chelate Membrane from Poly(vinyl alcohol)/Poly(N-salicylidene allyl amine) Blend. II. Effect of Co(II) Content on Oxygen/Nitrogen Separation", J. Appl. Polym. Sci. 58, 2373-2379 (1995).

Chow, G-M., I. A. Ovid'ko and T. Tsakalakos, Eds., "Nanostructured Films and Coatings", Kluwer Academic Publishers, Dordrecht, NL (2000).

Ciferri, A., Ed., "Supramolecular Polymers", Marcel Dekker, Inc., New York, NY (2000).

Collman, J. P., J. I. Brauman, K. M. Doxsee, T. R. Halbert, S. E. Hayes and K. S. Suslick, "Oxygen Binding to Cobalt Porphyrins", J. Am. Chem. Soc. 100, 2761-2766 (1978).

Collman, J. P., R. R. Gagne, C. A. Reed, T. R. Halbert, G. lang and W. T. Robinson, "Picket Fence Porphyrins. Synthetic Models for Oxygen Binding to Hemoproteins", J. Am. Chem. Soc. 97, 1427-1439 (1975).

Davis, M. E., "Organizing for better Synthesis", Nature 364, 391-393 (1993).

Drago, R. S., J. Gaul, A. Zombeck and D. K. Straub, "Preparation and catalytic Oxidizing Potential of Polymer Supported Chelating Amine and Schiff Base Complexes", J. Am. Chem. Soc. 102:3, 1033-1038 (1980).

Drechsler, U. and Hanack, M., "Towards Semiconducting Polynuclear Bridged Complexes Incorporating Phthalocyanines", in "Comprehansive Supramolecular Chemistry", J. L. Atwood, J. E. D. Davies, D. D. MacNicol, F. Vögtle, J-M. Lehn and M. W. Hosseini, Eds., vol.9, Pergamon Press, Oxford, UK (1996), pp 283-311.

Galal, A., N. F. Atta, S. A. Darwish and A-B. M. Abdallah, "Electrochemistry and Characterization of Conducting Poly(3-methylthiophene) Electrodes Containing Ferrocene Moieties", Bull. Chem. Soc. Jpn. 70, 1769-1776 (1997).

General Electric Plastics, Polymerland, Huntersville Business Park, 12200 Herbert Wayne Court, Suite 150, Huntersville, NC 28078, Phone # 1-800-PLASTIC and Fax # 1-888-PLASTIC.

Hipps K. W., L. Scudiero, D. E. Barlow, M. P. Cooke, "A self-organized 2-dimensional bifunctional structure formed by supramolecular design", J. Am. Chem. Soc. 124 (10), 2126-2127 (2002).

Hupp, J. T. and S. T. Nguyen, "Functional Nanostructured Molecular Materials", The Electrochemical Society Interface. Fall (2001).

Imamura, S. and J. H. Lunsford, "Separation of Oxygen from Air by $[Co^{(II)}(bpy)(Terpy)]^{2+}$ Complexes in Zeolite Y", Langmuir 1 (3), 326-330 (1985).

Inabe, T., "Novel Phthalocyanine-Based Conductors: Tunable $\pi-\pi$ Stacking Structure through the Steric and Chemical Interactions and Axial Ligands", J. Porphyrins Phthalocyanines 5, 3-12 (2001).

Jones, R. D., D. A. Summerville and F. Basolo, "Synthetic Oxygen Carriers Related to Biological Systems", Chem. Rev. 79 (2), 139-179 (1979).

Kobayashi, N., J. Mack, K. Ishii and M. J. Stillman, "Electronic Structure of Reduced Symmetry Peripheral Fused-Ring-Substituted Phthalocyanines", Inorg. Chem. 41, 5350-5363 (2002).

Kosal, M. E. and K. S. Suslick, "Microporous Porphyrin and Metalloporphyrin Materials", J. Solid State Chem. 152, 87-98 (2000).

Kurdi, J. and A. Y. Tremblay, "The Determination of Interaction Parameters in the Characterization of Polyetherimide Gas Separation Membranes Using Horvath-Kawazoe Model", Desalination, 148, 341-346 (2002), chapter IV.

Kurdi, J. and A. Y. Tremblay, "Preparation of Defect-Free Asymmetric Membrane for Gas Separations", Journal of Applied Polymer Science, 73 (8) 1471-1482 (1999), chapter II.

Lei, Z., X. Han, Y. Hu, R. Wang and Y. Wang, "Synthesis and Catalytic Oxidation Properties of Polymer-Bound Cobalt Complexes", J. Appl. Polym. Sci. 75, 1068-1074 (2000).

Lever, A. B. P., M. R. Hempstead, C. C. Leznoff, W. Liu, M. Melnik, W. A. Nevin and P. Seymour, "Recent Studies in Phthalocyanine Chemistry", Pure and Appl. Chem. 58, 1467-1476 (1986).

Li, G. Q. and R. Govind, "Separation of oxygen from Air Using Coordination Complexes: A review", Ind. Eng. Chem. Res. 33, 755-783 (1994).

Martell, A. E. and D. T. Sawyer, "Oxygen Complexes and Oxygen Activation by Transition Metals", Plenum Press, New York, NY (1988).

Niederhoffer, E. C., J. H. Timmons and A. E. Martell, Thermodynamics of Oxygen Binding in Natural and Synthetic Dioxygen Complexes", Chem. Rev. 84, 137-203 (1984).

Nishide, H., E. Soda, H. Mizuma and E. Tsuchida, "Specific Oxygen-Binding to a Polymer-Supported N,N'-DisalicylidenethylenediaminoCobalt complex", Macromol. Symp. 105, 191-197 (1996).

Nishide, H., T. Suzuki, R. Nakagawa, K. Itakura and E. Tsuchida, "Chemically Specific Surface Diffusion of Oxygen through a Porous Membrane Modified with Cobalt Porphyrin on its Pore Surface", J. Phys. Chem. 99, 12312-12317 (1995).

Nishide, H., T. Suzuki, R. Nakagawa and E. Tsuchida, "Enhanced Oxygen Diffusion through a Porous Membrane Chemically Modified with Cobalt Porphyrin on its Pore Surface", J. Am. Chem. Soc. 116, 4503-4504 (1994).

Ohya, H., V. V. Kudryavtsev and S. I. Semenova, "Polyimide Membranes – Applications, Fabrications, and Properties", Kodansha LTD. and Gordon & Breach Science Publishers S. A., Tokyo, JP (1996).

Pinnavaia, T. J. and M. F. Thorpe, Eds., "Access in Nanoporous Materials", Plenum Press, New York, NY (1995).

Simándi, L. I., "Catalytic Activiation of Dioxygen by Metal Complexes", Kluwer Academic Publishers, Dordrecht, NL (1992).

Suslick, K. S., N. A. Rakow, M. E. Kosal and J-H. Chou, "The Materials Chemistry of Porphyrins and Metalloporphyrins", J. Porphyrins Phthalocyanines 4, 407-413 (2000).

Tanev, P. T., M. Chibwe and T. J. Pinnavaia, "Titanium-containing Mesoporous Molecular Sieves for Catalytic Oxidation of Aromatic Compounds", Nature 368, 321-323 (1994).

Taylor, R. J., R. S. Drago and J. P. Hage, "A reversible O_2 Binding System: $Co(CN)_5^{3-}$ Inside Zeolite Y", Inorg. Chem. 31, 253-258 (1992).

Taylor, R. J., R. S. Drago and J. E. George, "Characterization of a Cobalt(II) Cyanide Complex inside Zeolite Y that reversibly Binds oxygen", J. Am. Chem. Soc. 111, 6610-6615 (1989).

Wang, R-M., C-J. Hao, Y-F. He, C-G. Xia, J-R. Wang and Y-P Wang, "Polymer-Bound Schiff-base Complex Catalyst for Effective Oxidation of Olefins with Molecular Oxygen", J. Appl. Polym. Sci. 75, 1138-1143 (2000).

Zhang, Z. and S. Lin, "Oxygen/Nitrogen Transport in Ionomer Composite Membranes containing a Cobalt Schiff base Complex", J. Appl. Polym. Sci. 74, 1071-1077 (1999).

Zhang, Z. and S. Lin, "Facilitated Oxygen Transport in an Ionomer Membrane containing Cobaltous ions", Macromol. Rapid Commun. 16, 927-933 (1995).

CHAPTER IX

Molecular Structuring to Improve the Performance and Stability of Polyetherimide Gas Separation Membranes through the Incorporation of Metal Complexes

J. Kurdi, and A. Y. Tremblay*

Department of Chemical Engineering, University of Ottawa, 161 Louis Pasteur, Ottawa, Ontario, K1N 6N5, Canada

*Corresponding author

André Y. Tremblay

Tel.: +1-613-562-5920; fax: +1-613-562-5172

E-mail address: tremblay@uottawa.ca

CHAPTER IX

Paper 8: Molecular Structuring to Improve the Performance and Stability of Polyetherimide Gas Separation Membranes through the Incorporation of Metal Complexes

J. Kurdi and A. Y. Tremblay
Department of Chemical Engineering, University of Ottawa, 161 Louis Pasteur,Ottawa, Canada, K1N 6N5

ABSTRACT

Polyetherimide (PEI) gas separation membranes were tailored at the molecular scale by incorporating nanostructured metallic complexes into the PEI network. The influence of these additives on the micropore size distributions of the membranes produced and on their performance for oxygen/nitrogen separation was investigated. Changing the metal within the same ligand had a significant influence on the microporosity and gas separation performance. Magnesium (II) phathalocyanine (MgPc) in PEI membranes was found to be an excellent additive to increase membrane performance for air separation. The performance of these membranes increases with increasing additive concentrations. Membranes with this additive also exhibit an improved stability as determined through the annealing process. Annealing these membranes caused a slight decrease in their gas permeance and total micropore volume but a significant increase in their membrane selectivity. The results show that the properties of the nanophase additive and nanophase-polymer interactions play a pivotal role in stabilizing and determining membrane performance for air separation.

Keywords: Polymer engineering, microporosity, gas separation membranes.

1 INTRODUCTION

Molecular engineering and molecular architecturing of novel materials having superior characteristics and properties are rapidly growing technologies that will be pervasive in all fields of science and engineering such as machines at molecular levels (Balzani et al.2000), electronic and optical devices (Pease et al. 2001, Timp, 1999), chemistry (Klabunde, 2001), supramolecular polymers (Ciferri, a., 2000; Schubert and Eschbaumer, 2002), polymer nanocomposites (Krishnamoorti and Vaia, 2002), thin film and coatings (Chow, 2000), metal-containing polymers (Chen et al. 1996, Sheats et al., 1985), high surface area materials including molecular sieves and catalysts (Ying, 2001, Pinnavaia and Thorpe, 1995, Tanev et al., 1994, Davis, 1993). The development of tailor-made materials is based on a common physicochemical fundamental that recognizes how materials are assembled starting from the atomic scale, to the nanoscale and ending at the bulk scale (Balzani et al. 2000). Common fabrication processes to produce these nanomaterials were reviewed in the literature (Ying, 2001, Hu and Shaw, 1999, Edelstein and Cammarata, 1998, Pinnavaia and Thorpe, 1995). One of these processes, involves the incorporation of a second organic or inorganic nanophase into polymeric materials. This technique was found to be successful in the production of novel superior plastics (Vaia, 2002). For example, it is estimated that using polymer nanocomposites by US vehicle manufacturers would save 1.5 billion liters of gasoline over one year reducing the emission of carbon dioxide by more than 4.5 billion kilogram (Vaia, 2002). In another application such as gas separations, the incorporation of transition metal complexes such as Schiff base oxygen carriers (Li and Govind, 1994, Martell and Sawyer, 1988, Niederhoffer et al. 1984) into polymeric membranes gave a significant improvement in performance of gas separation membranes. For example, the permeability and selectivity of oxygen over nitrogen were increased with increasing the Co(II) content in poly(vinyl alcohol)/poly(N-salicylidene allyl amine) blend membranes (Choi et al. 1995) or in Cobalt (II)-neutralized sulfonated EPDM (Ethylene-Propene-Diene terpolymer) ionomer membranes (Zhang and Lin, 1999, 1995). In other studies, a trade off between permeability and selectivity was observed. Increasing the content of the oxygen carrier (Cosalen) in polycarbonate membranes leads to a decrease in the permeability of oxygen

and nitrogen gases but an increase in the selectivity of oxygen over nitrogen. These results were also obtained with the addition of Cosalen to polyurethane (Chen et al. 2000). It was also reported that the conditions of the permeation test such as upstream pressure and temperature affect membrane performance (Nishide et al. 1995, 1994; Zhang and Lin, 1999, 1995). The above results show different membrane performance for different systems. There is no general rule for the results obtained from the incorporation of transition metal complexes into a specific polymeric membranes on membrane performance. However, many studies attribute these results to a structural diffusion factor using X-ray diffraction measurements (Chen and Lai, 1996) or diffusion models (Nishide et al. 1995). The correlation between the micropore size distribution and the performance of gas separation membranes was not investigated. For this reason and due to the importance of this correlation (Viva and Krishnamoorti, 2002 cited in Krishnamoorti and Viva), we have selected five different metal complexe additives classified into two groups: The first group includes metal (II) phthalocyanines of three different metals: Cobalt (CoPc), Iron (FePc) and Magnesium (MgPc) and the second group includes 1,1'-Bis(di-I-propylphosphino)Ferrocene(1,5-cyclooctadiene)Rhodium (I) tetrafluoroborate), (Rh-DiPFc) and Cobalt (II) 2,3-naphthalocyanine (CoNPc). These additives were incorporated into polyetherimide/N-methylpyrrolidinone solutions to prepare asymmetric flat membranes. For the purpose of comparison, the additives CoPc and CoNPc have been selected from our previous work as membranes produced using this adititve showed the best air separation performance among other Cobalt complexes (Kurdi and Tremblay, chapter VIII). The micropore size distributions of these membranes were determined using nitrogen adsorption and the Horvath-Kawazoe slit model. The membrane performance for separation of oxygen from air was also tested. The correlation between the performance of gas separation membrane and its micropore size distribution for each of the above five additives was discussed. The stability and durability of membrane performance for air separation were examined for membranes containing CoPc and MgPc additives through an annealing process and performance test.

2 EXPERIMENTAL

2.1 Materials

Polyetherimide (PEI, Ultem® 1000) was obtained from General Electric Plastics, USA, in pellet form and was dried in a vacuum oven (725 mm Hg vacuum) at 140°C for 24 hours. methyl alcohol (BDH, microscopic grade), hexanes (BDH, reagent grade), and isopropyl alcohol (OmniSolv®, EM Science, water 0.05% max) were supplied by (VWR CANLAB, QC, Canada), anhydrous 1-methyl-2-pyrrolidinone (Aldrich, 99.5 %, reagent grade, water < 0.005%) was supplied from Sigma-Aldrich Canada LTD, ON., Canada. Five different metal complexes shown in Table 9.1 were supplied from Sigma-Aldrich Canada LTD, ON., Canada except Rh-DiPFc was supplied from Strem Chemicals, INC., MA, USA. These metal complexes and anhydrous N-methylpyrrolidinone were used as supplied but under dried nitrogen atmosphere. All other solvents were used without any further purification. Medical air (PRAXAIR, Ottawa, ON., CA) was used to test the membrane for oxygen separation. Ultra high purity gases, nitrogen and helium (PRAXAIR, Ottawa, ON., CA) were used in the nitrogen adsorption measurements. All gases were used as supplied without purification.

2.2 Membrane preparation

Casting solutions were prepared using polyetherimide (PEI), anhydrous N-methyl-2-pyrrolidinone (NMP) and one of the additives shown in Table 9.1. The preparation was under a nitrogen atmosphere using a glove bag placed in a fume hood. We kept the ratio of PEI to the total weight of solution at 23 percent by weight. The ratio of additive to PEI was 1, 3, 10 and 15% (weight additive/weight PEI). One PEI membrane was prepared without additive served as a base case.

The same preparation procedures were followed for all samples. All mixing and casting was carried out under a nitrogen atmosphere in order to not expose materials to the atmospheric air. A particular additive was first dissolved in NMP using a Nalgene polypropylene jar having a screw cap under a nitrogen atmosphere in order to not expose materials to the atmospheric air. Dissolving was done by rolling the sealed jars at room temperature for many days until a clear solution was obtained. The polymer was then

Table 9.1 Metal complexes used in this study.

Group	Abbreviations	Chelate complex name	Chemical structure
1	CoPc	Catalog No. 30,769-6 Cobalt(II) phthalocyanine	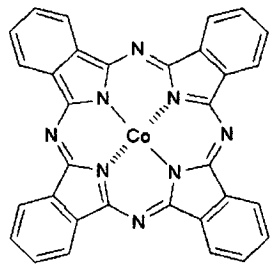
	FePc	Catalog No. 37,954-9 Iron (II) phthalocyanine	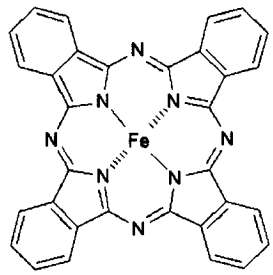
	MgPc	Catalog No. 40,273-7 Magnesium (II) phthalocyanine	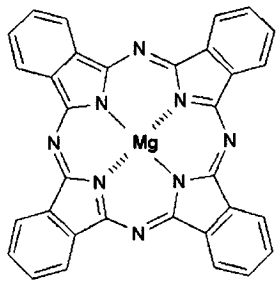
2	Rh-DiPFc	Catalog No. 45-0205 1,1'-Bis(di-I-propylphosphino) ferrocene (1, 5-cyclooctadiene)	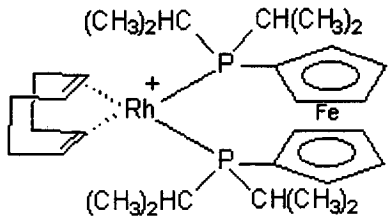
	Co(2,3NPc) CoNPc	Catalog No. 38,192-6 Cobalt(II) 2,3-naphthalocyanine	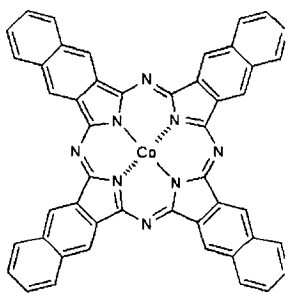

All additives in Table 9.1 were supplied from Aldrich, Sigma-Aldrich Canada LTD, On., Canada, except the additive Rh-DiPFc was supplied from Strem Chemicals, Inc., MA, USA.

added to the dissolved additive/NMP solution under nitrogen atmosphere, sealed and rolled again for many days until a clear homogenous casting solution was obtained.

The solution was cast onto a clean glass plate at room temperature using a knife gap of 250 μm. The film was quickly immersed for 5 minutes in a coagulation bath containing isopropyl alcohol. The coagulated film was moved to a methanol bath where it was kept for 16 hours. Finally the film was immersed in a bath of hexanes for two days. The membrane was dried in air for three days. We cut three circular coupons of 65 mm diameter from each membrane film. These coupons were used in the permeation tests and the rest of the film was cut into small strips in order to be used in the nitrogen adsorption measurements.

2.3 Determination of the micropore size distribution

A standard procedure was used to determine the micropore size distribution. An automated volumetric porosity analyzer ASAP 2000M produced by Micromeritics (GA, USA) was used to measure the nitrogen adsorption isotherm. Approximately 1 gram of small strips of each membrane sample were weighed to +/- 0.0005 grams. The small strips were placed inside a sample tube and degassed at 0.002 ± 0.0005 mm Hg and temperature at 40 °C for 12 hours. Nitrogen adsorption was performed at 77 K using a liquid nitrogen bath. Ultra high purity gases, nitrogen and helium were used for adsorption and purging the sample. The automated volumetric porosity analyzer ASAP 2000M produced by Micromeritics (GA, USA) was used to measure the nitrogen adsorption isotherm. The Horvath-Kawazoe slit model was used to calculate the micorpore size distribution from the measured isotherm data. The method and the determination of the parameters used in Horvath-Kawazoe model for nitrogen and polyetherimide were explained in our previous work (Kurdi and Tremblay, chapter IV).

2.4 Permeation test

The same permeation test was used for all samples. A test cell having an effective cross-flow section of 20 cm^2 was used. The upstream side of the cell was pressurized with medical air at 12.8 bar gauge and the retentate flow was set at 400 ml (STP)/min. The permeate was discharged to the atmosphere. A soap bubble flowmeter was used to

measure the volumetric permeate gas flow. An automatic gas sampling valve having a sample volume of 0.5 cm^3 was connected in line with the permeate. The valve as connected to a gas chromatograph to measure the oxygen concentration in the permeate gas stream. The oxygen concentration was corrected for the difference in the thermal conductivity between oxygen and nitrogen using the following equation (Academy of China, 1972):

$$y_{corr} = \frac{\left(\frac{y}{40}\right) * 100}{\left(\frac{y}{40}\right) + \left(\frac{100 - y}{42}\right)} \quad (1)$$

Where y is the percentage of oxygen concentration in the permeate stream as calculated by gas chromatography and y_{corr} is the corrected value. The oxygen permeance and nitrogen permeance were determined as explained elsewhere (Kurdi and Tremblay, chapter II). The total gas permeance is the sum of permeances of oxygen and nitrogen. The true selectivity was considered to be the ratio of oxygen permeance to nitrogen permeance.

3 RESULTS AND DISCUSSION

3.1 Influence of additives on the microporosity of PEI membranes

The micropore size distributions of the membranes prepared using the additives shown in Table 9.1 and one membrane without additive were plotted in Figure 9.1 for group (1) additives and Figure 9.2 for group (2) additives. It is clear that all additives increased the total differential micropore volume of the polymer. This can be attributed to an increase in the connectivity and accessibility among the micropores of the polymeric network of PEI and the possible creation of new micropores at the interface between the dispersed nanoparticles and the polymer network.

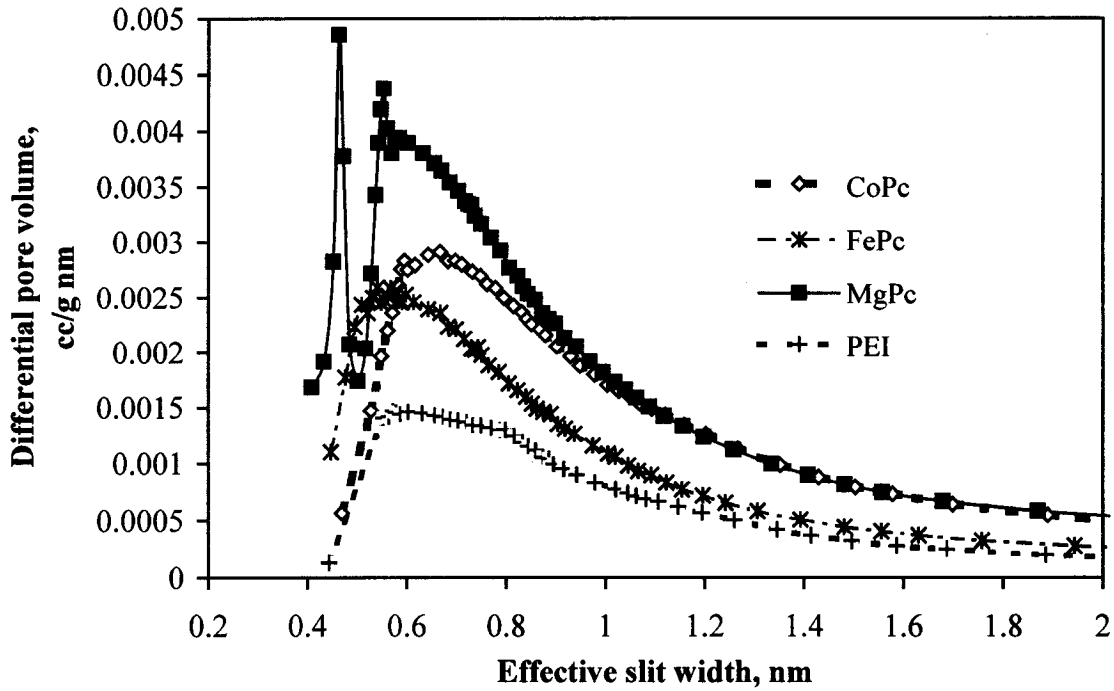

Figure 9.1 Micropore size distribution for PEI membranes cast from solutions containing group (1) additives shown in Table 9.1 and one without additive. Differential pore volume (cm^3/g nm) vs. effective slit width in nm. Casting solutions contain 3 % additive/PEI by weight.

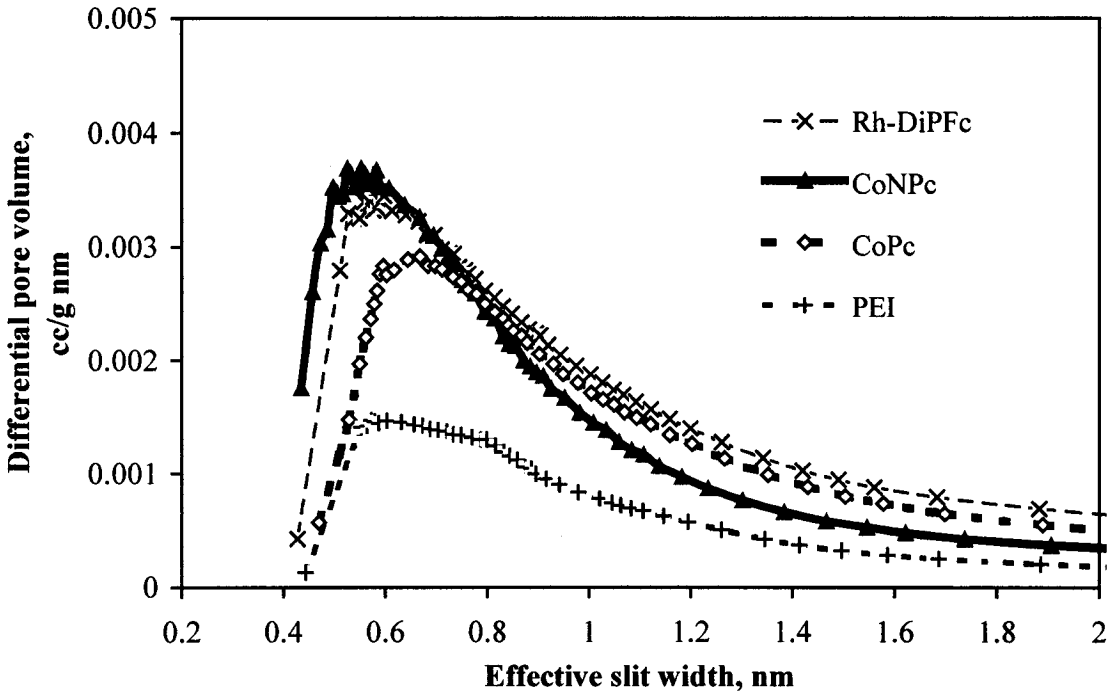

Figure 9.2 Micropore size distribution for PEI membranes cast from solutions containing group (2) additives shown in Table 9.1 and one without additive. Differential pore volume (cm^3/g nm) vs. effective slit width in nm. CoPc additive was included for the purpose of comparison. Casting solutions contain 3 % additive/PEI by weight.

In the first group, Figure 9.1, changing the metal (II) in the phthalocyanine complexes leads to a change in the micropore size distribution within the membranes. This was attributed to different properties and characteristics of the dispersed nanoparticles and the affinity between each of these complexes and polyetherimide chains. The smallest mode in the distribution and the greatest micropore volume was for the membrane containing the MgPc additive. This indicates that the complex has a higher affinity to PEI and a better connectivity. MgPc is not a planar molecule but the magnesium atom is placed outside the plane over the center of the macrocyclic moiety. It has a shuttlecock shape as explained by McKeown (1998). This leads to an enhancement in the π–π intermolecular interactions operating through the Mg atom (Mizuguchi, 2001) forming a nanocrystallic structure (Breeze et al. 2001, Mizuguchi, 2001). The alkaline property of Mg in phthalocyanines was reported to form complexes having an improved solubility in aromatic polar solvents (McKeown, 1998). Therefore, a better dispersion and the smaller nanophases of MgPc expected in NMP lead to a greater micropore volume compared to that obtained using other additives in group (1).

Magnesium (II) is a hard Lewis acid while Co(II) and Fe(II) are at the borderline between soft and hard Lewis acids (Pearson, 1997). Therefore, MgPc is a harder base than CoPc and FePc that leads to a higher affinity of this complex to a hard base solvent such as methanol. For this reason, the presence of the double peak in the micropore size distribution of the membrane containing MgPc was attributed to the presence of methanol in its structure. This was confirmed in our lab as the double peak change to a single peak upon further drying. The double peak was not observed when methanol was not used in membrane preparation.

According to the hard soft acid base (HSAB) principle (Pearson, 1997) hard acids prefer to coordinate to hard bases, and soft acids prefer to coordinate to soft bases. The affinity of the hard base, MgPc to polyetherimide is greater than for CoPc and FePc because the imide group is a hard base (Benrabah et al. 1995). This higher affinity leads to a smaller mode in the micropore size distribution for membranes containing MgPc.

Membranes containing FePc have a smaller mode in their micropore size distribution compared to membranes containing CoPc because of the higher affinity of the former to the imide groups in PEI. This can be explained through the lower electron

affinity of FePc than CoPc. Fe has a greater positive charge than Co (Liao and Scheinder, 2002) and as a result is more attracted by the imide group in PEI.

In the second group, Figure 9.2, replacing the phthalocyanine in Cobalt(II) complex by naphthalocyanine i.e. adding four aromatic rings leads to an increase in the micropore volume and a decrease in the mode and skewness of the micropore size distribution. This can be attributed to an increase in the aromatic (nucleophillic) environment that increases the $\pi-\pi$ stacking interactions leading to microporous nanoscale structures (Inabe, 2000). This also tends to increase the affinity of the CoNPc to PEI chains as well as to the NMP solvent. The cationic rhodium (1) bearing the air stable and crystalline diphosphine 1,1'-bis-(diisopropylphosphino) Ferrocene (Rh-DiPFc) has the same micropore volume as a membrane with CoNPc but a very small shift to a larger size especially for larger micropore sizes. The micropore size distribution of a membrane containing CoPc was added to Figure 9.2 for the purpose of comparison.

3.1.1 Effects of MgPc concentration

For most incorporated metallic complexes such as CoPc into PEI, increasing the additive concentration leads to an increase in the total micropore volume but no change in the shape of the micropore distribution as previously discussed by Kurdi and Tremblay, (chapter VIII). However, this is not the case with the incorporation of MgPc. The micropore size distributions of membranes containing different concentrations of this additive were plotted as shown in Figure 9.3. The possibility of forming a double peak due to the presence of methanol is higher for lower concentrations as found for membranes containing 1 and 3 % additive. This means that the higher concentrations of 10 and 15 % additive formed different nanoparticles that hosted less methanol. With an increase in the concentration of the additive, the mode in the micropore size distribution remained constant while the volume of the micropore of pore size between 0.6-2 nm decreased. In this pore size range, membranes containing 10 % additives had the lowest micropore volume. This was even lower than the PEI micropore volume in the range 0.9 to 2 nm. This indicates that incorporating MgPc into PEI has a great benefit in reducing the number of larger micropores that are responsible for decreasing the selectivity of gas separation membranes. The greater affinity of MgPc is responsible for the tighter

structure and narrow pore size distribution for membranes containing higher concentration of 10 and 15 % of Magnesium phthalocyanine.

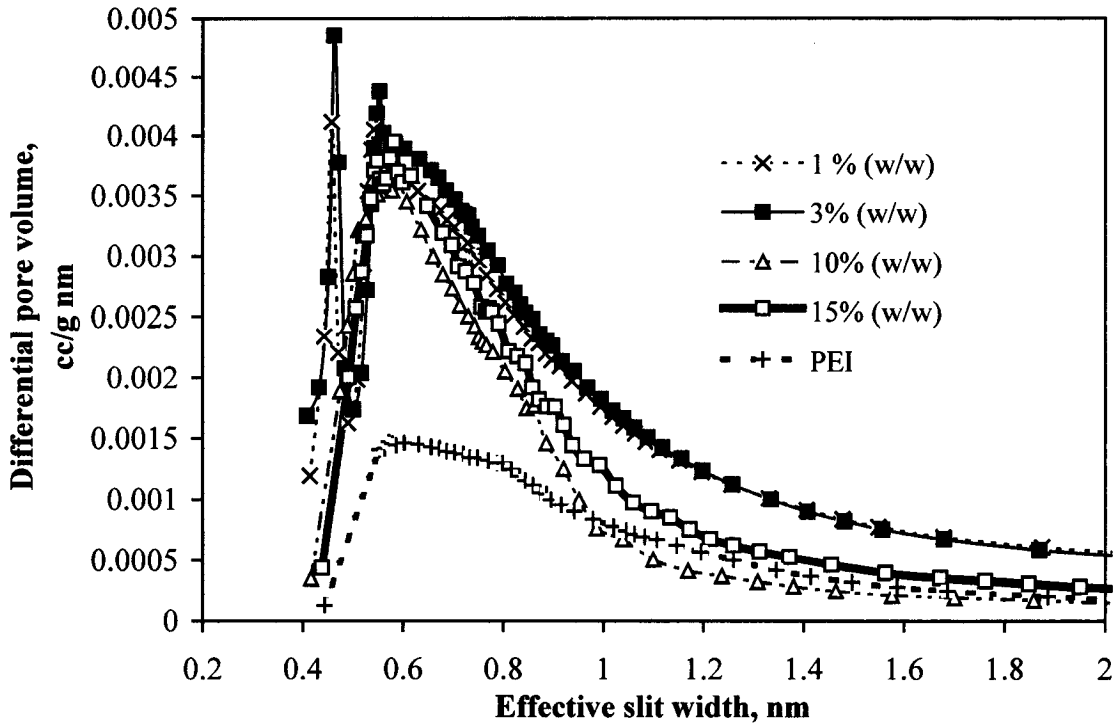

Figure 9.3 Micropore size distribution for PEI membranes cast from solutions containing MgPc additive at concentrations 1, 3, 10 and 15 % (w/w), and one without additives. Differential pore volume (cm^3/g nm) vs. effective slit width in nm.

3.1.2 Effects of drying and annealing of PEI membranes containing MgPc or CoNPc

Polyetherimide membranes containing 3 % of MgPc or CoNPc were dried and annealed in a vacuum oven under 725 mm Hg vacuum pressure and temperature of 90 °C for 48 hours. The micropore size distributions of these membranes before and after drying were plotted in Figure 9.4 for MgPc and in Figure 9.5 for CoNPc additive. It is clear that drying and annealing lead to decrease in the membrane micropore volume for both additives. The first peak in the micropore size distribution of membrane containing MgPc disappeared due to the removal of the residual methanol as previously discussed in this work. The decrease in the micropore volume after drying and annealing is attributed to the shrinkage of the composite membranes as well as removal of solvents.

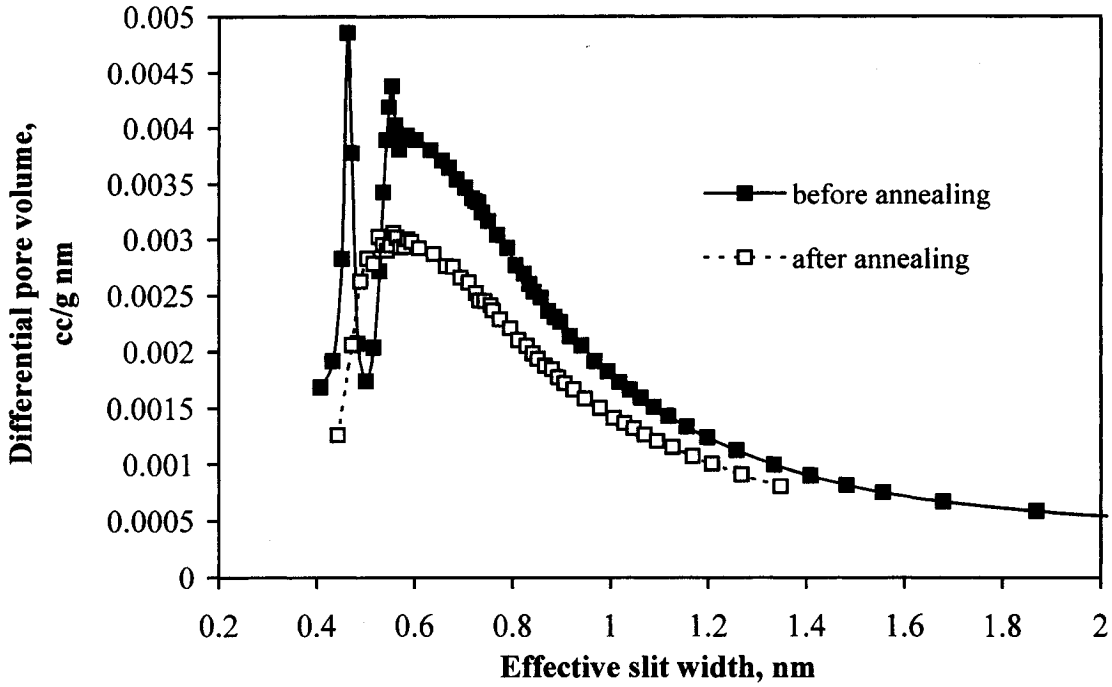

Figure 9.4 Micropore size distribution for PEI membranes cast from solutions containing MgPc additive at concentration 3 % (w/w), before and after annealing process in oven under 725 mm Hg vacuum pressure and temperature of 90 °C for 48 hours. Differential pore volume (cm^3/g nm) vs. effective slit width in nm.

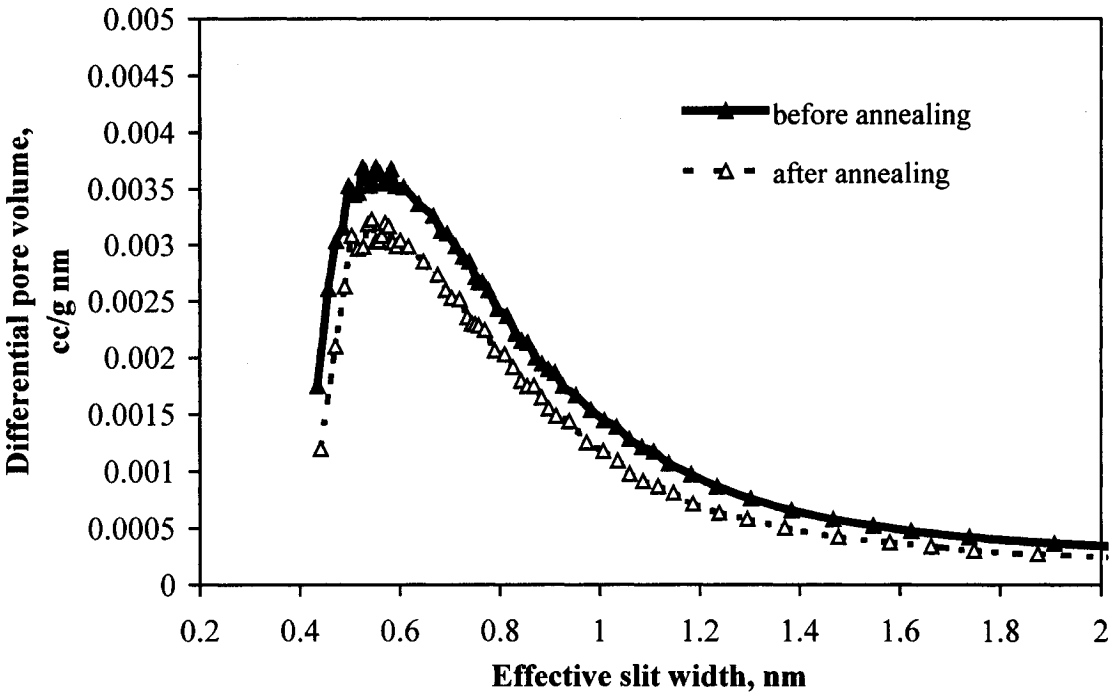

Figure 9.5 Micropore size distribution for PEI membranes cast from solutions containing CoNPc additive at concentration 3 % (w/w), before and after annealing process in oven under 725 mm Hg vacuum pressure and temperature of 90 °C for 48 hours. Differential pore volume (cm^3/g nm) vs. effective slit width in nm.

3.2 Influence of additives on the O_2/N_2 separation of PEI membranes

The gas permeances of membranes containing additives shown in Table 9.1, group (1) were plotted versus the additive weight ratio as shown in Figure 9.6. The membranes containing the additives CoPc and MgPc were first tested for permeation. They were then, dried and annealed in a vacuum oven under 725 mm Hg vacuum pressure and temperature of 90 °C for 48 hours and retested. The results of both annealed membranes were plotted in Figure 9.6. It is clear that the permeance of the non-annealed membranes containing CoPc and FePc increased with increasing additive concentration. The permeance of non-annealed MgPc membranes decreased slightly with increasing additive concentration. These results are consistent with the relatively constant microporosity shown in Figure 9.3. The slight decrease in permeance was attributed to a small decrease in the micropore volume between 0.6 and 2 nm. Comparing membranes containing MgPc before and after annealing, the decrease in the permeance is lower at higher additive concentrations in the range 0.9 to 2 nm. This indicates that the increase in the concentration of the additive leads to an increase in the stability of the PEI membrane. It was reported that the MgPc is the most effective additives among other metal phthalocyanines to inhibit the thermal degradation and increase the stability of polymers such as polyesters, polyamide and aromatic heterocyclic polymers (Moser and Thoms, 1983). The results of our work are consistent with previous studies found in the literature. Membranes containing CoPc exhibit a larger decrease in the permeance especially at higher concentration that may be attributed to different shrinkage between PEI and the CoPc nanoparticles. Larger variations in the data and the higher permeance for membranes containing FePc are attributed to the disorder and impurities that influence the structure of FePc nanoparticles (Evangelisti et al. 2002).

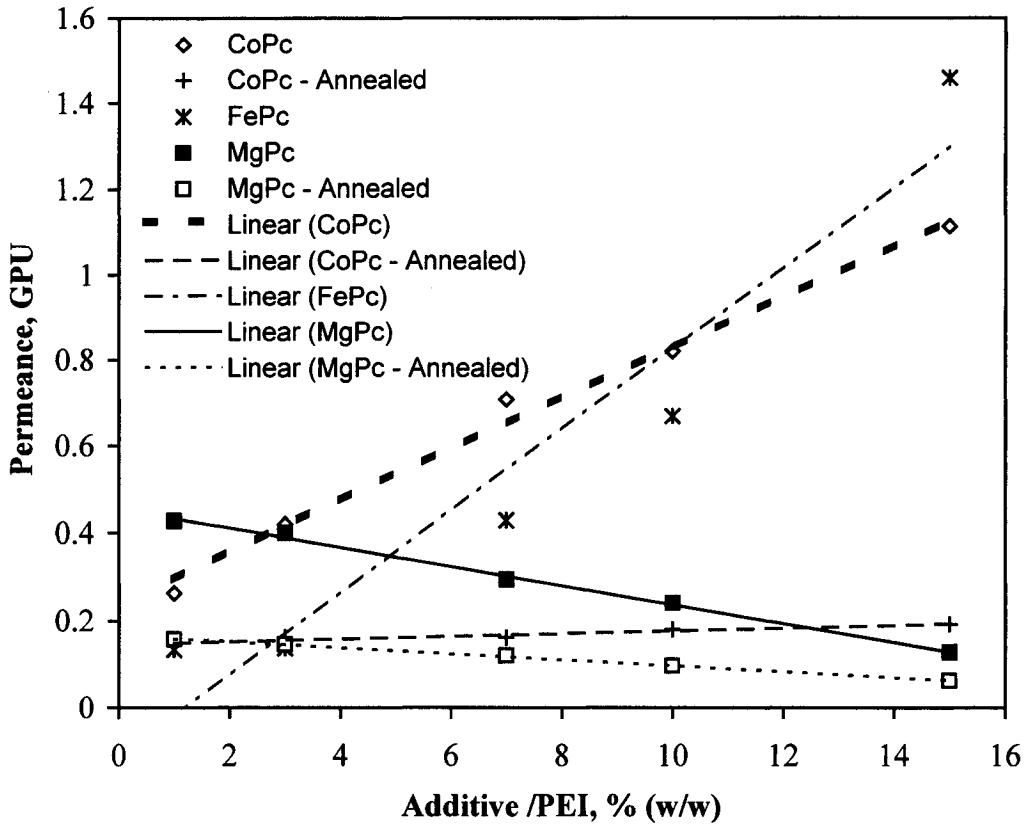

Figure 9.6 Plot of the total permeance, GPU vs. the percentage of the (additive/PEI) ratio in the casting solution for air separation by membranes containing group (1) additives shown in Table 9.1. Permeation test was included membranes containing CoPc and MgPc which were annealed in an oven under 725 mm Hg vacuum pressure and temperature of 90 °C for 48 hours.

The permeances of membranes containing group (2) additives versus the concentration of these additives were plotted in Figure 9.7. Although the membrane containing the additive Rh-DiPFc has a similar micropore size distribution to membranes containing CoNPc. It has a higher permeance that can be attributed to the bulky structure of this additive compared to the planar structure of the CoNPc. The electrophillic property known from the reducing activity of Rh-DiPFc for aldehydes and ketones (Burk et al. 1994) leads to a lower affinity to imide groups in PEI. The bulky structure inhibits aggregating the Rh-DiPFc and enhances its solubility. Therefore, smaller nanophases and less affinity to PEI lead to an increase in micropore volume at different sizes as seen in Figure 9.2.

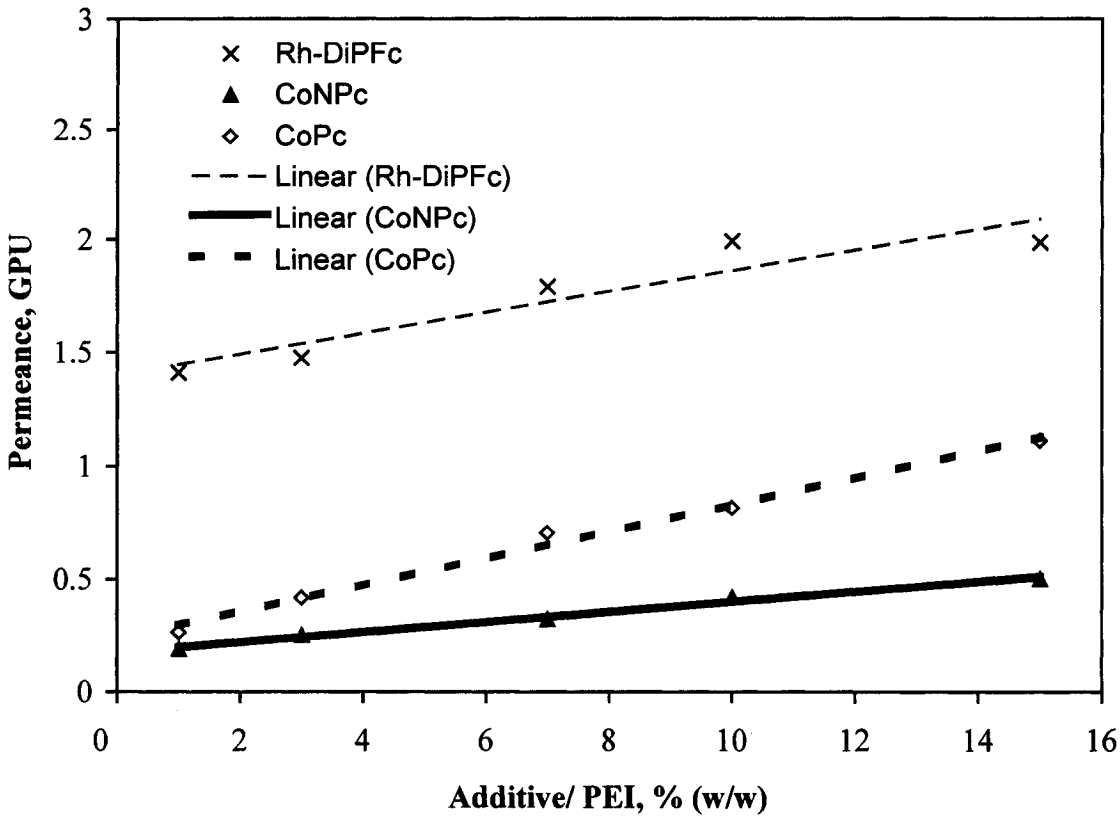

Figure 9.7 Plot of the total permeance, GPU vs. the percentage of the (additive/PEI) ratio in the casting solution for air separation by membranes containing group (2) additives shown in Table 9.1.

The selectivity of membranes containing group (1) additives was also plotted versus additive concentration as shown in Figure 9.8. The selectivity of annealed membranes containing CoPc and MgPc were also included. The selecitivity trade off with permeance is clear for all membranes except the ones containing the MgPc additive. The selectivity of membranes containing MgPc was largely increased with increasing additive concentrations. An increase in the MgPc concentration from 1% to 15% (w/w) leads to an increase in selectivity from 2.28 to 5.39 before annealing and from 2.67 to 5.46 for annealed membranes. A slight increase in the selectivity upon membrane annealing is observed. However, the annealing of membranes containing CoPc leads to a decrease in the selectivity especially at low additive concentrations.

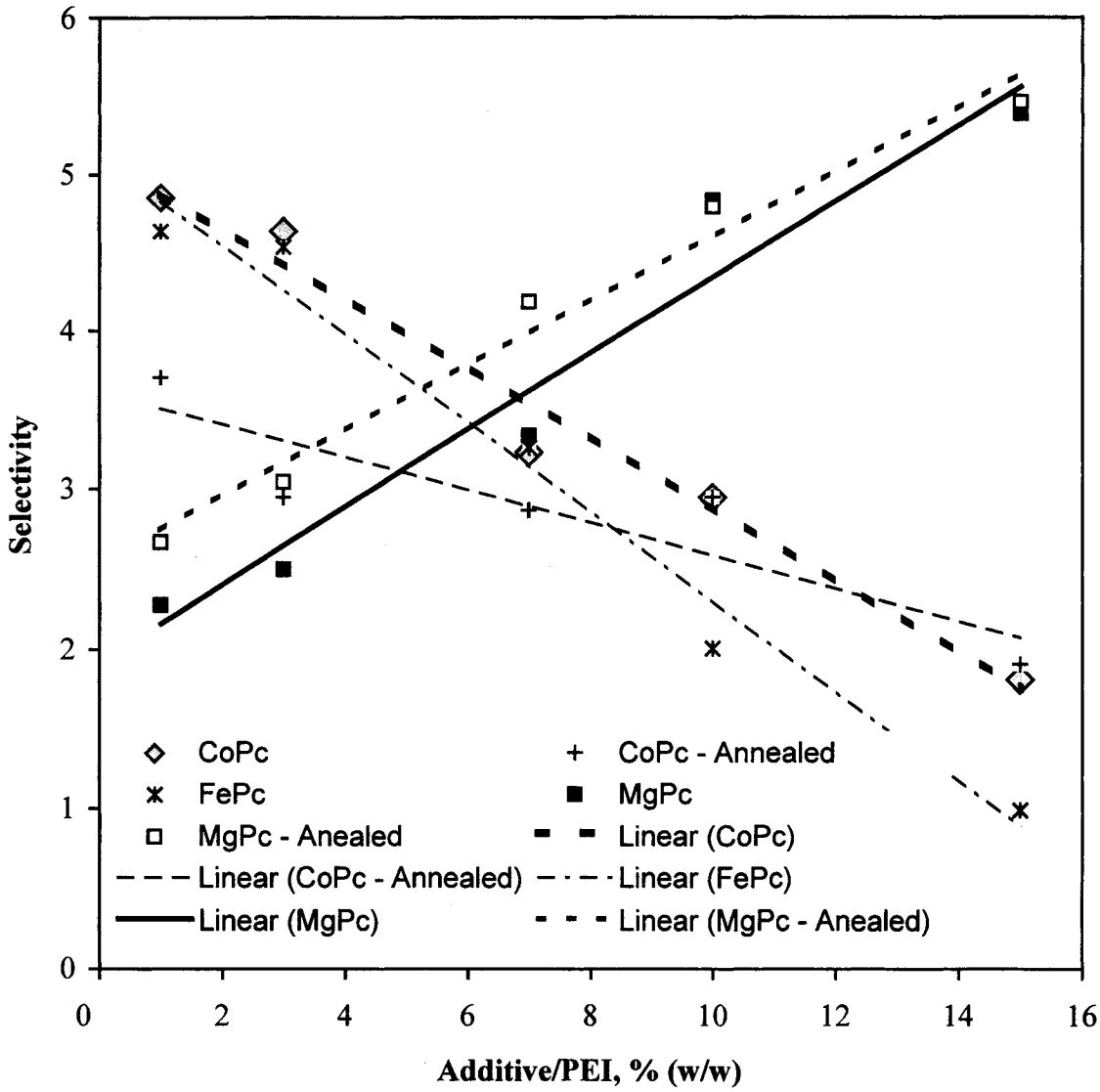

Figure 9.8 Plot of O_2/N_2 selectivity vs. the percentage of the (additive/PEI) ratio in the casting solution for air separation by membranes containing group (1) additives shown in Table 9.1. Permeation test was included membranes containing CoPc and MgPc which were annealed in an oven under 725 mm Hg vacuum pressure and temperature of 90 °C for 48 hours.

The selectivity of membranes containing group (2) additives decreases with increasing additive concentrations following the trade off behavior as shown in Figure 9.9. Membranes containing Rh-DiPFc had macroporous defects in their skin layer indicated by their inability to separate oxygen from air. The presence of the nonselective pore larger than 0.8 nm can be seen in Figure 9.2.

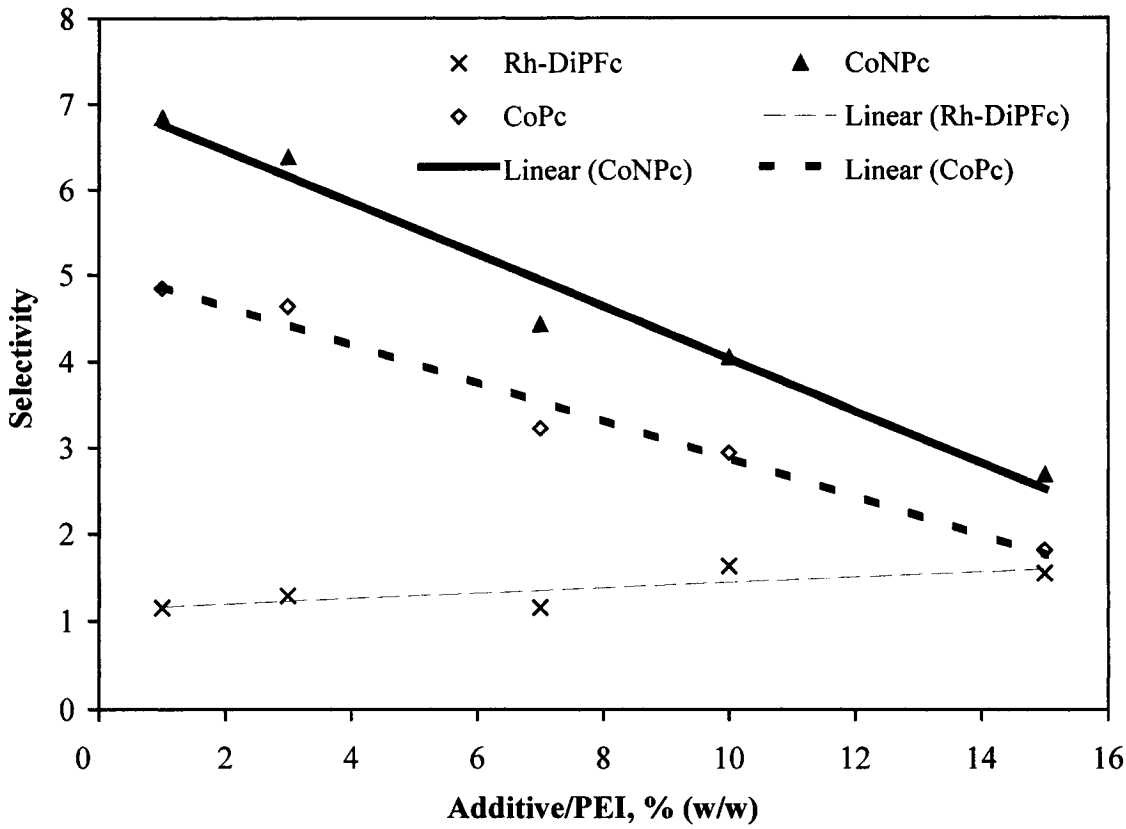

Figure 9.9 Plot of O_2/N_2 selectivity vs. the percentage of the (additive/PEI) ratio in the casting solution for air separation by membranes containing group (2) additives shown in Table 9.1. Additive CoPc was included for the purpose of comparison.

To study the performance of the above membranes for oxygen/nitrogen separation, the selectivity versus the air permeance was plotted for membranes containing group (1 and 2) additives as shown in Figure 9.10. Membranes containing Rh-DiPFc were excluded because they were not selective to oxygen. It is clear from Figure 9.10 that the highest performance before annealing is obtained for the membrane containing (CoPc) when the permeance is greater than 0.36 GPU but at lower than this permeance the membrane containing CoNPc had the best performance.

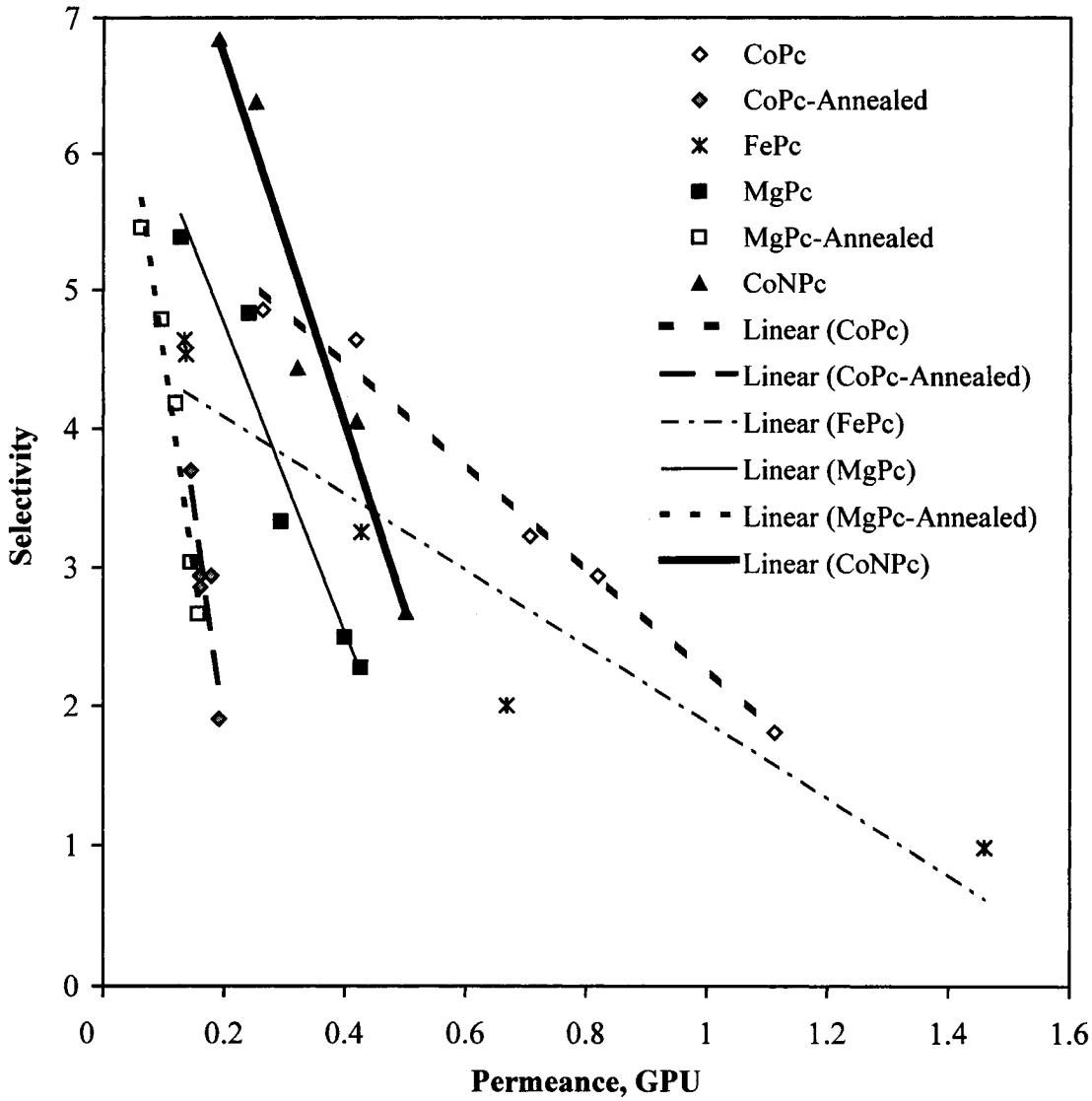

Figure 9.10 Performance plot of O_2/N_2 selectivity vs. the total permeance, GPU for air separation by membranes containing additives shown in Table 9.1. Membranes containing Rh-DiPFc was excluded as it is not selective to O_2/N_2 separation.

Comparing the annealed membranes containing MgPc with the annealed ones containing CoPc as shown in Figure 9.10, it is clear that membranes containing MgPc maintained a high performance for oxygen separation from air especially at higher additive concentrations as the performance line goes up while it goes down in case of CoPc. The performance is highly improved with an increase in the content of MgPc. The MgPc additive was the only one to provide an increase in selectivity when its concentration was increased. All other additives showed a decrease in

selectivity with an increase in additive concentration as seen in Figure 8.8 (chapter VIII in this thesis) and Figure 9.8 (this chapter).

At higher MgPc concentrations, annealing had the least effect on permeance and selectivity compared to CoPc. The MgPc additive tends to increase the stability of the membrane as the permeance was maintained after the annealing process as seen in Figure 9.6. This result agrees well with the reported ability of MgPc to inhibit the thermal degradation and increase the stability of polymers (Moser and Thoms, 1983).

4 CONCLUSIONS

Incorporating of metallic complexes as additives into polyetherimide was found to be a useful method to structure this polymeric material at the molecular scale. The micropore volume increased significantly on the inclusion of planar additives. It was found that PEI membranes containing a bulky additive such as (Rh-DiPFc) could not separate oxygen from air due to the presence of macroporous defects in the skin layer of the membrane. CoPc forms high performance gas separation membranes. However, its performance was reduced with the annealing process. On the other hand, MgPc was found to be the best additive as it forms a membrane with a narrow micropore size distribution that improved by increasing the additive concentration. The stability of the composite material was also significantly improved as the annealing process tends to increase membrane selectivity without a decrease in the micropore volume and with only a slight decrease in membrane permeance. This result was attributed to the high affinity of MgPc to PEI as well as for the solvent used. This explains why increasing the content of MgPc leads to a finer membrane structure and a significant improvement in membrane performance. It was concluded that MgPc is a promising additive that can be used to improve the stability and the performance of polyetherimide gas separation membranes.

REFERENCES

Academy of China, Physics Institute of Dalian, "Gas Chromatography", Science Press Inc. of China, China (1972).

Balzani, V., A. Credi, F. M. Raymo and J. F. Stoddart, "Artificial Molecular Machines", Angew. Chem. Int. Ed. 39, 3348-3391 (2000).

Benrabah, D., R. Arnaud and J-Y. Sanchez, "Comparative *ab initio* Calculations on Several Salts", Electrochim. Acta 40 (13-14), 2437-2443 (1995).

Breeze, A., A. Salomon, D. Ginley, and B. Gregg, "Photovoltaic Cells based on Conducting polymers and Perylene Diimides", NCPV Program Review Meeting, Lakewood, Colorado, 14-17 October (2001).

Burk, M. J., T. G. P. Harper, J. R. Lee and C. Kalberg, "Efficient Rhodium-Catalyzed Hydrogenation of Aldehydes and Ketones", Tetrahedron Lett. 35 (28), 4963-4966 (1994).

Chen, S. H., K. C. Yu, S. L. Houng, J. Y. Lai, "Gas transport properties of HTPB based polyurethane/Cosalen membrane", J. Membrane Sci. 173(1), 99-106 (2000).

Chen, S. H. and J. Y. Lai, "Polycarbonate/(N,N'-dialicylidene ethylene diamine) Cobalt(II) complex Membrane for Gas Separation", J. Appl. Polym. Sci. 59, 1129-1135 (1996).

Chen, L., H. Xu and C-Z Yang, "The Study of Metal-Schiff Base Coordinated Polyurethane", Polym. Adv. Technol. 8, 335-338 (1996).

Choi, M. J., C. K. Park and Y. M. Lee, "Chelate Membrane from Poly(vinyl alcohol)/Poly(N-salicylidene allyl amine) Blend. II. Effect of Co(II) Content on Oxygen/Nitrogen Separation", J. Appl. Polym. Sci. 58, 2373-2379 (1995).

Chow, G-M., I. A. Ovid'ko and T. Tsakalakos, Eds., "Nanostructured Films and Coatings", Kluwer Academic Publishers, Dordrecht, NL (2000).

Ciferri, A., Ed., "Supramolecular Polymers", Marcel Dekker, Inc., New York, NY (2000).

Davis, M. E., "Organizing for better Synthesis", Nature 364, 391-393 (1993).

Edelstein, A. S. and R. C. Cammarata, Eds., "Nanomaterials: Synthesis, properties and Applications", Institute of Physics Publishing, Bristol, UK (1998).

Evangelisti, M., J. Bartolomé, L. J. de Jongh and G. Filoti, "Magnetic properties of α-iron(II) Phthalocyanine", Phys. Review B66, 144410-144420 (2002).

General Electric Plastics, Polymerland, Huntersville Business Park, 12200 Herbert Wayne Court, Suite 150, Huntersville, NC 28078, Phone # 1-800-PLASTIC and Fax # 1-888-PLASTIC.

Hu, E. L. and D. T. Shaw, "Synthesis and Assembly", chapter (2) in "WTEC Panel Report on: Nanostructure Science and Technology, R&D Status and Trends in Nanoparticles, Nanostructured Materials, and Nanodevices", Loyola College Baltimore, MD 21210, USA (September, 1999).

Inabe, T., "Novel Phthalocyanine-Based Conductors: Tunable $\pi-\pi$ Stacking Structure through the Steric and Chemical Interactions and Axial Ligands", J. Porphyrins Phthalocyanines 5, 3-12 (2001).

Klabunde, K. J., Ed., "Nanoscale Materials in Chemistry", John Wiley and Sons, Inc., New York, NY (2001).

Krishnamoorti, R. and R. A. Vaia, Eds., "Polymer nanocomposites: Synthesis, Characterization and Modeling", American Chemical Society, Washington, DC (2002).

Kurdi, J. and A. Y. Tremblay, "The Determination of Interaction Parameters in the Characterization of Polyetherimide Gas Separation Membranes Using Horvath-Kawazoe Model", Desalination, 148, 341-346 (2002), chapter IV.

Kurdi, J. and A. Y. Tremblay, "Preparation of Defect-Free Asymmetric Membrane for Gas Separations", Journal of Applied Polymer Science, 73 (8) 1471-1482 (1999), chapter II.

Li, G. Q. and R. Govind, "Separation of oxygen from Air Using Coordination Complexes: A review", Ind. Eng. Chem. Res. 33, 755-783 (1994).

Liang, L., J. Liu and X. Gong, "Thermosensitive Poly(N-isopropylacrylamide)-Clay Nanocomposites with Enhanced Temperature Response", Langmuir 16, 9895-9899 (2000).

Liao, M-S. and S. Scheinder, Comparative Study of Metal-Porphyrins, -Porphyrazines and –Phthalocyanines", J. Comput. Chem. 23, 1391-1403 (2002).

Martell, A. E. and D. T. Sawyer, "Oxygen Complexes and Oxygen Activation by Transition Metals", Plenum Press, New York, NY (1988).

McKeown, N. B., "Phthalocyanine Materials: Synthesis, Structure and Function", Cambridge University Press, Cambridge, UK (1998).

Mizuguchi, J., "$\pi-\pi$ Interactions of magnesium Phthalocyanine as Evaluated by Energy Partition Analysis", J. Phys. Chem. A 105, 10719-10722 (2001).

Moser, F. H. and A. L. Thomas, "The Phthaolcyanines, Vol.1, CRC Press, Inc., Boca Raton, FL (1983).

Niederhoffer, E. C., J. H. Timmons and A. E. Martell, Thermodynamics of Oxygen Binding in Natural and Synthetic Dioxygen Complexes", Chem. Rev. 84, 137-203 (1984).

Nishide, H., T. Suzuki, R. Nakagawa and E. Tsuchida, "Enhanced Oxygen Diffusion through a Porous Membrane Chemically Modified with Cobalt Porphyrin on its Pore Surface", J. Am. Chem. Soc. 116, 4503-4504 (1994).

Nishide, H., T. Suzuki, R. Nakagawa, K. Itakura and E. Tsuchida, "Chemically Specific Surface Diffusion of Oxygen through a Porous Membrane Modified with Cobalt Porphyrin on its Pore Surface", J. Phys. Chem. 99, 12312-12317 (1995).

Pearson, R. G., "Chemical Hardness", Wiley-VCH, Weinheim, DE (1997).

Pease, A. R., J. O. Jeppesen, J. F. Stoddart, Y. Luo, C. P. Collier and J. R. Heath, "Switching Devices Based on Interlocked Molecules", Acc. Chem. Res. 34, 433-444 (2001).

Pinnavaia, T. J. and M. F. Thorpe, Eds., "Access in Nanoporous Materials", Plenum Press, New York, NY (1995).

Schubert, U. S. and C. Eschbaumer, "Macromolecules Containing Bipyridine and Terpyridine Metal Complexes: Towards Metallosupramolecular Polymers", Angew. Chem. Int. Ed. 41, 2892-2926, 2002).

Sheats, J. E., C. E. Carraher, Jr. and C. U. Pittman, Jr., "Metal-Containing Polymeric Systems", Plenum Press, New York, NY (1985).

Tanev, P. T., M. Chibwe and T. J. Pinnavaia, "Titanium-containing Mesoporous Molecular Sieves for Catalytic Oxidation of Aromatic Compounds", Nature 368, 321-323 (1994).
Timp, G., Ed., "Nanotechnology", Springer-Verlag, New York, NY (1999).

Vaia, R. A., "Polymer Nanocomposites Open a New Dimension for Plastics and Composites", The AMPTIAC Newsletter 6 (1) 17-24 (2002).

Ying, J. Y., Ed., "Nanostructured Materials", Academic Press, San Diego, CA (2001).

Zhang, Z. and S. Lin, "Oxygen/Nitrogen Transport in Ionomer Composite Membranes containing a Cobalt Schiff base Complex", J. Appl. Polym. Sci. 74, 1071-1077 (1999).

Zhang, Z. and S. Lin, "Facilitated Oxygen Transport in an Ionomer Membrane containing Cobaltous ions", Macromol. Rapid Commun. 16, 927-933 (1995).

CHAPTER X

DISCUSSION AND CONCLUSIONS

The tailoring and characterizing of materials at a molecular scale to develop novel rigid polymeric molecular sieves for high performance gas separation membranes was the main objective of this thesis. The importance of this research is not only for the development and characterization of membrane materials for gas separations but also for material interactions and characterization at an atomic scale required in many fields of nanoscience. In the WTEC Panel Report on Nanostructure Science and Technology (Siegel, 1999), it was reported that nanotechnologies face two important challenges: (1) knowing the interaction between the nanoscale building blocks and their surrounding and (2) characterizing the materials at finer size scales. The thesis has dealt with both challenges and significant fundamental contributions have resulted.

The order of the thesis was not as usual from fundamental theories to experimental work, then results and applications. This can be attributed to our finding fundamental problems in the characterization method such as the discrepancy in the reported intermolecular force parameters. These physicochemical parameters are of a great importance to define the supramolecular interactions in addition to their essential use in material characterization.

In the first part of this work, chapters II and III, computational chemistry was a helpful tool to qualify the intermolecular interactions and complexes stability and the demand for determination of the intermolecular force parameters had appeared through the calculation of the micropore size distribution of membrane materials.

In our first paper (chapter II), membrane preparation was our first step. Our selection for a glassy polymer (PEI) was guided by the literature trend for gas separation membranes. The paper reviewed in a simple way material selection and membrane preparation. Differently from the saturated literature trend to have a thinner skinned asymmetric membrane, our concern was to architecture polymer network at an atomic scale within the skin layer. There is a lack of information related to this topic in the literature. Our first attempt in the incorporation of polyaniline into polyetherimide membranes to modify material structure and properties was not successful. Then an

alternative plan was set to explore the role of additives salt such as Li NO_3 in pore forming inside the polymer network. A successful experimental program was carried out to establish an architecturing fabrication method named later by Coagualtion Post-Leaching Method. Interactions among different molecules were discussed based on experimental observations found in the literature. From this paper, we have recognized that the weak or strong interactions (supramolecular interactions) among different molecules are a key to understanding the molecular engineering assembly of bulk materials. In the second paper (chapter III), we were seeking two goals. First, to determine the interaction among different molecules in order to illustrate molecular structuring during membrane fabrication and second, to characterize the material structure at a molecular scale. Computational chemistry and physicochemical principles were found to be powerful tools in determining the interaction and stability of different systems. The successful results enabled us to explain membrane architecturing through the coagulation preparation method. The formation and stability of molecular coordination complexes have an important role in material structuring the membrane at the microscopic scale. The nanocoiling around these complexes is possible as indicated by the molecular modeling of polymer chains using computational chemistry. The agreement among physicochemical principles, computational chemistry and other supported experiments for the obtained data related to molecular interactions indicates the validity of our results. For membrane material characterization at a molecular scale, work of Calvo et al. (1997) encouraged us to determine the micropore size distribution of polymeric membranes. They used the Micropore Method, which is based on micropore filling mechanism and using an empirical universal equation (Harkin and Jura, 1944) for adsorbate thickness. Because of the amorphous and hydrophobic nature of PEI similar to activated carbons used by Horvath and Kawazoe (1983), the Horvath-Kawazoe (HK) model of slit pore geometry was selected for the determination of the micropore size distribution of the PEI polymeric membranes. The same intermolecular interaction parameters were used because the polarizability and diamagnetic susceptibility of PEI were not available in literature in addition to the need for a structural model for PEI. Therefore, the determination of the interaction parameters of PEI membranes using the HK model was the topic of the third paper in chapter IV.

In the third paper in chapter IV, The HK parameters for N_2-PEI system were determined based on molecular properties and computational chemistry. The determination of the total effective polarizability of PEI was not an easy task. No similar determination was found in literature. The main ideas that concluded in advance in the fundamental work were used. For examples, the total polarizability of PEI was determined form the refractive index for the non-polar part and from the dipole moment for the polar part. The theoretical correlation between the dipole moment and the polar polarizability was one of the important fundamental contributions in this work. The diamagnetic susceptibility of PEI was determined from group contribution method based on the chemical structure of PEI repeat unit. Computational chemistry was used to determine the dipole moment of PEI. Modeling of the PEI structure and possible interactions were discussed. Computational chemistry was also used to determine the distance between two interacting polymer chains. The results of this paper indicate the importance of the interaction parameters in interpreting the gas adsorption isotherms to obtain valid micropore size distributions. The chain thickness of PEI has an important role in polymer membrane characterization. Because computational chemistry was used, a reasonable micropore size distribution was obtained for PEI membranes. The determined parameters were used in our last two papers in chapters VIII and IX.

Chapters V, VI and VII address the literature discrepancy in the determination of these parameters and their most direct evaluation from experimental results. Our important contribution in this subject was the link between the microscopic pair molecular interaction and the macroscopic interactions among molecules. Intermolecular force parameters were determined from the cohesive energy and the X-ray diffraction experiments. A new set of equations was developed for the determination of the intermolecular parameters at different temperatures and pressures. The direct determination of the interaction energy coefficient between two molecules from molecular properties was investigated. The discrepancy between theory and experiments in determination of the interaction energy coefficient was attributed to the repulsive electron correlation term. In literature, the determination of this term is considered a very difficult task. Our contribution was in establishing a simple equation to determine this repulsive electron correlation term.

The fundamental work in chapters V, VI and VII is an important contribution, which enabled us to establish a new model for the characterization of materials at a molecular scale. The new model was supported by different computational and experimental work such as the determination of the isosteric heat of adsorption of nitrogen on PEI polymer and there are many modeling works for the structure of N_2-PEI system. The work related to the new model was not included because of the maximum capacity and limited number of pages in this thesis. However, our new contributions will be published in referred journals.

In the last two papers in chapters VIII and IX, the objective was to improve the sieving characteristics of PEI membrane materials. The incorporation of nanoparticles into polymers to form a hybrid material having a large interfacial area that increases while decreasing the size of the nanoparticles. The strength of the adhesive energy between the phase of the nanoparticle and the polymer phase lead to a uniform definite slit width that became dominant when a very large interfacial area is formed. The shape and stereo-structure of the surface of the nanoparticles also had an impact on the resulting material structure. Supramolecular interactions such as hydrogen bonding or π–π intermolecular interactions play an important role in increasing the packing density and producing a tighter structure. Based on these concepts, twelve metal-ligand complexes were incorporated into polyetherimide during membrane preparation. PEI membranes containing these additives were tested for their performance for oxygen separation from air. The micropore size distributions of these membranes were determined from the corresponding nitrogen adsorption isotherms. In order to have a polymeric molecular sieve, the micropore size distribution has to become narrow and sharp. A very successful novel contribution was resulted in this work. The incorporation of magnesium phthalocyanine (MgPc) into polyetherimide membrane material lead to narrowing the micropore size distribution especially when additive/PEI, 10 % by weight is used. This membrane showed significant improvement on its ability to separate oxygen from air over membranes obtained using other additives.

The stability of PEI membrane material was also improved by the incorporation of MgPc. The stability of these membranes was excellent as membrane gas permeation was not influenced by an annealing process.

Comparing performance of studied membranes using Robeson's plot

As we are concerned with the development of polymeric materials for gas separation membranes, it is necessary to compare the results of this work with recent literature data. Material perfomance in membranes for the separation of O_2 from air can be compared through the trade-off curve of O_2/N_2 separation obtained by Robeson in 1980 and 1991 (Baker, 2002) as shown in the following illustration:

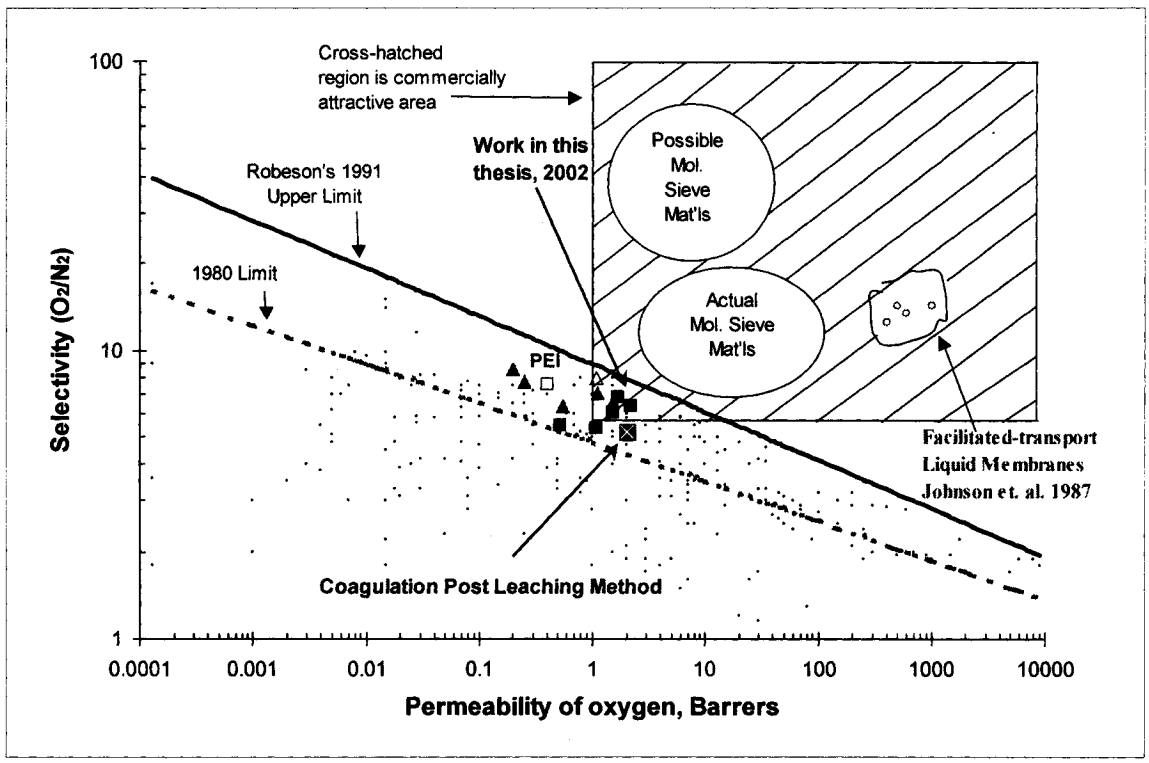

Figure 10.1 Trade-off curve plot of O_2/N_2 selectivity vs. O_2 permeability for most known materials illustrated by Robeson (1991). Open circle is for facilitated-transport liquid membranes (Johnson et al. 1987). Open square is for dense PEI film. Solid triangle is for Zeolite4A/Matrimide®/plasticizer mixed matrix films (Mahajan et al. 2002). Open triangle is for carbon molecular sieve (CMS 800-2)/Ultem® 1000 mixed matrix film (Vu et al. 2003). Solid square with a cross inside is for a membrane prepared by the coagulation post-leaching method (chapters II and III in this thesis). Solid square is for nanostructured metal complexes/polyetherimide membranes used in this thesis (chapters VIII and IX).

The selectivity was determined from the ratio of oxygen permeance to nitrogen permeance. The permeability was calculated from the product of the permeance obtained in this work and the effective thikness of the membrane. Because we have asymmetric membranes, the effective thickness of the membrane was considered to be equal to the thickness of the dense skin layer with neglecting the resistance of the sublayer for gas transport. The thickness of the skin layer was estimated to be 10 μm as an average determined from the micrograph of the cross-section of the prepared membranes obtained using Scan Electron Microscopy as shown below:

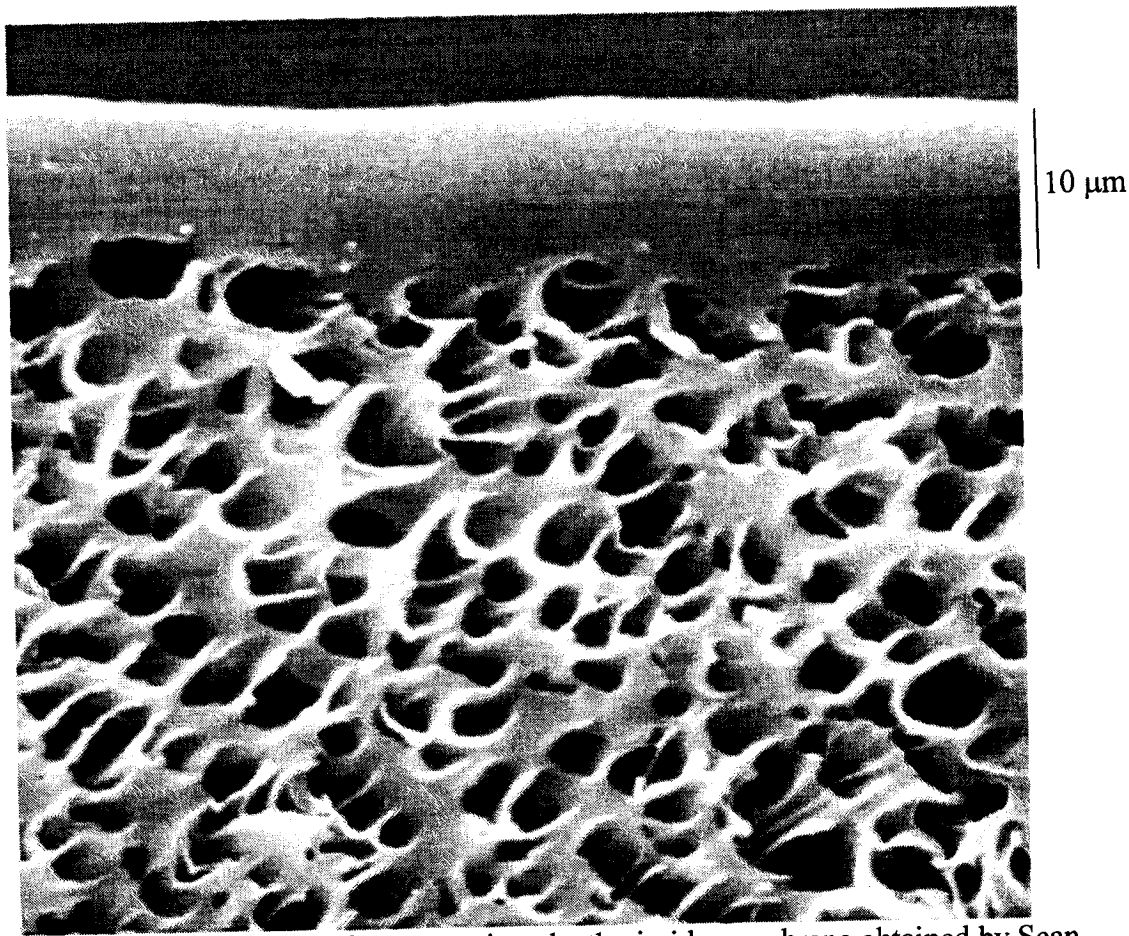

Figure 10.2 Micrograph of asymmetric polyetherimide membrane obtained by Scan Electron Micrposcopy (X 3000).

Recent data for the performance of membrane materials used for O_2/N_2 separation were obtained from Koros' school. Mixed matrix composite materials were prepared from blending molecular sieving domains within a polymer matrix. Mahajan et al.

(2002) reported that membrane performance for O_2/N_2 separation was improved when Zeolite4A/Matrimide®/plasticizer mixed matrix film was used. Vu et al. (2003) used carbon molecular sieve (CMS 800-2)/Ultem® 1000 mixed matrix film to enhance the performance of polyetherimide membrane for O_2/N_2 separation.

It is clear from the trade-off curve plot shown above that material development for membrane gas separation was enhanced by Koros and his coworkers through pushing the results of mixed matrix materials tawords the commercial area in the plot. On the other hand, nanostructured materials produced in this work also show good results that lie within the lower corner of the commercial area in the plot. Therefore, the achievement of this work is competitive with recent literature advanced research.

The facilitated-transport membranes reported by Johnson et al. (1987) show also promising results. However, their low stability (Baker, 2002) and limitations of using low upstream pressure and lower driving forces (Nishide et al. 1994, 1995; Zhang and Lin, 1995, 1999) create a strong barrier that should be overcome in the future.

From the results of this thesis, it is clear that the nanostructuring of polymeric materials confirmed by changes in material porosity at the molecular scale is the key to improve material performance for gas separation membranes.

RECOMMONDATIONS

In this work, incorporation of different additives as nanophases into polyetherimide matrix was illustrated. The same preparation procedures were used for the comparison purpose. The area of optimization of membrane morphology for the used additives was not investigated. Therefore we recommond the following for a related future study:

1. Optimizing membrane morphology for each additive.
2. Using different non-solvents and preparation procedures.
3. Using small angle X-ray diffraction for further membrane characterization.
4. Improving material characterization techniques and interpretation at a molecular scale.

REFERENCES

Baker, R. W., "Future Dirctions of Membrane Gas Separation Technology", Ind. Eng. Chem. Res., 41, 1393-1411 (2002).

Calvo, J. I., P. Prádanos, A. Hernández, W. R. Bowen, Nidal Hilal, R. W. Lovitt and P. M. Wolliams, "Bulk and Surface Characterization of Composite UF Membranes: Atomic Force Microscopy, Gas Adsorption-Desorption and Liquid Displacement Techniques, J. Membr. Sci., 128, 7-21 (1997).

Harkins, W. D. and G. J. Jura, "Surfaces of Solids. XIII. A Vapor Adsorption Method for the Determination of the Area of a Solid without the Assumption of a Molecular Area and the Areas Occupied by Nitrogen and Other Molecules on the Surface of a Solid", J. Am. Chem. Soc., 66, 1366-1373 (1944).

Horvath, G. and K. Kawazoe, "Method for the calculation of effective pore size distribution in molecular sieve carbon", Journal of chemical engineering of Japan, 16 (6), 470-475 (1983).

Johnson, B. M., R. W. Baker, S. L. Matson, K. L. Smith, I. C. Roman, M. E. Tuttle and H. K. Lonsdale, "Liquid Membranes for the Production of Oxygen-Enriched Air", J. Membr. Sci., 31 (1), 31-67 (1987).

Mahajan, R., R. Burns, M. Schaeffer and W. J. Koros, "Challenges in Forming Successful Mixed Matrix Membranes with Rigid Polymeric materials"' J. Appl. Polym. Sci., 86, 881-890 (2002).

Nishide, H., T. Suzuki, R. Nakagawa, K. Itakura and E. Tsuchida, "Chemically Specific Surface Diffusion of Oxygen through a Porous Membrane Modified with Cobalt Porphyrin on its Pore Surface", J. Phys. Chem. 99, 12312-12317 (1995).

Nishide, H., T. Suzuki, R. Nakagawa and E. Tsuchida, "Enhanced Oxygen Diffusion through a Porous Membrane Chemically Modified with Cobalt Porphyrin on its Pore Surface", J. Am. Chem. Soc. 116, 4503-4504 (1994).

Robeson, L. M., "Correlation of Separation Factor versus Permeability for Polymeric Membranes", J. Membr. Sci., 62, 165-185 (1991).

Siegel, R. W., WTEC Panel Report on "Nanostructure Science and Technology, R&D Status and Trends in Nanoparticles, Nanostructured Materials, and Nanodevices", Loyola College Baltimore, MD 21210, USA (September, 1999).

Vu, D. Q., W. J. Koros and S. J. Miller, "Mixed Matrix Membranes Using Carbon Molecular Sieves: I. Preparation and Experimental Results", J. Membr. Sci., 211, 311-334 (2003).

Zhang, Z. and S. Lin, "Oxygen/Nitrogen Transport in Ionomer Composite Membranes containing a Cobalt Schiff base Complex", J. Appl. Polym. Sci. 74, 1071-1077 (1999).

Zhang, Z. and S. Lin, "Facilitated Oxygen Transport in an Ionomer Membrane containing Cobaltous ions", Macromol. Rapid Commun. 16, 927-933 (1995).

REFEREED CONFERENCES

The results of this work were presented in refereed journals (see corresponding chapters) and refereed conferences (oral presentation by person underlined) as follows:

1. Kurdi J. and **A. Y. Tremblay** (2002). The Determination of Interaction Parameters in the Characterization of Polyetherimide Gas Separation Membranes Using Horvath-Kawazoe Model., International Congress on Membranes and Membrane processes, Toulouse, France, July 7-12, 2002 (Ph. D. work).

2. **Kurdi J.** and A. Y. Tremblay (2001). Preparation and characterization of nanoporous polyetherimide gas separation membranes, 51st Canadian Chemical Engineering Conference, Halifax, October 14-17, 2001 (Ph. D. work).

3. **Harlick, P. J. E.**, Kurdi, J and A. Y. Tremblay, Theoretical evaluation of a novel dual membrane gas permeator, 51st Canadian Chemical Engineering Conference, Halifax, October 14-17, 2001 (Research assistant's work).

4. **Kurdi, J.** and A. Y. Tremblay, The influence of casting solution structure on the porosity of polyetherimide gas separation membranes, International Congress on Membranes and Membrane processes, Toronto, Ontario, Canada June 12-18, 1999 (Ph.D. work).

APPENDIX

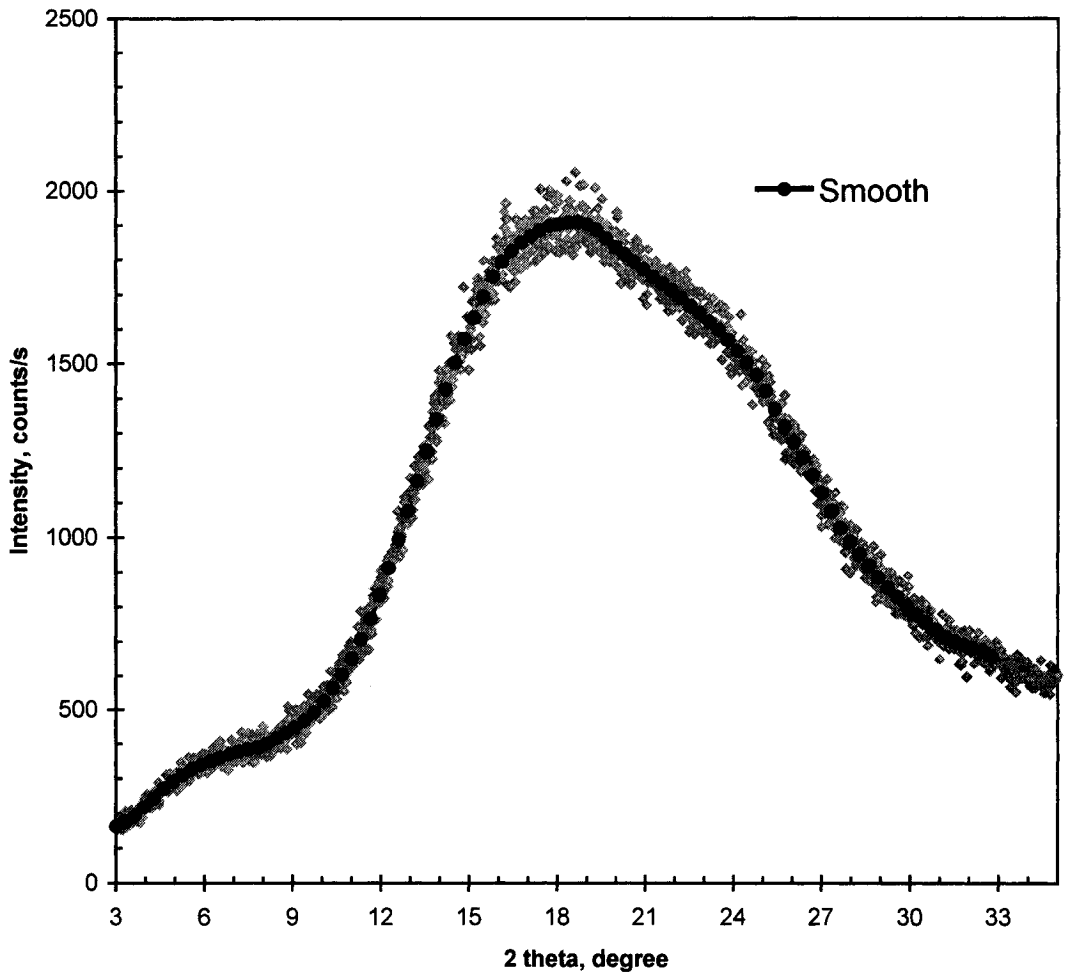

Figure A.1 Wide-angle X-ray diffraction measurements of asymmetric polyetherimide membrane described in section 3.2, chapter V, page 88.

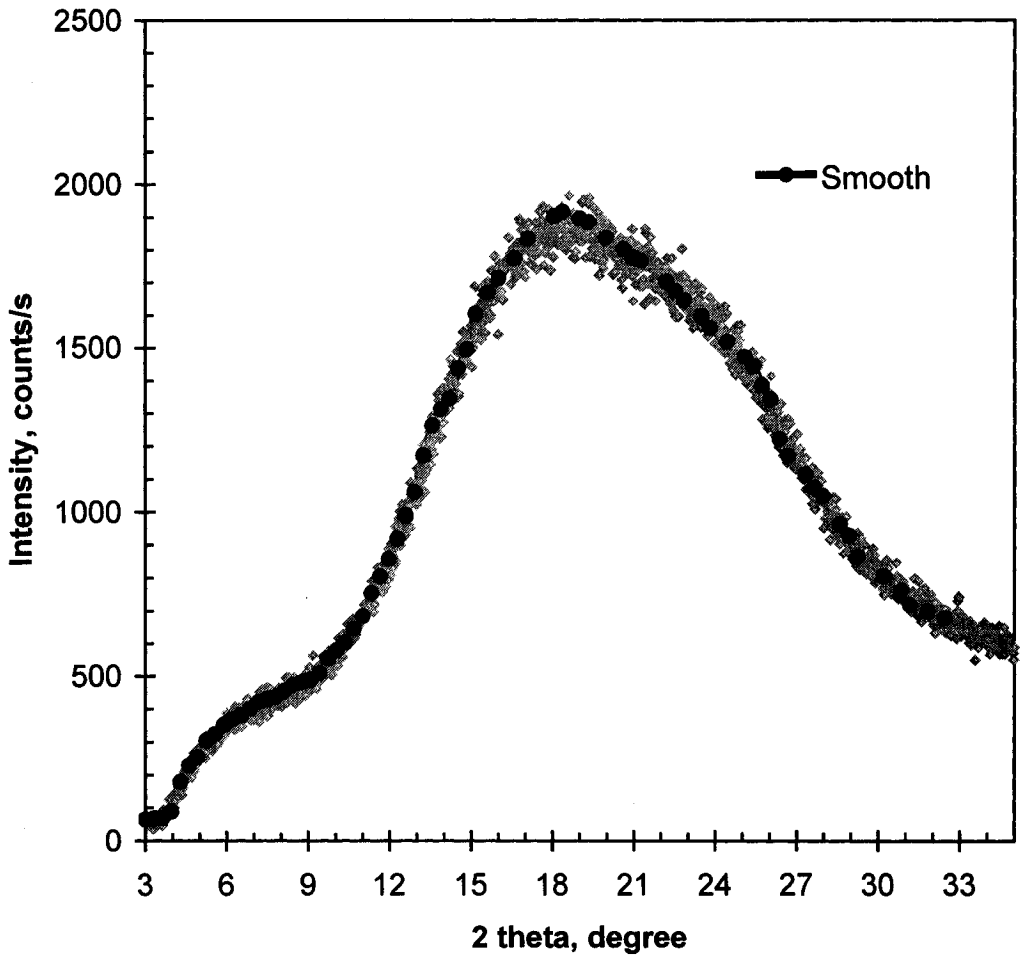

Figure A.2 Wide-angle X-ray diffraction measurements of symmetric polyetherimide film described in section 3.2, chapter V, page 88.

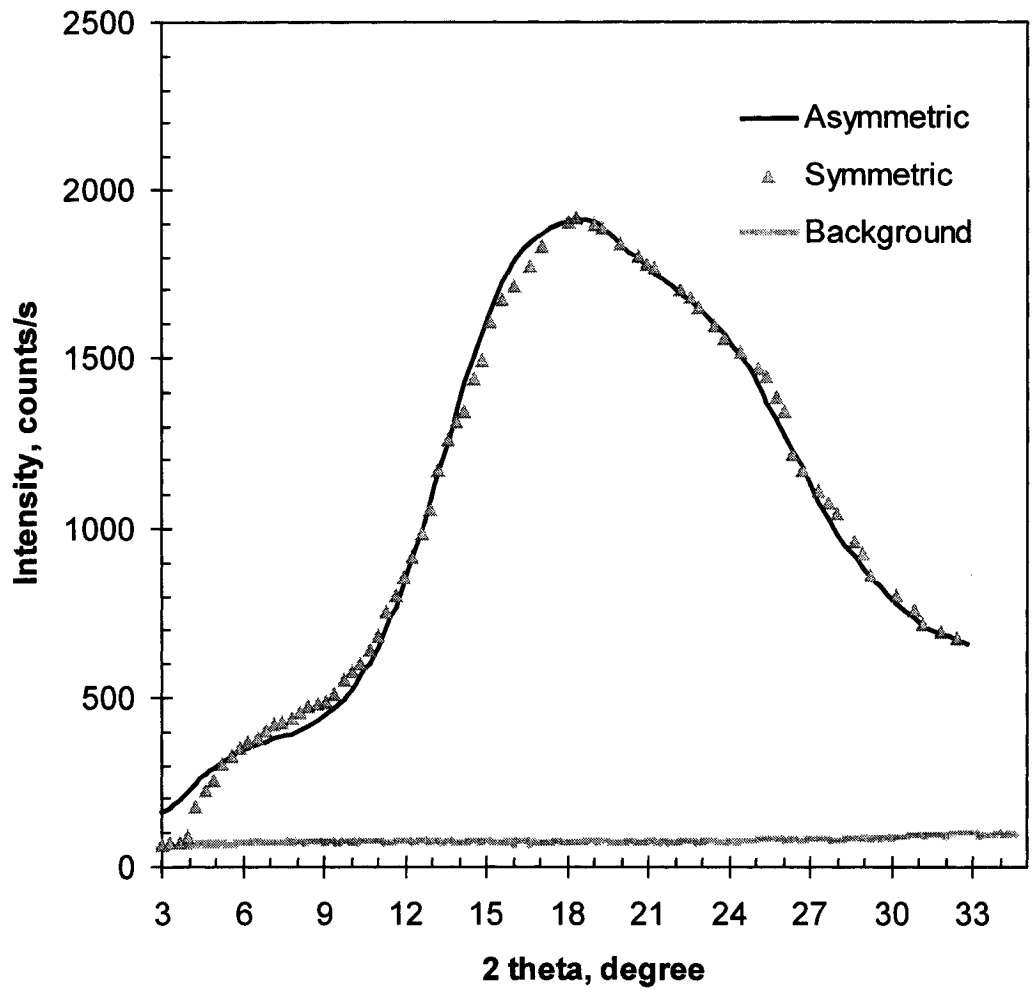

Figure A.3 The above two X-ray diffraction spectra were plot in this figure for the purpose of comparison. The background was taken at the same conditions without the sample in place.